THE UNIVERSITY *of* EDINBURGH

Peptide and peptidomimetic leads for the inhibition of MDM2-mediated ubiquitination of p53

A thesis submitted for the degree of

Doctor of Philosophy in

Organic Chemistry

Edinburgh University - 2013

Nicolas Petitjean

Supervisor: Dr. Alison Hulme

DECLARATION

I hereby declare that I am the author of this thesis. The work described in this thesis is my own and any contribution by others has been clearly stated and acknowledged. I can also confirm that no part of this thesis has been previously submitted for any other degree or professional qualification.

Nicolas Petitjean.

Acknowledgments

Firstly I would like to thank my main supervisor Dr. Alison Hulme for giving the opportunity to conduct this research in her laboratories and to Prof. Kathryn Ball my second supervisor. I would like to thank them for their advice, guidance and support over the last 4 years. I would like to thank everyone in the Hulme group, Phil Dorgan, Jill Hanna, Felicia Landi and Sarah Boys for all the good moments spent during my MSc, but also Helen Niblock, Kevin Ralston, Heather Johnston and Sarah Thomas for the day-to-day breaks. A special thanks to Lore Troalen for the mutual support during the long HPLC-pizza nights. I also would like to thank the Biology crew for helping me to learn the biological techniques, especially Euan Murray, Suzanne Petterson, Vikram Narayan, Vivien Landre, Anne-Sophie Huart and Emma Pion.

A huge thank to all the support staff at the university, especially Juraj Bella, Marika de Cremoux and Lorna Murray for their help with the NMR; John Knox, Derek Burgess, Raymond Borwick and Tim Calder in Stores.

I thank Janice Bramham for the help on the circular dichroism and Andrew Cronshaw on the MALDI at the Swann Building, Logan Mackay on the Mass spectrometer at SIRCAMS and Catherine Botting for the trypsin experiments at the University of St Andrews. More generally I thank the University of Edinburgh for providing the facilities and CRUK for funding.

I would like to thank the French and other friends (Géraldine Escher, Yan Jauffret, Anne-Frédérique Pecharman, Marine Raman, Jon Lowther, Anne Germeroth, Craig and Natalie Potter) for good laughs and support.

I am thankful to my family for all the support and encouragement given through my years of study. A special thought goes out for my younger brother Philippe who has passed away during this adventure. This thesis is for you. The most special thanks goes out to Aline for the mutual support, strength and love given all those years. You give me so much energy. Thank you with all my heart.

Table of contents

Abbreviations

°C	Degree Celsius
µL	Microlitre
A_{280}	Absorbance at $\lambda = 280$ nm
aa	Amino acid
Ac	Acetyl
AChE	Acetylcholinesterase
Asc	Ascorbate
ATP	Adenosine-5'-triphosphate
BLAST	Basic Local Alignment Search Tool
Boc	*Tert*-butoxycarbonyl
bp	Base pair
br	Broad
BRCA1	Breast cancer 1
BSA	Bovine Serum Albumin
CD	Circular dichroism
CuAAC	Copper-catalysed Azide-Alkyne cycloaddition
d	Doublet
DCM	Dichloromethane
DIC	N,N-Diisopropylcarbodiimide
DIPEA	Diisopropylethylamine
DMF	N,N-Dimethylformamide
DMSO	Dimethyl sulfoxide
DNA	Deoxyribonucleic acid
DNA-PK	DNA protein kinase
DTT	Dithiothreitol
E. coli	*Escherichia coli*
ECL	Electro chemiluminescence
EDTA	Ethylenediaminetetraacetic acid
ELISA	Enzyme-Linked ImmunoSorbent Assay
equiv.	Equivalent
ESI	Electrospray ionization
Et	Ethyl
Fmoc	9*H*-Fluoren-9-ylmethoxycarbonyl
Fmoc-OSu	*N*-(9-Fluorenylmethoxycarbonyl) succinimide
FTIR	Fourier Transform Infrared spectroscopy
GST	Glutathione S-transferase
h	Hours
HCT116	Human colon carcinoma cell line (variant T116)

HEK293	Human embryonic kidney 293 cells
HEPES	4-(2-hydroxyethyl)-1-piperazineethanesulfonic acid
His	Histidine
HDAC	Histone Deacetylase
HIV	Human immunodeficiency virus
HOBt	1-Hydroxybenzotriazole
HPLC	High Performance Liquid Chromatography
HRMS	High Resolution Mass Spectrometry
HRP	Horseradish peroxidase
Hz	Hertz
IPTG	Isopropyl β-D-1-thiogalactopyranoside
IR	Infrared
J	Coupling constant
LIM	Linear interaction motif
m	Multiplet
m/z	Mass to charge ratio
mAb	Monoclonal antibody
MDM2	Murine double minute 2
MDM4	Murine double minute 4 (MDMX)
mL	Millilitre
mmol	Millimoles
mol	Moles
mRNA	Messenger RNA
M_w	Molecular weight
MW	Microwave
NES	Nuclear Export Signal
Ni-NTA	Nickel nitrotriacetic acid
NLS	Nuclear Localisation Signal
NMR	Nuclear Magnetic Resonance
OD_{600}	Optical density at $\lambda = 600$ nm
o/n	Overnight
p53	Tumour suppressor protein 53
pAb	Polyclonal antibody
PAGE	PolyAcrylamide Gel Electrophoresis
PBS	Phosphate buffered saline
PBS-T	Phosphate buffered saline Tween
PDB	Protein Data Bank
q	Quartet
res.	Residues
R_f	Retention factor
RING	Really Interesting New Gene
RLU	Relative Luminescence Unit

RNA	RiboNucleic Acid
rpm	Revolutions per minute
RPMI	Roswell Park Memorial Institute
rt	Room temperature
s	Singlet (NMR) or strong (IR)
SDS	Sodium dodecyl sulfate
SPPS	Solid Phase Peptide Synthesis
t	Triplet
TBTA	Tris-[(1-benzyl-1*H*-1,2,3-triazol-4-yl)methyl]amine
TfN_3	trifluoromethanesulfonyl azide
TIS	Triisopropylsilane
t-Bu	*tert*-butyl
TFA	Trifluoro Acetic Acid
THF	Tetrahydrofuran
TLC	Thin Layer Chromatography
TOF	Time of flight
t_R	Retention time
Tris	Tris(hydroxymethyl)aminomethane
Trt	Trityl
USP	Ubiquitin specific Protease
UV	Ultraviolet
V	Volume
w	Weight
wt	Wild type
δ	Chemical shift
λ	Wavelength

Abstract

The tumour suppressor p53 is essential for genome stability and loss of its function can lead to human cancer. The functional roles of p53 are regulated by a variety of mechanisms, some of which are not well understood. However, the murine double minute 2 (MDM2) protein, a major negative regulator of p53, has been found to be overexpressed in many human cancer cell lines in which p53 was not mutated; thus establishing MDM2 as a target for cancer therapeutics. MDM2 is defined as both an oncoprotein and an E3-ubiquitin ligase; its interactions with p53 are controlled through multiple domains, providing different possible pathways to inhibit MDM2 and therefore reactivate p53 function. Previous work undertaken in the Ball laboratory has shown that the MDM2 RING domain plays a critical role in p53 ubiquitination; thus screening for modulation of its activity by small molecules could provide new leads for the inhibition of the E3 ligase activity of MDM2.

The MDM2 RING domain was cloned, expressed and purified so that it could be studied using a series of *in vitro* experiments. The generation of a library of short (12-mer) peptides as potential inhibitors of the MDM2 RING domain was investigated using phage display against His-tagged RING protein to screen the peptide ligands. In order to study the specificity of these peptides towards MDM2 (res. 396-491 and 396-479) compared with MDM4 and BRCA1, the MDM4 RING domain (res. 395-490 and 395-478) and BRCA1 (res. 1-304) domain were expressed and purified for further characterisation. A small selection of peptides was isolated and their binding affinity and activity as MDM2 inhibitors evaluated by *in vitro* ELISA, affinity chromatography and ubiquitination assays. One peptide in particular, KCCYFETHMPRH, was found to bind to MDM2 and was able to inhibit MDM2-mediated ubiquitination of p53 *in vitro*. Preliminary optimisation of this peptide by alanine scan revealed a peptide with a 2-fold increased potency.

Since peptides provide comparatively weak therapeutic leads due to a combination of poor cellular uptake and susceptibility to cleavage by proteases, cyclic peptidomimetics based upon this lead were developed using side-chain to side-chain cyclisation. These peptidomimetics were successfully generated by the synthesis and incorporation of novel *N*-propargylated glycine and *N*-azidoalkyl glycine building blocks into a peptide sequence by Solid Phase Peptide Synthesis (SPPS). Following a Copper-catalysed Azide-Alkyne Cycloaddition (CuAAC) on solid phase or in solution, these peptoid-peptide hybrids were isolated, purified and characterised.

Lay Abstract

The tumour suppressor protein p53 is known to safeguard our genetic information. However, this protein sometimes loses its ability to function as a protector. For this reason, the p53 protein has been widely studied to understand how its malfunction leads to the development of human cancer and, more particularly, the mechanisms by which it is regulated. The murine double minute 2 (MDM2) protein is a regulator that inhibits the function of p53. MDM2 is therefore considered as a good anti-cancer target. One region of MDM2, called the RING (Really Interesting New Gene) domain provides a target for finding new inhibitors of MDM2.

The focus of this thesis was the isolation of short chain peptides which bind specifically to the target MDM2 RING. A range of different biological techniques were used to achieve this, including phage display which allows selection of a few peptides based on their binding affinity to the biological target. Peptides that bound to the MDM2 RING domain were isolated, one of which in particular has shown interesting activity. Since peptides provide weak therapeutic leads, a new method was developed to modify them and increase their resistance. In future work, the active compound will be further studied and optimised as a new anti-cancer therapeutic. This new method will be applied to a variety of known active compounds and other similar methods will be developed.

Nomenclature

Recommended abbreviations for cyclic peptides are described by the IUPAC system (2004). The prefix cyclo is often used for ring closure by elimination of hydrogen and the prefix anhydro for ring closure by elimination water. However there is no clearly defined abbreviation for ring closure of cyclic peptides by triazole formation. For this reason, the cyclised peptidomimetics developed in this thesis will be described with the prefix C (for cyclised). The prefix U (for uncyclised) will refer to uncyclised peptidomimetics. An example for peptidomimetic 22 is shown below:

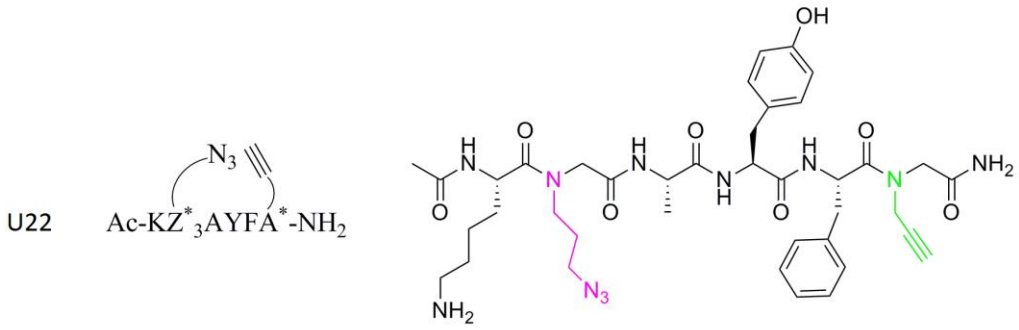

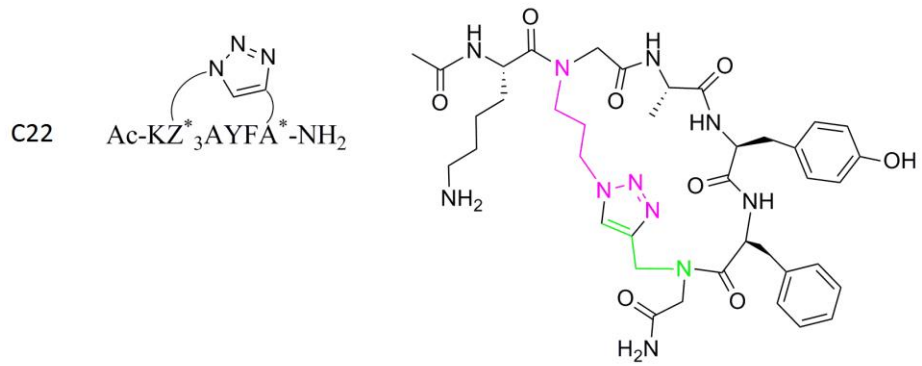

As there are no cysteines in the peptidomimetics synthesised, there should be no confusion between them.

CHAPTER 1

Isolation and identification of potential inhibitors of the MDM2 RING domain

1.1 Introduction

1.1.1 Causes of cancer

Cancer is defined by the development of abnormal and aggregated cells (tumours) that have escaped the normal growth process[1]. Because cancer cells indefinitely divide and escape programmed cell death (apoptosis), they can perturb normal tissues. If this growing mass of cells remains untreated, it may spread through the host and eventually cause death. Therefore, it is essential to understand the processes involved in the development of cancer.

Tumours can arise from different specialised cell types. The majority of tumours arises from epithelial tissues. Adenocarcinomas and squamous cell carcinomas are mostly found in the mouth, oesophagus, stomach, intestines, skin, pancreas, lung, liver, ovary, bladder, prostate and breast. Other tumours can arise from non-epithelial tissues throughout the body such as connective tissues (sarcomas), blood-forming tissues (leukaemias, lymphomas) or from cells of the central and peripheral nervous system (gliomas, neuroblastomas).

Cancers occur with different frequencies within the human population and have been shown to be associated with environmental stresses and lifestyle factors (Figure 1.1-1).

Figure 1.1-1. (a) Estimated worldwide cancer mortality in 2008. (b) The ten most common cancer deaths in males worldwide in 2008. (c) The ten most common cancer deaths in females worldwide in 2008. NHL: Non-Hodgkin's Lymphoma. Reproduced with permission.[2]

Mainly two classes of genes, tumour suppressor genes (genes that normally suppress tumour proliferation) and oncogenes (genes that favours tumour formation upon activation) are thought to be altered in the cellular machinery during cancer development.[3] Mutations in either of these genes may allow a cell to escape normal regulatory mechanisms and proliferate freely.[4] It is therefore essential to understand how these genes contribute to cellular decisions including whether to divide or undergo apoptosis. The identification of partners of these oncogenes and tumour suppressors is therefore critical for the understanding of their function and regulation.

1.1.2 Protein-Protein Interactions

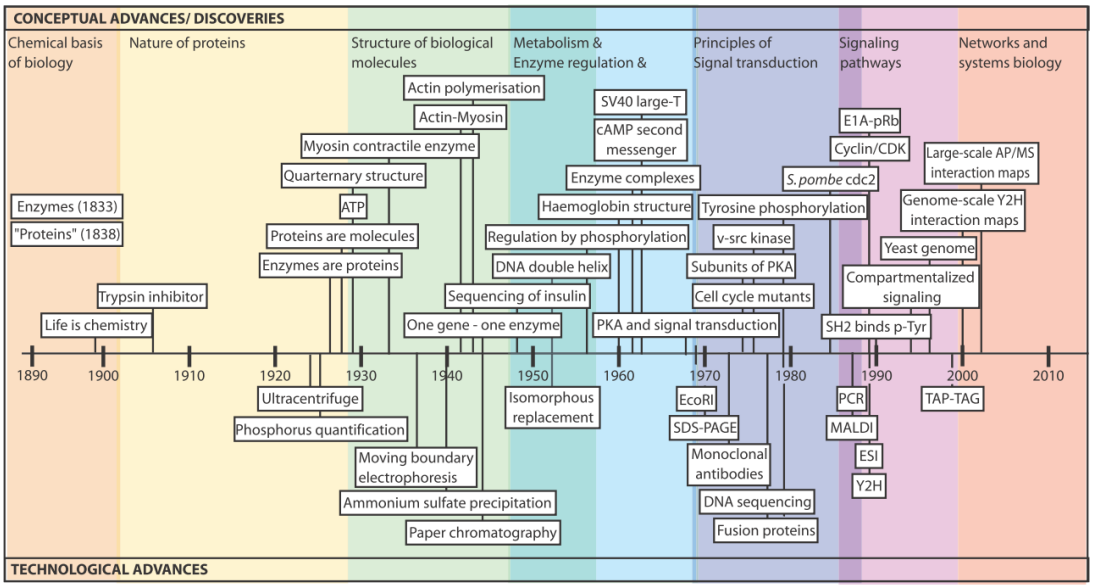

Figure 1.1-2. Timeframe of PPI research. Discoveries are indicated in the top part, technological advances are shown in the bottom part. Reproduced with permission.[5]

The improved understanding made over the past century of the structure and function of biological molecules and in the field of signal transduction and signalling pathways (Figure 1.1-2) together with technological advances such as electrophoresis, DNA sequencing and PCR have developed the field of protein-protein interactions (PPIs).

PPIs play a major role in mediating functions such as maintenance of cellular organisation, regulation of protein concentrations, metabolism and cell signalling.[6-10]

Until recently, protein-protein interactions (PPIs) were believed to occur only through the interactions of well-ordered domains. However, domains only represent a fraction of the primary amino acid sequence of protein.[11] The remaining amino acids form unstructured regions flanking the domains that are more ordered. These intrinsically disordered sequences are often rich in polar and charged amino acids (Gln, Ser, Pro, Glu, Lys) and can be of significant length.[12] In absence of a target, the relative flexibility of linkers allows the domain to search the target. When bound to the target, the linker can fold, act as a lid, help the protein to orientate towards the target (Figure 1.1-3).[12]

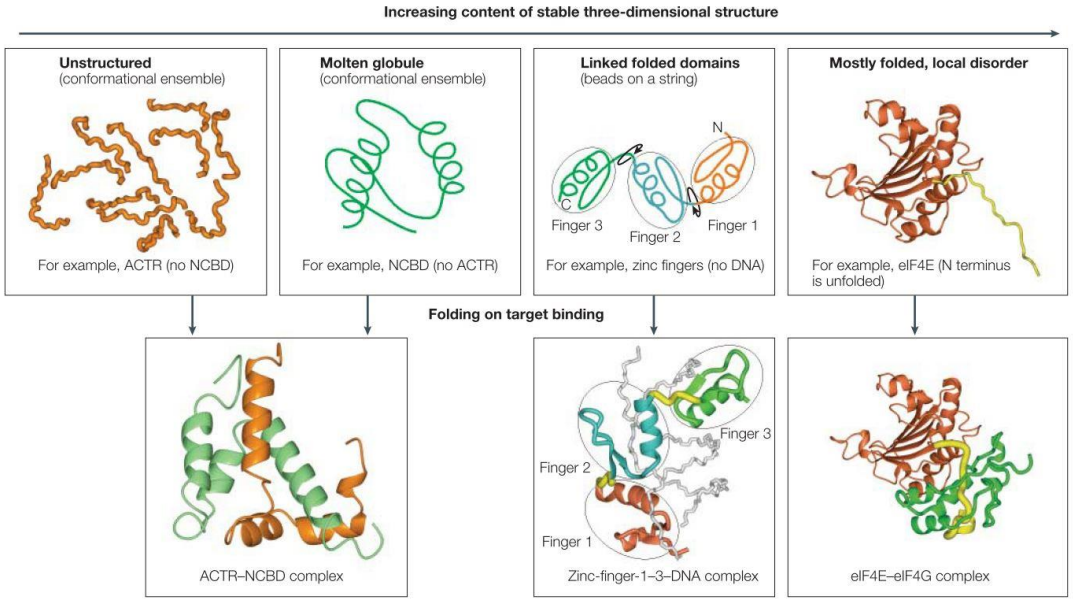

Figure 1.1-3. Folding of proteins upon target binding. Reproduced with permission.[12]

Proteins can form complexes through their domains; indeed p53, a tumour suppressor, can form a tetramer through its tetramerisation domain (more details in section 1.1.3). MDM2 (mouse double minute 2), its main negative regulator, can form a homodimer or a heterodimer with MDM4 (Section 1.1.6). Inside these domains, α-helix, β-sheets, and β-hairpin structures have been observed and shown to interact with other domains. This is the case for p53 protein, the N-terminus of which forms an α-helix and binds the N-terminal hydrophobic pocket of MDM2. Key residues involved in a PPI are called hot spots[13]. Bogan and Thorn have compiled a database of alanine mutants for which the change of free energy of binding has been measured and reported that a few residues such as arginine, tyrosine and tryptophan, a positively charged amino acid and two hydrophobic aromatic amino acids respectively, were more likely to be hot spots than other amino acids.[13] Tyrosine and tryptophan are capable of hydrogen bonding, hydrophobic interaction or π-interactions. Arginine is also capable of hydrogen bonding, salt-bridge formation with its guanidinium motif which displays a pseudo-aromatic character with its delocalised π-system. PPI are not very deep. In these interactions, exclusion of solvent is achieved by contacts of energetic unimportance, offering protection of hot spots from bulk solvent. These solvation and dielectric conditions increase the interaction strength for electrostatic and hydrogen

bonding. This can explain why arginine, tyrosine and tryptophan are favoured since they are capable of both hydrophobic and hydrogen bonding interactions.

Regions within an interaction domain that display a specific sequence pattern or linear interaction motif (LIM) contain usually three to eight residues, that play a key role in binding, and only two to four may be essential.[9,11,14] LIMs have specific functions, which include localisation signals, phosphorylation sites or binding regions such as the identified PXXP motif which has been shown to bind the SH3 domain.[15,16] Unlike large domains, which are easily detectable by sequence comparison, linear motifs are very difficult to discover using alignment methods because of their short lengths. Cell-based proteomic screens for the p53-MDM2 interaction have been used to achieve the identification of such motifs and find potential new inhibitors. With the construction of the [L/I/V/M]-[W/Y/F]-X-X-[L/I/V/M] consensus motif for this interaction and the identification of Nutlin-3 modulated protein by mass spectrometry, a new set of peptides were shown to mind full length MDM2. Cyclophilin B was finally identified as a novel *in vivo* MDM2 binding protein.[17]

1.1.3 Loss of p53 function, activation and regulation

The p53 protein was independently discovered by three groups in 1979 and was observed in an oligomeric complex with the Simian Virus (SV) oncogene product, the large T antigen, in SV40 transformed cells.[18-20] The p53 gene, cloned for the first time in 1983,[21] was found to be located in the short arm of chromosome 17 in humans. It has been shown that allelic deletions of chromosome 17p occur in at least 30% of brain tumours and at least 60% of tumours in lung, breast and colon. Interestingly, these were shown to correlate with p53 mutations,[22-27] most of which give rise to mutations in the DNA binding domain of the p53 protein (Figure 1.1-4). Overall, p53 mutations have been observed with different frequencies in many cancer types (Figure 1.1-5).

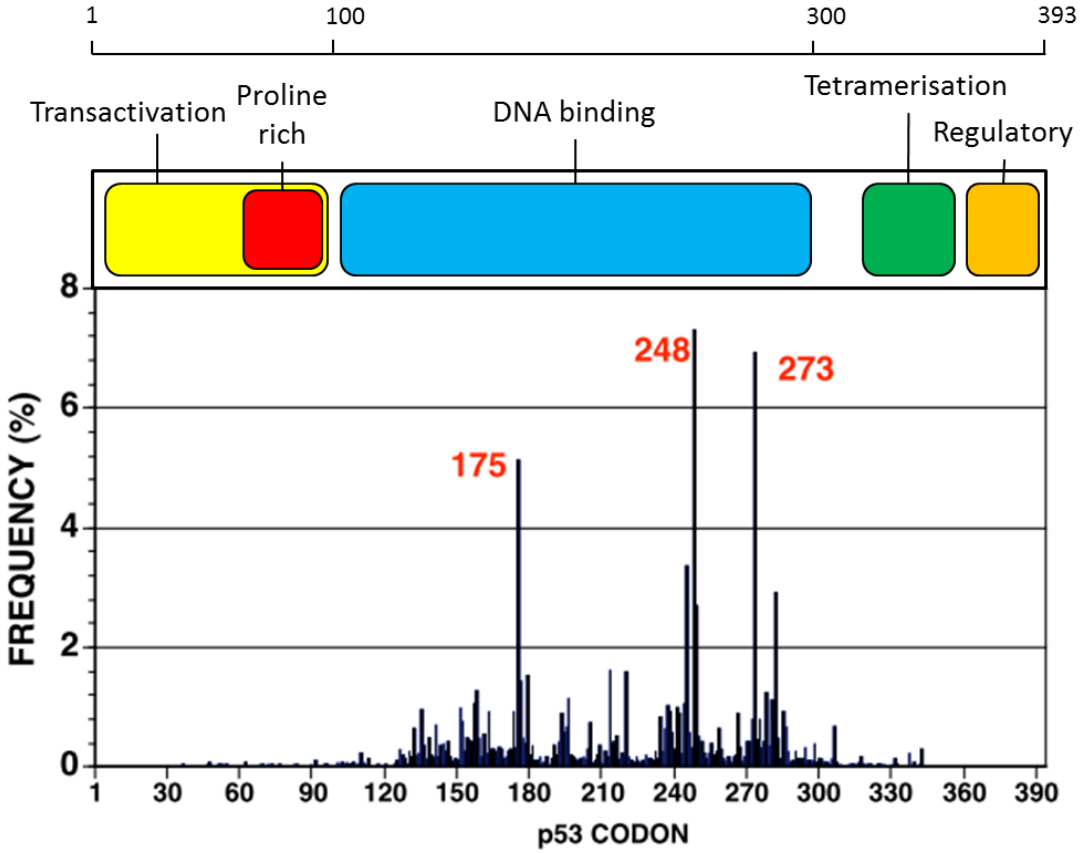

Figure 1.1-4. Distribution of p53 mutations. 393 amino acids. Most mutations appear in the DNA binding domain (blue); transactivation domain (yellow); proline-rich domain (red); oligomerisation domain (green); regulatory domain (orange). Residues with most frequent mutations are written in red.[28]

Cancer type	Number of cases (#)	Number of mutations (#)	Frequency (%)
Breast carcinoma	14389	3390	23.56
Colorectal carcinoma	9183	3967	43.2
Lung (NSCLC)	6126	2314	37.77
Head and Neck SCC	5654	2185	38.65
Ovarian carcinoma	4401	1997	45.38
Bladder carcinoma	4271	1156	27.07
Hepatocellular carcinoma	3327	945	28.4
Glioblastoma	2706	633	23.39
Gastric carcinoma	2467	739	29.96
Esophageal SCC	2444	1136	46.48
Prostate ca.	1395	205	14.7
Astrocytoma	1247	451	36.17
B-Chronic Lymphocytic Leukemia	1200	144	12
Pancreatic cancer	1107	342	30.89
Acute Myelogenous Leukemia	852	78	9.15
Osteosarcoma	816	158	19.36
Soft Tissue Sarcomas	791	73	9.23
Cervical Cancer	766	44	5.74
Endometrial tumor	724	184	25.41
Non-Hodgkin's Lymphomas	708	137	19.35
B-cell Lymphoma	638	101	15.83
Sarcoma	627	36	5.74
Thyroid Carcinoma	603	58	9.62
Brain Tumor	599	155	25.88
B-Acute Lymphoblastic Leukemia	564	77	13.65
Renal cell ca.	528	70	13.26
Gliomas	481	112	23.28
Esophageal ADC	424	248	58.49
Myelodysplastic synd.	422	29	6.87
B-Lineage Diffuse Large Cell L	357	59	16.53
Adult T-cell Leukemia	328	54	16.46
Skin Squamous Cell Carcinoma	312	132	42.31
Lung (SCLC)	288	148	51.39
Basal Cell Carcinoma	284	124	43.66
Follicular lymphoma	274	27	9.85
Rectal ca.	261	116	44.44
Urothelial TCC	260	111	42.69
Esophageal ADC (Barrett)	253	77	30.43
Colorectal adenoma	238	14	5.88
Nasopharyngeal carcinoma	232	34	14.66
Melanoma	210	54	25.71
Multiple Myeloma	209	20	9.57
Uterine cancer	189	71	37.57
Wilm's tumor	177	21	11.86
Hepatic angiosarcomas	169	5	2.96
Neuroblastoma	147	4	2.72
Mantle Cell Lymphoma	143	23	16.08
Oligodendrioglioma	143	28	19.58
Urothelial ca.	143	73	51.05
Colorectal Carc. Metast.	142	77	54.23

Figure 1.1-5. Frequency of p53 mutations in various cancers. Data were obtained from the UMD-p53 mutation database.[28]

The *p53* gene codes for a transcription factor that is involved in cell cycle arrest, apoptosis and DNA repair.[29] Although not required for normal development in mice,

the tumour suppressor *p53* is essential for maintaining the integrity of the genome as its deletion dramatically increases the risk of cancer.[30] For example, Li Fraumeni Syndrome (LFS) is a cancer predisposition syndrome characterised by early onset tumours[31] and is associated with germline mutations in the *p53* gene.[32] Loss of p53 function can also be observed with wild-type p53 through the action of repressors and negative regulators of p53. Indeed, amplification of the *hdm2* gene leads to the overexpression of the protein Human Double Minute 2 (HDM2), an E3 ubiquitin ligase known to repress p53 activity.[33] HDM2 is overexpressed in about 7% of all human tumours with an amplification range of 2- to 10-fold and soft tissue tumours were found to have the highest frequency of HDM2 overexpression (about 20%) closely followed by osteosarcomas (about 16%).[34]

Cellular stresses may trigger cellular transformation to prevent damage. Without surveillance, this would lead to cancer and ultimately to the death of the host. To avoid such an outcome, depending on the intensity, the duration and the type of stress (DNA damage, telomere shortening, chromosomal aberration, hypoxia, temperature shock, nutrient depletion or oncogene activation) and through a multitude of interactions, the p53 pathway is activated and leads to either cell cycle arrest, DNA repair, differentiation, senescence, anti-angiogenesis or apoptosis (Figure 1.1-6).[35-37]

Following a stress, sensors recognising the nature of the damage induce signal transduction cascades triggering upstream proteins to activate p53 via post-translational modifications. Indeed, p53 can be stabilised and activated by phosphorylation, acetylation, methylation, sumoylation and neddylation at different sites on the protein, depending on the nature of the stress.[31,34-37] Once activated, p53 can act as a transcription factor to transactivate or repress downstream genes (Figure 1.1-6).

Since p53 is able to induce cell cycle arrest or a programmed-cell death, it is also critical to control p53 activity to avoid such outcomes and allow normal proliferation under non-stressed conditions.

The half-life of p53 has been estimated to be about 30 minutes in the absence of cellular stress and about 2.5-3.5 hours after stress-induced damage such as ionising

radiation or UV radiation.[38,39] More recently, it has been shown that the activity of p53 can also be controlled by MDM2 binding to *p53* mRNA, resulting in accumulation of MDM2 at the polysome, inhibition of the E3 ligase activity of MDM2 and stimulation of p53 synthesis.[40] It has been shown using mouse models lacking the *mdm2* gene (*mdm2*$^{-/-}$ mice) that the mice die during the embryonic stage. This early embryonic lethality could be rescued by deleting the *p53* gene, thus demonstrating the importance of MDM2 as a critical negative regulator of p53 *in vivo.*[41,42]

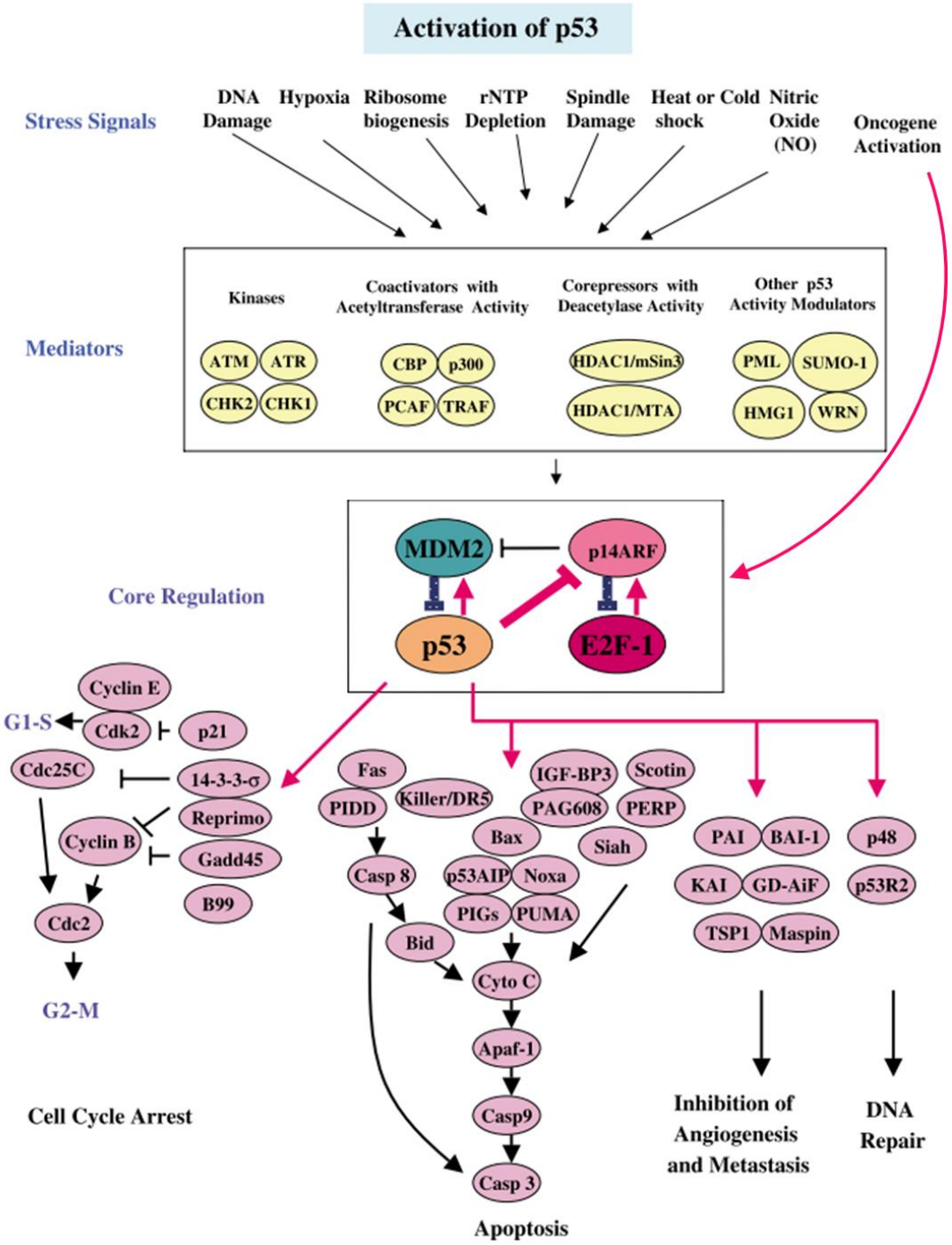

Figure 1.1-6. Activation of p53 following a stress: upstream and downstream genes of p53 mediate the different outcomes in response to cellular stress. Triangle-headed arrows represent an activation while T-shaped arrows mean an inhibition of the subsequent genes. Modified with permission.[43]

The conformation of p53 seems to be important for its functions and outcome. Indeed, Heat-shock protein 90 (Hsp90), a molecular chaperone essential for the correct folding and assembly of many proteins, is able to bind p53 and positively modulate p53 DNA binding. In the absence of Hsp90, p53 loses its wild-type conformation and its DNA binding function when incubated at 37°C.[44] Another piece of evidence highlighting the importance of p53 conformation is the existence of p53 in different oligomeric states. p53 can be found as a monomer, dimer or tetramer (or more precisely a dimer of dimers). Indeed, a tetramerisation domain (res. 324-355) has been identified at the C-terminus of p53. Although an equilibrium exists between the different oligomeric states of p53, the tetramer is required for p53-specific DNA binding.[45,46]

Considering the function of p53 as a tumour suppressor, it is also essential to keep p53 at low levels in the absence of damage. p53 regulatory proteins include transcriptional coactivators, ubiquitin ligases, enzymes involved in post translational modifications and others.[43,47,48] Degradation of p53 is mainly managed through the ubiquitination process (discussed in detail in Chapter 1.1.5),[49] either to keep p53 at basal levels under normal conditions or to return to steady state levels after cellular stresses.

p53 degradation can occur in an MDM2-dependent or MDM2-independent manner. It has been established that the last 30 amino acid residues and the oligomerisation domain of p53 are essential for MDM2-dependent degradation.[50] Degradation of a protein via the proteasome usually requires attachment of a polyubiquitin chain to specific sites on the protein. However, MDM2 does not seem to polyubiqitinate p53 on its own but rather mediates multiple monoubiquitination events in HCT116 cells.[51] The RING (Really Interesting New Gene) domain of MDM2 which catalyses the ubiquitination of p53 is widely documented and is discussed in Sections 1.1.5 and 1.1.6. Other studies have revealed the importance of the acidic domain of MDM2 in p53 ubiquitination, as a deletion within the acidic domain led to monoubiquitination but not degradation of p53, which could be due to the loss of p300 binding.[52,53]

The exact sub-cellular location of p53 degradation has been the subject of some controversy. p53 has three nuclear localisation signals (NLS) and two nuclear export signals (NES).[54,55] MDM2 also possesses such domains, which brings more complexity to the understanding of the process. Activated p53 is mainly found in the

nucleus but is also found in the cytoplasm where it has a shorter half-life . It was therefore suggested that p53 is degraded in the cytoplasm (Figure 1.1-7).

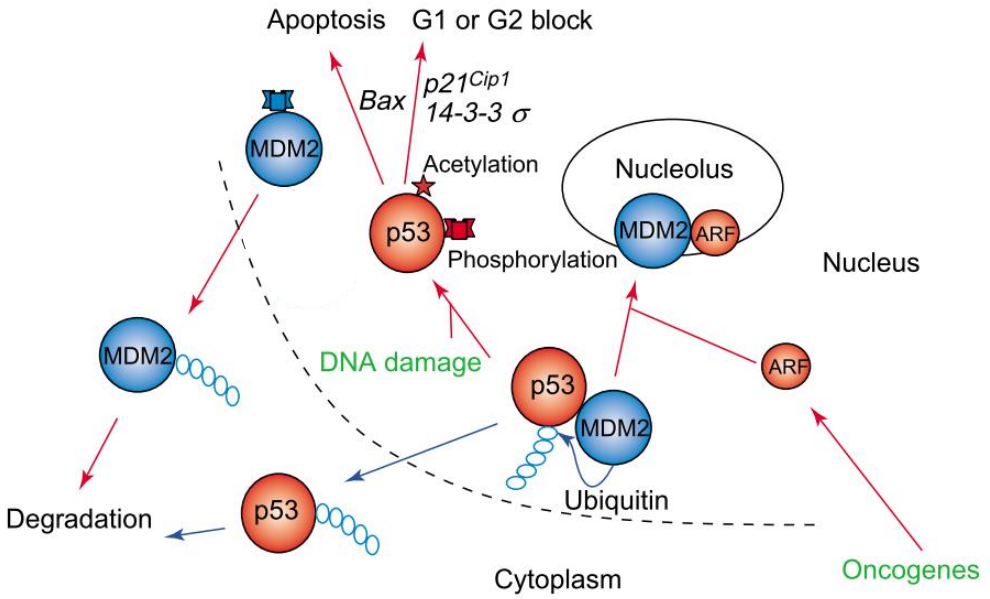

Figure 1.1-7. MDM2 and p53 transport within the cell. Flag: phosphorylation; star: acetylation; Triangle-headed arrows represent an activation while T-shaped arrows mean an inhibition of the subsequent protein. Modified with permission.[56]

While mutant p53 lacking an NES failed to be exported by MDM2, the NES of MDM2 was not required for p53 export. Although it was initially believed that MDM2 transports p53 to the cytoplasm for degradation directly, a later study revealed that wild-type MDM2 promotes cytoplasmic translocation upon ubiquitination of p53 either by activation of the NES of p53, or by enhancing accessibility to, or association with, nuclear export factors.[57] Subsequent studies have demonstrated that even when p53/NES$^-$ and MDM2/NES$^-$, both of which are strictly nuclear, were expressed, p53 could be degraded by nuclear proteasomes.[58]

p53 degradation can also occur in an MDM2-independent manner. Indeed, other E3 ligases such as Pirh2, COP-1, ARF-BP1 and CHIP are able to drive p53 proteasomal degradation[49,59] and therefore broaden the spectrum of regulation of the p53 response.

1.1.4 MDM2

Isolated for the first time in 1987 as an amplified gene from a transformed mouse 3T3 cell line and sequenced in 1991,[60] the *mdm2* gene has been associated with the abnormal presence of paired acentric chromatin bodies (or double minutes[61]). The *mdm2* gene consists of 12 exons. There are two promoters, P1 and P2, which generate at least two proteins, the full length of about 90 kDa and a shorter one of about 76 kDa synthesised through an internal initiation at an AUG located in exon 4.[62] p90 is the negative regulator of p53 while p76, lacking the N-terminus of the full-length MDM2,[63] seems to be an activator of p53.[64] P1 directs the synthesis of RNA transcripts beginning at exon 1 of *mdm2* and P2 directs the synthesis of RNAs from exon 2 of *mdm2*. The consequences of having two promoters are not clear since the first initiation codon is located in exon 3. The analysis of the expression of the *MDM2* gene in human tumours revealed the existence of other MDM2 protein isoforms and alternative or aberrantly spliced *MDM2* mRNA (reviewed in ref. [65]).

As mentioned previously, the *MDM2* gene has been strongly associated with tumour formation. In the study by Momand *et al,*[34] 3889 samples from 28 different tumour types were examined for *MDM2* amplification. 7% of all human tumours screened had *MDM2* amplification, observed in 19 different tumour types. The highest frequency was observed in soft tissue tumours with 20%, osteosarcomas with 16% and oesophageal carcinomas with 13%. When considering only the tumour types carrying *p53* mutations or *MDM2* amplification, only four tumours had both *p53* and *MDM2* alterations out of a total of 93 tumours.

The human MDM2 protein (HDM2) is composed of 491 amino acids and contains several domains that are conserved between species[66,67] (Figure 1.1-8). The p53 binding domain of MDM2 is located at its N-terminus (res. 29-128) which binds to and inhibits the N-terminal transactivation domain of p53.[68] The nuclear localization sequence (NLS) (res.181-185) and the nuclear export sequence (NES) (res.191-199) mediate the ability of MDM2 to reversibly shuttle between the nucleus and the cytoplasm.[69] The central region of the MDM2 protein contains an acidic domain which: (a) mediates the interaction between the ribosomal protein L5 and its associated 5S ribosomal RNA (rRNA);[70] (b) has been shown to bind the BOX-V of p53;[71-73] and

(c) has also been shown contribute to the ubiquitination of p53.[74] This acidic domain is followed by a zinc finger domain (res. 300-332) whose functional role is still unclear. Finally, the RING domain (res. 429-491) of MDM2 contains two extra zinc fingers which are necessary for the structural conformation of the RING domain and also for its function in ubiquitinating p53 and itself (discussed in Section 1.1.6). [75]

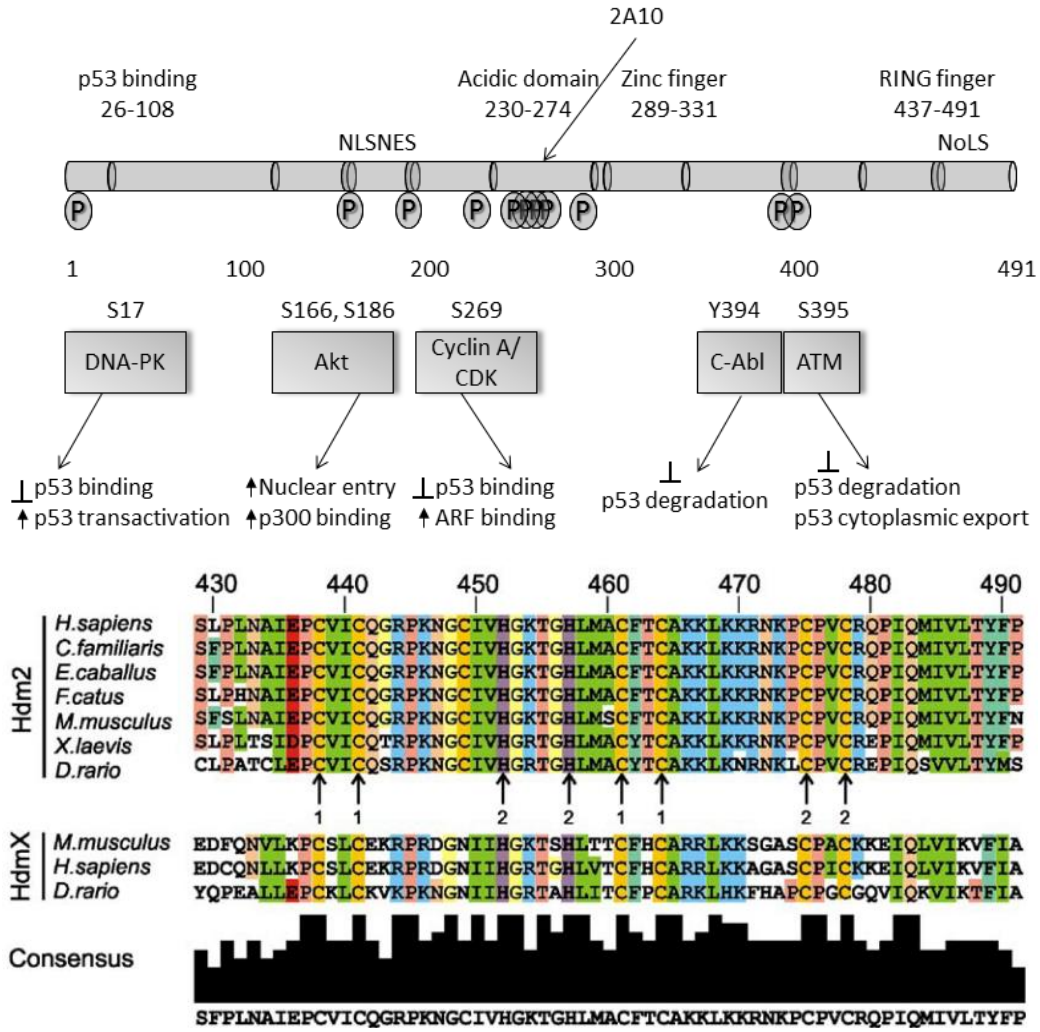

Figure 1.1-8. (top) Domain organisation of HDM2. res.181-185: NLS; res. 191-199: NES. MDM2 phosphorylation sites and corresponding partners and events. Phosphorylation sites are indicated with the letter P in an ellipse, a vertical arrow indicates stimulation while an inverted "T" indicates an inhibition. (bottom) Sequence alignment of the RING domains of HDM2 and HDM4 (HDMX) between species; conserved amino acids are coloured based on their properties or role in the RING: ligand cysteines (gold), ligand histidine (purple), aliphatic (green), basic (blue), red (acidic), aromatic residues (turquoise), serine, proline and threonine (pink), glycine (yellow), asparginine and glutamine (beige). Arrows with numbers 1 or 2 show the residues interacting with zinc sites 1 or 2 in the RING domain. reproduced with permission (bottom panel).[76,77]

Of the different domains, the N-terminal domain, the acidic domain and the RING domain are of particular interest as they can be specifically targeted to inhibit the p53-MDM2 interaction and therefore enhance the activity of wild-type p53. Indeed, the N-terminus of p53 has been extensively studied. It is now well known that the N-terminus of p53, containing the transactivation domain, is able to bind to the N-terminus of MDM2 leading to the inhibition of p53 transcriptional activity.[68,78] In addition, p53 is able to induce the expression of MDM2, through the p53 DNA binding site of the *mdm2* gene, which creates an auto-regulatory feedback loop between MDM2 and p53.[79] The acidic domain of MDM2 has been shown to be essential for the negative regulation of p53 acetylation via the inhibition of the acetyltransferases p300/CBP and the association of MDM2 with histone deacetylase 1 deacetylase (HDAC1).[80]

MDM2 can be regulated at the post-translational level by different modifications. For example, MDM2 can be modified by multi-site phosphorylations (reviewed in ref [76]). Indeed, several kinases such as ATM,[81] DNA-PK,[82] MK2[83], cyclinA-CDK1/2,[84] c-Abl[85] and others are able to phosphorylate MDM2 to decrease its interaction with p53 (Figure 1.1-8).

Other studies have shown that kinases such as Akt can phosphorylate and activate MDM2 by blocking the interaction with its negative regulator ARF.[86,87] MDM2 is also able to bring about self-ubiquitination (discussed in Section 1.1.6) leading to its own degradation. This raises the question of how the balance between MDM2 auto- and substrate-induced-ubiquitination is regulated. To this effect, it has been shown that MDM2 can be sumoylated by the SUMO E3 ligases Ubc9, PIAS1 and PIASxβ *in vivo* and it has been suggested that sumoylation can differentially modulate the MDM2 E3 ligase activity by preventing MDM2 auto-ubiquitination.[88,89]

Other proteins have been identified that interact with MDM2.[90,91] These either function upstream to modify MDM2 or are downstream proteins regulated by MDM2. The protein ARF ($p14^{ARF}$ in humans and $p19^{ARF}$ in mouse) binds to MDM2 and sequesters it into the nucleolus[92] which results in the activation of p53. It has also been observed that ARF is able to block self-degradation of MDM2 (Figure 1.1-9).[93] The ribosomal protein L11 can also sequester MDM2 into the nucleolus, resulting in the stabilisation

of p53.[94] Hypoxia-inducible factor 1α (HIF-1α) directly binds MDM2 thereby preventing the nuclear export of p53 and protecting p53 from degradation by MDM2.[95] Further, MDM2 associates with the transcriptional activator Sp1 and prevents its interaction with its related DNA, thus blocking Sp1-dependent gene transcription.[96]

Major proteins interacting with MDM2 are summarised in Figure 1.1-9.

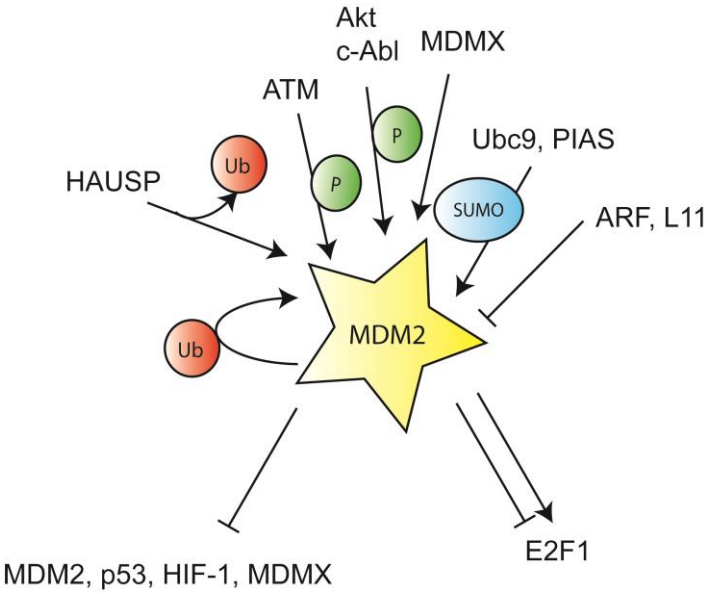

Figure 1.1-9. Major proteins interacting with MDM2. Straight Triangle-headed arrows represent an activation while T-shaped arrows mean an inhibition of the subsequent proteins. Ub (red) stands here for ubiquitination, P (green) for phosphorylation, SUMO (blue) for sumoylation.

In some cases, MDM2 can have a dual role as an activator or inhibitor of the same protein. For example, MDM2 can interact with the E2F1/DP1 complex and stimulate the growth promoting activity of E2F1 but also block its apoptotic activity.[97]

As mentioned earlier, the human *MDM2* gene has been found to be overexpressed in 7% of all screened tumours. In those *MDM2* amplification-positive tumours, *p53* was mostly wild-type. It is therefore essential to find compounds able to disrupt the MDM2-p53 protein complex as this will relieve negative regulation of p53 by MDM2, thus allowing p53 to function as a tumour suppressor. Phe^{19}, Trp^{23}, Leu^{26} residues on p53 have been shown to be crucial for the stability of the MDM2-p53 complex.[98]

Based on this discovery, many inhibitors have been identified (discussed in Chapter 1.1.7), of which one of the most widely used and active molecules is Nutlin 3a.[99]

1.1.5 The ubiquitination pathway

Cell cycle progression is tightly regulated by the synthesis and degradation of regulatory proteins. The degradation of these proteins is mainly driven by the ubiquitin-proteasome pathway in an ATP-dependant manner.[100] Ubiquitin is a 76 amino acid protein and is highly conserved between species.[101] Ubiquitination of a protein involves a multi-step enzymatic reaction. First, ubiquitin is attached to an enzyme E1 (Ubiquitin-activating enzyme) via a thioester bond between the active-site cysteine of the E1 and the C-terminal glycine (Gly^{76}) of ubiquitin. The ubiquitin in the E1-ubiquitin complex is then transferred to an enzyme E2 (Ubiquitin-conjugating enzyme) by trans-thioesterification. Finally, the ubiquitin is covalently bound to the target protein through amide formation between Gly^{76} of ubiquitin and the ε amino group of an internal lysine of the target protein. This last attachment is dependent on an E3 Ubiquitin-ligase enzyme (see below). A polyubiquitin chain can be formed by linking each ubiquitin to a specific lysine residue on the previously attached ubiquitin. This polyubiquinated protein is finally recognised and degraded by the 26S proteasome (Figure 1.1-10) and the ubiquitin recycled. This process involves de-ubiquitinating enzymes (DUBs). While the E1 enzyme is the product of a single gene with two isoforms,[102] the E2 family is more diverse. The crystal structures of several E2s have been solved and have provided some hints on how E2s bind E3s.[103,104]

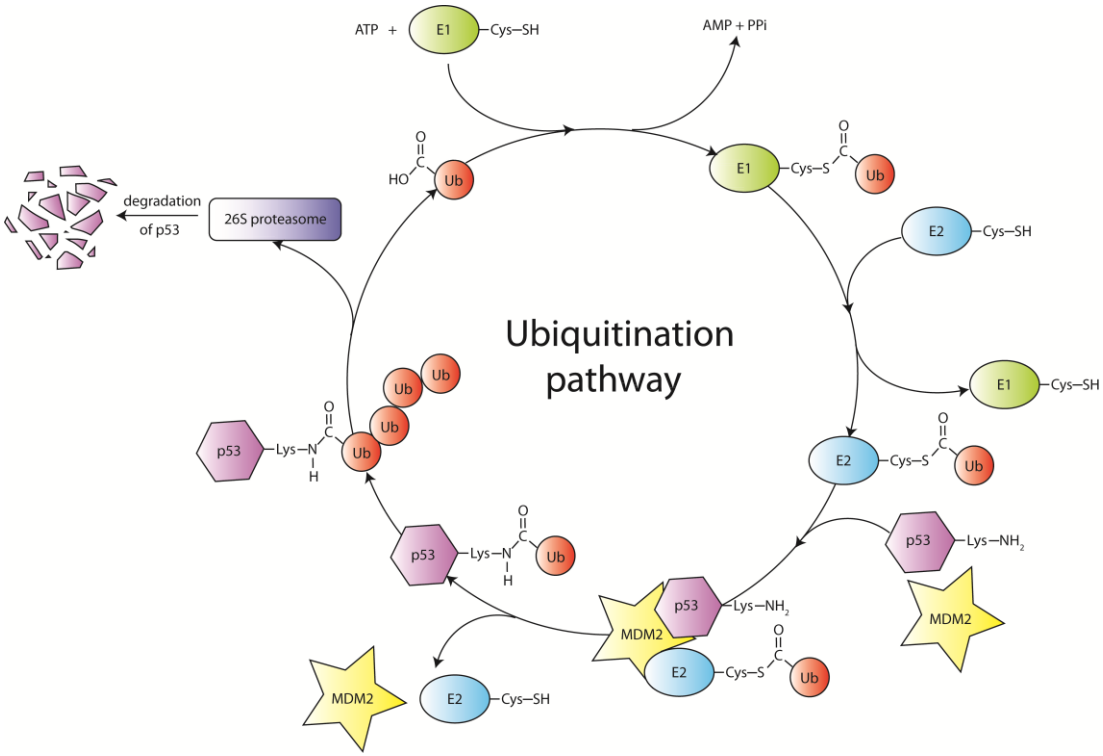

Figure 1.1-10. Overview of the ubiquitination pathway showing MDM2-mediated degradation of p53.

There are two major classes of E3s: HECT (Homologous to E6-AP Carboxyl Terminus) domain E3s and RING (Really Interesting New Gene) domain E3s. HECT domain E3s bind ubiquitinated E2 (E2~Ub); the ubiquitin is then transferred to the active site cysteine on the HECT domain before being attached to a lysine of the target protein also bound to the HECT E3. In the case of RING domain E3s, the ubiquitin is transferred directly from the E2~Ub thioester to the target protein, the E3 acting as a scaffold to bring the activated E2~Ub and the target protein in close proximity (Figure 1.1-11).

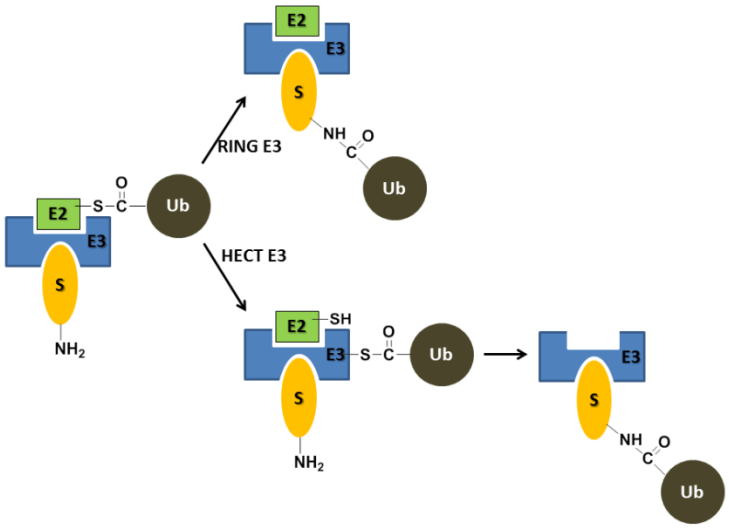

Figure 1.1-11. Transfer of ubiquitin from E2 to the target, via HECT E3 or RING E3.[105]

RING domains usually range in length from 40 to 100 amino acids. They are characterised by eight cysteines and histidines coordinating two zinc ions and arranged in a cross-braced structure [$CX_2CX_{(9-39)}CX_{(1-3)}HX_{(2-3)}C/HX_2CX_{(4-48)}CX_2C$].[106] The mechanism of ubiquitin chain elongation by RING E3's is still unclear. However, it has been noted that homo or heterodimerisation of RING E3 ligases is quite common and that this dimerisation process tends to enhance ubiquitination activity relative to the monomeric species. Indeed, BRCA1 (BReast Cancer 1) displays a much greater ubiquitination activity when associated as a heterodimer with BARD1.[107] The MDM2/MDM4 heterodimer is another such example and will be discussed in detail in Section 1.1.6. Manfred Koegl and co-workers have suggested the existence of a fourth ubiquitination factor, named E4. In yeast, the E3 UFD4, involved in ubiquitin chain polymerization, is unable to initiate polyubiquitination in the presence of the E2 UBC4 alone but requires an addition factor, UFD2 (ubiquitin fusion degradation protein 2) which has been termed E4.[108]

Ubiquitination can lead to different outcomes (Figure 1.1-13), depending on the number of ubiquitins attached, where the ubiquitins are attached on the target protein and how the ubiquitin chain is linked together (for monoubiquitination, see review[109]). Ubiquitin has seven conserved lysines (Lys^6, Lys^{11}, Lys^{27}, Lys^{29}, Lys^{33}, Lys^{48} and Lys^{63}) where polyubiquitin chains can occur. Despite the tremendous potential statistical complexity, the polyubiquitin chain formation generally occurs through

Lys[48], Lys[63] and Lys[29].[105] The main proteasomal degradation signal seems to operate via polyubiquitin chains linked through a Lys[48]-Gly[76] isopeptide bond[110] (Figure 1.1-11, Figure 1.1-12 and Figure 1.1-13) where a minimum chain of four ubiquitins is needed. It has also been found that Lys[63]-Gly[76] polyubiquitin chains are involved in kinase activation[111] and DNA repair.[112]

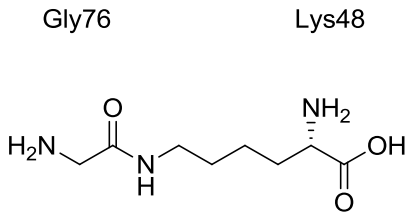

Figure 1.1-12. Lys[48]-Gly[76] isopeptide bond involved polyubiquitin chains for degradation signal.

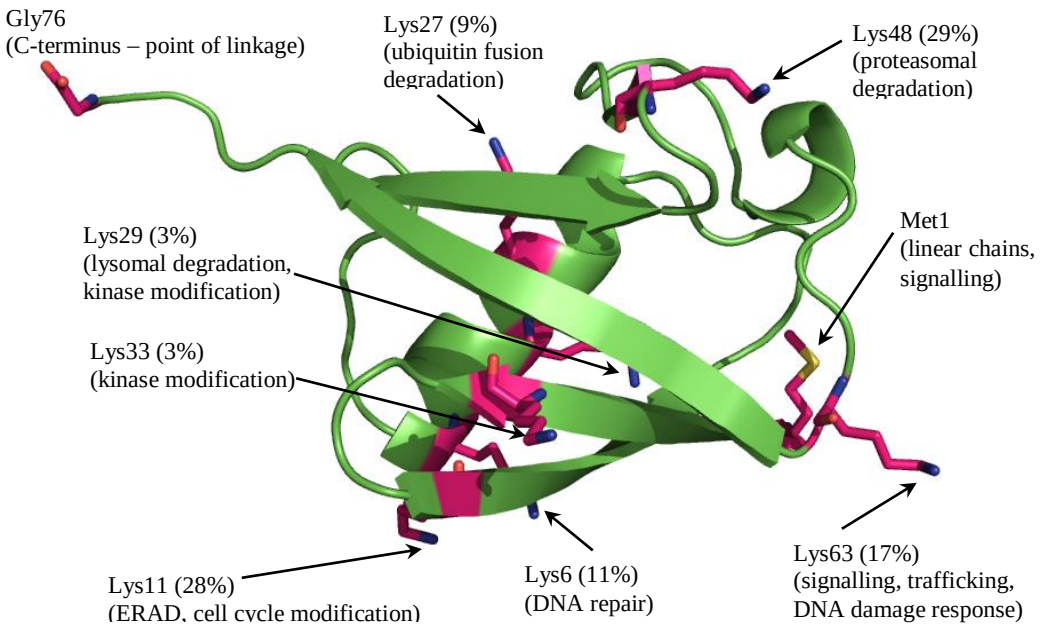

Figure 1.1-13. Ubiquitin and its lysine residues. Side-chains of lysines and N-terminal methionine are shown (carbons in red, amine in blue and sulfur in green). Percentages represent the relative occurrence of side-chain linkage.[113]

Under stress, p53 may be de-ubiquitinated. This role is fulfilled by Herpes Associated Ubiquitin-Specific Protease (HAUSP; also known as USP7), first identified as a p53 interacting protein stabilising p53 by ubiquitin removal.[114] In 2004, extra complexity was revealed as MDM2 is also a substrate for HAUSP.[115]

Some small proteins display a high degree of homology with ubiquitin. These ubiquitin-like proteins can be involved in post-translational, single or multiple modification of substrate proteins and their mechanisms of action are very similar to the ubiquitination pathway. Small ubiquitin-related modifier-1 (SUMO-1) is a 101 amino acid protein which shares 48% homology with human ubiquitin and is conserved between species.[116] Many proteins have been shown to be modified by conjugation with SUMO-1. In particular, following UV exposure, p53 has been shown to be sumoylated on Lys^{386}, which leads to the activation of a transcriptional response by p53.[117] As mentioned earlier, MDM2 can be sumoylated. This process is believed to compete with the ubiquitination of MDM2 (either by itself, or by other E3-ligase enzymes), which adds another dimension to the regulation of p53 protein levels by MDM2. NEDD8 (neural precursor cell-expressed developmentally downregulated) is another ubiquitin-like protein. p53 can be neddylated in an MDM2-dependant manner, which results in the attenuation of the transactivation function of p53.[118] MDM2 itself can also be neddylated, which results in an increase in its half-life.[119]

1.1.6 MDM2/MDM4 and their RING domains

The MDM2 RING domain is essential for its E3 ubiquitin ligase activity and also for RNA binding activity; however, the mechanism for the latter is still unclear.[120] Using UbcH5b/c as an ubiquitinated E2,[121] MDM2 functions as an E3-ubiquitin ligase responsible for the ubiquitination and proteasomal degradation of p53. In particular, its RING domain is necessary for this function. The overall structure of the MDM2 RING domain is similar to that of the other RING domains reported so far with a compact ββαβ motif,[77] a small hydrophobic core and two zinc ions which play a critical role in maintaining the structure. Unlike the common C3HC4 zinc coordination pattern displayed in most RING domains, the MDM2 RING domain has a C4H2C2 zinc coordination pattern that binds to two zinc atoms per molecule in a cross-braced system (Figure 1.1-14). If the RING structure is disrupted by mutating any of the eight residues which coordinate to the zinc atoms, MDM2 is unable to promote the degradation of p53.[75,122] Further, the RING domain of MDM2 has been shown to be required for MDM2 to bring about p53 nuclear exclusion.[57] It has been found that

deletion of the last twelve amino acid residues from the C-terminus of MDM2 conserves the RING structure but abrogates its E3 ligase activity.[123] More recently, it has been suggested that mutation of key residues in the RING domain of MDM2 induces a conformational change in the protein, thereby affecting MDM2-mediated transrepression of p53.[74]

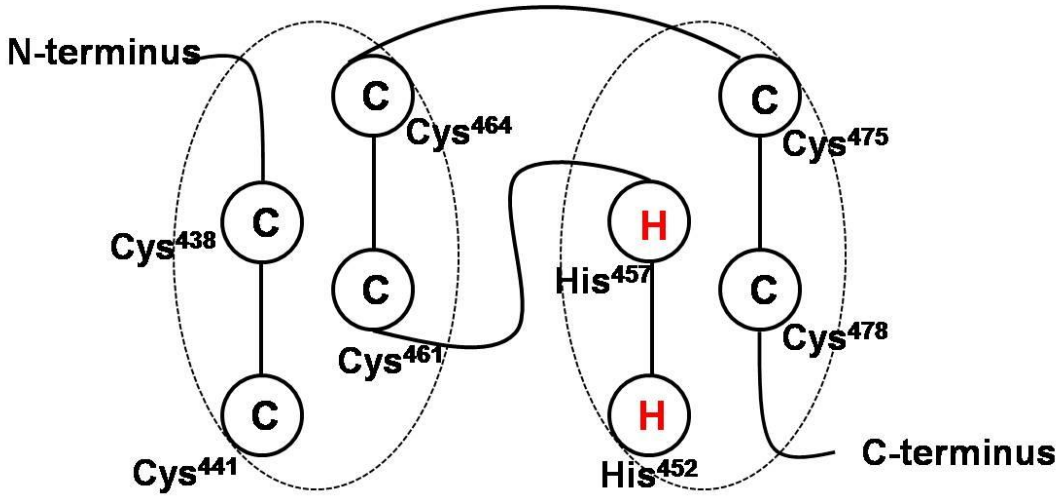

Figure 1.1-14. Schematic structure of the RING domain of MDM2. MDM2 has a unique pattern, C4H2C2, unlike the other RING domains, displaying a C4HC3 pattern.

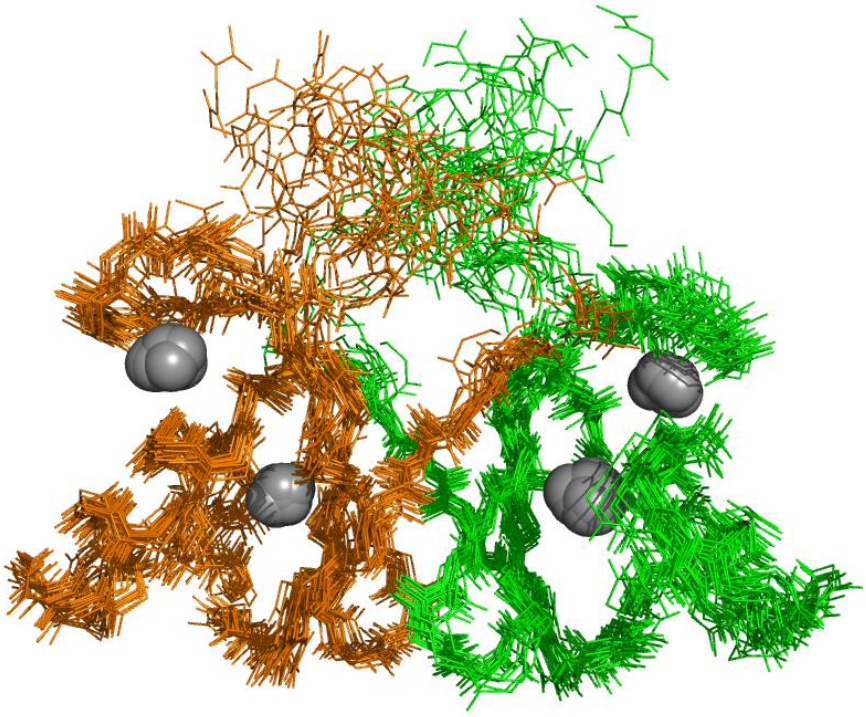

Figure 1.1-15. Solution structure of the HDM2 RING domain. Superposition of the 20 lowest energy structures of HDM2 RING domain homodimer (subunits orange and green). Zinc sites are in grey (PDB : 2HDP).[77]

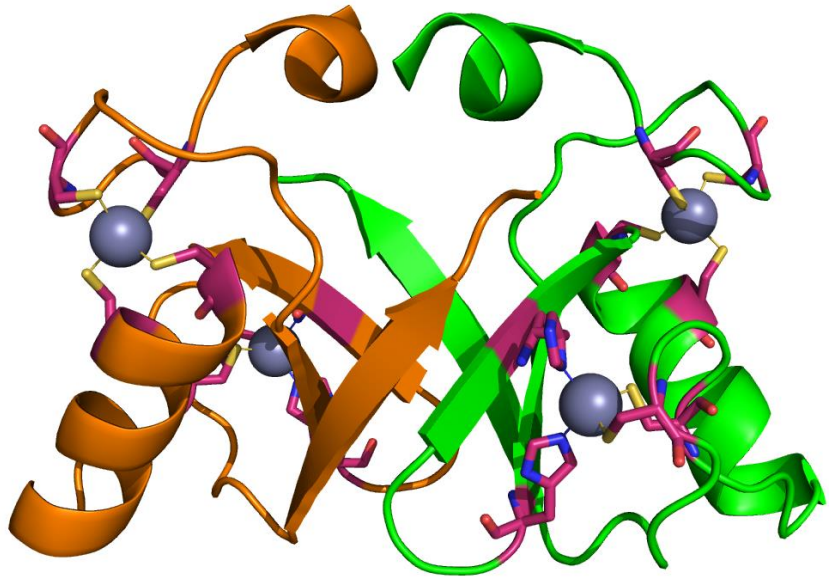

Figure 1.1-16. Structure of the MDM2/MDMX RING domain heterodimer. Ribbon structure of the MDM2/MDMX RING domain heterodimer. MDM2 RING domain is represented in orange, MDMX RING domain in green; zinc ions as grey spheres; residues coordinating are shown as sticks, the carbons of which are magenta, the nitrogens blue, sulfurs in yellow (PDB : 2VJE).[124]

NMR structures have confirmed that the MDM2 RING domain homodimerises (Figure 1.1-15)[77] and a crystal structure revealed the existence of a heterodimer with MDMX,[125] also called MDM4, an MDM2-related protein. This heterodimer formed

between their respective RING domains has been confirmed by NMR structures[124] (Figure 1.1-16). The interaction of MDMX with p53 and MDM2 has brought a greater complexity to the system. MDMX also contains a RING domain and has many similarities with MDM2. MDM2 and MDMX RING domains are the only known RING domains to contain an ATP binding site. Despite its lack of E3-ubiquitin ligase activity, MDMX has been shown to enhance MDM2's substrate ubiquitination function by reducing its autoubiquitination.[126,127] Acting as a negative regulator, MDMX has also been shown to interact with the N-terminus of p53.[128,129] As it binds to the same site on p53 as MDM2, MDMX therefore controls MDM2-mediated regulation of p53.[130] MDMX can be ubiquitinated and degraded by MDM2.[131]

1.1.7 Strategies for reactivating the p53 pathway and examples of known inhibitors of the p53-MDM2 interaction

With the knowledge acquired about the p53 pathway over the past thirty years, different strategies to activate the pathway have been investigated. These strategies depend on the characteristics of p53 and MDM2 (mutants, wild-type or overexpressed). One could restore p53 function on a mutant p53 by inducing a wt-p53 native conformation.[132] Finding a molecule able to disrupt the p53-MDM2 interaction could also reactivate p53 function. This could be achieved by identifying molecules that bind directly to MDM2, p53 and family members or indirectly by binding to others partners of these two proteins. These inhibitors could have different effects; for example disruption of p53's transactivation function or prevention of its degradation, ultimately leading to cell cycle arrest or apoptosis.

Several reviews have reported numerous molecules targeting p53 as anticancer therapy (for details, reviews[133-135]). A non-exhaustive list of non-peptidic inhibitors of the p53-MDM2 is provided in Figure 1.1-17 and p53-MDM2-related peptidomimetic inhibitors will be discussed in the chemistry introduction, Section 2.3.1.4.

The N-terminal region of MDM2 that binds to p53 has been mapped onto res. 19-102 and the transactivation domain of p53 that binds MDM2 onto res. 15-29.[98] X-ray

structures of N-terminal MDM2 revealed a deep hydrophobic structure pocket where residues Phe[19], Trp[23] and Leu[26] of α-helical p53 peptide (from wild-type p53) are the points of contact[98] (PDB entry: 1YCR). Over the past decade, the number of identified inhibitors of this interaction has increased exponentially. The p53-MDM2 interaction has also been studied by NMR.[136,137] The NMR structure of uncomplexed MDM2 has been resolved, revealing interesting conformational changes upon p53 binding.[138] Two peptides, PMI (TS**F**AEY**W**NL**L**SP) and pDI (LT**F**EHY**W**AQ**L**TS), both found by phage display in independent studies have been identified as efficient inhibitors of the p53-MDM2 interaction. Interestingly, these peptides, displaying the same three key residues Phe[19], Trp[23] and Leu[26] as in wild-type p53, were more active than the native p53 peptide (QET**F**SDL**W**K**L**LP).[19,31]

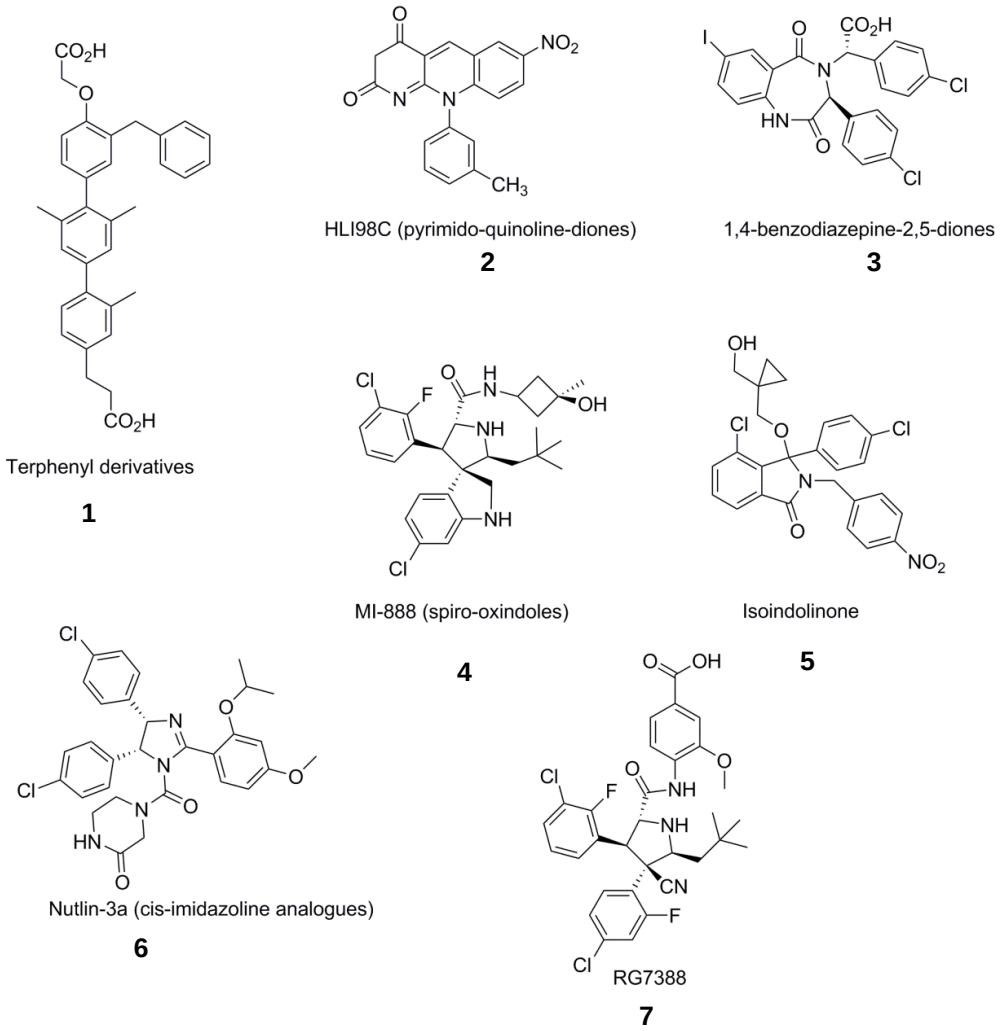

Figure 1.1-17. Examples of non-peptidic small molecule inhibitors of the N-terminal p53-MDM2 interaction found in literature.[139-144]

Some non-peptide small molecule inhibitors of the N-terminal p53-MDM2 interaction have also been developed (Figure 1.1-17). These include terphenyls **1**,[143] chalcones,[145] benzodiazepinediones **3**,[142] isoindolinones **5**,[141,144] spiro-oxindoles **4** [140,146,147] and Nutlins **6**.[99] Among these classes, the *cis*-imidazoline Nutlins [Nutley (New Jersey) inhibitors] seem to be one of the most promising classes. With an IC_{50} of approximately 90 nM and 150 times more potent than its enantiomer, Nutlin-3a **6** was the most potent inhibitor of its class until recently.[139] Indeed, optimisation of Nutlin-3a by Hoffmann-Laroche has given RG7112 with a 4-fold greater potency than Nutlin-3a; RG7388 **7**, the second generation clinical inhibitor is fifteen times more selective and potent than its predecessor.[148] The binding interactions of Nutlin-3a with MDM2 have been determined by NMR[137] and match those of MDM2 binding to Nutlin-2 as determined by X-ray crystallography[99] (Figure 1.1-18; PDB entry: 1RV1).

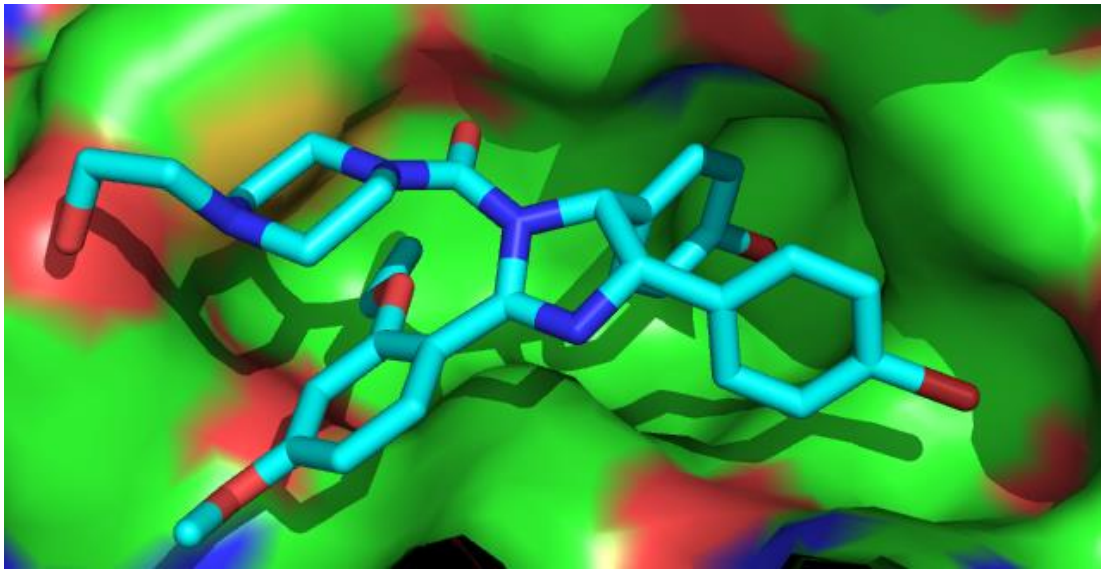

Figure 1.1-18. Crystal structure of MDM2 bound to nutlin-2. Carbon atoms are drawn in white, oxygen in red and nitrogen in blue.[99]

Nutlin-3a occupies the hydrophobic pocket of MDM2 where residues Phe^{19}, Trp^{23} and Leu^{26} of p53 bind. The effects of Nutlin appear to be cell-line dependent. Interestingly, when exposed to Nutlin-3a, the viability of normal human skin and mouse embryo fibroblasts was much higher than in wild-type p53 cancer cell lines. Since 2005, Nutlin-3a has been studied in many different tumours and has been shown to act synergistically with some other inhibitors thus overcoming drug resistance.[149-151]

Notably, Nutlin-3a is unable to prevent MDM2-mediated ubiquitination of p53 and the RING domain of MDM2 is required for full efficiency of Nutlin-3a.[74] Due to the similarities between MDM2 and MDMX, inhibitors of the p53-MDM2 complex have also been shown to inhibit the p53-MDMX interaction, but to a lesser degree.[152] X-ray crystal structures of a p53 peptide bound to MDMX revealed that the binding sub-pocket where Leu^{26} fits is smaller (PDB entry: 3DAB) in MDMX than in MDM2.[153,154] The task of finding inhibitors specifically designed for MDMX has now been undertaken.[155]

Specific inhibitors of the E3 ligase activity of MDM2 have also been developed, but show relatively low efficiency.[156-159] Interestingly, some of these have been shown to selectively inhibit *in vitro* MDM2-mediated p53 ubiquitination but not MDM2 auto-ubiquitination. In summary, although many inhibitors of MDM2-p53 have been identified, each of these has clear limitations, such as their limited cell permeability, proteolytic degradation, poor solubility; they would have to be administered intravenously. Thus, it would be beneficial to develop a highly efficient, modified and specific inhibitor of the MDM2-mediated degradation of p53.

As seen through this section, the discovery of inhibitors such Nutlin-3a has driven the research in the p53-MDM2 field. Most of these inhibitors bind to the N-terminus of MDM2. However, few inhibitors targeting the RING domain of MDM2 have been found.[156-159] Instead of focusing the effort on the N-terminal MDM2-p53 interaction, the approach will consist in the development of novel inhibitors targeting the MDM2 RING domain. These inhibitors may either disrupt the MDM2 homodimer, the MDM2/MDM4 heterodimer or the E2-MDM2-p53 complex and should prevent p53 degradation and enhance p53 activity.

1.2 Development of a peptide lead against the ubiquitination of p53.

1.2.1 Cloning, expression and purification of MDM2, MDM4 and BRCA1 fragments

In order to perform peptide-phage display, MDM2 RING domains fragments were expressed. Due to the sequence similarity of MDM4 with MDM2, the equivalent fragments were also expressed in order to observe whether any selectivity was observed. pTrcHis B was chosen as a vector in order to express a His-tagged protein as close as the original protein of study. Indeed the restriction enzyme sites are closer to the EK cleavage site than other vectors. Double digested pTrcHis B (Section 4.4.5, Figure 4.4-1) and amplified MDM4 fragments (supplied by Suzanne Petterrson) were loaded on agarose gels (Figure 1.2-1) and single bands corresponding to double digested plasmid and double digested insert were excised (under UV) and purified using the QIAquick gel extraction kit protocol (Qiagen).

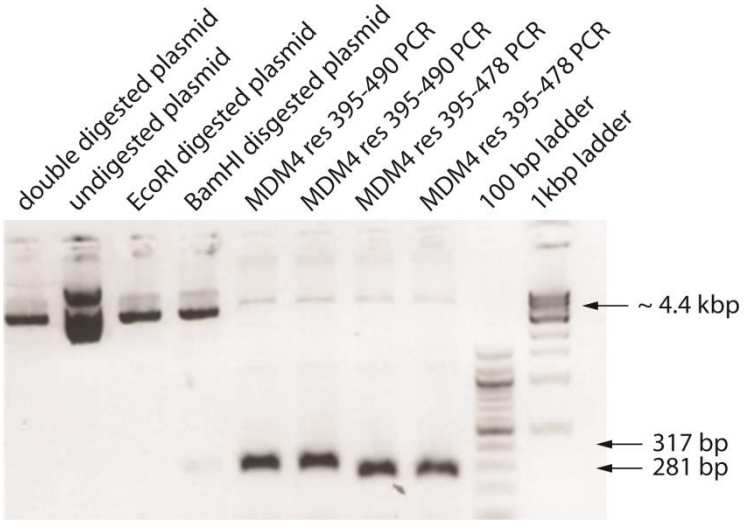

Figure 1.2-1. Digested plasmid DNA and MDM4 fragment DNAs. Samples were loaded onto a 1% agarose gel (w/v) containing 0.5 µg/mL ethidium bromide. Gel visualised under UV light.

Excised bands of desired DNA were purified following the QIAquick gel extraction kit protocol (Qiagen). DNA concentrations were measured with a NanoDrop® spectrometer at 260 nm (Labtech) and were found to be:

$[\text{pTrcHis B}]_{\text{digested}} \sim 4$ ng/µL

[MDM4 res.396-491] ~ 4 ng/µL

[MDM4 res.396-479] ~ 8 ng/µL

DH5α cells were transformed at both 1:1 and 3:1 insert to vector ratios. At the 3:1 ratio, colonies of transfected cells were observed on ampicillin-resistant LB agar plates for both MDM4 res. 395-490 and MDM4 res. 395-478. However at the 1:1 ratio only MDM4 395-478 ligated product gave rise to colonies of transformed DH5α cells **(**Figure 1.2-2**).**

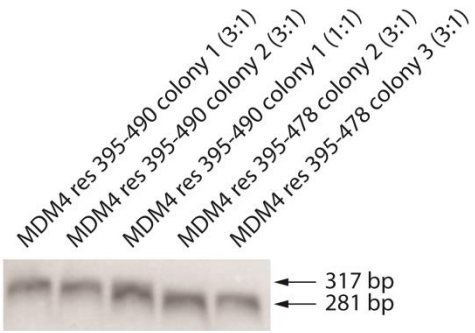

Figure 1.2-2. PCR products of colonies resulting from ligation between MDM4 inserts and double digested pTrcHis B plasmid. Samples were loaded onto a 1% agarose gel (w/v) containing 0.5µg/mL ethidium bromide. Gel visualised under UV light.

BL21(DE3) expression competent cells used for the expression of non-toxic proteins were used. Once the culture has grown to OD_{600} ~ 0.5, transformation of BL21(DE3) cells with plasmid DNA followed by induction with 1 mM IPTG, lysis and sonication of centrifuged cells provided the unpurified lysates containing the proteins His-tagged MDM4 res. 395-490, or res. 395-478. Purification of His-tagged MDM4 fragments (as well as any other His-tagged proteins made in this project) was carried out using Ni-NTA beads to capture the His-tagged proteins. After the washing steps, proteins were eluted with an imidazole-based buffer and collected into fractions (Figure 1.2-3).

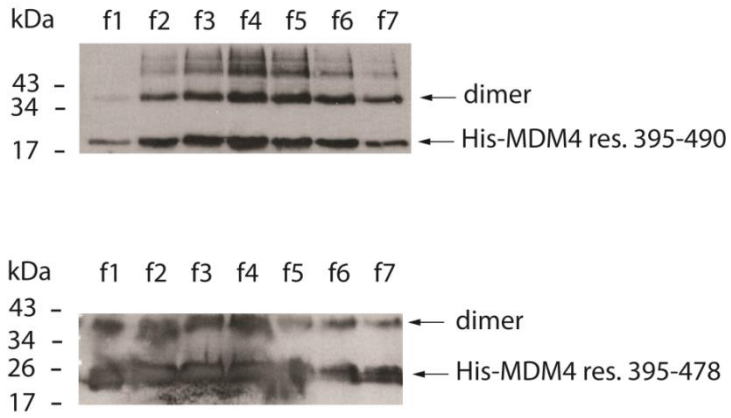

Figure 1.2-3 Collected fractions (f1-f7) of MDM4 res 395-490 (upper panel) and res. 395-478 (lower panel). 10 µL of samples in buffer were run on a 12% SDS-PAGE. MDM2 was detected with anti-His antibody.

Upper bands were observed on western blots. The first upper band mass is approximately twice the mass of His-tagged MDM4 fragments. The identity of these bands as the dimer and further oligomeric forms (observed with longer exposure times) was confirmed by DTT titration (Figure 1.2-4). However, the dimer band only decreased slightly in intensity, even at high concentrations of DTT, suggesting a strong homodimer interaction. Interestingly, it appears that the extra twelve amino acids enhance the dimer cohesion.

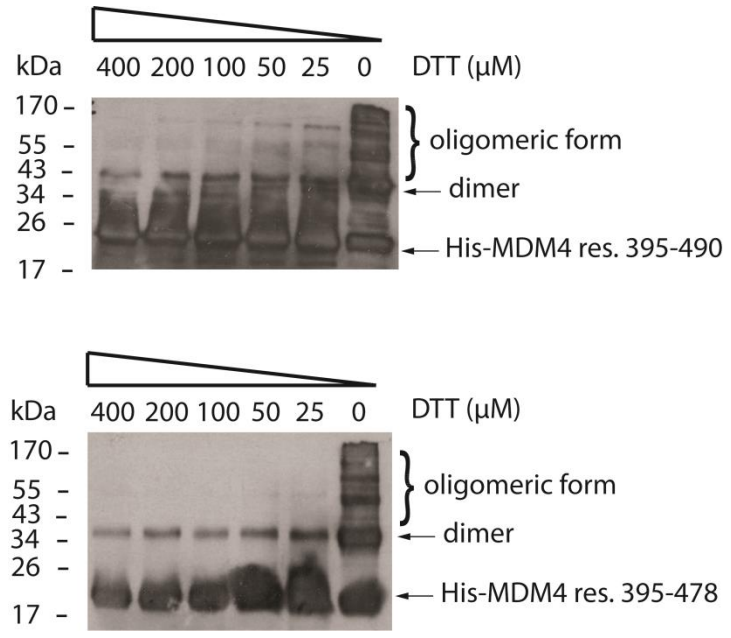

Figure 1.2-4 DTT titration of His-tagged MDM4 fragments (MDM4 res. 395-490 f1 and MDM4 res. 395-478 f2). 10 µL of samples in buffer were run on a 12% SDS-PAGE. MDM2 was detected with anti-His antibody.

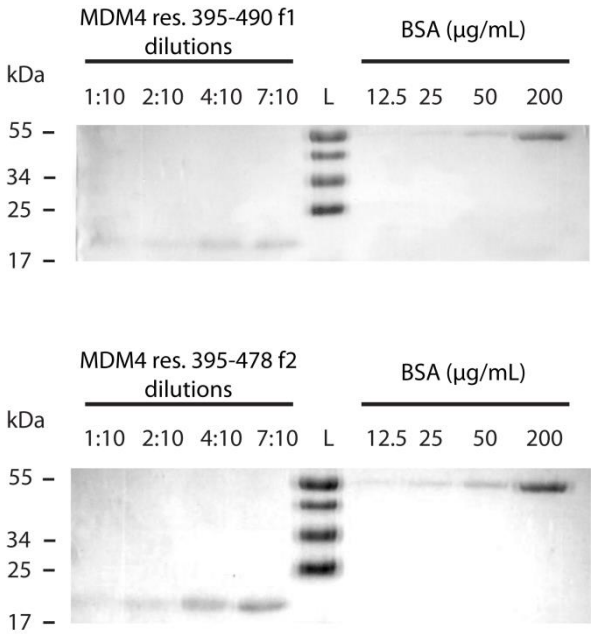

Figure 1.2-5. MDM4 concentration determination by BSA titration. 10µL of each sample in SDS buffer were loaded in wells and run by electrophoresis on 12% SDS-PAGE gels followed by Coomassie staining.

Protein fragment concentrations were calculated by BSA titration (Figure 1.2-5) and found to be of 7 µg/mL for MDM4 res. 395-490 f1 and MDM4 res. 395-478 f2.

Digested pTrcHis B plasmid with MDM2 fragments in DH5α (courtesy of Suzanne Petterrson) were used to transform BL21(AI) competent cells. Addition of 0.2% arabinose to the growth culture medium (OD_{600} ~ 0.5) of the plasmid in BL21(AI), followed by lysis and sonication of centrifuged cells provided unpurified lysates containing His-tagged MDM2 fragments res. 396-491 and res 396-479. Purification of the lysate was carried out with the same approach as for His-tagged MDM4 fragments (Figure 1.2-6) using Ni-NTA beads to capture his tagged proteins and imidazole-based elution buffer.

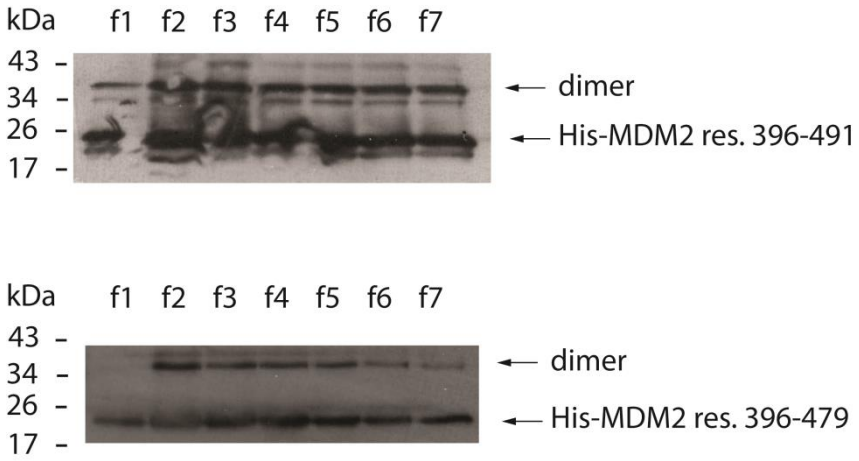

Figure 1.2-6 Collected fractions of MDM2 res 396-491 (upper panel) and res. 396-479 (lower panel). Samples were run on a 12% SDS-PAGE. MDM2 was detected with anti-His antibody.

Concentrations of MDM2 fragments were measured by BSA titration and were found to be 15 µg/mL for MDM2 res. 396-491 f2 and 7 µg/mL for MDM2 res. 396-479 f2. The BRCA1 RING domain res. 1-103 was chosen to check the specificity of the phage-display peptides raised against MDM2 and MDM4. The E3 ligase BRCA1 is an excellent control; it has a C4HC3 RING domain structure located at the N-terminus of the protein, whereas MDM2 bears a C4H2C2 RING structure. Using the extraction kit RNeasy from Qiagen, full mRNA was extracted from the HCT116 cell line. Using an optimised protocol from Kathryn Ball's laboratories, reverse transcription afforded the corresponding cDNA.[160] The BRCA1 insert needed for the subsequent ligation into the plasmid pTrcHis B vector (Invitrogen) was obtained by performing PCR on the cDNA with primers designed for BRCA1 (Section 4.4.5, Table 4.4-2).

Successful digestion of the BRCA1 insert and the pTrcHis B vector with the restriction enzymes EcoRI and BamHI was followed by electrophoresis of these inserts on a 1% agarose gel containing 0.5 µg/mL ethidium bromide. Purification of the desired DNA fragments was performed using the QIAquick gel extraction kit protocol (Qiagen). Ligation between the two purified DNA fragments was attempted at 1:1 and 3:1 molar ratios (vector : insert). However, transformation of the DH5α competent cells followed by incubation overnight at 4°C on ampicillin resistant plates showed no colonies, suggesting a failed ligation.

Thus, instead, the commercially available BRCA1 res. 1-304 (Addgene) was used, this is already ligated with the vector pET151D topo and is provided in DH5α cells. The corresponding protein was expressed in BL21(DE3) cells by induction with 0.4 mM IPTG as described in literature.[107] Induction conditions were optimised (1 h, 2 h or 4 h incubation time, at room temperature or 37°C) and from western blots (Figure 1.2-7) of collected fractions of BRCA1 res. 1-304 purification, a two-hour induction at 37°C was shown to give the best results. This result was confirmed by ELISA (Figure 1.2-8).

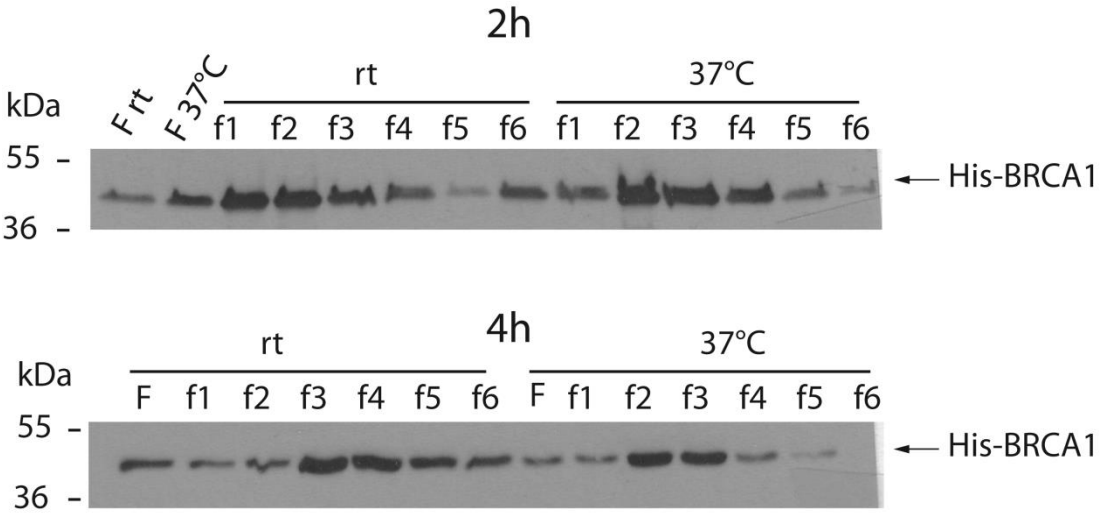

Figure 1.2-7. Optimisation of BRCA1 res. 1-304 induction conditions. Fractions collected after 2 h at room temperature or at 37°C (upper panel); 4 h at room temperature or 37°C (lower panel). 10 µL of each fraction in buffer were run on a 12% SDS-PAGE. BRCA1 was detected with anti-His antibody.

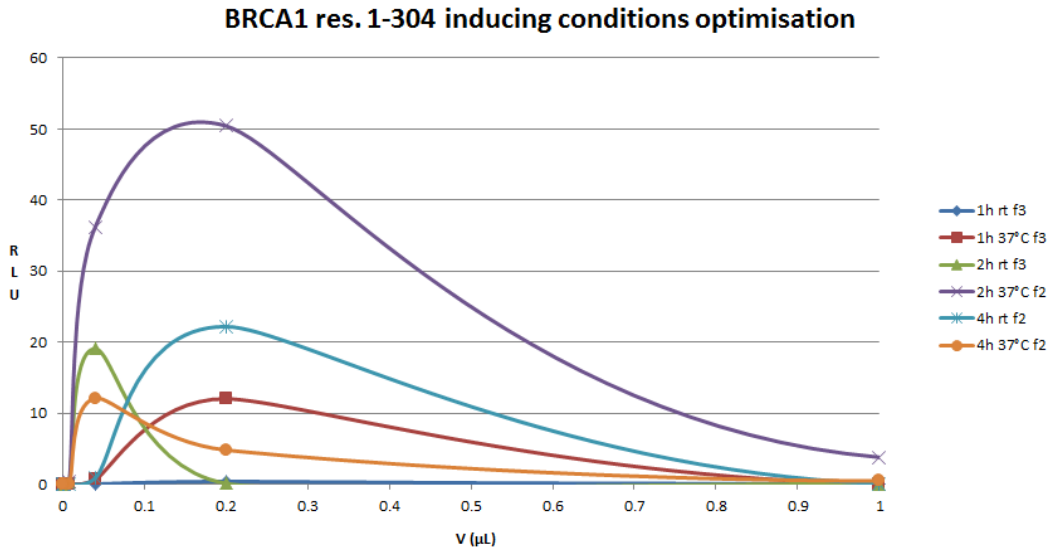

Figure 1.2-8. ELISA for the optimisation of BRCA1 res. 1-304 induction conditions.

The purified protein concentration was measured by BSA titration and was found to be 25 µg/mL (Figure 1.2-9).

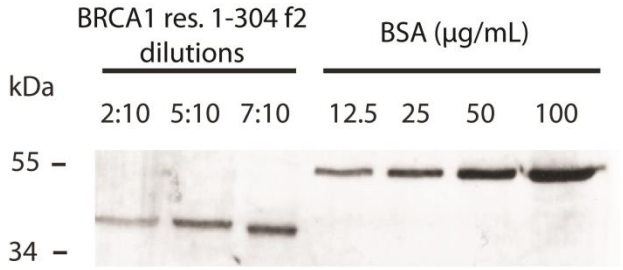

Figure 1.2-9. BRCA1 1-304 f2 concentration determination by BSA titration. 10µL of each sample in SDS buffer was loaded into wells and run by electrophoresis on 12% SDS-PAGE gels followed by Coomassie staining.

Successful expression and purification of fragments from MDM2, MDM4 and BRCA1 allowed phage display (Section 1.2.2) to be carried out as well as ELISA , *in vitro* affinity chromatography and *in vitro* ubiquitination experiments (Section 1.2.3).

1.2.2 Phage Display

1.2.2.1 Previous work

The MDM2 RING domain contains one ATP binding site (res. 448-455, 'GCIVHGKT') (Figure 1.4-1), which provides a basis for the rationale for looking for short peptide inhibitors of the ATP site in order to disrupt RING domain function. As the interface between a structured domain and a LIM is small, potential inhibitors should be able to compete for direct binding and to displace pre-bound complexes. Classical methods, such as high throughput screening to discover such inhibitors are usually expensive and time consuming. Therefore, new strategies to converge more quickly towards drug leads are needed. Target guided strategies offer a good alternative. Among them, phage peptide display[161] (reviewed in ref. [162]) is an *in vitro* technique used to identify interactions between a receptor and a library of phage-displayed peptides. This technique allows for rapid screening of several hundred million phage-displayed peptides.

Phages are viruses that can infect and replicate in bacterial cells such as the bacterium *Escherichia coli* (*E. coli*). In phage display, the bacteriophage (usually M13 phage) is engineered such that a specific peptide is expressed as a fusion with a coat protein by encoding with the circular single stranded phage. This results in the display of a peptide at the surface of the phage. Since DNA encoding the peptide is embedded within the phage, this allows the identification of the sequence of residues of the peptide displayed on the phage. Briefly, a library of phage-displayed peptides is incubated with a plate coated with the target, unbound phage is washed away and bound phage is eluted. The eluted phage is then amplified in *E. coli*, and used as a new input library. This process is repeated two to three times in order to obtain peptide-displaying phage that show high specificity towards the target (Figure 1.2-10). Finally, individual phage colonies are analysed by DNA sequencing.

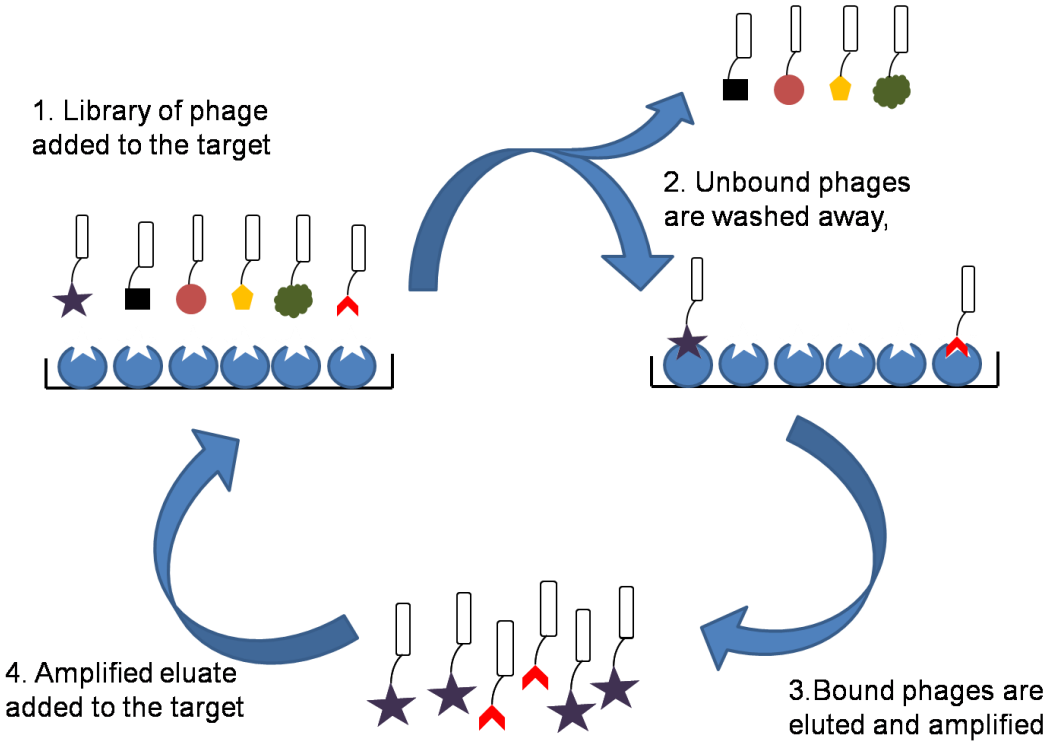

Figure 1.2-10. General phage display process. A well from a 96-well plate is coated with a protein. A library a compounds (more than 2 billion) is added to the well. After the third or fourth round, a consensus binding sequence (identified by sequencing the phage DNA) could be observed.

In this thesis, phage display was applied to the MDM2 RING domain. Potential ligands were isolated and identified and these ligands (peptides) were studied to evaluate their binding toward MDM2 and their ability to inhibit MDM2-mediated ubiquitination of p53.

So far, no inhibitor of the MDM2 RING domain ATP binding site and few inhibitors of the MDM2 RING domain itself have been discovered. Previous studies from Kathryn Ball's laboratory and others have highlighted the importance of the last twelve amino acids at the C-terminus of MDM2 in regulating p53 ubiquitination.[123] Indeed, the tail has been shown to be critical for MDM2's E3 ligase activity. Previous work in the Ball group has led to the successful cloning of different fragments of MDM2 and MDMX RING domains: MDM2 res. 396-491, MDM2 res. 396-479, MDM4 res. 395-490 and MDM4 res. 395-478. Phage display has been performed on MDM2 res. 396-491, and MDM2 res. 396-479, with non-specific elution or ATP elution. Biopanning during phage display was carried out until the fourth round (see Section 4.10 for more details and phage display protocol).[163] The fourth round of the phage display are data from previous work and are summarised in Figure 1.2-11.[163]

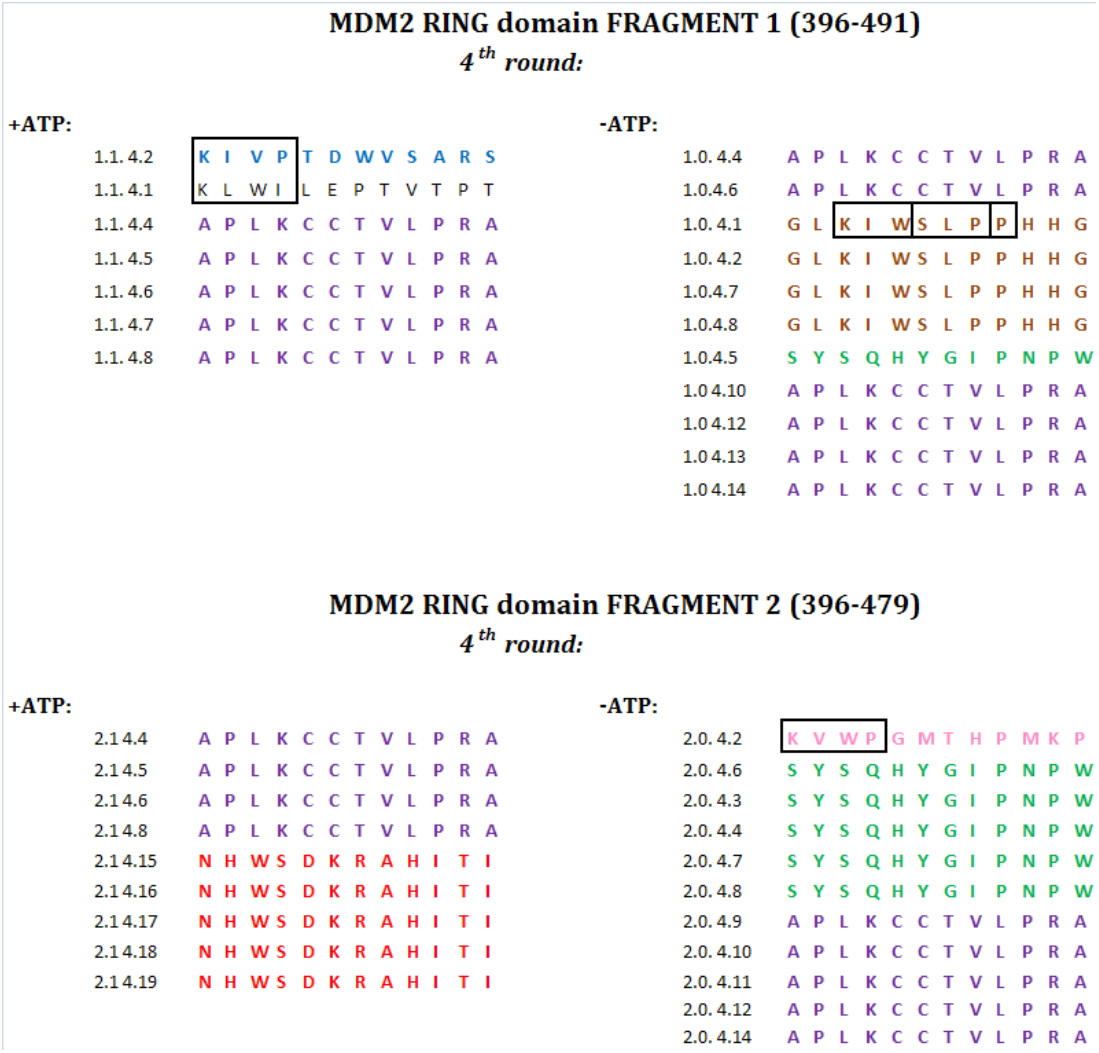

Figure 1.2-11. Amino acid sequences from the fourth round of phage display on MDM2 res.396-491 and res.396-479. Phage binding to MDM2 res.396-491 and res.396-479 were eluted by ATP (left columns) or non-specific elution (0.2 M glycine-HCl; right columns). The fourth round phage were amplified and resulting single phage colonies from titered plates were purified and subjected to DNA sequencing. Among all the sequences obtained, highly represented sequences are highlighted with colours. Black borders highlight different consensus sequences observed in the fourth round.

Unfortunately, the lack of diversity from the fourth round did not allow the observation of any consensus sequences. Instead, single colonies from the third round were submitted for DNA sequencing (35 colonies for MDM2 res. 396-491; 36 colonies for MDM2 res. 396-479). Sequences are reported in Figure 1.2-12 and Figure 1.2-13.

1.2.2.2 Sequencing results

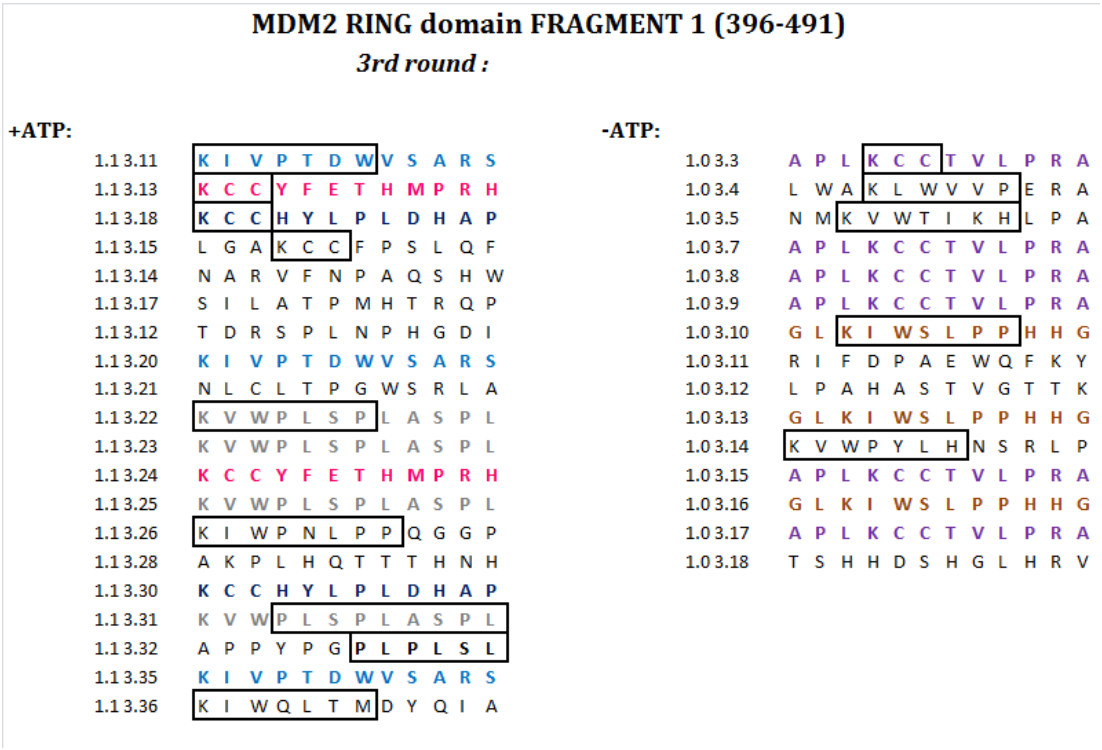

Figure 1.2-12. Amino acid sequences from the third round of phage display on the MDM2 res.396-491. Phage binding to MDM2 res.396-491 were eluted by ATP (left columns) or non-specific elution (0.2 M glycine-HCl; right columns). The third round phage were amplified and resulting single phage colonies from titered plates were purified and subjected to DNA sequencing. Among all the sequences obtained, highly represented sequences are highlighted with colours. Black borders highlight different consensus sequences observed in the third round.

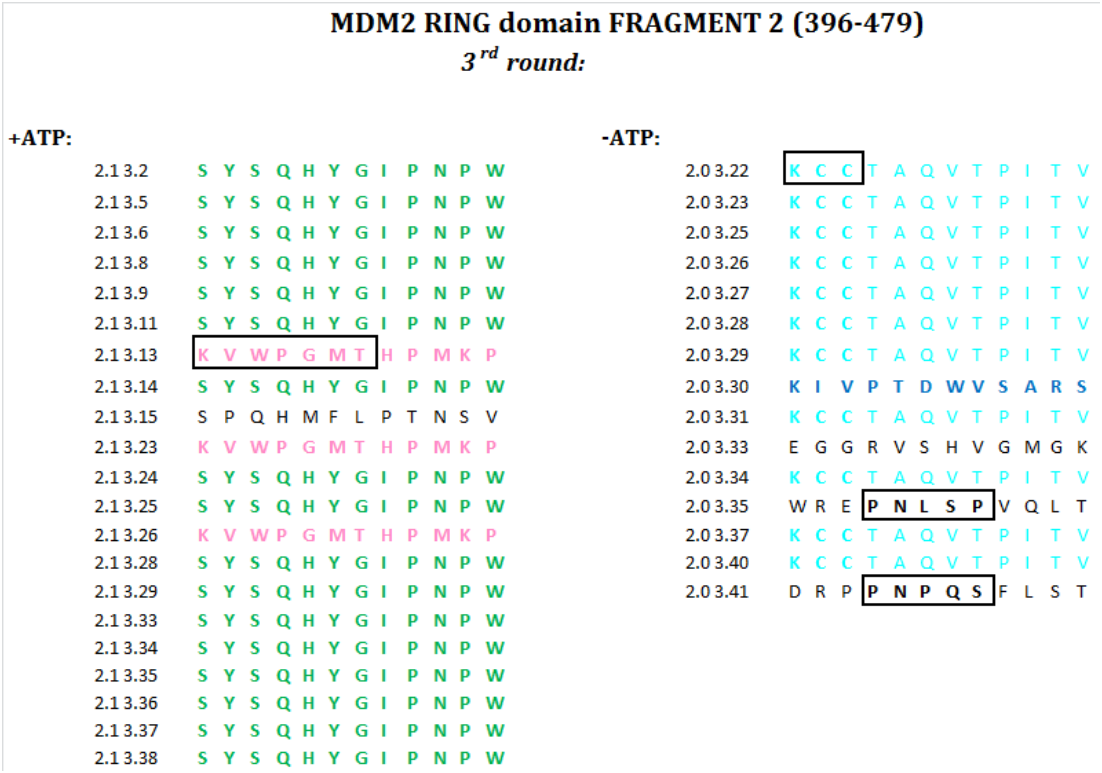

Figure 1.2-13. Amino acid sequences from the third round of phage display on the MDM2 res.396-479. Phage binding to MDM2 and res.396-479 were eluted by ATP (left columns) or non-specific elution (0.2 M glycine-HCl; right columns). The fourth round phage were amplified and resulting single phage colonies from titered plates were purified and subjected to DNA sequencing. Among all the sequences obtained, highly represented sequences are highlighted with colours. Black borders highlight different consensus sequences observed in the third round.

Figure 1.2-14. Consensus sequences a, b and c found in the third round of phage display. Sequences were aligned using ClustalW2, with no gaps allowed. The star represents an identical amino acid in the alignment, two dots represent high similarity. Colours are defined by ClustalW2 as such: red for small and hydrophobic, blue for acidic, magenta for basic, green for hydroxyl, sulfhydryl and glycine

Using the ClustalW2 alignment tool a few consensus sequences were identified and peptides containing these consensus sequences are summarised in Figure 1.3-14 ranked according to the hydrophilicity of the amino acids. Two clear motifs were observed: K[V/I/L]W and KCC, **(a)** and **(b)** respectively. The third category **(c)** shows a higher frequency of amino acids (P, L, S) within the peptide rather than a real consensus.

a

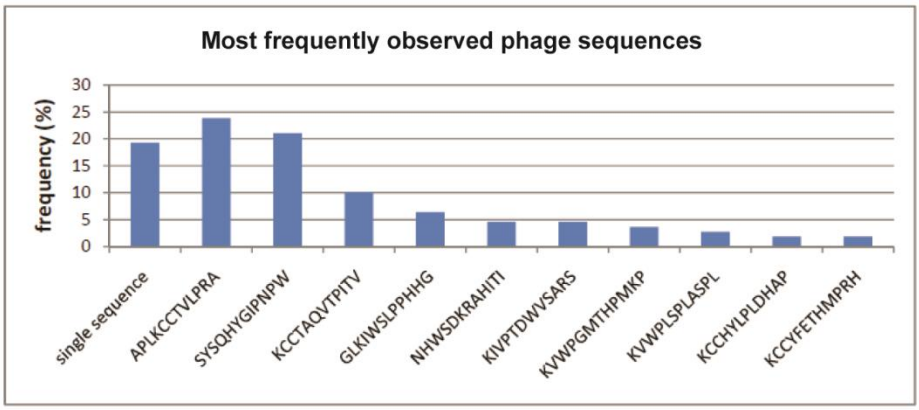

b

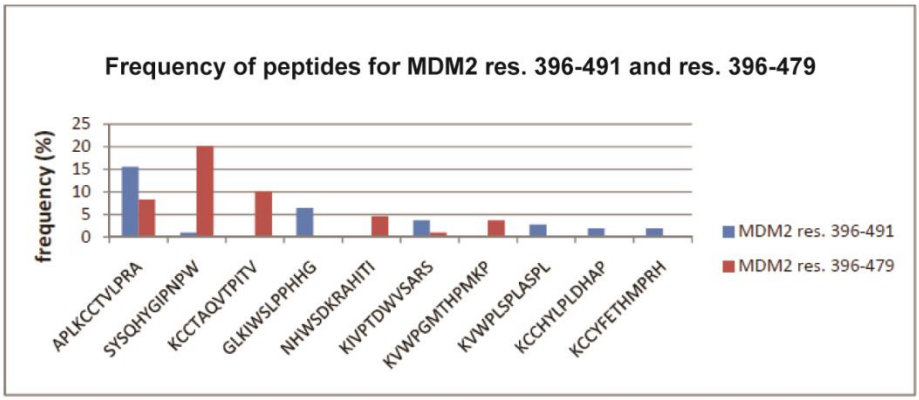

c

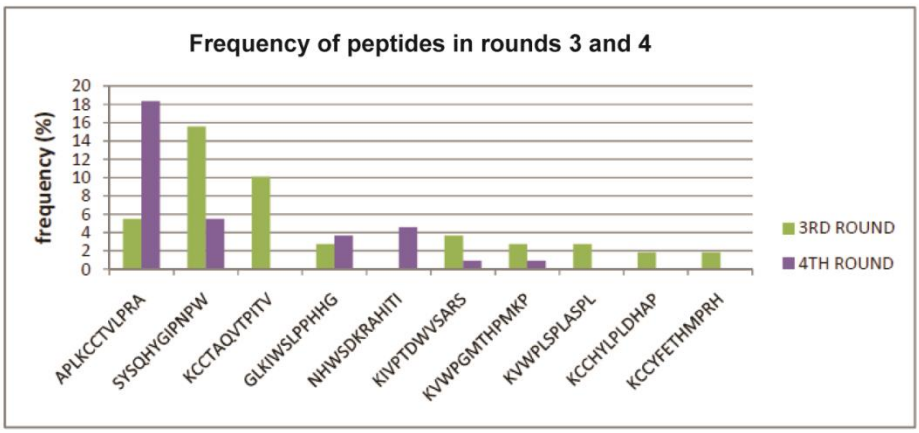

Figure 1.2-15. Summary of frequently seen phage-peptide sequences in the phage display. (a) Frequency of occurrence of the most common phage-peptide sequences accross the third and fourth rounds of phage display. (b) Frequency of Frequency of occurrence of the most common phage-peptide sequences for MDM2 res. 396-491 and res. 396-479 across the third and fourth rounds of phage display. (c) Frequency of the most common phage-peptide sequences in each of the third and fourth round of phage display. The total number of successfully obtained sequences was 109.

The distribution of phage-peptides by frequency of observation are summarised in Figure 1.2-15, in the whole phage display **(a)** or according to which target the

phage-peptide sequences have been found to bind to **(b)** or according to the round of biopanning the sequences has been obtained from **(c)**. Interestingly, the phage-peptide sequences which are the most represented in the third round are not necessarily the most represented in the fourth round. However, these observations are to be viewed with caution. Indeed, although the handpicking of colonies during the phage display process was random, the number of selected samples was small compared to total number of colonies and overall selection of samples will not be a statistical representation of the entire library.

1.2.2.3 BLAST Alignment and relevance of phage-peptide hits

All the sequences obtained from phage display were checked through the Basic Local Alignment Search Tool (BLAST: http://blast.ncbi.nlm.nih.gov/Blast.cgi) using the Homo Sapiens database. Although it was not expected to find any sequences with 100% identity, best alignment scores together with cancer relevance were selected. A few interesting hits were identified which commanded attention as their extracted sequences exist in ubiquitin-related proteins, RING finger domains and E3 ligases. Indeed, since MDM2 is an E3 ligase for p53, it is particularly interesting to observe fragments from family members of deubiquitinating enzymes (USP, UCH). However, no such protein has yet been shown to interact with p53 or MDM2.

From those alignments, sequences were extracted from the original proteins and purchased as biotinylated peptides along with biotinylated peptides from the phage-peptide sequences. The peptides purchased are listed in Figure 1.2-16. Most peptides resulted from phage display. The others were obtained using BLAST searches for simultaneous high scores and relevant proteins.

	Biotinylated peptides	related protein (BLAST)
Pept.55	Biotin-SGSG-APLKCCTVLPRA	
Pept.56	Biotin-SGSG-SYSQHYGIPNPW	ubiquitin-like modifier activating enzyme 7
Pept.57	Biotin-SGSG-LRC**QNYGIP**PVN	ubiquitin-like modifier activating enzyme 7
Pept.58	Biotin-SGSG-SHSG**SYSQH**MNH	Zinc finger E-box-binding homeobox 1
Pept.59	Biotin-SGSG-NHWSDKRAHITI	
Pept.60	Biotin-SGSG-ELFKTPADKRFF	
Pept.61	Biotin-SGSG-GDK**FKTPA**KVGL	ubiquitin associated protein 1
Pept.62	Biotin-SGSG-GLKIWSLPPHHG	
Pept.63	Biotin-SGSG-VEE**IWSLEP**ENF	ubiquitin C-terminal hydrolase UCH37
Pept.64	Biotin-SGSG-KLWILEPTVTPT	
Pept.65	Biotin-SGSG-KRK**PTVTPT**VNR	ubiquitin specific peptidase 8
Pept.66	Biotin-SGSG-ED**EPTVVPT**TSA	ring finger protein 111
Pept.67	Biotin-SGSG-HVQPGAPPALDL	
Pept.68	Biotin-SGSG-QA**PGSPPAL**RIP	ubiquitin specific protease 43
Pept.69	Biotin-SGSG-KCCHYLPLDHAP	
Pept.70	Biotin-SGSG-KCCYFETHMPRH	
Pept.71	Biotin-SGSG-IEQF**CCYF**KELP	ubiquitin specific protease 3
Pept.72	Biotin-SGSG-KIVPTDWVSARS	
Pept.73	Biotin-SGSG-KVWPGMTHPMKP	
Pept.74	Biotin-SGSG-SDL**THPMK**TSHP	ubiquitin specific protease 36
Pept.75	Biotin-SGSG-LGAKCCFPSLQF	
Pept.76	Biotin-SGSG-NA**RVFNPA**QSHW	
Pept.77	Biotin-SGSG-IKRVFDPALNLF	ubiquitin protein ligase E3B
Pept.78	Biotin-SGSG-SDTISRLHVSMT	
Pept.79	Biotin-SGSG-SHHIPSYQWPLH	
Pept.80	Biotin-SGSG-HQPI**SHHIP**ATA	ring finger protein 111
Pept.81	Biotin-SGSG-SILATPMHTRQP	
Pept.82	Biotin-SGSG-SYSQHYGIPNPW	
Pept.83	Biotin-SGSG-TDRSPLNPHGDI	
Pept.84	Biotin-SGSG-TLPAFGPRAHVL	
Pept.85	Biotin-SGSG-TMGFTAPRFPHY	
Pept.86	Biotin-SGSG-WPFPHNTPPSFI	
Pept.87	Biotin-SGSG-AKPLHQTTTHNH	
Pept.88	Biotin-SGSG-APPYPGPLPLSL	
Pept.89	Biotin-SGSG-EGGRVSHVGMGK	
Pept.90	Biotin-SGSG-KCCTAQVTPITV	
Pept.91	Biotin-SGSG-KIWPNLPPQGGP	
Pept.92	Biotin-SGSG-KIWQLTMDYQIA	
Pept.93	Biotin-SGSG-KVWPYLHNSRLP	
Pept.94	Biotin-SGSG-LPAHASTVGTTK	
Pept.95	Biotin-SGSG-LWAKLWVVPERA	
Pept.96	Biotin-SGSG-NMKVWTIKHLPA	
Pept.97	Biotin-SGSG-RIFDPAEWQFKY	
Pept.98	Biotin-SGSG-TSHHDSHGLHRV	
Pept.99	Biotin-SGSG-WREPNLSPVQLT	
Pept.100	Biotin-SGSG-SPQHMFLPTNSV	
Pept.101	Biotin-SGSG-DRPPNPQSFLST	

Figure 1.2-16. Biotinylated peptides resulting from phage display and BLAST search. The proteins from which the peptides have been extracted are specified next to the corresponding peptides. Coloured sequences are highly represented sequences. Black bold sequences represent the alignment from a peptide and its corresponding phage-peptide.

1.2.3 Evaluation of binding affinity and activity of biotinylated lead peptides against the MDM2-p53 interaction

1.2.3.1 *In vitro* ELISA

To evaluate the affinity and the specificity of the selection of peptides found by phage display and refined with BLAST, ELISA experiments were performed on His_6-MDM2 res. 396-491, His_6-MDM2 res. 396-479, His_6-MDM4 res. 395-490 and His_6-MDM4 res. 396-478. Two different approaches are possible when evaluating new peptide leads using ELISA (see Figure 1.2-17 and Figure 1.2-18). The first consists of coating the plate with the target protein, then adding the biotinylated peptide followed by the addition of a HRP-linked streptavidin. In the second approach the plate is coated with streptavidin first, then one peptide per well is added, followed by the addition of the target protein. An addition of anti-His antibody, rabbit anti-mouse antibody and ECL would detect any binding between the protein and the peptide.

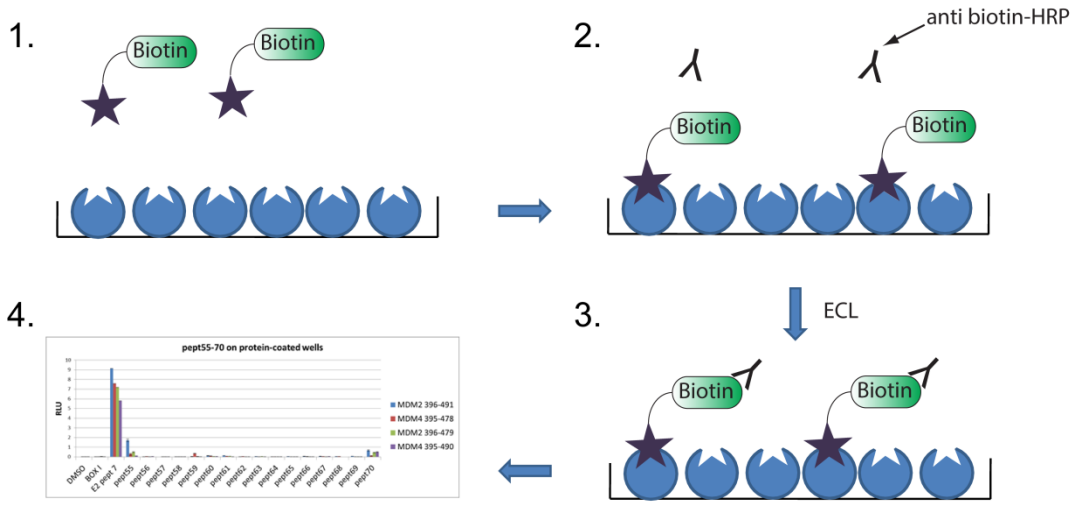

Figure 1.2-17. ELISA using immobilised protein. 1. Biotinylated peptide is incubated in protein-coated well. 2. HRP-linked streptavidin binds the biotinylated peptide. 3. ECL is added to the washed wells. 4. Plate is read for signal.

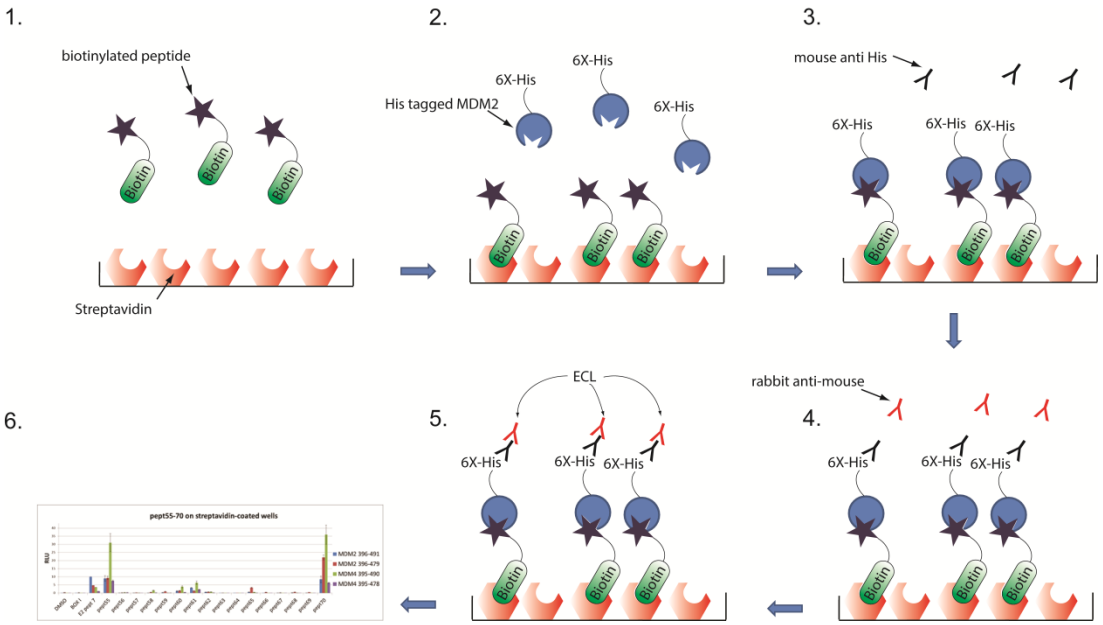

Figure 1.2-18. ELISA using immobilised peptides. 1. Biotinylated peptide is immobilised on a streptavidin-coated well. 2. Protein is incubated in well. 3. Primary antibody bind the protein. 4. Secondary antibody binds the primary antibody. 5. ECL is added to the washed wells. 6. Plate is read for signal.

Coating the plate first with protein has the advantage of using only one antibody which should give less background. However, in presence of a basic buffer, the protein is denatured. In the second approach, the protein retains its conformation. Therefore, different sets of results are to be expected.

For each ELISA method, 2.5 µg of peptide per well was used, antibodies were used at a 1:2000 dilution and binding was detected by electrochemical luminescence (50 µL ECL mix per well) and was quantified at 450 nm using a Fluoroskan Ascent FL apparatus (Labsystems). The ELISA experiments were repeated in triplicate (Sections 4.8.3 and 4.8.4).

Results of ELISA using the protein-coated method are shown in Figure 1.2-19 and Figure 1.2-20.

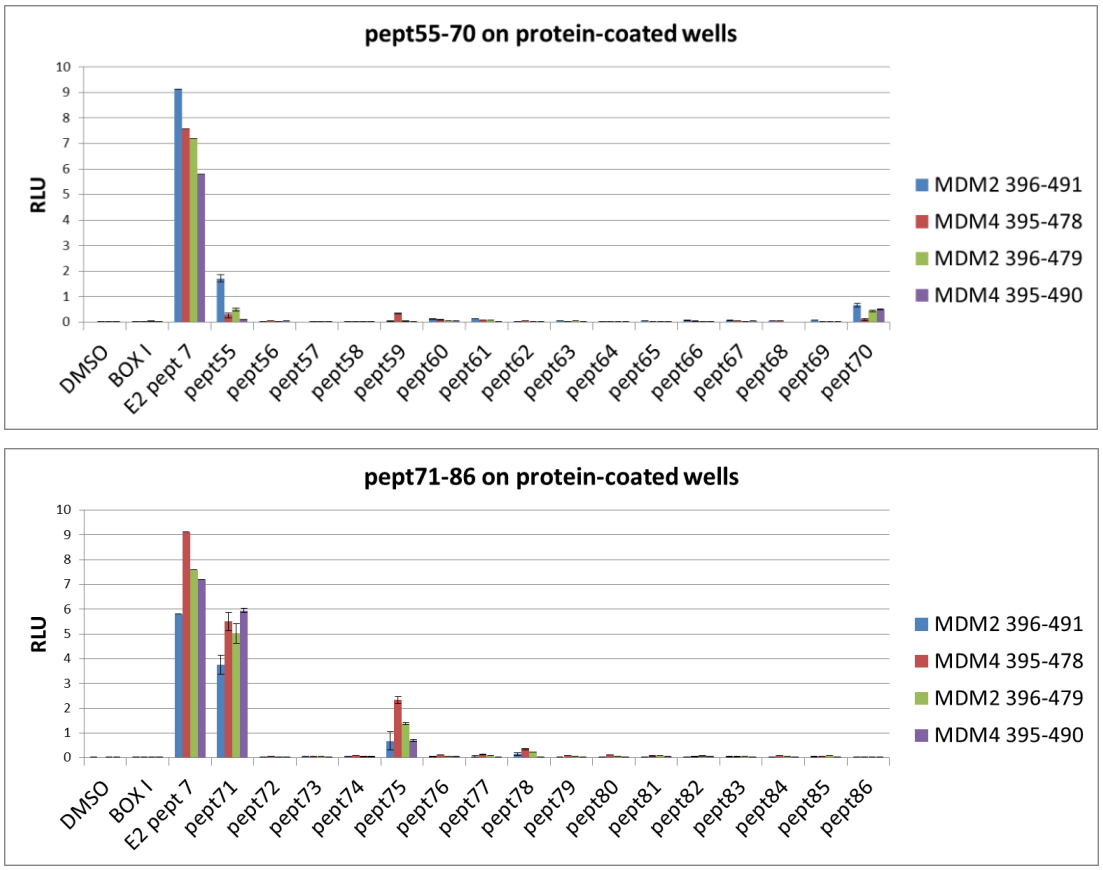

Figure 1.2-19. peptide ELISA on MDM2 res. 396-491, MDM2 396-479, MDM4 res. 395-490, MDM4 395-478, coating the wells with protein first and then biotinylated peptides (pept.55-86). 1:2000 diluted HRP-linked streptavidin was used. Protein concentrations were normalised prior to addition. Detection after addition of ECL with luminescence read on a plate reader and analysed with the Fluoroskan Ascent software.

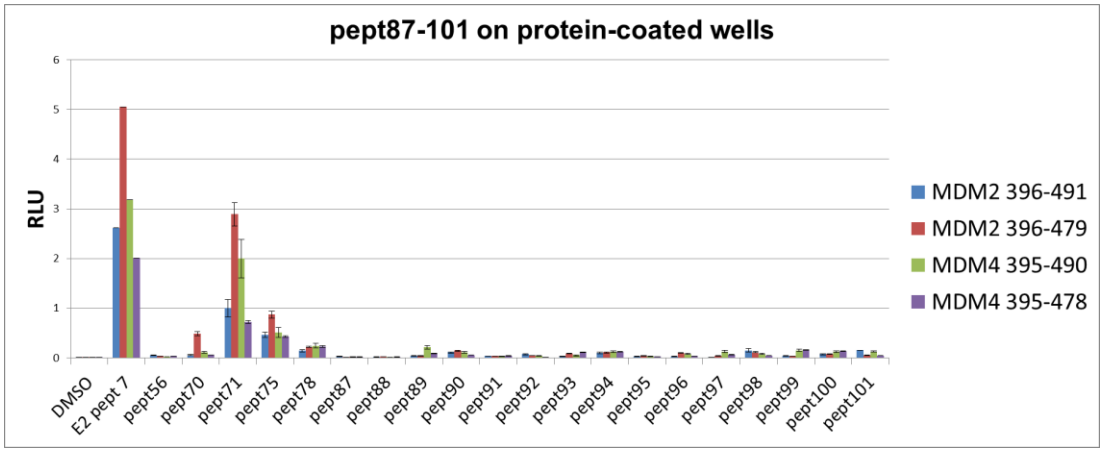

Figure 1.2-20. Peptide ELISA on MDM2 res. 396-491, MDM2 396-479, MDM4 res. 395-490, MDM4 395-478, treating the wells first with protein and then with biotinylated peptides (pept.87-101). 1:2000 diluted HRP-linked streptavidin was used. Protein concentrations were normalised prior to addition. Detection after addition of ECL with luminescence read on a plate reader and analysed with the Fluoroskan Ascent software.

According to this approach, pept.55, pept.70, pept.71 and pept.75 appear to bind MDM2, with sequences APL**KCC**TVLPRA, **KCCYF**ETHMPRH, IEQF**CCYF**KELP, LGA**KCC**FPSLQF, respectively. Bold characters highlight consensus residues.

Results of ELISA using the peptide-coated method are shown in Figure 1.2-21 and Figure 1.2-22.

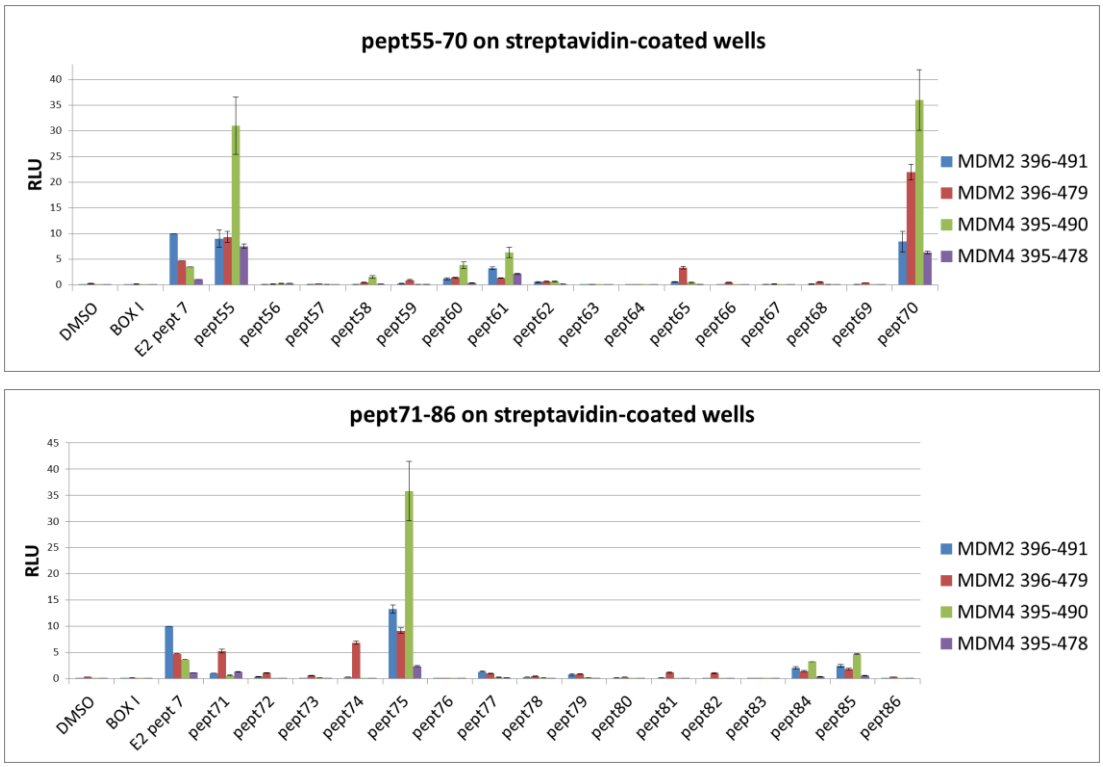

Figure 1.2-21. Peptide ELISA on MDM2 res. 396-491, MDM2 396-479, MDM4 res. 395-490, MDM4 395-478, treating the wells with streptavidin and then with biotinylated peptides (pept.55-86). 1 µg of streptavidin, 5 µg of biotinylated peptides, 1:800 diluted anti-His primary antibody and 1:2000 diluted rabbit anti-mouse secondary antibody were used. Protein concentrations were normalised prior to addition. Detection after addition of ECL with luminescence read on a plate reader and analysed with the Fluoroskan Ascent software.

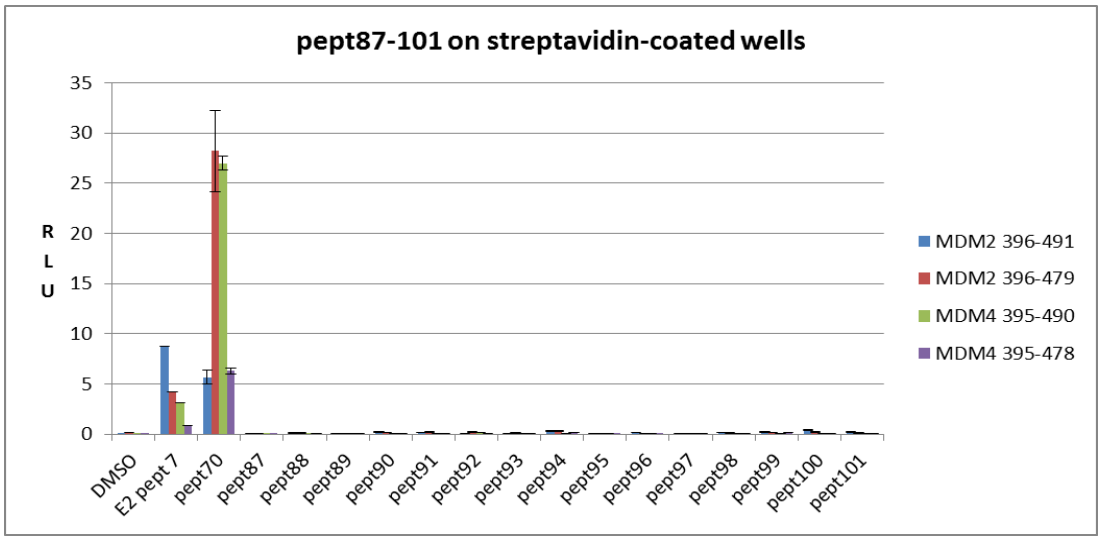

Figure 1.2-22. Peptide ELISA on MDM2 res. 396-491, MDM2 396-479, MDM4 res. 395-490, MDM4 395-478, treating the wells with streptavidin and then with biotinylated peptides (pept.87-101). 1 µg of streptavidin, 5 µg of biotinylated peptides, 1:800 diluted anti-His primary antibody and 1:2000 diluted rabbit anti-mouse secondary antibody were used. Protein concentrations were normalised prior to addition. Detection after addition of ECL with luminescence read on a plate reader and analysed with the Fluoroskan Ascent software.

The two different ELISA methods display different results. The first and second approaches suggest that pept.55, pept.70, pept.71 and pept.75 are potential binders. The different intensities of signals observed in the two methods are in accordance with the change of conformation of the proteins; as in the first approach, the target protein is denatured to be displayed on the well and may display a different conformation. Pept.70 and pept.71 best illustrate these differences. Pept.70 binds strongly using the streptavidin-coated ELISA method but not so much using the protein-coated ELISA method. In contrast, pept.71 seems to have a higher binding affinity using the protein-coated ELISA method. The change in conformation is enough to select one peptide rather than the other. However, it is interesting to note that the selected peptides have the same **KCC** consensus motif.

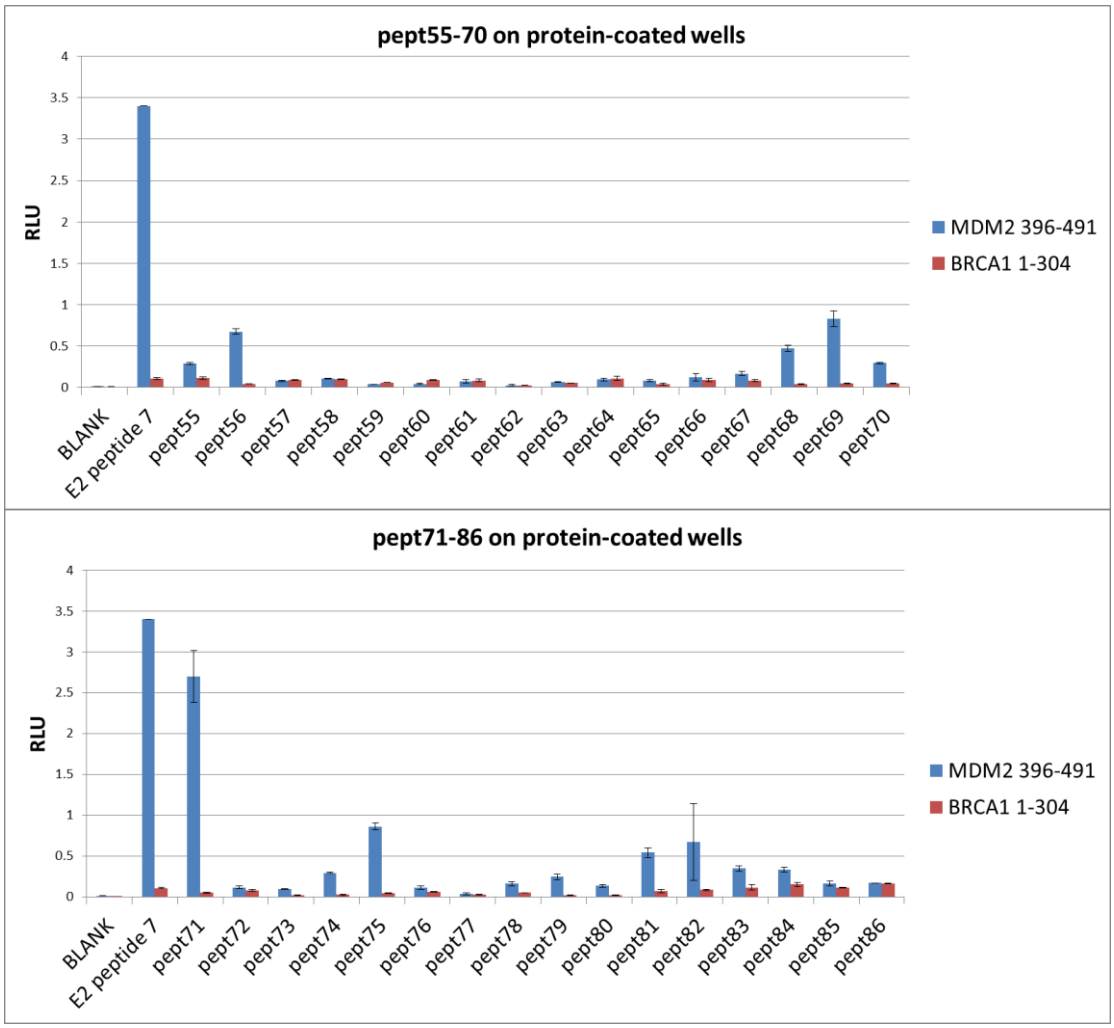

Figure 1.2-23. Peptide ELISA on MDM2 res. 396-491 and BRCA1 res. 1-304, treating wells first with protein and then with biotinylated peptides (pept.55-86). 1:2000 diluted HRP-linked streptavidin was used. Protein concentrations were normalised prior to addition. Detection after addition of ECL with luminescence read on a plate reader and analysed with the Fluoroskan Ascent software.

The peptides found by phage display were shown to bind MDM2 res. 396-491 and not BRCA1 res.1-304 (Figure 1.2-23). Based on this experiment, pept.70 has an affinity six times higher and pept.71 sixty six times higher for MDM2 res. 396-491 than for BRCA1 res.1-304, which suggests selective binding for the MDM2-MDM4 family.

1.2.3.2 *In vitro* pull-down experiments

Pull-down experiments rely on the affinity of a protein to a peptide attached to beads. Successive washes followed by cleavage of the protein from the peptide by heat in

SDS sample buffer and afforded the protein sample ready for western blotting. This experiment is similar in principle to the streptavidin-coated ELISA method.

To confirm the binding of the lead peptides to MDM2, pull-down experiments were used as an alternative method to evaluate binding. These affinity chromatography experiments were performed on full-length MDM2 detected by a 2A10 antibody, as described in the Material and Methods section, and the corresponding western blots are shown in Figure 1.2-24. E2 peptide 7 (biotin-SGSG-SQWSPALTVSKVLLSICSLL) is a UbcH5a-truncated peptide and has been shown in the K. Ball laboratories to be a good binder of full-length MDM2 and was chosen as positive control (unpublished data). Full-length MDM2 and 2A10 were chosen as this system afforded a clean and sensitive signal.

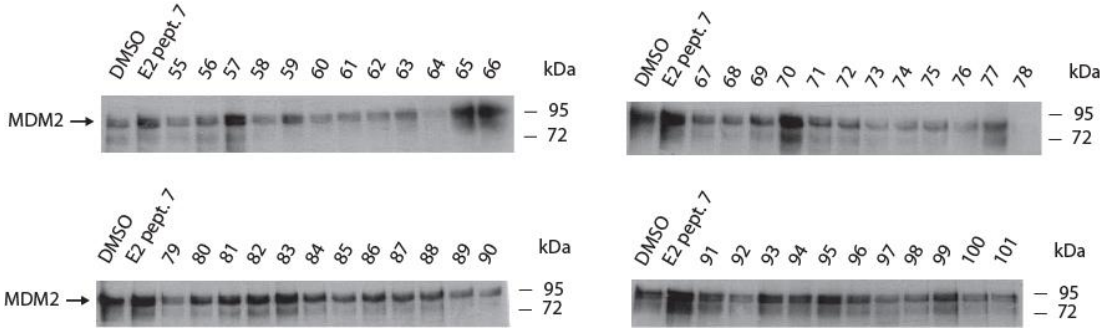

Figure 1.2-24. *in vitro* pull-down experiments on biotinylated pept.55-101 with full-length MDM2. Biotinylated peptides were added to streptavidin-agarose beads. 40 ng MDM2 was then incubated with the beads. Samples were then heated up with sample buffer and run by western blotting. MDM2 was detected with 2A10 antibody.

The initial quantity of purified protein recommended in a general protocol designed in the Ball and Hupp laboratories was 150 ng protein per tube, but this led to a large background signal, suggesting a non-specific binding of MDM2 to the beads.[164] Reducing the amount of full-length MDM2 to 20 ng was enough to detect the strongest binding peptides, but not the positive control. Finally, 40 ng of full-length MDM2 was chosen as a compromise as it allowed the detection of the positive control E2 peptide 7 with limited background (Figure 1.2-24).

The data suggest that pept.57 (LRCQNYGIPPVN) and pept.70 (KCCYFETHMPRH) seem to be the strongest binders to full-length MDM2. However, a signal was detected for every peptide and the negative control, DMSO, which suggests a non-specific

binding of full-length MDM2 with the streptavidin beads. Pull-down experiments with the most promising peptides were also performed on MDM2-transfected H1299 cell lysates. However, only the positive control gave rise to any detectable signal.
The *in vitro* pull-down results being in accordance with the ELISA experiments in which peptide sequences were displayed in the presence of non-denatured MDM2 fragments, any further required ELISA experiments should be carried out using the streptavidin-coated approach.

1.2.3.3 *In vitro* ubiquitination assay

After checking the binding of purchased peptides, their ability to prevent the ubiquitination of p53 from full-length MDM2 was assessed. This is most readily achieved *in vitro* through the addition ATP, E1, E2 (UbcH5), ATP, ubiquitin, the E3 (MDM2), the target to be ubiquitinated (p53) and a peptide. The ubiquitination pathway was described in Figure 1.1-10. In the absence of a potent peptide, MDM2 would act as a template to bring the ubiquinated E2 in proximity with p53 and allow the transfer of ubiquitin to p53. A peptide preventing the ubiquination of p53 by MDM2 could either block the interaction of p53 with MDM2 or block the interaction of the ubiquitinated E2 with MDM2. After an incubation of 15 min at 30°C, sample reactions were stopped with sample buffer with DTT, heated and run by western blotting. Each band above the p53 band represents p53 with an extra ubiquitin attached (p53-Ub). If no p53-Ub is observed in the presence of a peptide, this peptide is able to prevent ubiquitination of p53 by MDM2 *in vitro*. Samples were run on precast electrophoresis gels (NuPage® Novex®, 4-12%). These manufactured gels are built with a gradient of the percentage of polyacrylamide. This allows a better separation between bands as the difference between each band is quite small (8.5 kDa).

MDM2 was titrated in order to use the amount of MDM2 necessary to observe poly- ubiquitination of p53 (Figure 1.2-25). A final concentration of MDM2 at 20 nM was chosen to carry out the ubiquitination experiments.

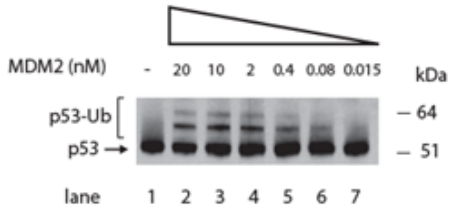

Figure 1.2-25. MDM2 titration for *in vitro* ubiquitination of p53. Samples contained a final p53 concentration of 23 nM.

Experiments used DMSO as a negative control and MDM4 39 as a positive control. MDM4 39 is a peptide from the C-terminus of MDM4 and had previously been shown to inhibit MDM2-mediated ubiquitination of p53 (unpublished data from the Ball laboratories). Results of the *in vitro* ubiquitination assay with pept.55-101 are shown in Figure 1.2-26.

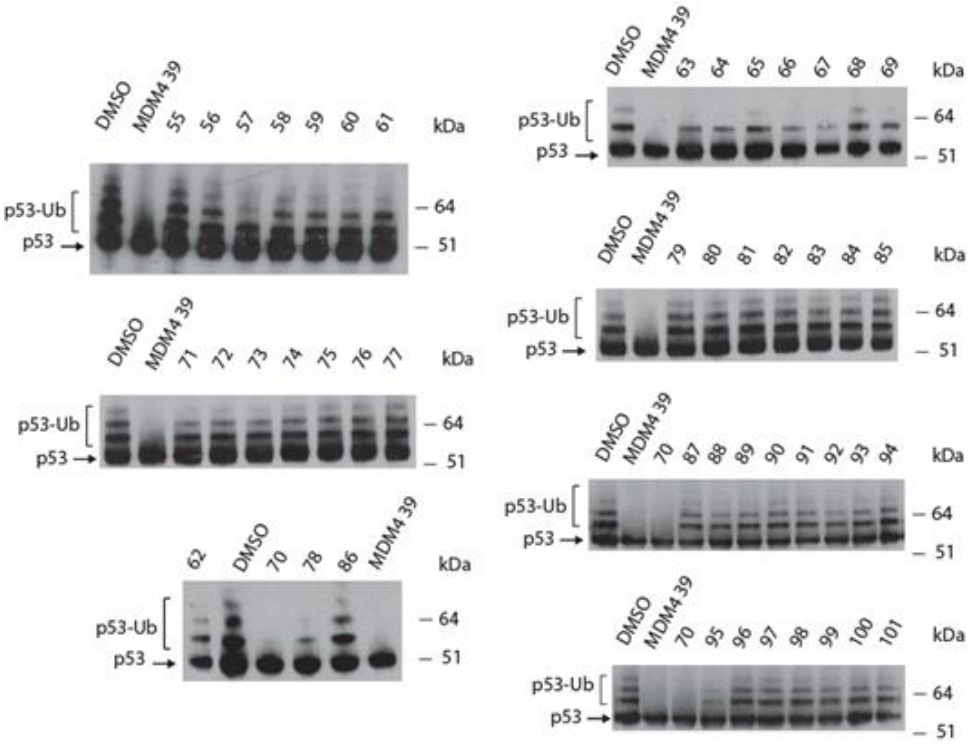

Figure 1.2-26. *In vitro* ubiquitination of p53 by full-length MDM2 in the presence of biotinylated peptides. Samples were incubated at 30°C for 15 minutes before stopping the reaction. DO-1 antibody was used for detection. DMSO was used as a negative control, MDM4 39 as a positive control. Samples contained a final concentration of 20 nM MDM2, 23 nM p53 and 50 µM biotinylated peptides.

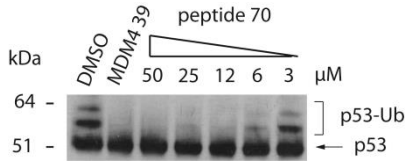

Figure 1.2-27. *In vitro* ubiquitination of p53 by full-length MDM2 in the presence of pept.70. Samples were incubated at 30°C for 15 minutes before stopping the reaction. DO-1 antibody was used for detection. DMSO was used as a negative control, MDM4 39 as a positive control. Samples contained a final concentration of 20 nM MDM2, 23 nM p53 and titrated pept.70 (3 to 50 µM).

These data show a clear inhibition of p53 ubiquitination by MDM2 with pept.70 (KCCYFETHMPRH) down to a final concentration of 6-12 µM. Other peptides, such as pept.78 (SDTISRLHVSMT) and pept.95 (LWAKLWVVPERA), displayed some activity although not complete inhibition even at 50 µM.

Together, these data suggest that pept.70 (KCCYFETHMPRH) is the strongest candidate as an inhibitor of the E3 ubiquitin ligase activity of MDM2 towards p53 *in vitro*. Moreover, pept.70 has already been shown to bind well in ELISA experiments where the biotinylated peptide is displayed on a streptavidin-coated surface and *in vitro* pull-down experiments. Moreover, and probably the most important feature of pept.70 so far is its ability to prevent the ubiquitination of p53 by MDM2 at 6-12 µM *in vitro* when most of the other peptides barely show a decrease in ubiquitination at 50 µM.

In order to assess the potential of pept.70, it should be subjected to further investigation, including ELISA, affinity chromatography and *in vitro* ubiquitination assays of alanine-mutated and truncated versions of pept.70.

1.2.4 Optimisation of peptide lead KCCYFETHMPRH

1.2.4.1 Alanine scan and truncation

Both Alanine-mutated and truncated peptide versions of $KC^{1}C^{2}YFETH^{1}MPRH^{2}$ (Table 1.2-1) revealed the importance of amino acid residues within this peptide. As shown by peptide-coated ELISA experiments (Figure 1.2-28), single mutations K1A, C2A, C3A, F4A, H8A were shown to significantly decrease the binding toward full-length MDM2 protein. In contrast, single mutations E6A and H12A slightly increased its binding. While the increased binding for pept.70-A6[§] is likely to be attributed to a charge effect, pept.70-A12 modification seems to be of lesser importance as suggested by the last C-amino acid truncation. Although pept.70-ΔC2 or pept.70-ΔC3 still show around 20% of pept.70 signal, any other truncation either side of the original peptides abrogates the binding to MDM2.

peptide	sequence
70	KCCYFETHMPRH
70-A1	**A**CCYFETHMPRH
70-A2	K**A**CYFETHMPRH
70-A3	KC**A**YFETHMPRH
70-A4	KCC**A**FETHMPRH
70-A5	KCCY**A**ETHMPRH
70-A6[§]	KCCYF**A**THMPRH
70-A7	KCCYFE**A**HMPRH
70-A8	KCCYFET**A**MPRH
70-A9	KCCYFETH**A**PRH
70-A10	KCCYFETHM**A**RH
70-A11	KCCYFETHMP**A**H
70-A12	KCCYFETHMPR**A**

peptide	sequence
70-ΔC1	KCCYFETHMPR
70-ΔC2	KCCYFETHMP
70-ΔC3	KCCYFETHM
70-ΔC4	KCCYFETH
70-ΔN1	CCYFETHMPRH
70-ΔN2	CYFETHMPRH
70-ΔN3	YFETHMPRH
70-ΔN4	FETHMPRH

Table 1.2-1. List of alanine-mutated and truncated peptide sequences.

[§] pept.70-E6A will now be referred as pept.70-A6; the other alanine mutations follow a similar pattern.

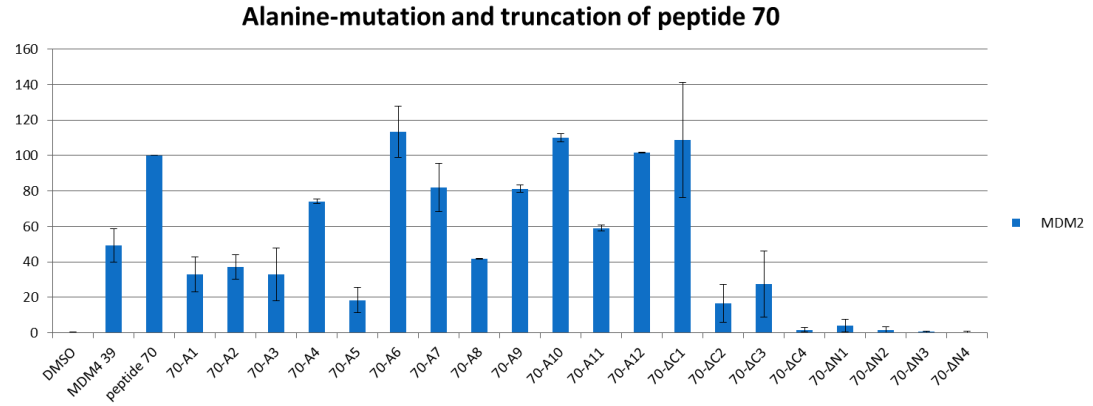

Figure 1.2-28. Binding affinity of alanine-mutated or truncated pept.70 towards full-length MDM2.

Western blots from *in vitro* pull-down experiments (Figure 1.2-29) barely show any binding between the alanine-mutated or truncated peptides and MDM2, which suggests that the first eleven residues are necessary for efficient binding. Only peptides pept.70-ΔC3, pept.70-A3 and pept.70-A12 appear to bind to full-length GST-tagged MDM2.

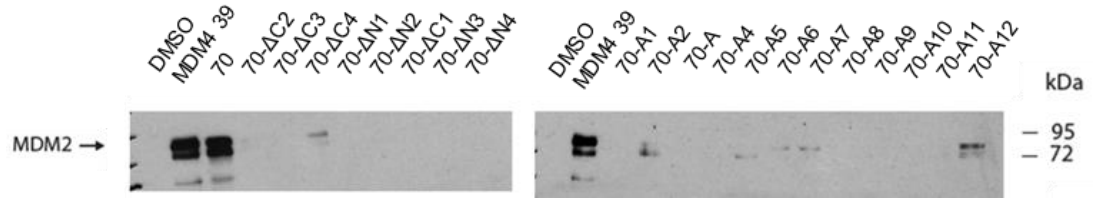

Figure 1.2-29. *in vitro* pull-down experiments of alanine-mutated or truncated pept.70 towards full-length MDM2.

In vitro ubiquitination experiments with peptides at a final concentration of 50 µM revealed that pept.70-A12 is at least as potent as pept.70 at inhibiting the *in vitro* ubiquitination of p53. This suggests that the last residue is more permissive but necessary to retain the ubiquitination. To a lesser extent pept.70-A7 and pept.70-A10 also displayed some activity. Interestingly, pept.70-ΔC1, which did show some binding toward MDM2 by ELISA, neither binds MDM2 in pull-down experiments nor is able to inhibit *in vitro* ubiquitination of p53. Titration of pept.70 and pept.70-A12 has even revealed a greater potency of pept.70-A12 (Figure 1.2-31) with activity retained down to 6 µM.

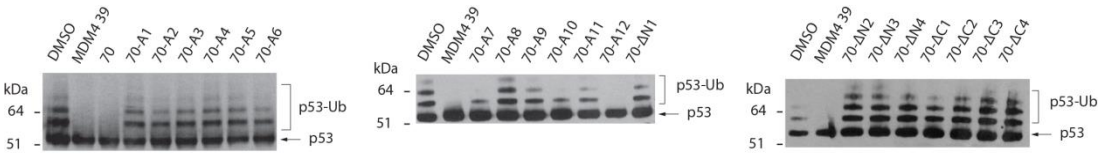

Figure 1.2-30. *In vitro* ubiquitination of p53 by full-length MDM2 in the presence of biotinylated peptides of alanine-mutated or truncated pept.70. Samples contained a final concentration of 20 nM MDM2, 23 nM p53 and 50 µM biotinylated peptides.

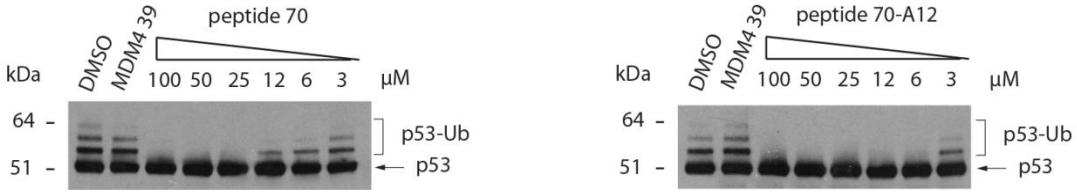

Figure 1.2-31. *In vitro* ubiquitination of p53 by full-length MDM2 with different concentrations of biotinylated alanine-mutated or truncated pept.70. Samples were incubated at 30°C for 15 minutes before stopping the reaction. DO-1 antibody was used for detection. DMSO was used as a negative control, MDM4 39 as a positive control. Samples contained a final concentration of 20 nM MDM2, 23 nM p53 and titrated pept.70 or Pet.70-A12 (3 to 100 µM).

Complementary ELISA experiments (Figure 1.2-32 and Figure 1.2-33) have confirmed the greater binding ability of pept.70-A12 compared to pept.70. Indeed, peptide titration revealed that an equivalent amount of pept.70-A12 displayed a higher binding affinity for full-length MDM2 than pept.70. Similarly, an increasing amount of full-length MDM2 had a bigger signal increase for a fixed amount of pept.70-A12 rather than for pept.70. Pept.33 and pept.34 have been chosen as random negative controls as they have shown no binding on previous ELISA experiments.

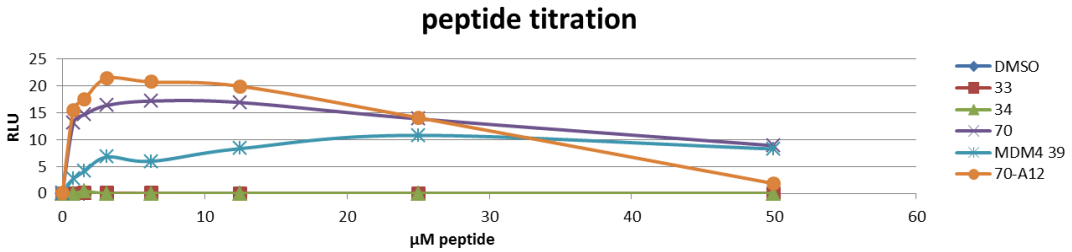

Figure 1.2-32. Binding affinity of pept.70 and pept.70-A12 towards full-length MDM2 with an increasing amount of peptide.

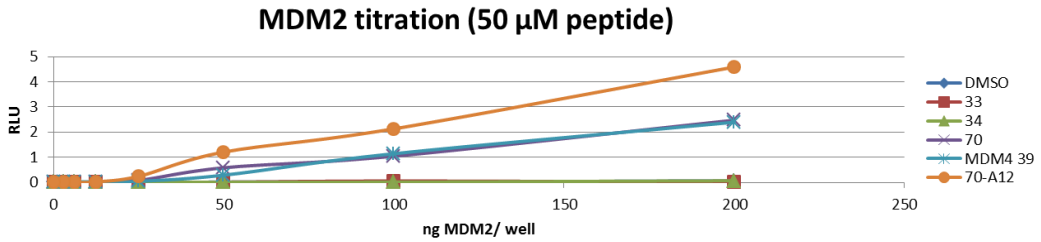

Figure 1.2-33. Binding affinity of pept.70 and pept.70-A12 towards full-length MDM2 with an increasing amount of protein.

Altogether, these data suggest that the first N-terminal amino acid residues are critical and outline the importance of the KCC motif identified during the phage display sequencing. Replacement with alanine of the any of the first three residues reduced the peptide affinity by more than half and truncation from the first N-terminal amino acid abrogates any binding. The C-terminal part of the peptide is slightly more permissive as truncation of the last C-terminal amino acid retains the binding affinity of the peptide with MDM2 but not its activity toward p53 ubiquitination. However, replacing the C-terminal histidine with an alanine actually improves the peptide's ability to inhibit MDM2-mediated p53 ubiquitination *in vitro* at a concentration as low as 6 µM, twice as effective as the original peptide activity.

1.2.4.2 Mutation of the C-terminal amino acid

The increased ability of pept.70-A12 to inhibit MDM2-mediated ubiquitination of p53 *in vitro* compared to pept.70 suggests that the histidine could be replaced but the twelfth amino acid should not be removed as mutation retains the binding affinity but truncation showed loss of activity. It would be therefore interesting to investigate mutations the C-terminus of pept.70 and see how it affects the peptide activity. The following peptides were purchased:

peptide	sequence
70	KCCYFETHMPR**H**
70-H12R	KCCYFETHMPR**R**
70-H12K	KCCYFETHMPR**K**
70-H12D	KCCYFETHMPR**D**
70-H12E	KCCYFETHMPR**E**
70-H12S	KCCYFETHMPR**S**
70-H12H	KCCYFETHMPR**H**
70-H12T	KCCYFETHMPR**T**
70-H12N	KCCYFETHMPR**N**
70-H12Q	KCCYFETHMPR**Q**

peptide	sequence
70-H12C	KCCYFETHMPR**C**
70-H12G	KCCYFETHMPR**G**
70-H12P	KCCYFETHMPR**P**
70-H12A	KCCYFETHMPR**A**
70-H12V	KCCYFETHMPR**V**
70-H12I	KCCYFETHMPR**I**
70-H12L	KCCYFETHMPR**L**
70-H12M	KCCYFETHMPR**M**
70-H12F	KCCYFETHMPR**F**
70-H12Y	KCCYFETHMPR**Y**
70-H12W	KCCYFETHMPR**W**

Unfortunately, due to time constraints, ELISA, *in vitro* pull-down experiments and *in vitro* ubiquitination assays are yet to be completed and it is hoped that they will be completed in the near future.

1.3 Conclusion

Successful cloning and expression of MDM2 and MDM4 fragments has enabled phage display to be carried out; and a few consensus sequences in the resultant hit sequences were observed. From those hits, several cancer-related or ubiquitin-related sequences have been identified, including IEQFCCYFKELP and SYSQHYGIPNPW, and these have been further investigated. ELISA assays together with pull-down experiments and ubiquitination assays showed that one twelve amino-acid long peptide in particular, KCCYFETHMPRH, was an interesting lead. Further investigation revealed that truncation on either side of the peptide abrogated its activity with respect to inhibition of ubiquitination of p53 by MDM2 *in vitro*. However, mutation of the C-terminal histidine into an alanine gave rise to a two-fold increase in potency. Although the lead peptide was active *in vitro*, it failed to show any binding in cell-based assays, a phenomenon that is quite common with peptides. Although its partition coefficient (estimated at log P = -0.87)[165] fits with Lipinski's rules, this peptide with more than five hydrogen bonding donors and ten hydrogen bonding acceptors, in common with many others, lies outwith Lipinski parameters. However, it is more and more frequent that researchers are moving away from this rule in order to reach new chemical entities, particularly when targeting protein-protein interactions. The design of peptidomimetics based on this peptide might increase its life time or cell permeability for a better activity in cell-based assays.

CHAPTER 2

Development of a new class of peptidomimetic

2.3 Introduction

2.3.1 Peptidomimetics

2.3.1.1 Different classes and structures

In order to understand protein-protein interactions (discussed in Chapter 1 Section 1.1.2), biochemists use peptides to either identify the active site of a protein or to identify the critical residues of an active peptide. Peptides as small as six amino-acid residues can be as active as the parent peptide or protein and fulfil the same role *in vitro* or in the cell.[166] Insulin was identified in the early twentieth century and purified in 1922. Since then, and more specifically over the past forty years, peptides have attracted attention as therapeutics with some success (Figure 2.3-1). CyclosporinA, discovered in 1972 and approved in 1983 is also worth noting. It is an immunosuppressant drug used to reduce the risk of organ rejection and its annual sales (including generic) are around 1 billion dollars. Angiotensin converting enzyme (*ACE*) inhibitors are used for the treatment of hypertension and congestive heart failure. The first ACE inhibitor is Captopril, approved in 1981 developed by Bristol-Myers Squibb has also reached over 1 billion dollars annual sales. Since Captopril, other ACE inhibitors such as Enalapril (Merck), Lisinopril (AstraZeneca), Trandolapril (Abbott), Cilazapril (Roche) and others have been developed. HIV-protease inhibitors. Saquinavir (Hoffmann-La Roche), Lopinavir and Ritonavir (Abbott; 1.4 billion dollar sales together in 2012), and Indinavir (Merck; 200 million dollar sales in 2010) (see also Figure 2.3-13) were launched on the market as HIV protease inhibitors between 1996 and 2000.[167]

In 2010, several other peptides reached over $1 billion/pa: glatiramer acetate (Copaxone; for multiple sclerosis; 10 aa's), leuprolide acetate (Lupron; for breast and

prostate cancer; 9 aa's), goserelin acetate (Zoladex; for breast and prostate cancer; 9 aa's) and octreotide acetate (Sandostatin; growth hormone inhibitor; 8 aa's).[168,169]

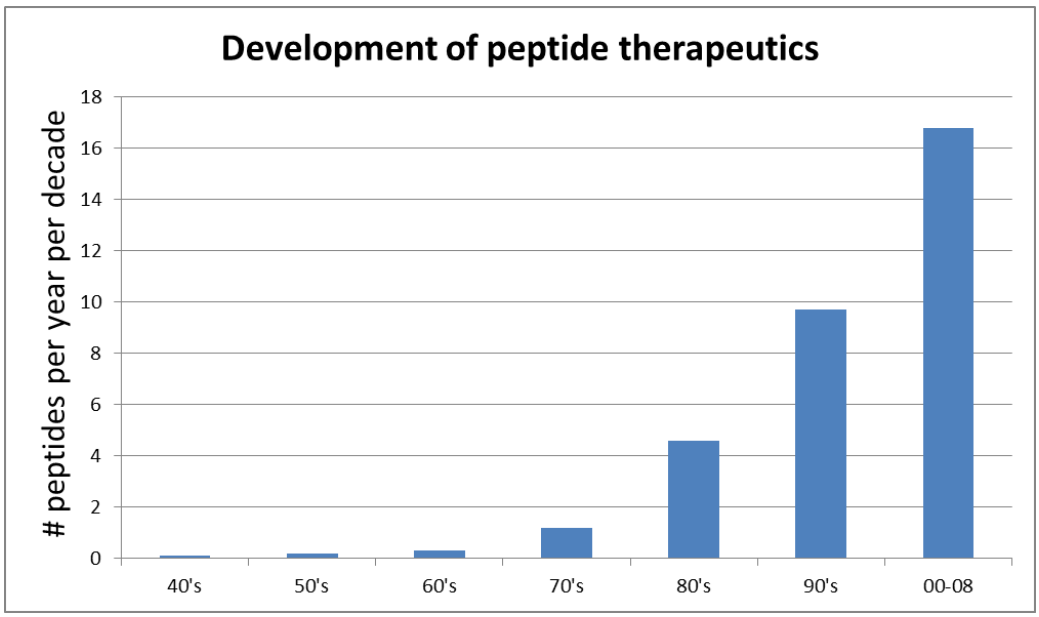

Figure 2.3-1. Peptides entering clinical study per year per decade. The data set includes a total of 435 peptides that entered clinical studies sponsored by commercial firms. Therapeutics and peptide vaccines were also included in the analysis[168]

Tufts Center for the Study of Drug Development and the Ferring Research Institute compiled publically available data and showed that a total of 334 peptides were reported as therapeutics since 1940. Of this data set, 41 are in Phase 1, 72 in Phase 2, 16 in phase 3. 149 peptides had been terminated and 54 had been approved for marketing.[168] The main categories for these approved peptides are oncology, obstetrics and gynaecology, allergy and immunology. Over the period 2001-2008, 10 peptides have been approved for the US market (Figure 2.3-2).

Company name	Generic name	Trade name	Treatment for	Year
Johnson & Johnson	Nesiritide	Natrecor, Noratak	Acutely decompensated congestive heart failure	2001
Lily	Teriparatide	Forteo	osteoporosis	2002
Trimeris	Enfuvirtide	Fuzeon	HIV-1 infection	2003
Praecis	Abarelix	Plenaxis	advanced prostate cancer	2003*
Elan	Ziconotide	Prialt	Severe and chronic pain	2004
Amylin	Pramlintide	Symlin	diabetes 1 and 2	2005
Amylin	Exenatide	Byetta	diabetes 2	2005
Ipsen	Lanreotide	Somatuline, Angiopeptin	acromegaly	2007
Amgen	Romiplostim	Nplate	Insufficient platelet production	2008
Ferring	Degarelix	Firmagon	advanced prostate cancer	2008

*Withdrawn from US market in May 2005 due to poor sales

Figure 2.3-2. FDA approvals 2001-2008.[168]

Peptides in clinical trials or on the market range from 2 to 50 amino acids. Their size distribution is shown in Figure 2.3-3.

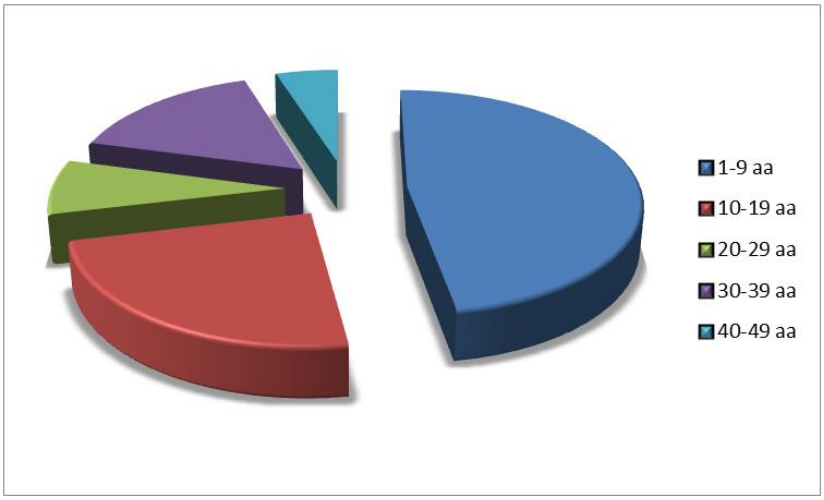

Figure 2.3-3. Size distribution of peptides (in terms of number of amino acids) on the market. Distribution established on 65 peptides.[169]

It is worth noting that many antibacterial peptides have been developed but few have been approved by FDA.[170] The decline was such that the Antibacterial Drug Development Task Force was launched in September 2012.[171] Major approved antibacterial peptides are the following: Nisin (DuPont) approved by the FDA in 1969, Caspofungin (Merck) in 2001, Daptomycin (Eli Lilly) in 2003, Micafungin (Astellas Pharma) in 2005, Anidulafungin (Pfizer) in 2006 and Telavancin (Theravance) in 2009.

High clearance, low membrane permeability and bioavailability of peptides usually limit their potential as oral drugs.[172,173] For these reasons, marketed peptides are mostly delivered via injection (i.e. insulin).
Due to their flexibility, short unbound peptides tend to be rather disordered in aqueous solution. However, they can adopt a conformation when bound to a protein.[174,175]

Peptidomimetics, as mimics of peptides, are designed with the purpose of retaining their activity toward the target and improving bioavailability and resistance to proteolysis. Different classes of peptidomimetics have been described over the past decades (Figure 2.3-4 and Figure 2.3-5).

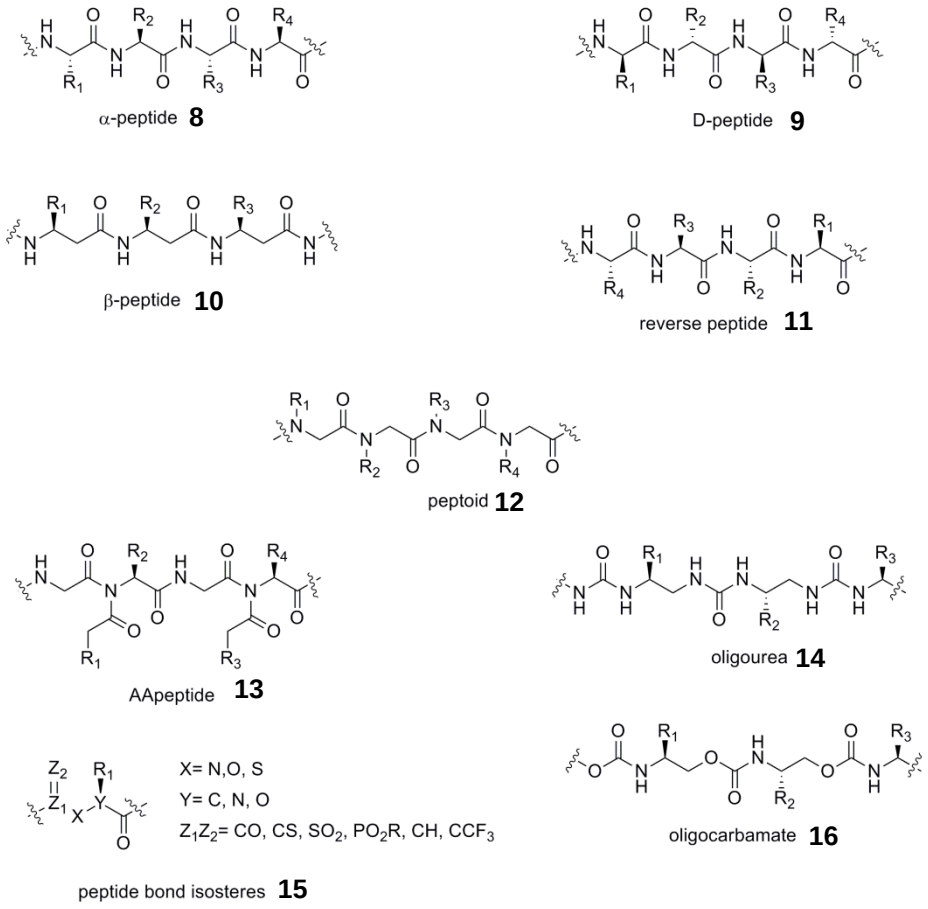

Figure 2.3-4. Examples of classes of peptidomimetics.

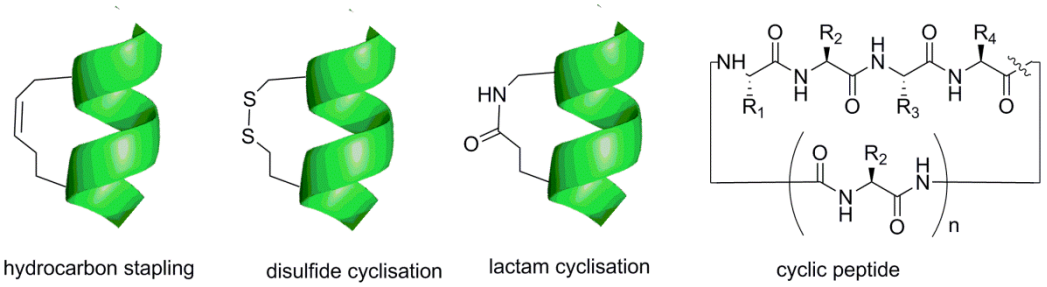

Figure 2.3-5. Examples of cyclised peptidomimetics.

A peptide's conformation is ultimately determined by its primary amino acid sequence. Amino acid properties and positions define the possible interactions that can occur

through the peptide. Interactions such as hydrogen bonding (through side-chains or the amide backbone), ionic bonding, disulphide bridging and hydrophobic interactions will influence the secondary structure of the peptide allowing the formation of α-helices, parallel or anti-parallel β-sheets or β-turns (Figure 2.3-6). However, the overall structure of peptides or proteins remains difficult to predict due to the numerous possible interactions. A specific conformation is usually required for activity and is often achieved upon binding on the target. Since many peptides adopt an α-helical conformation when bound to the target, great effort has been put into the design of peptidomimetic in which the molecule adopt this desired conformation.

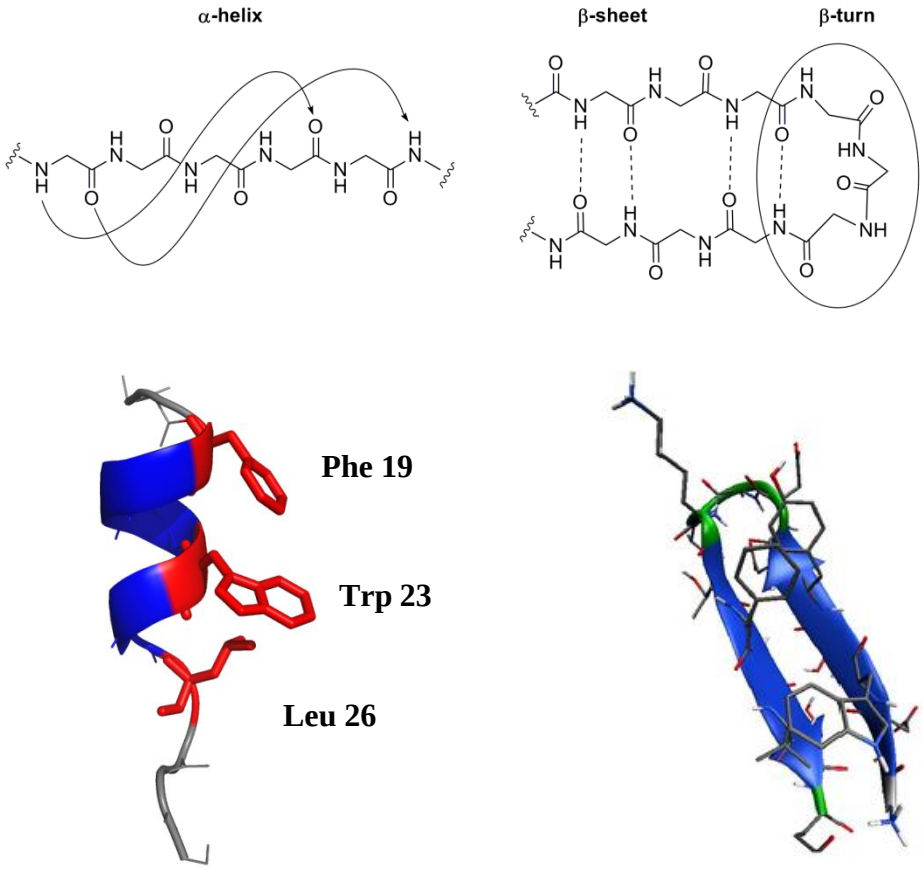

Figure 2.3-6. Possible modes of hydrogen bonding in a peptide. In the bottom panel, ribbon representations of the p53 peptide (left) and a fragment of B1 domain of protein G (GB1).[176,177]

D-amino acid containing peptides, also known as D-peptides, such as **9**,[178] offer the advantage of resistance to protease degradation and are synthesised in a similar manner

to L-peptides. Key residues of an α-helical D-peptide might face the target in as the equivalent L-peptide does.

β-peptides **10** are composed of β-amino acids and can form different helical structures, the 8-helix, 10-helix, 12-helix, 14-helix, 10/12-helix[179] (Figure 2.3-7, Figure 2.3-8).

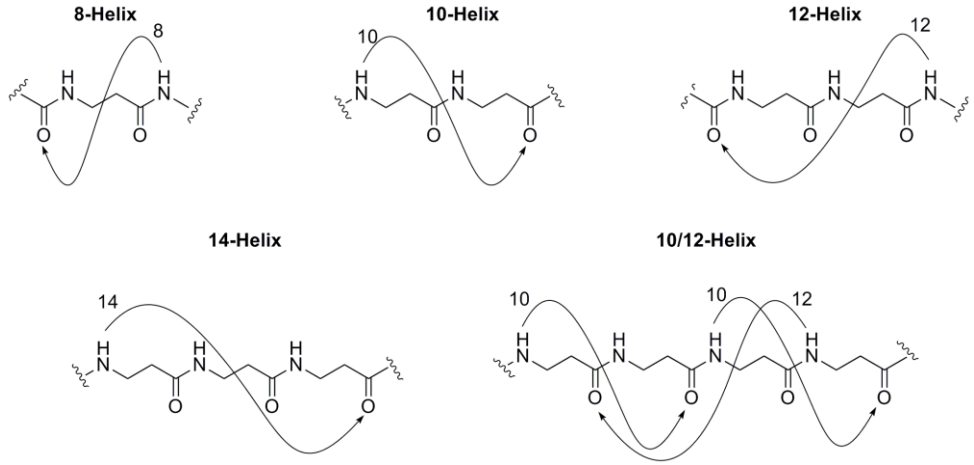

Figure 2.3-7. Common helical structures in β-peptides.[179]

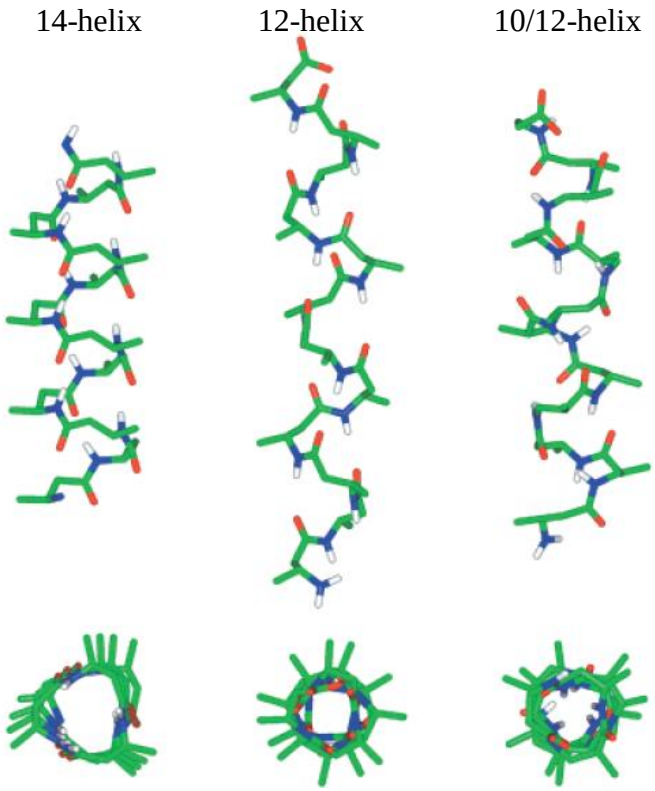

Figure 2.3-8. Structure of 14-helix, 12-helix and 10/12-helix. Carbon atoms in green, nitrogen in blue, oxygen red, and amide hydrogen in white (other hydrogens are omitted for clarity). Reproduced with permission.[179]

The Rana group has designed oligocarbamate **14** and oligourea **16** as peptidomimetics of the Tat peptide H-GlyArgLysLysArgArgGlnArgArgArg-OH.[180] These peptidomimetics have been shown to be non-toxic to the cell and inhibit Tat-TAR interactions *in vivo*.

Peptoids **12**, poly N-substituted glycines, have been used in many fields. The Bradley group has designed peptoids based on the Tat peptide and used them as cell penetrating moeities.[181]

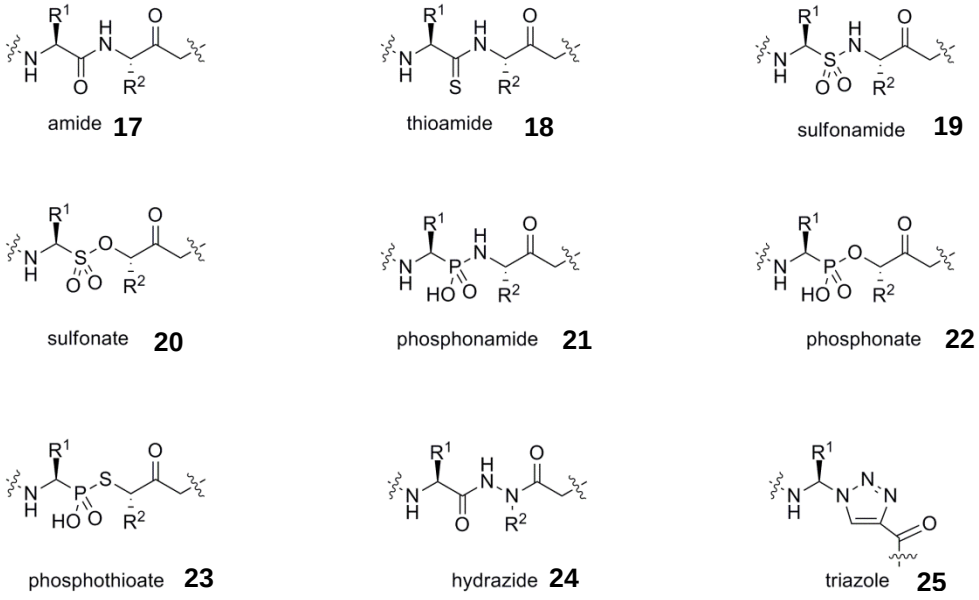

Figure 2.3-9. Examples of peptide bond isosteres [182-186]

Numerous peptide bond isosteres have been reported (Figure 2.3-9) such as thioamides **18**,[182] sulphonamides **19**,[183] sulfonates **20**,[184] phosphonamidates **21**, phosphonates **22** or phosphothioates **23**,[185] and hydrazides **24**[186] (non-exhaustive list). Another final example is the substitution of an amide bond with a triazole. These 1,4-disubstitued 1,2,3-triazoles seem to show similar hydrogen-bonding properties to amide bonds. They have been incorporated in derivatives of amprenavir, an HIV-1 protease inhibitor[187] or in derivatives of a cyclic peptide as tyrosinase inhibitors.[188]

Most peptidomimetic structures have their cyclic homologues; cyclic peptides[188] such as **26** and peptoids[189-191] such as **27, 28** and **29** have been developed, either by head-to-tail cyclisation[189,191] or by side-chain to side-chain cyclisation. There are many options for length and the rigidity of the linker, the bridge location between

side-chains, as well as the reaction to form the bridge; each can potentially modify the conformation of the cyclic peptidomimetic. Whether for side-chain to side chain or head-to-tail cyclisation, lactam and disulfide bridge formation are the most commonly utilised historically.

Hybrids of these peptidomimetics can be made by mixing different subunits. Among them, peptoid-peptide hybrids[192-194] **30**, **31** and **32** can be mentioned as well as β-peptide-peptide **33**,[195,196] β-peptoid-peptide hybrids and α,β-peptoids **34.**[197]

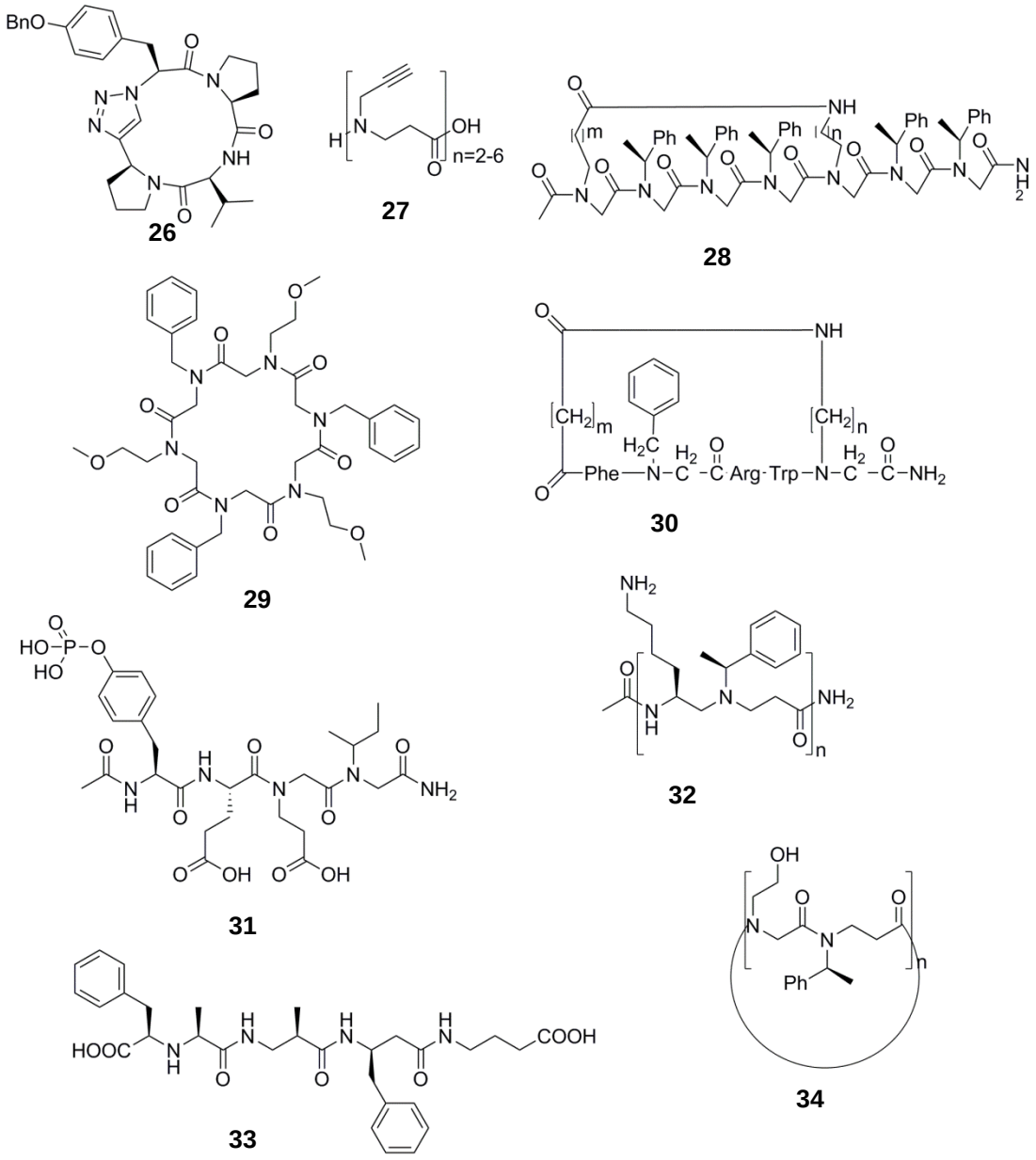

Figure 2.3-10. Examples of cyclised peptidomimetics.[188-193,195-197]

Molecular "stapling" refers to side-chain to side-chain cyclisation to lock a specific conformation. Typically this is achieved using side-chains which are both projected on the face of the peptide facing away from the target and thus are spaced at 3.6 residues per turn for an ideal α-helical peptide. The position of the bridge is often crucial as the bridge could interfere with molecular recognition (Figure 2.3-11).

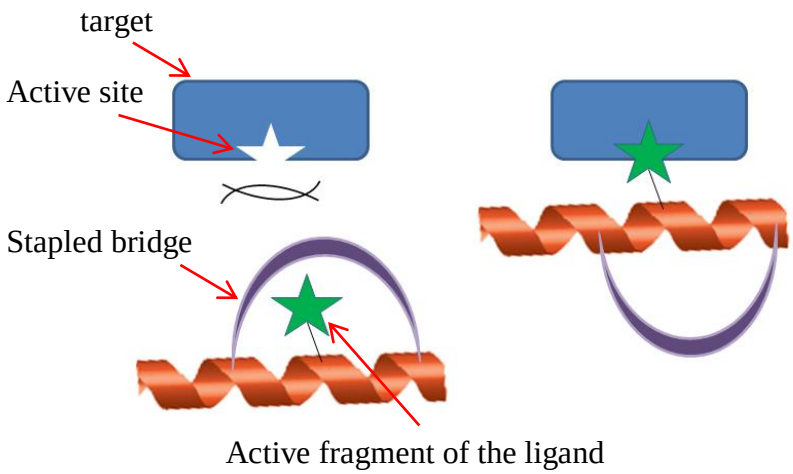

Figure 2.3-11. Importance of stapling position. The target is represented in blue; in green the ligand fitting the active site; the bold black line represents the bridge.

This helical conformation can be stabilised with lactam ,[198] salt[199] or disulphide (**35**)[200] bridge formation, with hydrophobic interactions (**37**),[201] metal ligation (**36**)[202,203] or hydrocarbon[204] stapling (**38**). To enhance helix stability, the Verdine Group has incorporated modified amino acids bearing olefinic side-chains in the peptide and has then connected, or "stapled", them across turns of the peptide them via olefin metathesis to form peptidomimetic **39**.[205] Other Ring-Closing Metathesis (RCM) examples have been reported since.[206-208]

As with peptides, peptoids stapled via lactam bridge formation such as **28** have been reported to display a stable helix.[190]

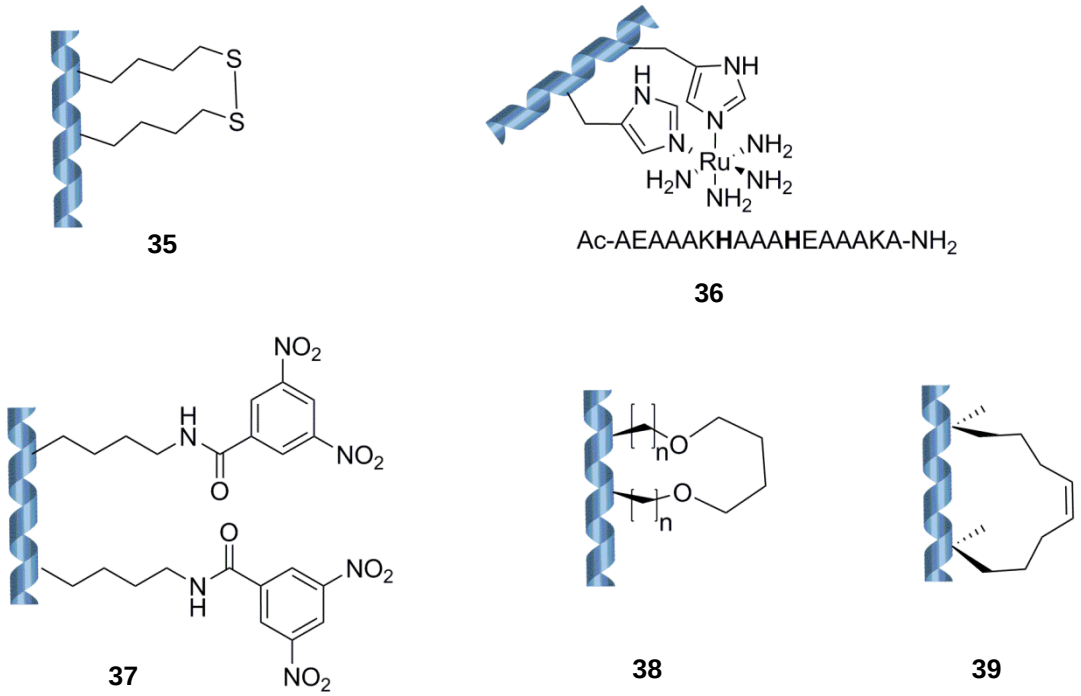

Figure 2.3-12. Examples of cyclised peptidomimetics with a stabilised α-helix.[200,201,203,204,207]

Some of the first peptidomimetics were designed to inhibit HIV-protease. Saquinavir **40**, Ritonavir **41**, Indinavir **42**, and Lopinavir **43** (Figure 2.3-13) were launched on the market as HIV protease inhibitors between 1996 and 2000.[167] Stapled peptidomimetic inhibitors are yet to be launched on the market.

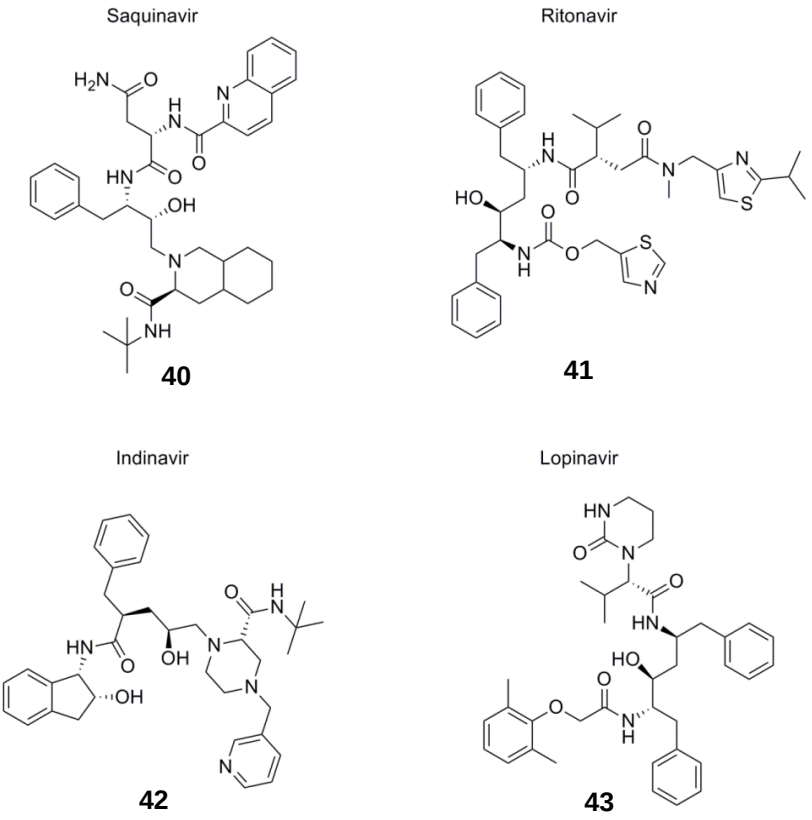

Figure 2.3-13. FDA-approved HIV-protease inhibitors.[167]

2.3.1.2 Cyclic peptoid-peptide hybrids

Linear peptoid-peptide hybrids were one the first hybrids to be studied **44**.[209] Cyclic peptoids **45**[210] or cyclic peptoid-organic hybrids **46**[211] were then reported (Figure 2.3-14).

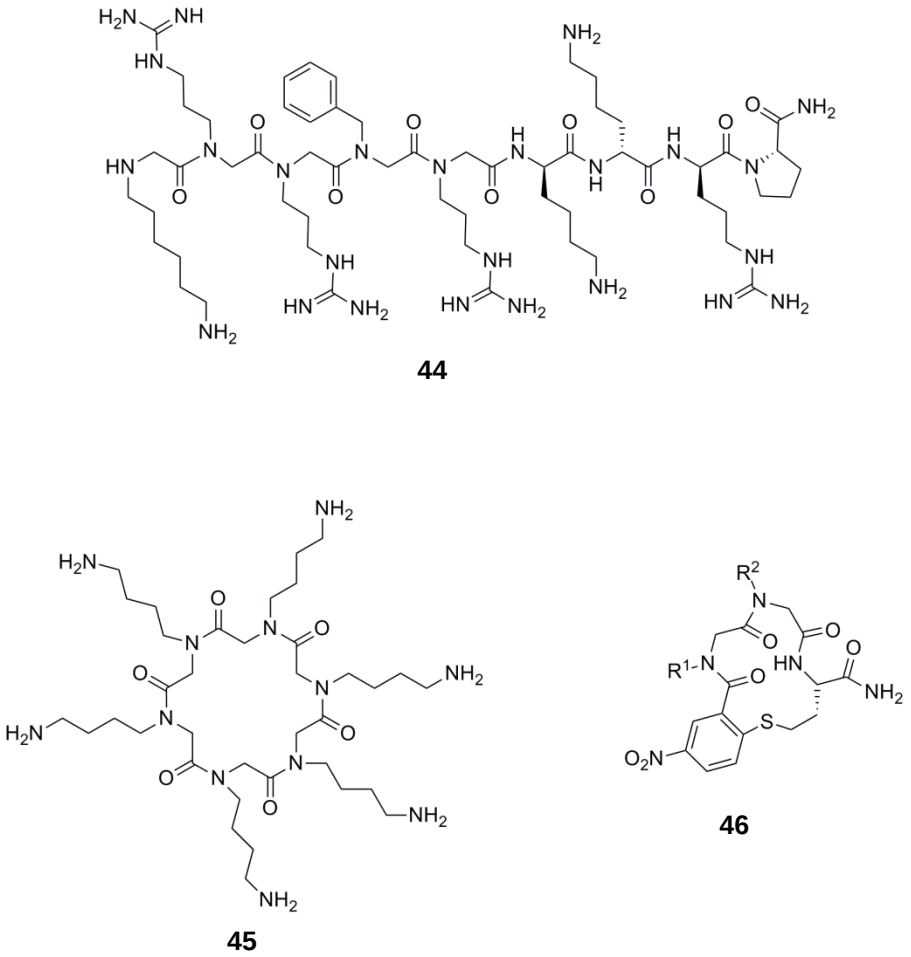

Figure 2.3-14. Examples of peptoid hybrids. Linear peptoid-peptide hybrid 44, cyclic peptoid 45, cyclic semi-peptoid 46.[209-211]

However, little has been reported about cyclic peptoid-peptide hybrids. Nevertheless, cyclic peptoid-peptide hybrids have been synthesised.[212] The Ghadiri group has recently reported the design of macrocyclic peptoid-peptide hybrids **48** as inhibitors of Class I Histone Deacetylases (HDAC) with equivalent activity to apicidin **47** (Figure 2.3-15), with IC_{50} values of 180 nM and 11 nM, respectively.[212]

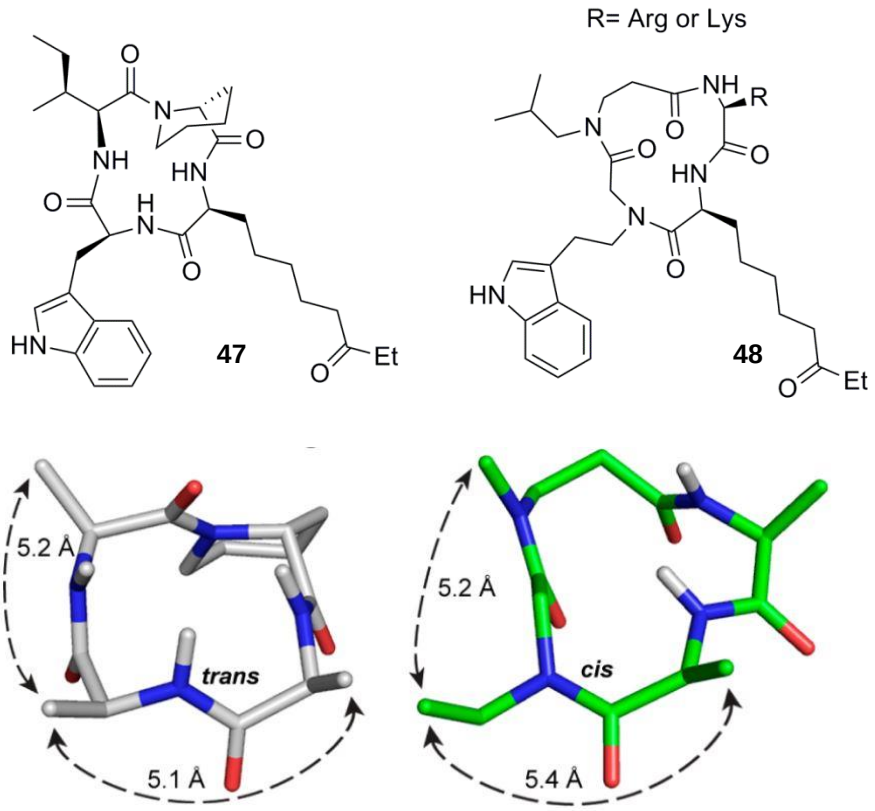

Figure 2.3-15. Apicidin 47 (left) and a cyclic peptoid-peptide hybrid mimic 48 (right). Side-chains in NMR structures were removed for clarity. Reproduced with permission.[212]

A common technique to generate a cyclic peptoid-peptide hybrid is to displace some of the side-chains of α-carbons to their adjacent nitrogens of a cyclic peptide.[213] The Blackwell group has synthesised such a molecule, **49**, based on a cyclic peptide **50**, the auto-inducing peptide I from *Staphylococcus aureu*s (Figure 2.3-16).[214]

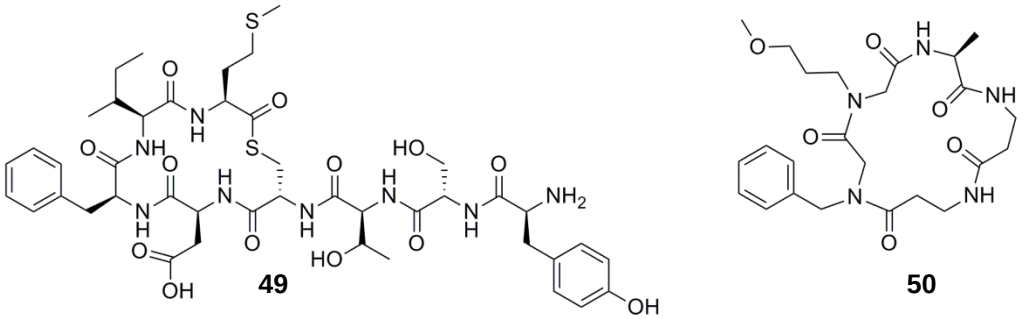

Figure 2.3-16. *S. aureus* peptide I autoinducing peptide 49 and its analogue 50.[214]

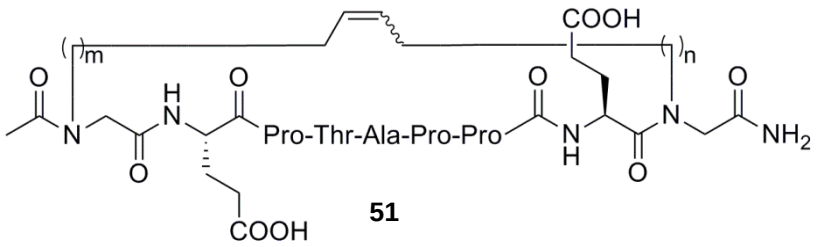

51

Figure 2.3-17. Peptoid-peptide hybrid cyclised by ring-closing metathesis.[215]

Cyclic peptoid-peptide hybrids such as **51** can be generated from a linear peptide by cyclisation through N-alkyl side-chains (Figure 2.3-17).[215]Cyclic peptoid-peptide hybrids formed through CuAAC triazole formation exist and will be discussed in Section 2.3.1.3.

However, to our knowledge, no peptoid-peptide hybrid has been reported with cyclisation through their N-alkyl propargyl or azido units.

2.3.1.3 Click chemistry and its applications

The concept of "click" chemistry was popularised by Sharpless and co-workers in 2001.[216] The term "click chemistry" was initially characterised by a set of criteria such as simplicity and modularity of a reaction, high yields, a wide scope, stereospecificity and simple isolation of the product. Although different reactions fall within this definition, the term "click chemistry" is often used to refer to the copper(I)-catalysed azide-alkyne cycloaddition (CuAAC).[217,218] Huisgen and co-workers originally developed the uncatalysed 1.3-dipolar cycloaddition in 1963.[219] However, the uncatalysed reaction usually gives rise to a mixture of the 1,4- and 1,5- regioisomers. In the search for a means of controlling this regioselectivity, copper catalysis has been found to offer an excellent method for the preparation of 1,4 triazoles.[220] Different copper sources can be used to catalyse this reaction; Cu(I) salts such as CuI can be used directly and usually require a nitrogen base (triethylamine, diisopropylethylamine, 2,6-lutidine, pyridine) to help stabilise the Cu(I) species. Alternatively, the method which is usually preferred consists of the use of a Cu(II) source in combination with a reductant, typically sodium ascorbate to generate Cu^{I} *in*

situ. Other additives such as tris-[(1-benzyl-1*H*-1,2,3-triazol-4-yl)methyl]amine (TBTA **52**) can be used in order to stabilise the Cu^{I} state of the catalyst (Figure 2.3-18).[221-223]

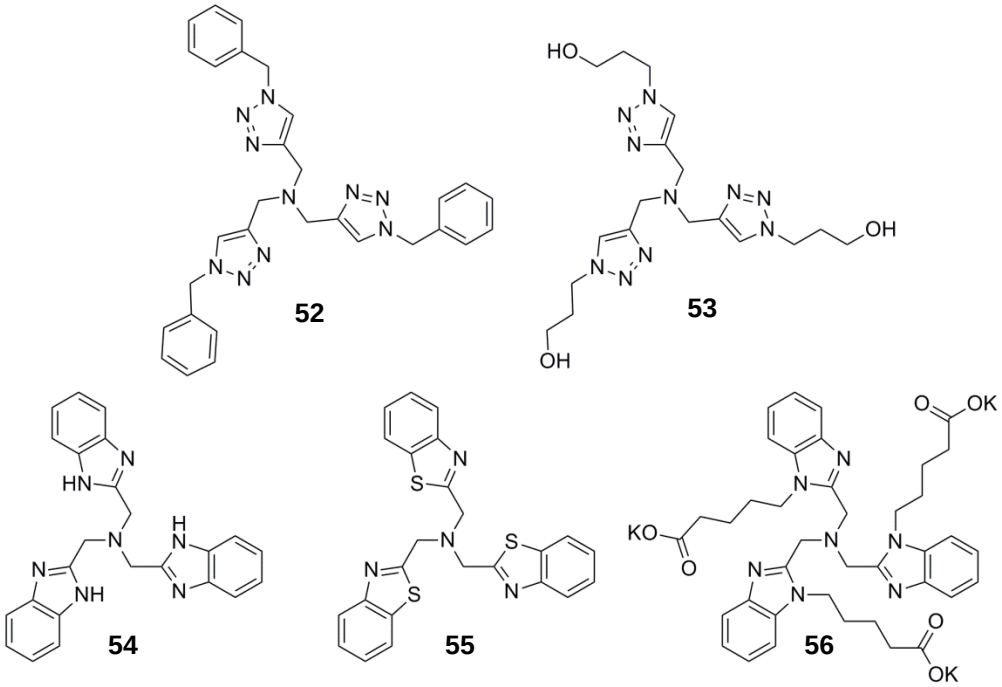

Figure 2.3-18. Commercially available ligands for CuAAC reactions.[221-223]

Although Cu(I) is toxic, therefore incompatible with living cells, the use of the ligand tris(3-hydroxypropyltriazolylmethyl)amine (THPTA) **53** was shown to have a protective effect on cells over the first five minutes, which was enough for CuAAC to occur on the surface of living cells.[222] A method was developed by Bertozzi *et al.* promoting a copper-free cycloaddition between fluorinated cyclooctynes and azides installed metabolically on cell surfaces (Figure 2.3-19).[224] Cycloaddition occurred as quickly as in copper-catalysed reactions and no toxicity was observed.

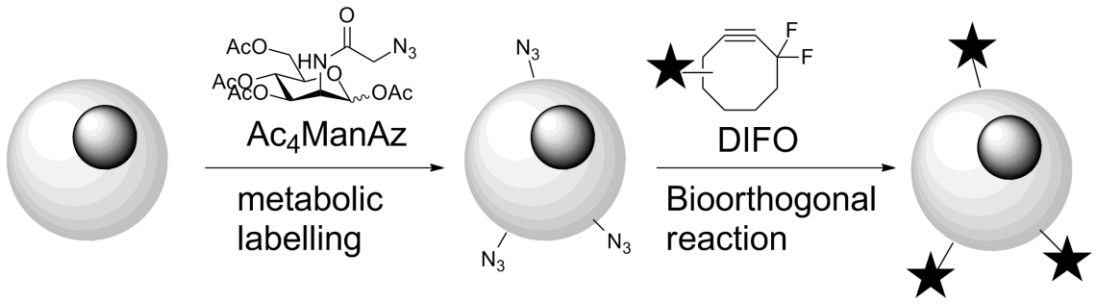

Figure 2.3-19. Metabolic labelling of the cell surface with Ac_4ManAz and detection of cell surfaces glycans using tagged cyclooctyne.[224]

With mild conditions including water as solvent without any co-solvent, tolerance of a wide pH range, and typically room temperature conditions, CuAAC is a versatile reaction, compatible with biological applications.

Click chemistry has been employed in a broad range of applications. Triazole formation has been used in the synthesis of branched polymers,[225] rotaxanes,[226] modified peptides, DNA analogues,[220] carbohydrate oligonucleotides conjugates,[227] in the functionalisation of nanoparticles,[228] in the generation of high-throughput libraries[229]. One striking example has been the optimisation of acetylcholinesterase (AChE) inhibitors through target-guided synthesis.[223] Indeed, using a library of tacrine and phenylanthridinium building blocks generating 104 potential products, 4 inhibitors (Figure 2.3-20), **57-60**, with dissociation constants in the femtomolar range have been identified when incubated with AChE for 1 day.[230] Following the success of enzyme-genenerated inhibitors of AChE, a similar strategy has been applied to assemble inhibitors of Carbonic Anhydrase II and has led to the *in situ* generation of inhibitors with low nanomolar dissociation constants.[231]

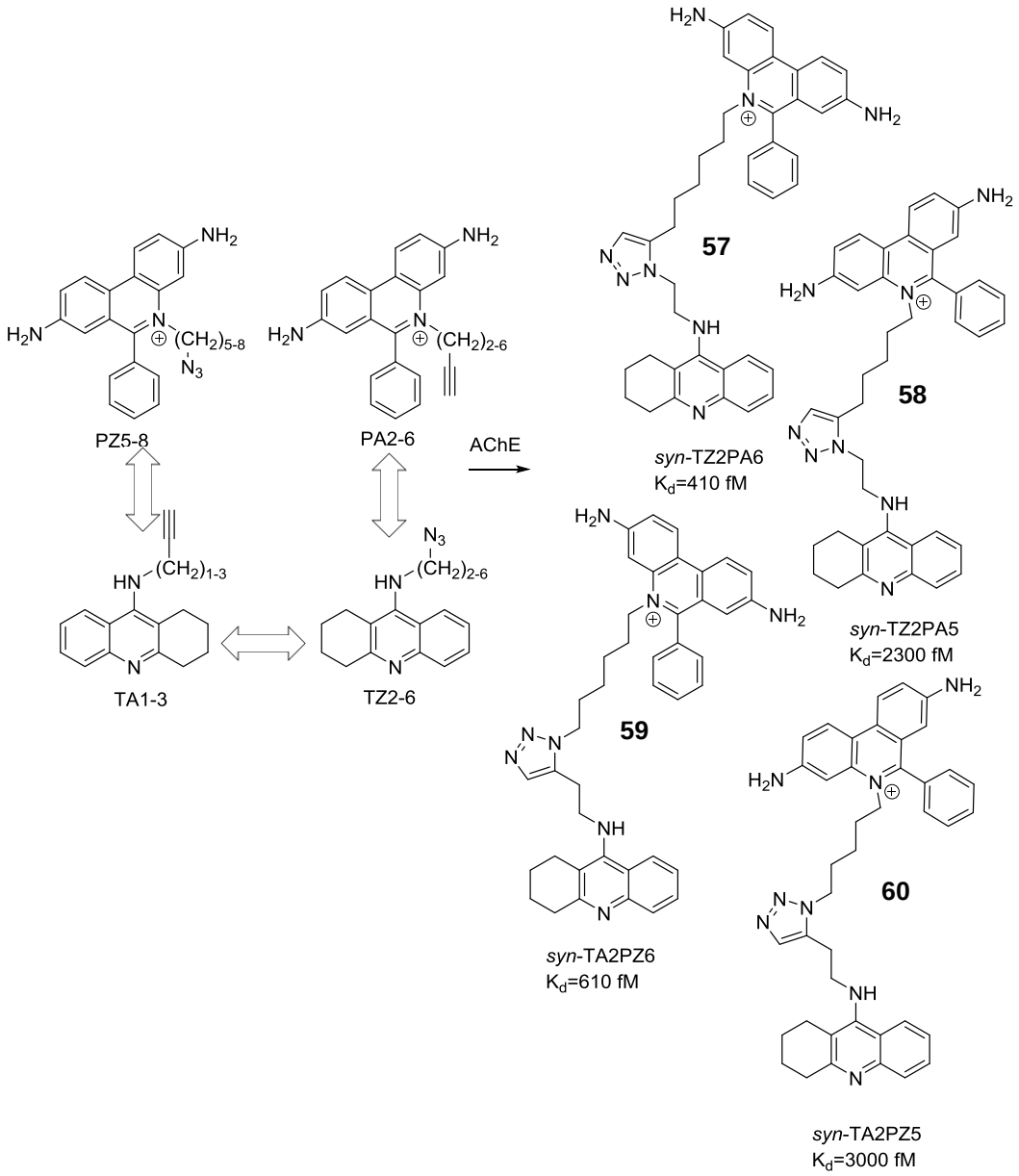

Figure 2.3-20. *In situ* click chemistry screening developed by Sharpless group. Double arrows indicate *in situ* pairs (52 combinations; 104 potential products). 4 products were selected following incubation with AChE: *syn*-TZ2PA6 **57**, *syn*-TZ2PA5 **58,** *syn*-TA2PZ6 **59,** *syn*-TA2PZ5 **60**. [230]

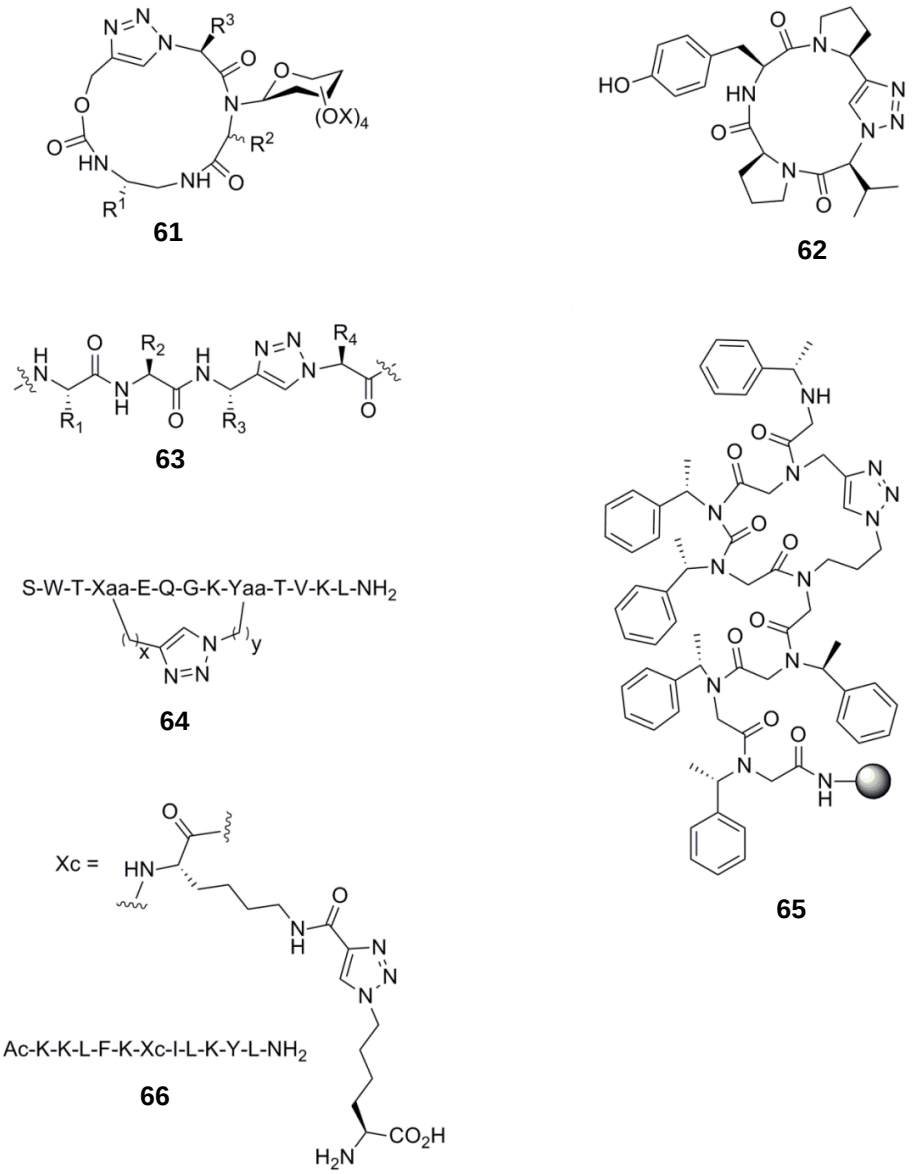

Figure 2.3-21. Examples of peptidomimetics with click chemistry. Glycopeptidomimetics **61**, cyclo-[Pro-Val-y(triazole)-Pro-Tyr] **62**, peptidomimetic synthesised by azide-alkyne ligation **63**, stapled peptide **64**, on-resin cyclised peptoid **65**, side-chain modification with triazole rings **66**.[232-236]

Very recently, triazole formation in peptidomimetic chemistry has seen a tremendous success (Figure 2.3-21). Using this reaction, glycopeptidomimetics **61** cyclic peptides **62** and have been successfully synthesised by head-to-tail cyclisation.[235,236] In a similar fashion to cysteine-assisted ligation, azide-alkyne ligation has enabled the synthesis of a peptidomimetic; the newly formed triazole is incorporated in the backbone of the peptide homologue **63** with the advantage of a comparable dipolar moment.[234] The

triazole can also be introduced on to side-chains as shown on peptidotriazole analogues **66** of an antimicrobial peptide.[233]

Triazole bridge formation has been applied to stapled peptides **64**[237,238] by introducing ω-azido- and ω-alkynyl-L-amino acids as building blocks.[239] Another group has formed a 3_{10}-helix on a peptide by introducing an *O*-propynyl serine **67**.[240]

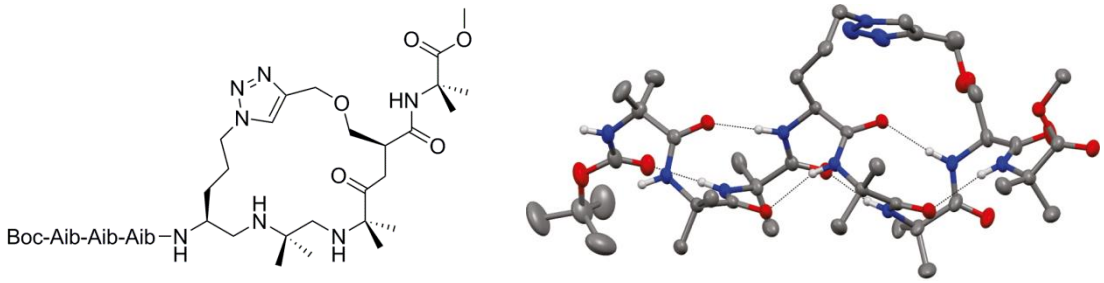

Figure 2.3-22. Stapled 3_{10}-helical aquaporin-4 **67** (left) and its X-ray crystal structure (right). The acyclic peptidomimetic was cyclised by click chemistry. Reproduced with permission.[240]

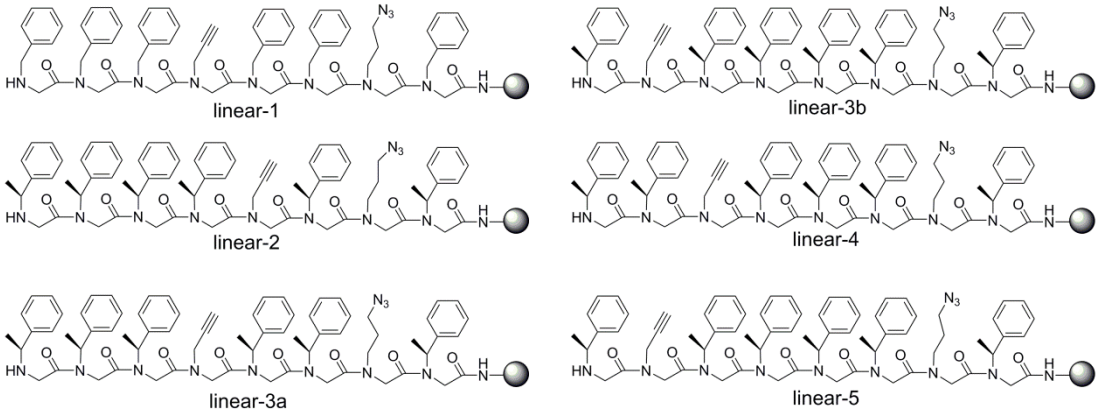

Figure 2.3-23. Peptoids used in cyclisation reactions with click chemistry.[232]

The Kirshenbaum group has used click chemistry on peptoids, creating a library of *N*-phenylethyl glycine peptoids **65** with click building blocks (Figure 2.3-23). Following cyclisation by CuAAC, HPLC revealed the presence of two main products, the cyclic monomer and the cyclic dimer. Linear-1 (*i*, *i*+3), linear-3a/3b (*i*, *i*+3) and linear-4 (*i*, *i*+4) had a monomer:dimer ratio of 2:1, 4:1 and 3:1 respectively. However, linear-2 (*i*, *i*+2) and linear-5 (*i*, *i*+5) offered a 1:1 and 1:2 ratio. This would suggest that intramolecular cyclisation is favoured by a pre-ordered helical conformation.[232]

2.3.1.4 Peptidomimetics in the p53-MDM2 interaction

As we have seen in Chapter 1 (Section 1.1.7), the numerous p53 interactions offer many options for the control of function through the disruption of PPIs. Regarding the p53-MDM2 interaction, most of the known active compounds interact with the N-terminus of MDM2. Non-peptidic small molecules have been discussed in Chapter 1 (Section 1.1.7). In the following section, peptidomimetics of the p53-MDM2 interaction (Figure 2.3-24) will form the main focus.

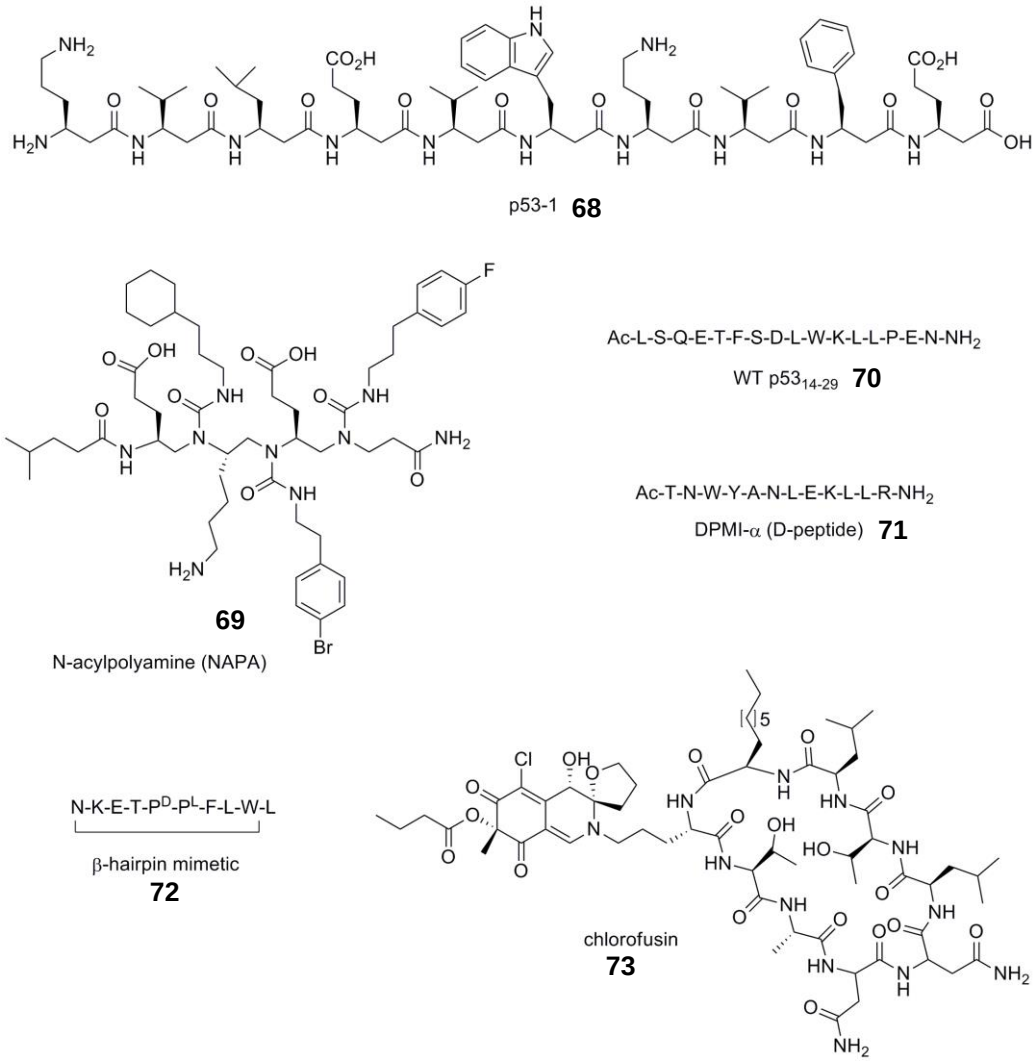

Figure 2.3-24. Peptidomimetic inhibitors of the p53-MDM2 interaction.[241-248]

The first class of inhibitors which have been investigated are cyclic peptides such as chlorofusin **73**, a 9-residue cyclic peptide composed of common and uncommon amino

acids has been described as one of the first inhibitors of the p53-MDM2 interaction.[242] A second class of inhibitors which have been investigated are β^3-peptides which form a 14-helix. Although the dimensions of a 14-helix are different from an α-helix, the 14-helix has almost three residues per turn. Therefore, the side residues should align nicely on key residues Phe^{19}, Trp^{23} and Leu^{26} of the p53 N-terminus upon binding which render 14-helical β^3-peptides well suited to this system.[241] Optimisation of β^3-peptide leads using *in silico* methods has been performed by adding a Cl atom at position 6 of tryptophan in the recently published β^3-peptide **68**.[243] β-Hairpin peptidomimetics have also been investigated. Indeed, the optimised inhibitor **72** (IC_{50} = 140 nM) has been synthesised using a β-Hairpin core with the three key residues attached and can mimic the p53-peptide α-helix.[249] Others have developed an *N*-acylpolyamine (NAPA) **69** scaffold and its flexibility enables its adaptation to either MDM2 or MDMX.[244] D-peptides, have been identified which target the p53-MDM2 interaction. However, they failed to cross the cell membrane without being encapsulated in liposomes displaying an integrin-targeting cyclic RGD peptide.[245]

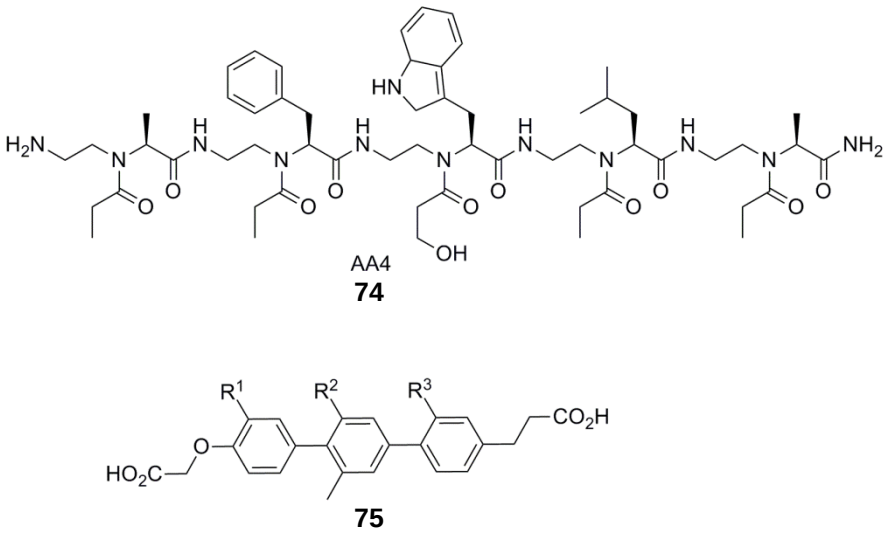

Figure 2.3-25. Peptidomimetic inhibitors of the p53-MDM2 interaction.[143,248]

Terphenyl derivatives **75** have been designed to inhibit the p53-MDM2 interaction. The phenyl rings of terphenyls adopt a conformation such that the R substituents in *ortho*- positions are displayed like amino acids along one face of α-helix.[143] AApeptides **74** (AA for *N*-acylated-*N*-aminoethyl) (Figure 2.3-25) have the same

length of backbone and same number of side-chain functional groups as their respective α-peptides.[248] Because of the *N*-substitutions on the amide bonds, higher flexibility of the backbone is expected which will affect the activity. These AApeptides have been applied to the p53-MDM2 interaction and some display a similar activity and increased resistance to degradation relative to the original peptide.[248]

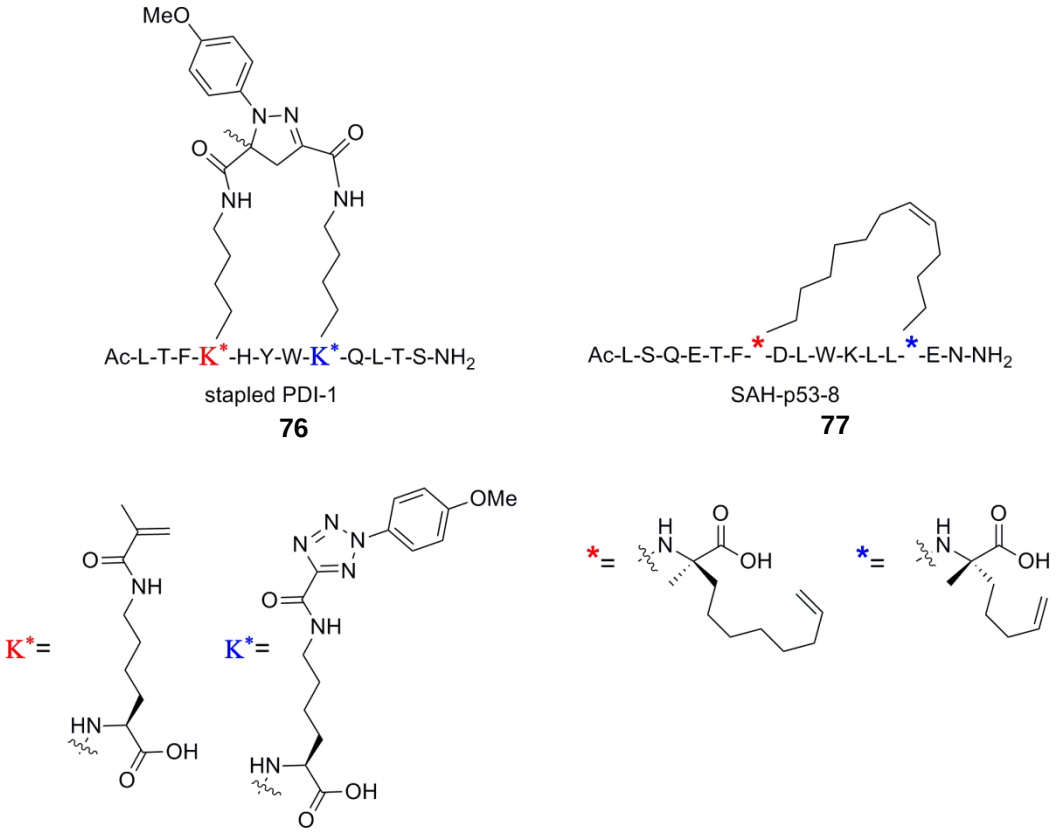

Figure 2.3-26. Peptidomimetic inhibitors of the p53-MDM2 interaction. Top panel: **76** and **77** are shown in their cyclised form; bottlom panel: building blocks used for the synthesis of **76** and **77**.[246,247]

Among the recent examples of the application of peptide stapling to the p53-MDM2 interaction through all-hydrocarbon[246] bridge formation, SAH-p53-8 peptidomimetic **77**, a hydrocarbon-stapled p53 peptide, has been found a 25-fold greater binding activity for human MDMX compared to human MDM2 and can act synergistically with Nutlin-3 to overcome p53 suppression. Photo-induced cycloaddition[247] has also been proved a useful to way to synthesise cyclic p53 peptide. One such analogue, dihydropyrazole **76,** has shown a 200-fold increase in the MDM2 activity relative to its linear version.

At the time when the project was started, only a few peptidomimetics had been reported where click chemistry had been used to staple peptides or peptoids. With the peptide lead discovered using phage display as described in Chapter 1 (Section 1.2.2), a peptide able to inhibit the MDM2-mediated ubiquitination of p53 *in vitro*, the question whether a method for the synthesis of cyclic peptoid-peptide hybrids via CuAAC could be designed was addressed. Peptide-peptoid hybrids were synthesised using a solid phase approach, and an efficient production of the different azide and alkyne building blocks for SPPS was required. The question of whether triazole formation could be conducted, both on solid support and in solution, was addressed.

2.4 Synthesis of amino acid derivatives

The identification of Ac-KCCYFETHMPRH-NH_2 as an active peptide able to inhibit MDM2-mediated ubiquitination of p53 *in vitro* was used as the basis for an investigation into a new class of peptidomimetics. At the start of the project, no peptoid-peptide hybrids generated using click chemistry with *N*-propargylated or *N*-azidoalkyl buiding blocks had been reported. For this reason, synthesis of building blocks (Figure 2.4-1) bearing *N*-alkyl alkynes or *N*-alkyl azides with different chain lengths were designed. Once the building blocks were available, Solid Phase Peptide Synthesis (SPPS) of a library of peptidomimetics based on the shorter peptide Ac-KCCYFE-NH_2 was anticipated. This SPPS library of twenty four linear peptoid-peptides was designed so that the peptoid building blocks were placed at different positions, allowing triazole bridge formation to be attempted both on solid support and in solution.

103 = A* **97-99** = Z^*_3-Z^*_5

Figure 2.4-1. Building blocks for the synthesis of peptoid-peptide hybrids.

2.4.1 Building block versus submonomer strategy

When the building blocks were designed, two main synthetic possibilities were available; they could either be synthesised *in situ* on the resin following the submonomer strategy introduced by Zuckermann,[250] or the complete amino acid derivative could be introduced just as for any classical Fmoc-protected amino acid. The submonomer strategy involves a two-step process to introduce the desired peptoid monomer (Scheme 2.4-1).

The first step is the acylation of an unprotected secondary amine with bromoacetic acid mediated by DIC. The second step is a nucleophilic substitution of the bromine by an amine thereby generating the peptoid monomer.

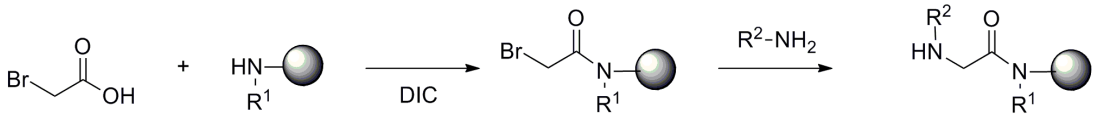

Scheme 2.4-1. Peptoid submonomer synthesis introduced by Zuckermann.[250]

However, in our case, the second step of this process would require the manipulation of relatively hazardous azido amines. For this reason, the approach of synthesising Fmoc-protected *N*-azidoalkyl glycines **97-99** (Section 2.4.2) has been chosen. It has the advantage of offering a building block readily available for any chemist or biologist familiar only with knowledge of SPPS. Moreover, once synthesised the monomer would be coupled in a single step instead of two and it could be more easily used with an automated peptide synthesiser or in manual parallel peptide syntheses. Also the azide group would be added to a relatively large building block precursor as the last step, providing greater safety in handling of the building block.

2.4.2 Generation of *N*-azidoalkyl Glycine

In the hunt for literature on the building blocks, no paper had yet reported the required *N*-alkyl azide Fmoc-protected peptoid building blocks. Closest to to the desired building blocks, the Bradley group had reported the synthesis of an Fmoc-protected lysine-like peptoid monomer (Scheme 2.4-2).[251]

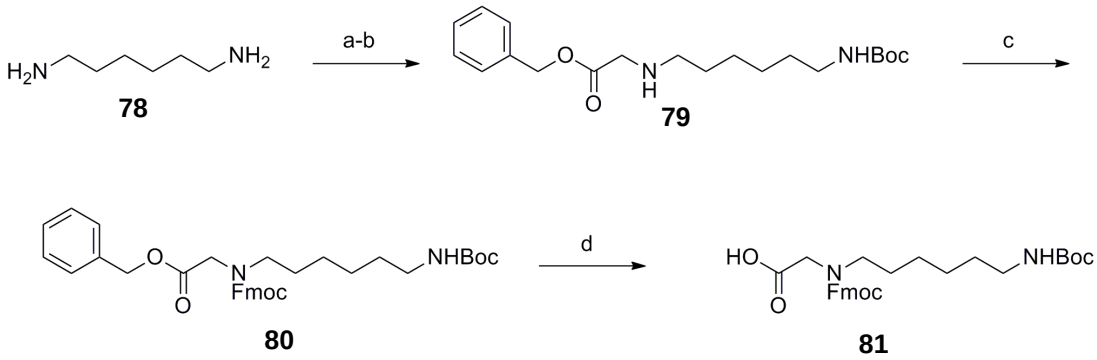

Scheme 2.4-2. Lysine-like monomer synthesis from the Bradley group. (a) Boc_2O (0.15 equiv.), DCM, 14 h; (b) benzyl 2-bromacetate (1 equiv.), Et_3N (3 equiv.), THF, 24 h, two steps 54%; (c) Fmoc-OSu (1 equiv.), THF, 5 h, 90%; (d) H_2 (1 atm), Pd-C, MeOH, 4 h, 80%.[251]

The *N*-azidoalkyl glycine monomer synthesis is directly inspired by this work and the synthetic steps are shown in Scheme 2.4-3.

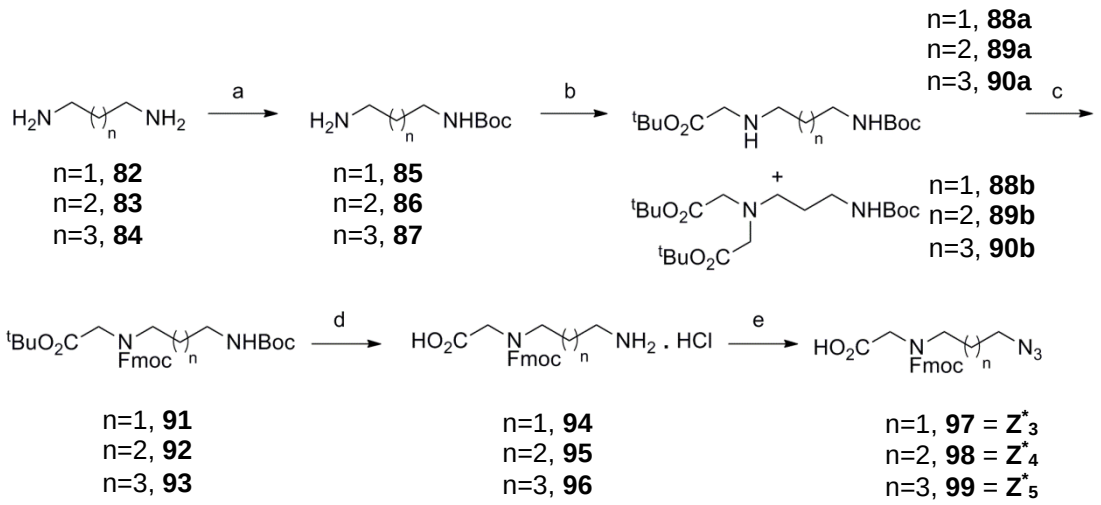

Scheme 2.4-3. Synthesis of *N*-azidoalkyl glycine monomers. (a) Boc_2O, DCM, rt, 18 h, **85** 96%, **86** 95%, **87** 94%; (b) *tert*-butyl 2-bromoacetate, Et_3N, THF, rt, 18 h, **88a** 54%, **89a** 51%, **90a** 62%; (c) Fmoc-OSu, DCM, rt, 18 h, **91** 94%, **92** 91%, **93** 88%; (d) i. 80% TFA in DCM, rt, 18 h; ii. AcCl in EtOH, 0°C, **94** 91%, **95** 90%, **96** 91%; (e) imidazole-1-sulfonyl azide.HCl, $NaHCO_3$, 2 mol% $CuSO_4$, **97** 87%, **98** 81%, **99** 89%.

Instead of the 1,6-hexanediamine, we used 1,3-propanediamine **82**, 1,4-butanediamine **83** and 1,5-propanediamine **84** as starting materials. The different chain lengths would hopefully give some insight into the preferred constraints when the peptoid-peptide hybrids are cyclised. Due to the presence of the two amino groups, mono *N*-*tert*-butoxycarbonyl protection was required. Di-*tert*-butyl dicarbonate was added to a solution containing an excess of diamine **82-84** (8 equiv.) in order to minimise di-Boc protection. After solvent evaporation, di-protected amines were occasionally observed but these were readily separated by filtration. The desired carbamates **85-87** required no further purification after extraction and could be synthesised on multigram scale to give pale yellow oils with excellent yield (up to 95%). The subsequent nucleophilic substitution reactions with *tert*-butyl 2-bromoacetate gave amino acetates **88a-90a** as pale yellow oils in reasonable yield (51-62%). Despite the slow addition of *tert*-butyl 2-bromoacetate, significant di-substitution occurred to give **88b-90b** which is the cause of only moderate yields of the desired products. The Fmoc moiety was introduced successfully on the amino acetates **88-90a** to give Fmoc carbamates **91-93** as colourless solids with excellent yields (88-94%). Deprotection of **91-93** with trifluoroacetic acid (TFA) followed by the addition of HCl in EtOAc [prepared by dropwise addition of AcCl in EtOH] in the reaction mixture gave the colourless amine

salts **94-95** after filtration and without further purification with excellent yields (90-91%).

In order to synthesise azides **97-99** on a large scale, an alternative, storable diazotransfer agent was preferred to the more common, but explosive, trifluoromethanesulfonyl azide (TfN_3).[252] Indeed, trifluoromethanesulfonic anhydride used to generate TfN_3 is very expensive and makes it unsuitable for large scale reactions. Rather than generating TfN_3 *in situ*, the use of imidazole-1-sulfonyl azide hydrochloride **100** (Scheme 2.4-4) was chosen.[253] This reagent presents the advantages of being a shelf-stable diazotransfer agent, it is relatively cheap to synthesise (63% yield) and has a comparable efficiency in transforming amines into azides relative to that of TfN_3.

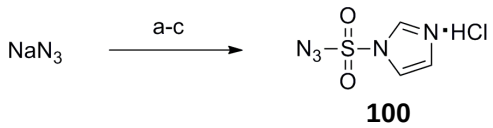

100

Scheme 2.4-4. Synthesis of imidazole-1-sulfonyl azide hydrochloride. (a) sulfuryl chloride, MeCN, 0°C to rt, 16 h ; (b) imidazole, 0°C to rt, 3 h; (c) HCl, EtOAc, 0°C. **100** 63%

The diazotransfer reagent **100** was initially used as described,[253] bringing together 1.2 equivalents of the azide with 1 equivalent of amine together with 2 equivalents of K_2CO_3 and 1 mol % of copper(II) sulphate for 16 h at room temperature. A minor adjustment was made to the equivalents of K_2CO_3 used (3 equiv.). However, the presence of the base sensitive Fmoc residue led to complete cleavage of Fmoc from the amino acid derivative. A search for milder bases which might avoid Fmoc cleavage was investigated; Na_2CO_3 and $NaHCO_3$ were used as bases. While Na_2CO_3 improved the yield with partial cleavage, $NaHCO_3$ offered the desired uncleaved azides **97-99** (**Z***$_3$-**Z***$_5$) with very good yield (81-89%).

2.4.3 Generation of *N*-propargylated Glycine

Although the required *N*-azidoalkyl glycine building blocks were unknown in literature, one paper has already reported the required *N*-propargylated glycine **103** (**A***).[254]

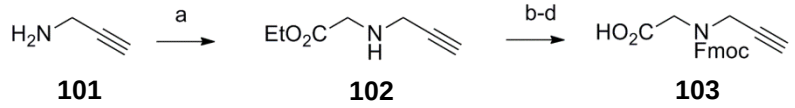

Scheme 2.4-5. Synthesis of *N*-propargylated glycine monomers in literature. (a) Et_3N, THF, 0°C to rt, o/n, **102** 84%; (b) 4 M NaOH, 1,4-dioxane-MeOH, rt, 30 min; (c) H_2O, pH 9-9.5; (d) Fmoc-OSu, MeCN, rt, o/n, **103** 82%.

We chose to adapt this synthesis for reasons of convenience. The reagents chosen were *tert*-butyl 2-bromoacetate, Fmoc-OSu and TFA as these were also used for the synthesis of azide building blocks **Z***$_3$-**Z***$_5$. (Scheme 2.4-6).

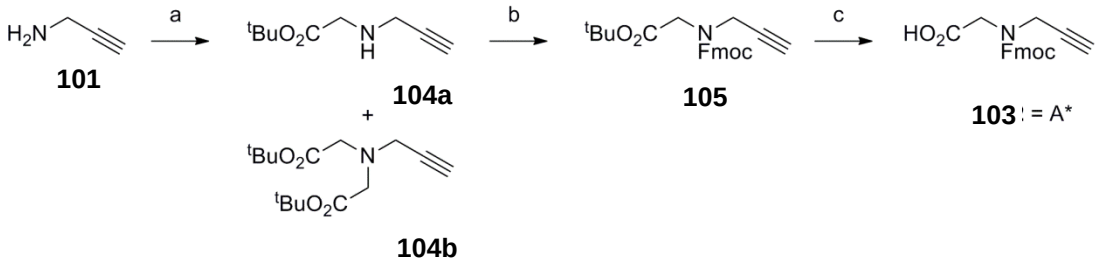

Scheme 2.4-6. Synthesis of *N*-propargylated glycine monomers. (a) *tert*-butyl 2-bromoacetate, Et_3N, THF, rt, 18 h, **104a** 50%; (b) Fmoc-OSu, DCM, rt, 18 h, **105** 81%; (c) 80% TFA in DCM, rt, 18 h, **103** 80%.

As seen for building blocks **97-99** (**Z***$_3$-**Z***$_5$), di-substitution of *tert*-butyl 2-bromoacetate on amine **101** occurred and strongly reduced the yield of **104a** (50% vs 84% in litterature). In contrast to the paper in which synthesis of **103** is described,[254] Fmoc protection was accomplished prior to acid deprotection to avoid Fmoc protection on the free acid.

Building blocks **A***(**103**) and **Z***$_3$-**Z***$_5$ (**97-99**) were successfully synthesised (see Appendix 1 for spectra). Due to the presence of the secondary amine after deprotection during classic Fmoc SPPS, it was anticipated that they would behave similarly to proline and coupling of the next amino acid may require a double coupling to ensure full conversion. The library of designed peptidomimetics would incorporate these

building blocks at specific positions and the linear peptoid-peptide hybrids obtained would be subjected to click chemistry in the attempt to create a library of cyclised peptoid-peptide hybrids.

2.5 Synthesis of acyclic and cyclic peptoid-peptide hybrids

2.5.1 Building block position strategy

Ac-KCCYFETHMPRH-NH_2 was found to inhibit MDM2-mediated inhibition of p53 *in vitro*. Its inability to enter cells (Section 1.2.3.2) sparked our interest in the development of peptidomimetics based on this peptide which might exhibit greater cell permeability and give rise to the design of a library of peptoid-peptide hybrids. Since no peptoid-peptide hybrids with such building blocks had been reported, the first concern was to establish the feasibility of incorporation of such building blocks by SPPS and then whether it was possible to cyclise these hybrids through the modified side-chains. No structural data was available on this peptide or its complexation with the MDM2 RING domain. However, for preliminary studies, a truncated version was chosen; based on the hypothesis that, although such short peptides have random structures in free solution, they might adopt more ordered structures when bound to the target or when cyclised. To minimise the number of peptides to be synthesised, we reduced the number of locations of peptoid building blocks to three positions out of six. Based on the peptide sequence KCCYFE, one of the cysteines and the glutamic acid was to be replaced by either $\mathbf{Z}^{*}_{3\text{-}5}$ or $\mathbf{A}^{*}$ and the other cysteine substituted by an alanine.

Finally, due to potential geometric constraints, three azide building blocks $\mathbf{Z^*_{3\text{-}5}}$ with different lengths of azidoalkyl chains were used and HPLC chromatograms of the peptide obtained compared to give some insight into favourable cyclisation conditions, on whether *i*, *i*+3 or *i*, *i*+4 spacing and the length of the cyclisation chain are suitable and have an impact on the purity of the target molecules, and whether these parameters can control the ratio of monomeric cyclisation over dimeric cyclisation. The list of target peptoid-peptide hybrids comprising both acetylated capped peptides and biotinylated peptides are shown in Figure 2.5-1.

(a)

U18/C18 Ac-KAA*YFZ$^*_3$-NH$_2$	**U23/C23** Ac-KAA*YFZ$^*_4$-NH$_2$	**U14/C14** Ac-KAA*YFZ$^*_5$-NH$_2$
U26/C26 Ac-KA*AYFZ$^*_3$-NH$_2$	**U20/C20** Ac-KA*AYFZ$^*_4$-NH$_2$	**U16/C16** Ac-KA*AYFZ$^*_5$-NH$_2$
U22/C22 Ac-KZ$^*_3$AYFA*-NH$_2$	**U21/C21** Ac-KZ$^*_4$AYFA*-NH$_2$	**U17/C17** Ac-KZ$^*_5$AYFA*-NH$_2$
U19/C19 Ac-KAZ$^*_3$YFA*-NH$_2$	**U25/C25** Ac-KAZ$^*_4$YFA*-NH$_2$	**U15/C15** Ac-KAZ$^*_5$YFA*-NH$_2$

(b)

U5/C5 Biotin-SGSG-KAA*YFZ$^*_3$-NH$_2$	**U10/C10** Biotin-SGSG-KAA*YFZ$^*_4$-NH$_2$	**U1/C1** Biotin-SGSG-KAA*YFZ$^*_5$-NH$_2$
U13/C13 Biotin-SGSG-KA*AYFZ$^*_3$-NH$_2$	**U7/C7** Biotin-SGSG-KA*AYFZ$^*_4$-NH$_2$	**U3/C3** Biotin-SGSG-KA*AYFZ$^*_5$-NH$_2$
U9/C9 Biotin-SGSG-KZ$^*_3$AYFA*-NH$_2$	**U8/C8** Biotin-SGSG-KZ$^*_4$AYFA*-NH$_2$	**U4/C4** Biotin-SGSG-KZ$^*_5$AYFA*-NH$_2$
U6/C6 Biotin-SGSG-KAZ$^*_3$YFA*-NH$_2$	**U12/C12** Biotin-SGSG-KAZ$^*_4$YFA*-NH$_2$	**U2/C2** Biotin-SGSG-KAZ$^*_5$YFA*-NH$_2$

(c)

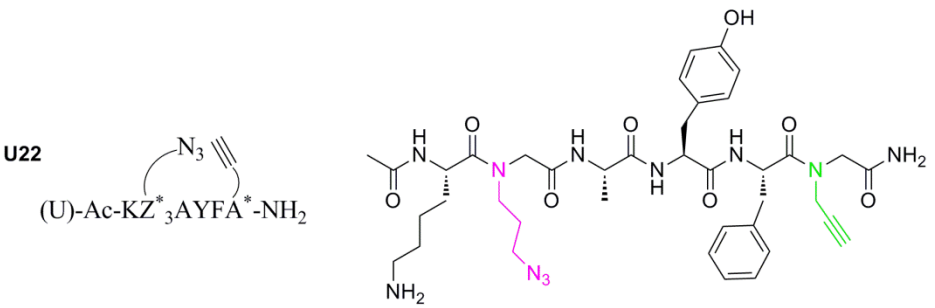

(d)

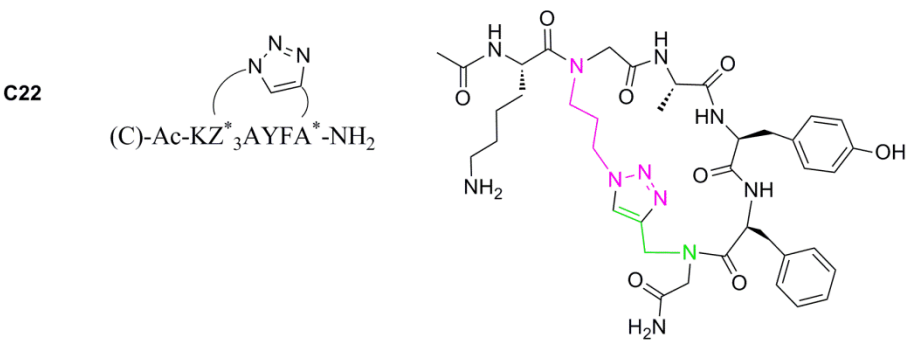

Figure 2.5-1. Library of peptoid-peptide hybrids to be synthesised. (a) List of acetylated-capped hybrids; (b) list of biotinylated hybrids with SGSG spacer; (c) example of an acyclic hybrid, **U22** ; (d) example of the corresponding cyclised hybrid, **C22**.

2.5.2 Fmoc SPPS applied to the library

Since the emergence of SPPS, a variety of linkers, side-chain protecting groups, cleavage cocktails and coupling agents have emerged and the peptide sequence will affect the choice of these parameters.[255]

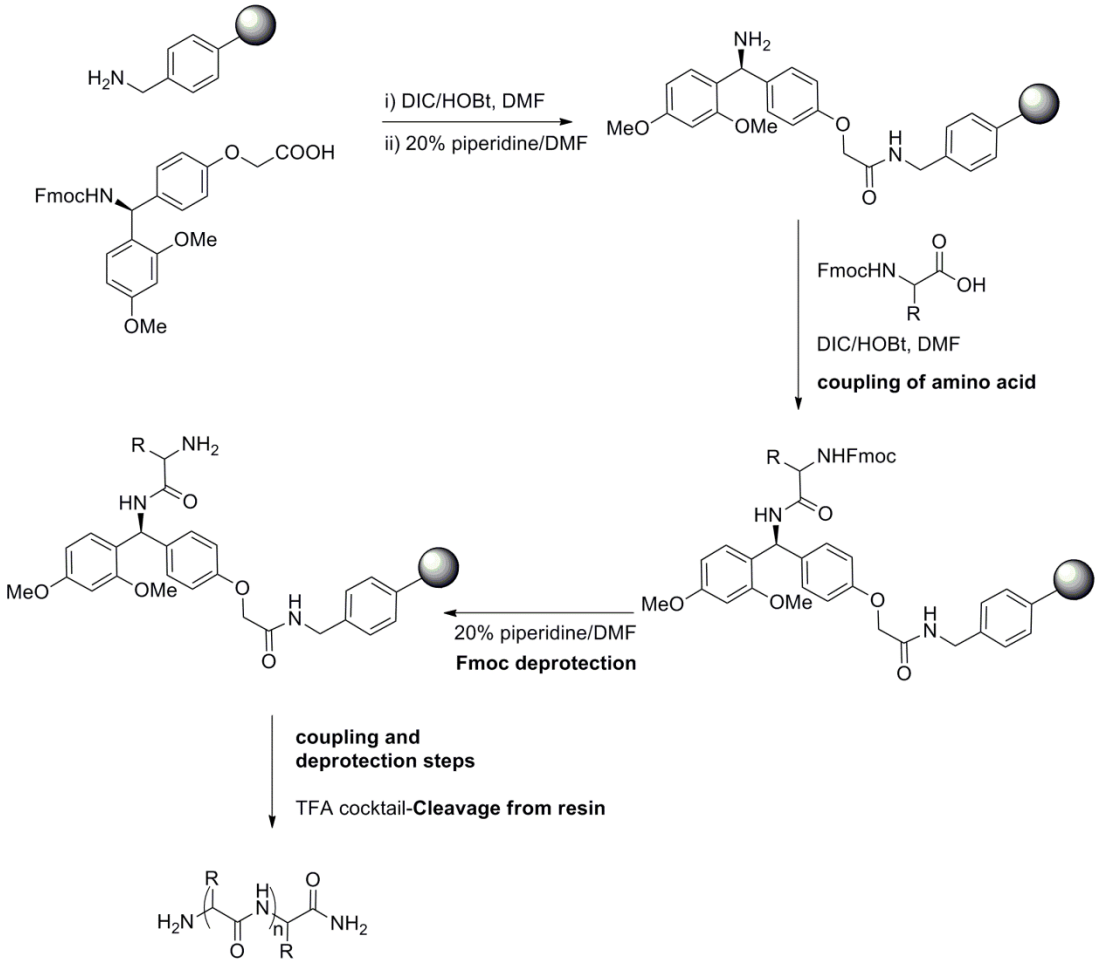

Scheme 2.5-1. General SPPS protocol for amino acid coupling on a Rink amide resin.

In Fmoc SPPS, side-chain protecting groups and resin linkers are commonly cleaved by trifluoroacetic acid (TFA). The matrix usually used is 1% divinylbenzene cross-linked polystyrene (PS).[255] Since some of the peptoid-peptide hybrids in the library bear biotin tags on their N-terminus, to maintain charge neutrality in the resultant peptides, aminomethyl-based polystyrene resin **106** was used with a Rink amide linker **107** to provide the Rink-amide-functionalised PS resin **108** (Scheme 2.5-2). With this resin, peptoid-peptide hybrids were either capped with biotin or an acetyl group at the N-terminus to avoid charged interactions between the ends.

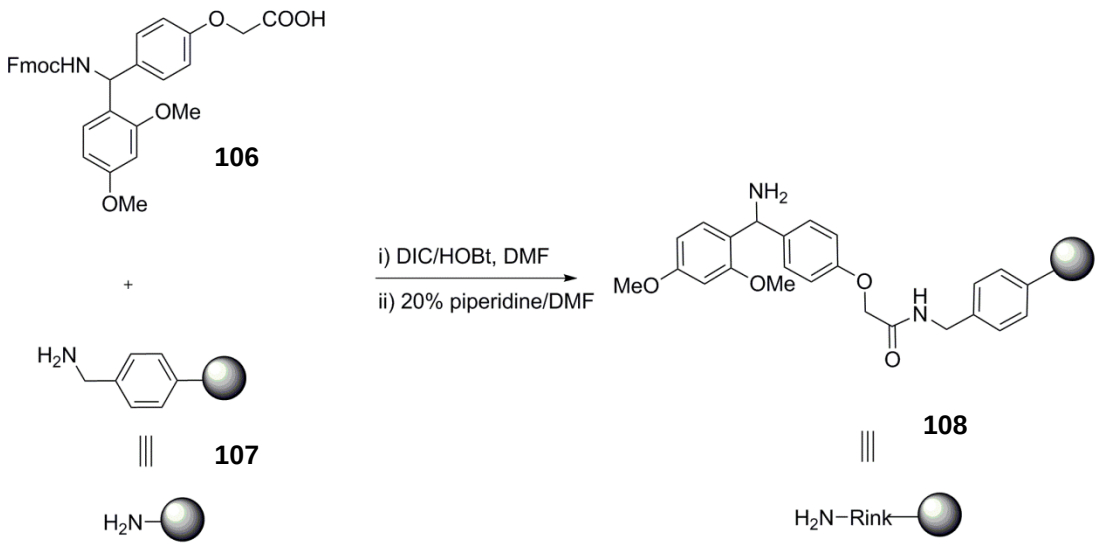

Scheme 2.5-2. Synthesis of the Polystyrene aminomethyl Rink amide resin.

Since more than half the common amino acids contain side-chains bearing reactive groups, protected-side-chain amino acids are commercially available. These side-chain protecting groups are generally acid sensitive so that they are not lost during Fmoc deprotection and will only be deprotected during final cleavage from the resin with a TFA cocktail. In the amino acid sequences of the current library, only Lysine, Tyrosine and Serine will require side-chain protection, and these are commercially available as Fmoc-Lys(Boc)-OH, Fmoc-Tyr(*t*Bu)-OH and Fmoc-Ser(*t*Bu)-OH.

Before the addition of an amino acid or its derivative, the Fmoc protecting group of the previous amino acid residue is removed, typically using 20% piperidine in DMF (v/v). Coupling conditions involved the addition of an excess (3 eq.) amino acid pre-activated with HOBt and DIC (3 eq. each). In order to verify the success of a coupling, colorimetric tests are available to test the presence or absence of a free primary or secondary amine. The ninhydrin test (Section 4.11.1), also known as the Kaiser test, is used to reveal the presence or absence of free primary amine;[256] free primary amines result in a dark blue solution when a few resin beads are exposed to the ninhydrin reagent mix. Proline, and more generally any secondary amine, is not systematically detected. For this reason, the more reliable chloranil test (Section 4.11.1) was used to check coupling on *N*-propargylated or *N*-azidoalkyl building blocks. When incubating the chloranil reagent, the observation of blue beads indicates the presence of secondary amines. Due to the lower efficiency of amino acid coupling on secondary amines, a second coupling reaction was often required. Indeed the

coupling reaction was often repeated to ensure complete conversion after coupling of lysine, A^* or Z^*_3-Z^*_3.

As shown in Figure 2.5-2, acyclic peptoid-peptide hybrids were successfully synthesised and characterised by HPLC and MALDI-ToF (all spectra are available in the electronic appendix). Purification by preparative HPLC afforded the desired acyclic hybrids with purity ranging from 68 to 99% (Section 2.5.3).

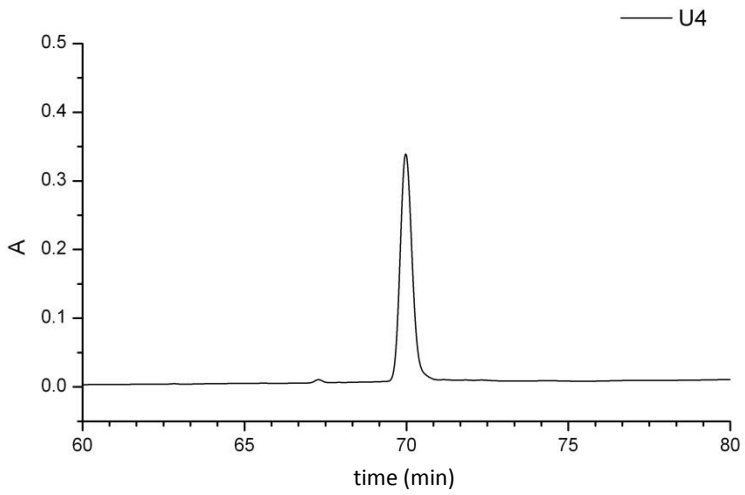

Figure 2.5-2. HPLC chromatogram of purified acyclic hybrid **U4** (U)-Biotin-SGSG-KZ^*_5AYFA^*-NH_2. Analytical and preparative HPLC experiments were carried out with method 4; signal was detected at 215 nm.

2.5.3 HPLC optimisation for acyclic hybrids

Acyclic peptides were cleaved from resin with the TFA cocktail TFA:TIS:H_2O (95:2.5:2.5; v/v), precipitated with cold ether, centrifuged, the solvent removed and the remaining pellet was lyophilised. HPLC conditions were initially optimised on an analytical set-up, but unfortunately the flow rate recommended for the scale-up from an analytical to preparative column could not be achieved due to instrument limitations. In order to achieve optimum peptide purities for biological testing on preparative scale, maximising the separation from truncated peptides of similar hydrophobicity, this meant that comparatively long run times were required.

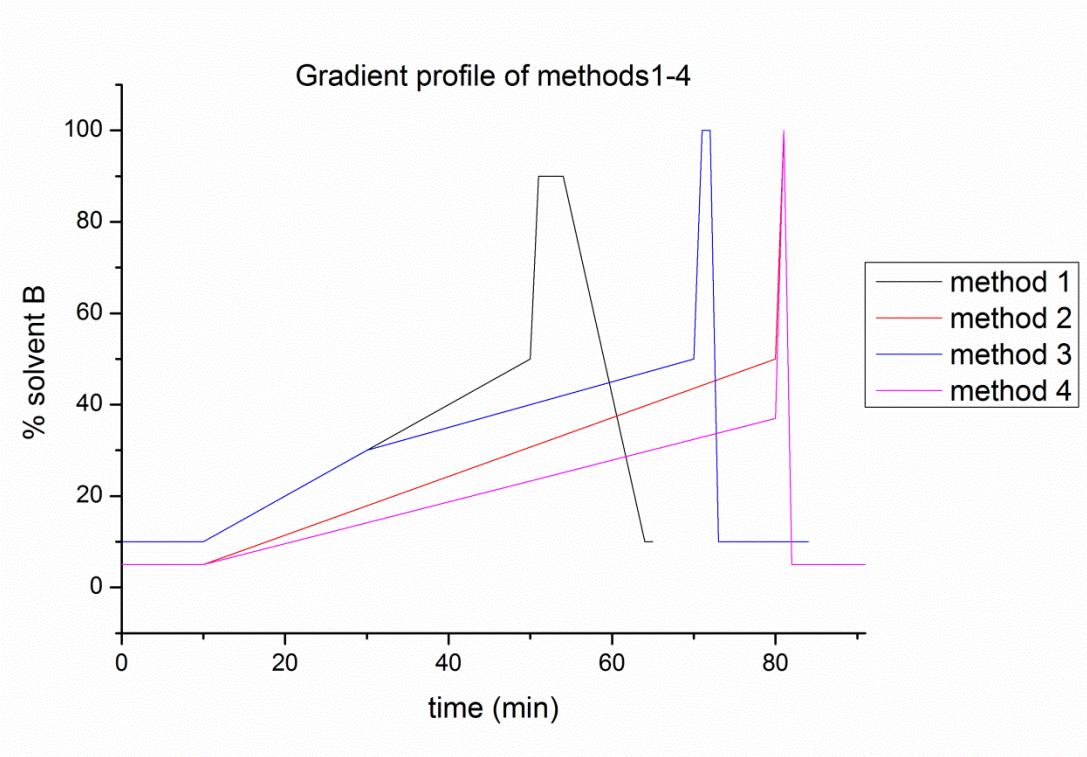

Figure 2.5-3. Gradient profile of methods 1 to 4. Method 1, 1% increase in solvent B per minute over 40 min; Method 2, 0.64% increase in solvent B per minute over 70 min; Method 3, 1% increase in solvent B per minute over 20 min followed by a 0.45% increase in solvent B per minute over 40 min; Method 4, 0.45% increase in solvent B per minute over 70 min.

To estimate the efficacy of a method, resolution factors were calculated as an indicator of peak separation; the resolution factor corresponds to twice the ratio of the difference of the retention time of the two peaks divided by the sum of the width *W* of each peak (Equation 2.5-1). An Rs value of 1.5 (or greater) is necessary for complete separation.

$$R_S = 2 \times \frac{[(t_R)_B - (t_R)_A]}{W_A + W_B}$$

Equation 2.5-1

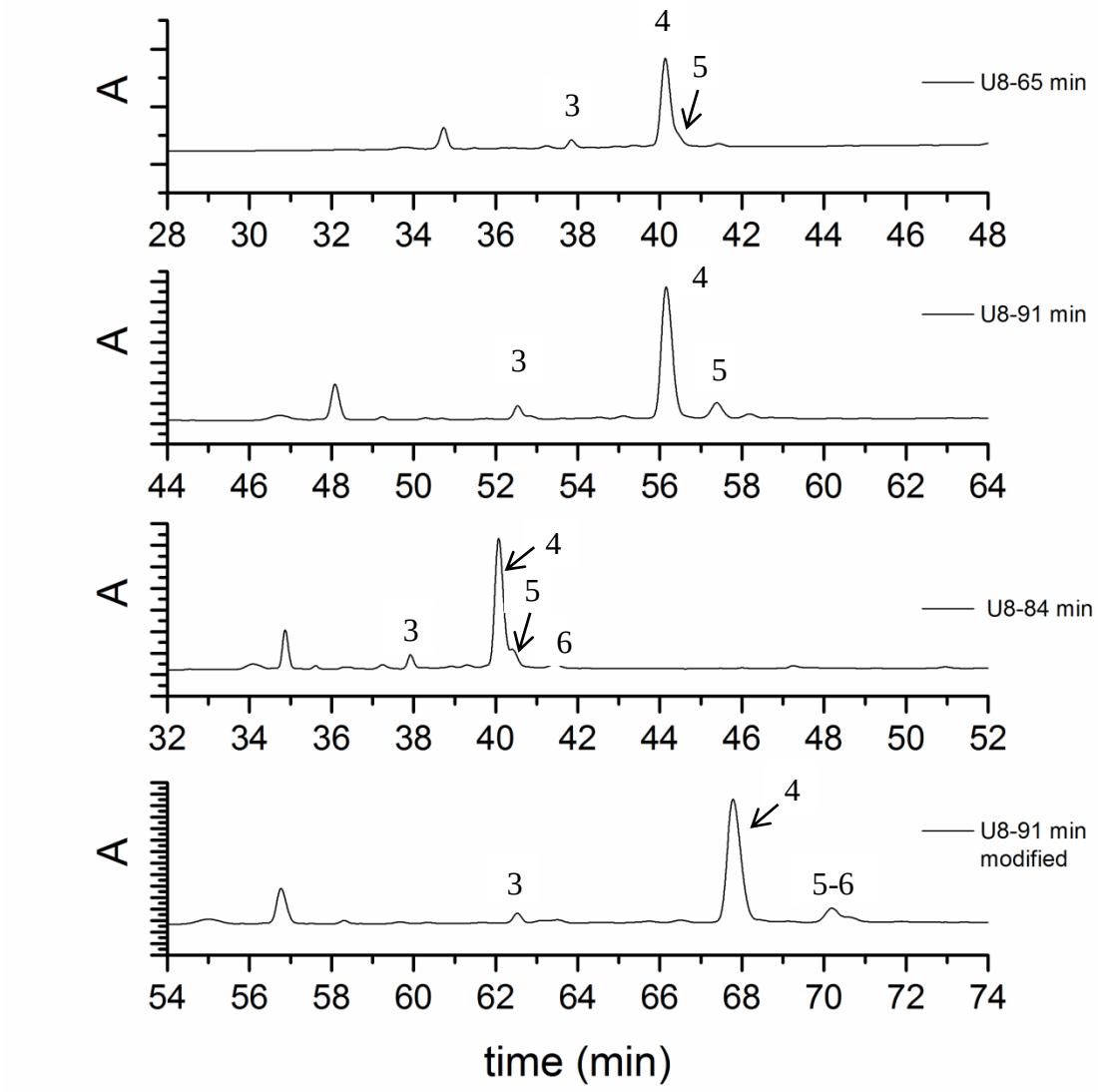

Figure 2.5-4. Optimisation of method for analytical HPLC on hybrid **U8** (U)-Biotin-SGSG-KZ*$_4$AYFA*-NH_2. Methods 1 to 4 are displayed from top to bottom. Signal was detected at 215 nm.

Rs values are reported alongside with retention times and peak width in Table 2.5-1.

	t_{R3} (min)	W_3 (min)	t_{R4} (min)	W_4 (min)	t_{R5} (min)	W_5 (min)	**Rs_{3-4}**	**Rs_{4-5}**
Method 1	37.85	0.48	40.13	1.41	-	-	**2.4**	-
Method 2	52.53	1.13	56.17	0.88	57.38	0.75	**3.6**	**1.5**
Method 3	37.93	0.48	40.07	1.42	-	-	**2.2**	-
Method 4	62.53	0.62	67.78	1.02	70.2	1.17	**6.4**	**2.21**

Table 2.5-1. Resolution factors for peaks 3 to 5 on methods 1-4.

Method 1 employed a 1% increase in solvent B per minute over 40 min but the chromatogram displayed 3 peaks in the vicinity of the acyclic hybrid (peak 4). A resolution factor, Rs_{3-4}, of 2.4 was observed but peak 5 is merged with peak 4 and needs to be separated. Optimisation consisted of separating peaks 3, 5 and 6 from peak 4. Method 2, with a gradient of 0.64% increase in solvent B per minute over 70 min was more successful as the resolution factors Rs_{3-4} of 3.6 and Rs_{4-5} of 1.5 were observed. With a 1% increase in solvent B per minute over 20 min followed by a 0.5% increase in solvent B per minute over 40 min, method 3 did not improve separation compared to method 2. Indeed, with an Rs_{3-4} of 2.2, the separation of peak 3 from peak 4 was worse than for the previous method. Method 4 was better than method 2 with a gradient of 0.45% increase in solvent B per minute over 70 min; indeed the observed Rs_{3-4} is 6.4 and Rs_{4-5} is 2.21. Unfortunately, the improvement in Rs_{4-5} is too small to hope for a better separation between peaks 4 and 5 without increasing the run time of the HPLC methods. Separation of peaks 4 and 5 was revealed as a substantial problem as it was felt that a decrease in the gradient of solvent B would be unlikely to improve this separation significantly, particularly on a preparative scale column. It should also be kept in mind that those methods were developed on a single compound and that other hybrid peptides, although similar, may behave differently. Nevertheless, method 4 was defined as the method to use for any further analysis or purification.

A scaling up calculation to transfer the method from the analytical to the preparative column suggested that a flow rate of 21.2 mL min^{-1} would be required for the preparative column. As the instrument could not achieve such a flow, the maximum

allowed flow rate, 5 mL min^{-1}, was chosen. Retention times for preparative HPLC were delayed by 12 to 17 minutes compared to analytical retention times. The final methods used for analytical methods and preparative separation of the uncyclised peptides by HPLC are shown in Table 4.11-1 Section 4.11.

Using these methods, the acyclic peptides were separated and obtained in high purity. Chromatograms are summarised in Figure 2.5-5.

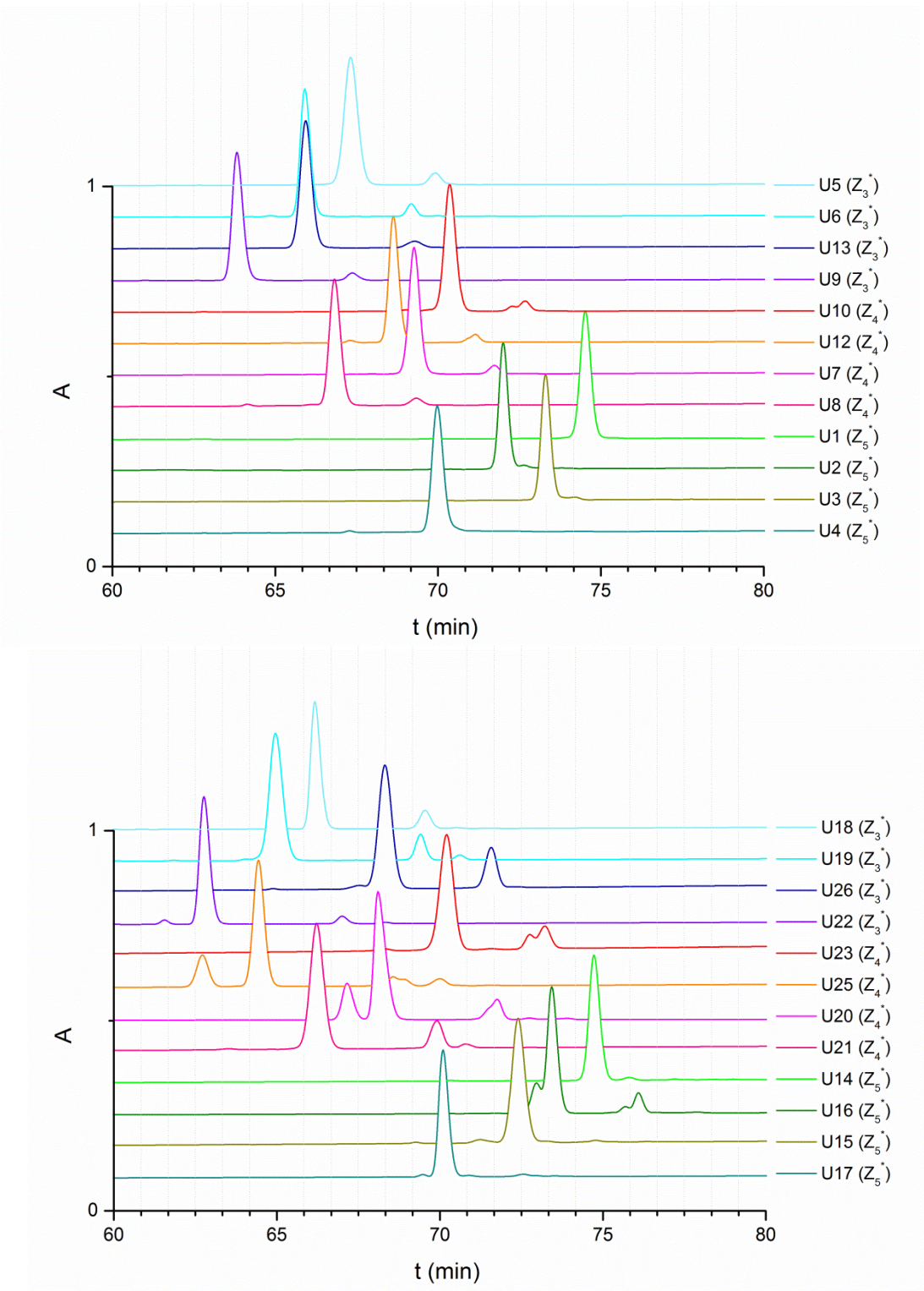

Figure 2.5-5. Analytical HPLC chromatograms after purification of uncyclised biotinylated hybrids (top panel) and uncyclised acetylated hybrids (bottom panel). HPLC experiments were carried out with method 4; signal was detected at 215 nm. Plots are rearranged according to the N-azidoalkyl chain length (Z^*_3-Z^*_5)

Very often, side products could not be separated on the preparative column (Figure 2.5-5) and this explains why some hybrids such as **U20 (Z^*_4)** (68%), **U25 (Z^*_4)** (69%), **U16 (Z^*_5)** (72%) or **U26 (Z^*_3)** (77%) were obtained with a lower purity. The other acyclic hybrids all have a purity of 80% or higher.

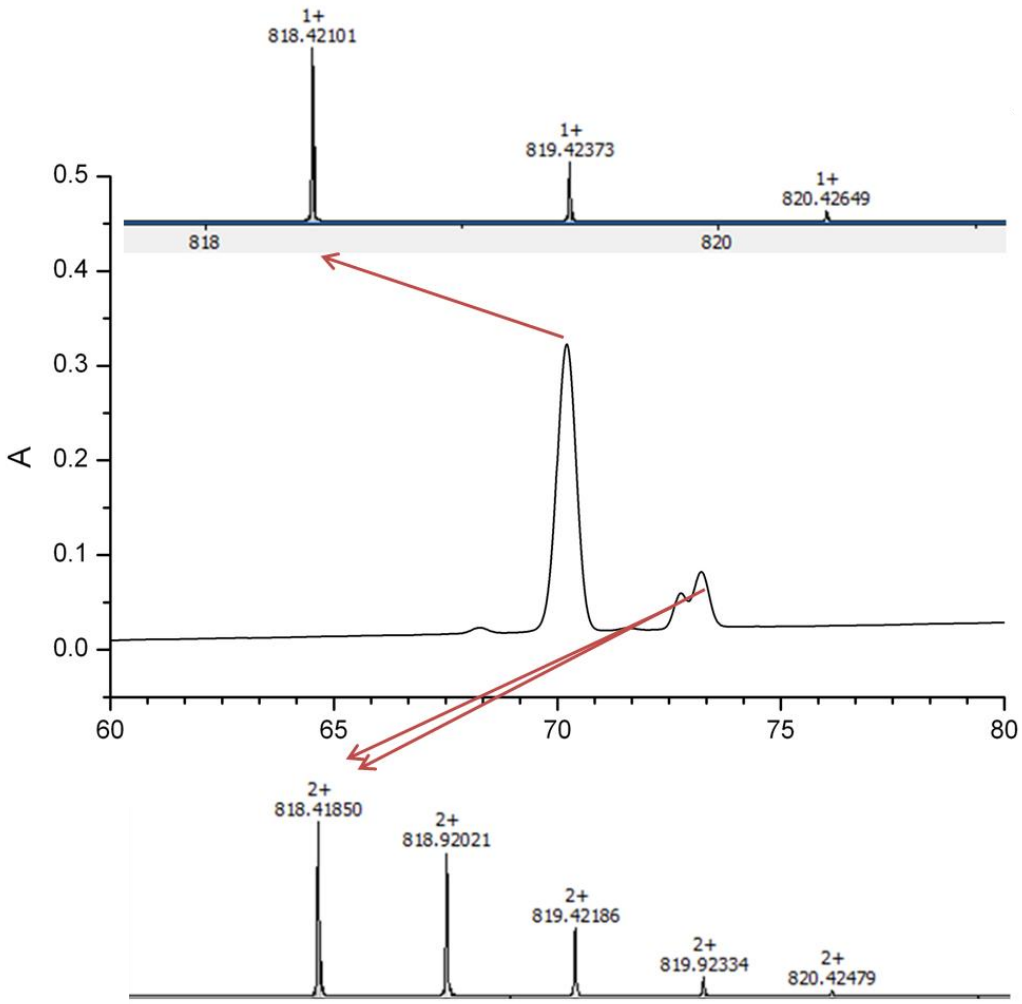

Figure 2.5-6. Identification of side peaks on **U23**. Extracted ion chromatograms at 818.4 (top panel; $[M+H]^+$) and (bottom panel; $[2M+2H^+]$) are matched to the UV spectrum (middle panel).

Compounds **U1-U26** have both the azide and alkyne functions. Therefore, intramolecular and intermolecular CuAAC products as well as uncatalysed triazole formation could be observed occur. Analysis on such products is difficult since the mass observed is the same as the starting material. Preliminary analysis on purified **U23 (Z^*_4)** identified the main product (t_R~ 70 min) with a mass corresponding to $[M+H]^+$ by ESI-MS (Figure 2.5-6, top panel) and side products (t_R~ 72-74 min) with a mass corresponding to $[2M+2H]^{2+}$ (Figure 2.5-6, bottom panel) by ion extraction.

$[M+H]^+$ has a different isotopic profile from $[2M+2H]^{2+}$. Indeed, $[M+H]^+$ displays a +1 mass shift between its isotopic peaks and $[2M+2H]^{2+}$ displays 0.5 mass shift. This might indicate the presence of a potential dimer. A second intermolecular and uncatalysed cycloaddition is possible but t_R would be similar to a t_R observed for **C1-C26**. This would suggest that the side products are linear products dimerised intermolecularly through uncatalysed cycloaddition and that cyclisation occurred once. This hypothesis also matches the facts that two small peaks with very similar t_R have this same $[2M+2H]^{2+}$ signature. Indeed, uncatalysed cycloaddition between one azide and an alkyne would provide both 1,4 and 1,5 triazoles. Possible dimers of **U23 (Z^*_4)** are shown in Scheme 2.5-3.

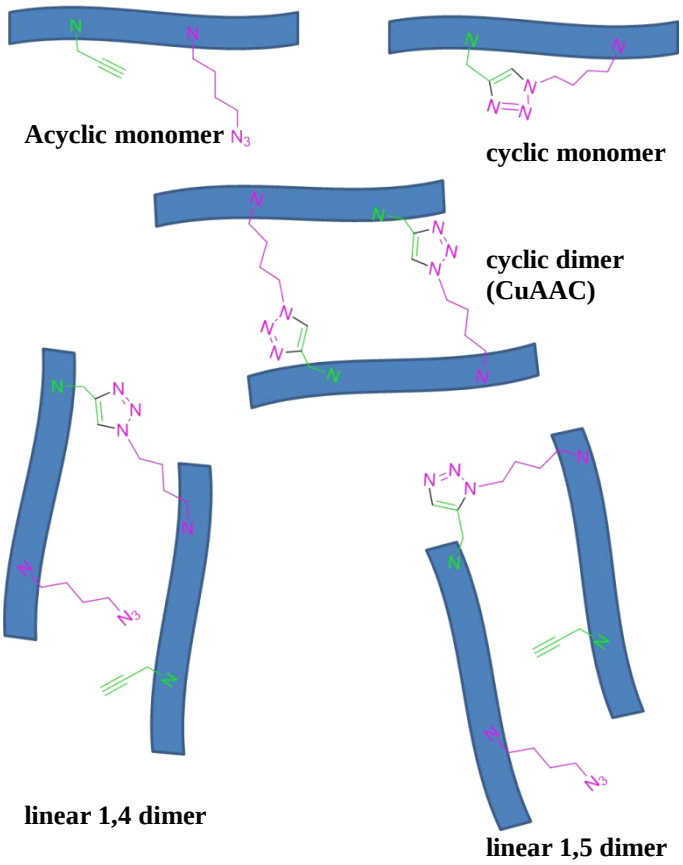

Scheme 2.5-3. Possible dimers formed by cycloaddition between azides and alkynes. 1,5-Dimer resulting from uncatalysed cycloaddition not shown.

On the basis of retention times it was felt that these 2M peaks observed in the ion chromatogram as their $[2M+2H]^{2+}$ ions at $t_R \approx 73$ min were most likely to represent the acyclic dimers rather the cyclic dimer as the acyclic dimers have an increased

hydrophobicity which compensates for the triazole contribution in hydrophilicity. Two triazoles would increase the hydrophilicity and lead to an earlier retention time of the cyclic dimer.

2.5.4 Off-bead and on-bead synthesis of cyclic hybrids

Two options were available for the cyclisation of the peptides (Figure 2.5-7). They could either be synthesised on-bead (Figure 2.5-7 **a**, **c**, **e**) or off-bead (Figure 2.5-7 **a**, **b**, **d**, **f**). The on-bead synthesis has several advantages. First, the cyclisation reaction could, in theory, be carried out at any time during the peptide synthesis either once the *N*-propargylated and *N*-azidoalkyl building blocks are attached or when the linear peptide is complete. As the peptide is on bead, the risk of intermolecular cyclisation should be reduced. Finally, excess reagent used for the triazole formation would be easily washed away. Off-bead synthesis requires the cleavage of the peptide from the resin. A purification step would be performed before triazole formation and one after cyclisation and should therefore offer a much cleaner cyclised product as more undesired products eluting in the same region as the cyclic monomer product should have been removed during the first purification step.

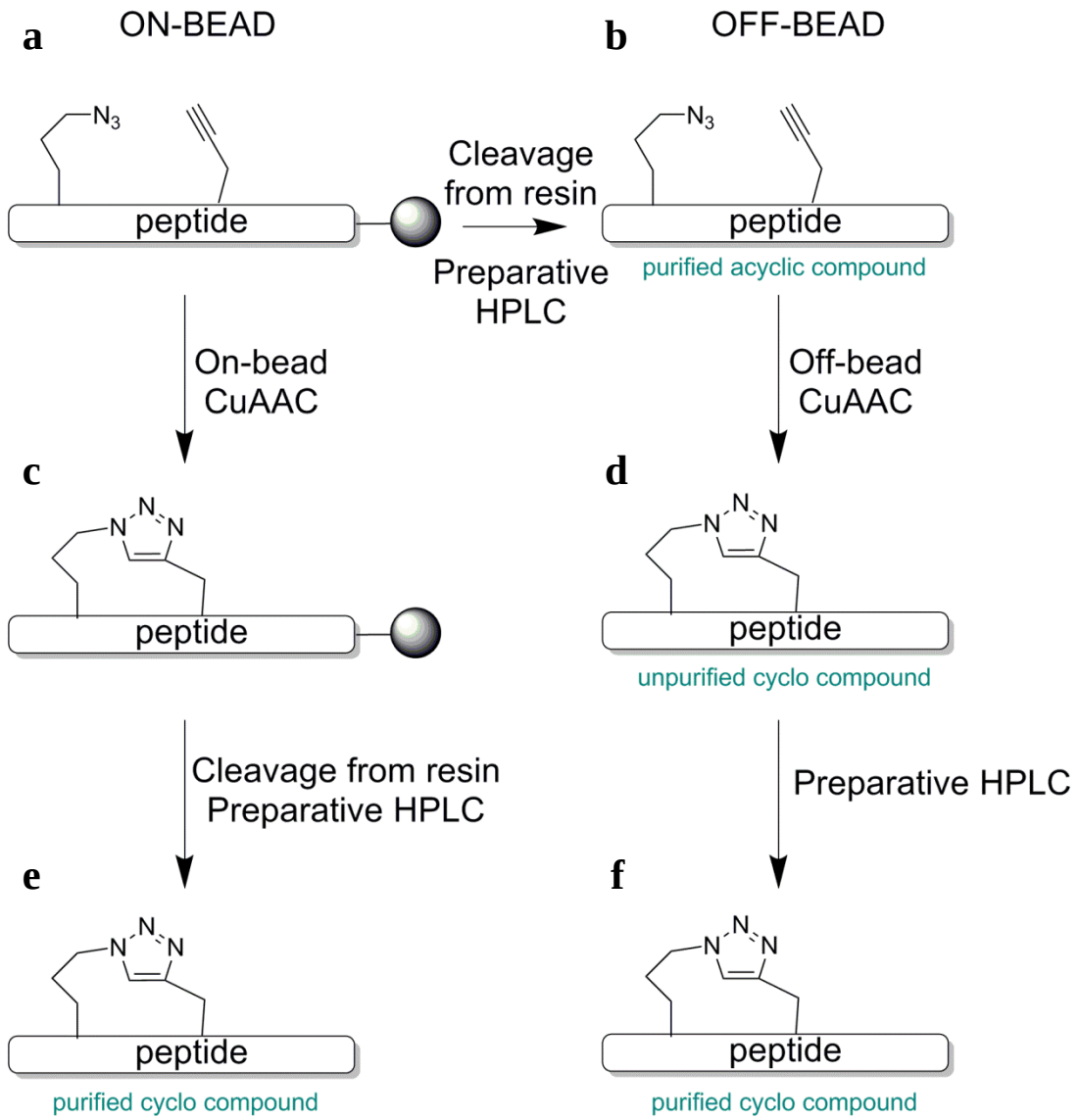

Figure 2.5-7. On-bead versus off-bead synthesis of cyclic peptoid-peptide hybrids. **(a)** unpurified acyclic peptoid-peptide hybrid; **(b)** acyclic peptoid-peptide hybrid cleaved from resin and purified by preparative HPLC; **(c)** unpurified peptoid-peptide hybrid cyclised by CuAAC on solid support; **(d)** unpurified peptoid-peptide hybrid cyclised by CuAAC in solution phase; **(e)** cyclic peptoid-peptide hybrid cleaved from resin and purified by preparative HPLC; **(f)** cyclic peptoid-peptide hybrid purified by preparative HPLC.

2.5.4.1 On-bead cyclisation

On-bead cyclisation conditions found in the literature[218,257,258] were tested on peptide **U9** (U)-Biotin-SGSG-KZ*$_3$AYFA*. Following cleavage from the resin and precipitation of the peptoid-peptide hybrid with cold ether, the peptoid-peptide hybrids were analysed by HPLC. Reactions could be followed by performing IR on solid support. The optimised HPLC Method 4 (Chapter 4.11) was applied to the purification of cyclic hybrids. With this method, acyclic hybrids were separated from their cyclic hybrid counterparts over 10 to 15 minutes, depending on the sample (HPLC chromatograms in Appendix 2). Retention times and purities are summarised in the following Tables; together the reaction conditions and the peak areas of the starting materials and products which were obtained using these are summarised in Table 2.5-2.

Table 2.5-2. Screening conditions for on-bead cyclisation.[218,257,258]

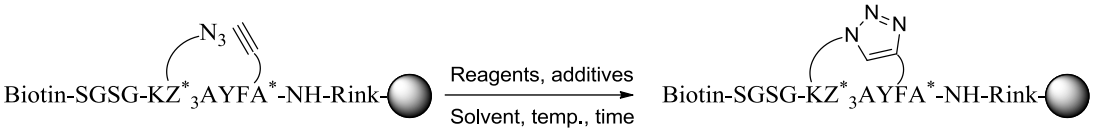

Entry	Reagents, addititves (equiv.)[a]	Temp., time	Solvent [ratio]	S.M. peak Area (%)	Product peak area (%)
1	CuI (3.0), DIPEA (3.0)	16 h, rt	MeCN	~ 33%	~ 36%*
2	CuI (13.0), NaAsc (7.0), DIPEA (17.0)	16 h, rt	DMF	< 2%	~ 69%
3	CuI (13.0), NaAsc (7.0), Lutidine (17.0)	16 h, rt	DMF	~ 7%	~ 55%
4	CuI (2.0), DIPEA (50.0)	16 h, rt	THF	~ 70%	~ 8%
5	$CuSO_4$ (8.0), DIPEA (16.0)	16 h, rt	*t*BuOH: H_2O [2:1]	~ 77%	~ 3%
6	$CuSO_4$ (0.2), NaAsc (0.4), TBTA (0.2)	16 h, rt	*t*BuOH: H_2O [2:1]	~ 81%	~ 3%

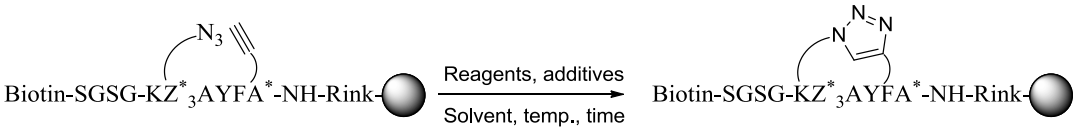

Entry	Reagents, addititves (equiv.)	Temp., time	Solvent [ratio]	S.M. peak Area (%)	Product peak area (%)
7	CuI (3.0), DIPEA (3.0)	72 h, rt	MeCN	~ 45%	~ 31%
8	CuI (13.0), NaAsc (7.0), DIPEA (17.0)	72 h, rt	DMF	< 3%	~ 69%
9	CuI (13.0), NaAsc (7.0), Lutidine (17.0)	72 h, rt	DMF	< 2%	~ 67%
10	CuI (2.0), DIPEA (50.0)	72 h, rt	THF	~ 66%	~ 10%
11	$CuSO_4$ (8.0), DIPEA (16.0)	72 h, rt	*t*BuOH: H_2O [2:1]	S.M. ~ 77%	~ 3%
12	$CuSO_4$ (0.2), NaAsc (0.4), TBTA (0.2)	72 h, rt	*t*BuOH: H_2O [2:1]	S.M. ~ 81%	~ 3%
13	CuI (3.0), DIPEA (3.0)	30 min, 60°C (MW)	DMF	S.M. ~ 3%	~ 64%
14	CuI (13.0), NaAsc (7.0), DIPEA (17.0)	30 min, 60°C (MW)	DMF	S.M. < 1%	~ 77%*
15	CuI (13.0), NaAsc (7.0), Lutidine (17.0)	30 min, 60°C (MW)	DMF	S.M. < 1%	~75%*
16	CuI (2.0), DIPEA (50.0)	30 min, 60°C (MW)	DMF	S.M. < 1%	~ 72%
17	$CuSO_4$ (8.0), DIPEA (16.0)	30 min, 60°C (MW)	DMF	S.M .< 1%	~ 74%
18	$CuSO_4$ (0.2), NaAsc (0.4), TBTA (0.2)	30 min, 60°C (MW)	DMF	S.M. ~ 4%	~ 70%

S.M.: starting material.
*presence of a side peak in the product peak.
[a]Masses and volumes were calculated based on 5 mg of resin with peptide **U9** with a theoretical loading value of 0.38 mmol/g.

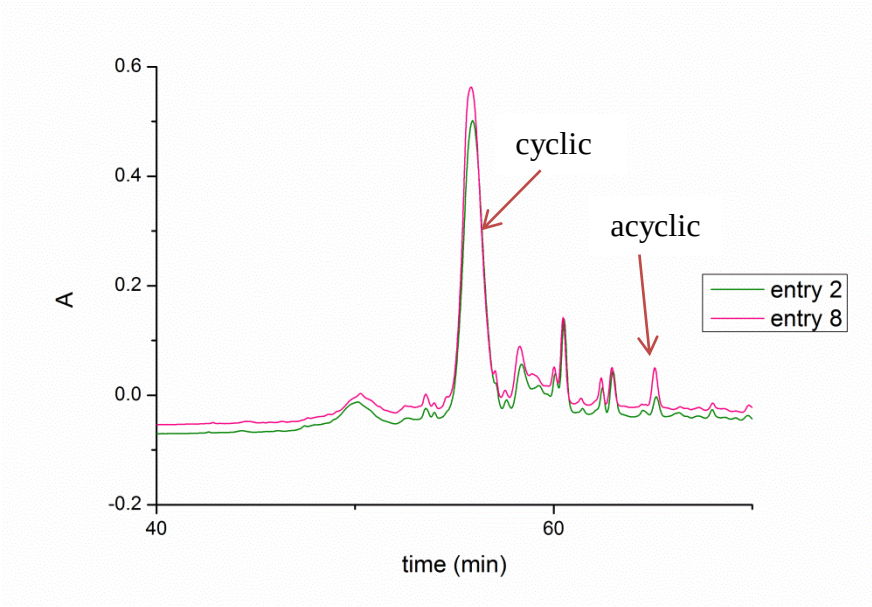

Figure 2.5-8. HPLC chromatograms (zoom 40-70 min) of reaction conditions **entry 2** and **8**. Analytical HPLC experiments were carried out using HPLC Method 4; signal was detected at 215 nm.

An increase in reaction time, from 16 h to 72 h, did not improve the conversion of starting material into the product (Figure 2.5-8).

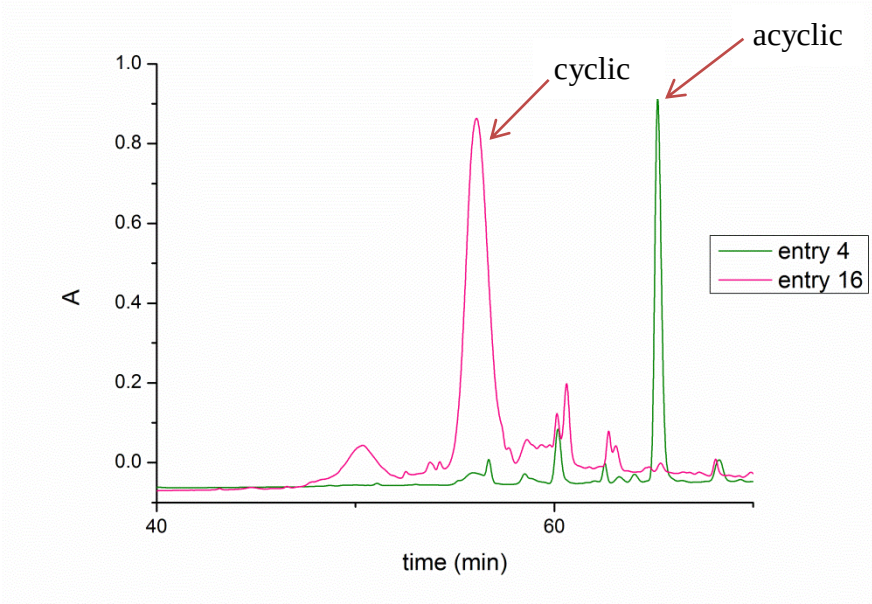

Figure 2.5-9. HPLC chromatograms (zoom 40-70 min) of reaction conditions **entry 4** and **16**. Analytical HPLC experiments were carried out using HPLC Method 4; signal was detected at 215 nm.

Under microwave conditions the yield was significantly improved (entries 4-6 vs entries 16-18; Figure 2.5-9). Indeed, almost complete conversion of starting material

was observed for entries 16-18 and peak areas of product reached approximately 70% compared with 5% under classic conditions of entries 4-6.

All entries in Table 2.5-2 were evaluated and overall it was determined that entries 2 and 14 gave the best outcomes in terms of both conversion and final yield and purity of product. Although under the reaction conditions shown in entry 14 faster conversion of the starting material was observed, these conditions resulted in a significant side-product peak which could not be separated from the product peak. Therefore, entry 2 conditions were chosen to carry out the on-bead cyclisation.

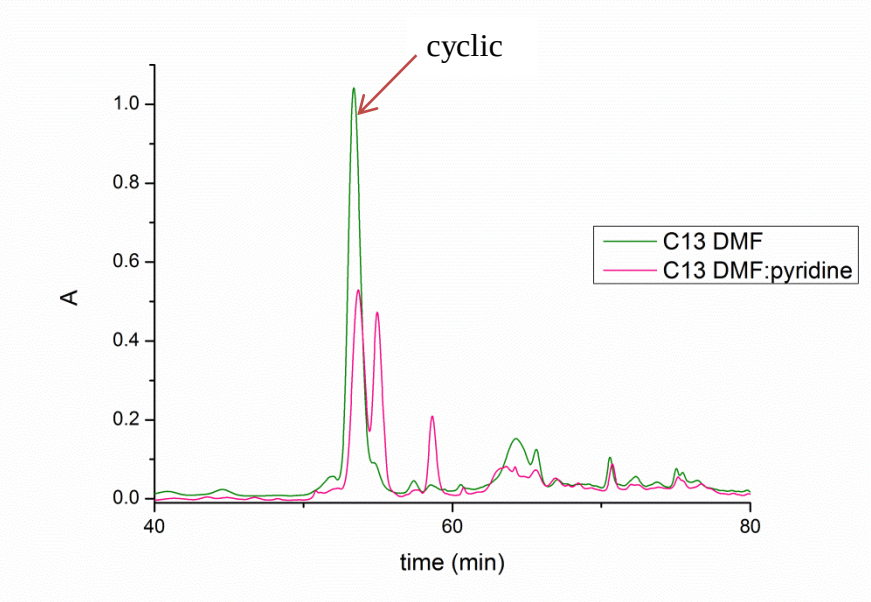

Figure 2.5-10. HPLC chromatograms (zoom 40-80 min) of reaction conditions **entry 2** with [7:3, (v/v)]. Analytical HPLC experiments were carried out using HPLC Method 4; signal was detected at 215 nm.

CuI is poorly soluble in DMF. For this reason, the reaction was tested in a solvent mix DMF:pyridine 7:3 (v/v) using entry 2 conditions [CuI (13.0 equiv.), NaAsc (7.0 equiv.), DIPEA (17.0 equiv.)]. Although CuI was solubilised with addition of pyridine, HPLC chromatograms (Figure 2.5-10) revealed the presence of numerous undesired peaks compared to the the reaction conducted in the absence of pyridine, possibly including a higher percentage of cyclic dimer. Therefore, pyridine was not used for reactions but it was used instead for washing CuI off the resin.

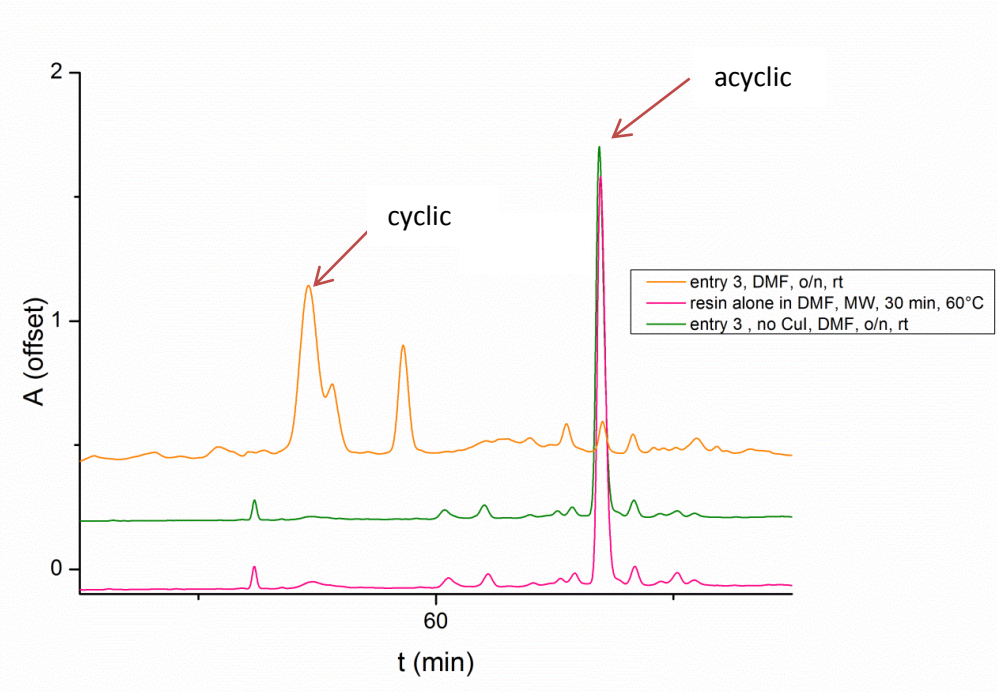

Figure 2.5-11. Reactions on resin with attached hybrid **U13** (U)-Biotin-SGSG-KA*AYFZ*$_3$-NH_2 in the absence of any Copper source. Chromatogram with the presence of copper (orange) is shown for comparison. Analytical HPLC experiments were carried out using HPLC Method 4 (see Section 2.5.3); signal was detected at 215 nm.

To check that cyclisation occurred through CuAAC, reactions were also performed without a copper source at higher temperature and these failed to yield the product (Figure 2.5-11). This may also suggest that linear dimers observed in HPLC chromatograms of purified acyclic hybrids did not form on the resin but rather when in solution in TFA, especially when the volume of TFA was reduced through evaporation, which ultimately led to a high concentration of product, favouring uncatalysed dimer formation.

Reactions could be followed either by cleaving the product from a few beads and analysing by HPLC, or by performing IR analysis on-bead.

IR is particularly convenient for the identification of azides as the azide peak shows a strong sharp signal at 2100 cm^{-1}. The monitoring of reactions involving the appearance or disappearance of azide within a larger molecule is therefore often possible.

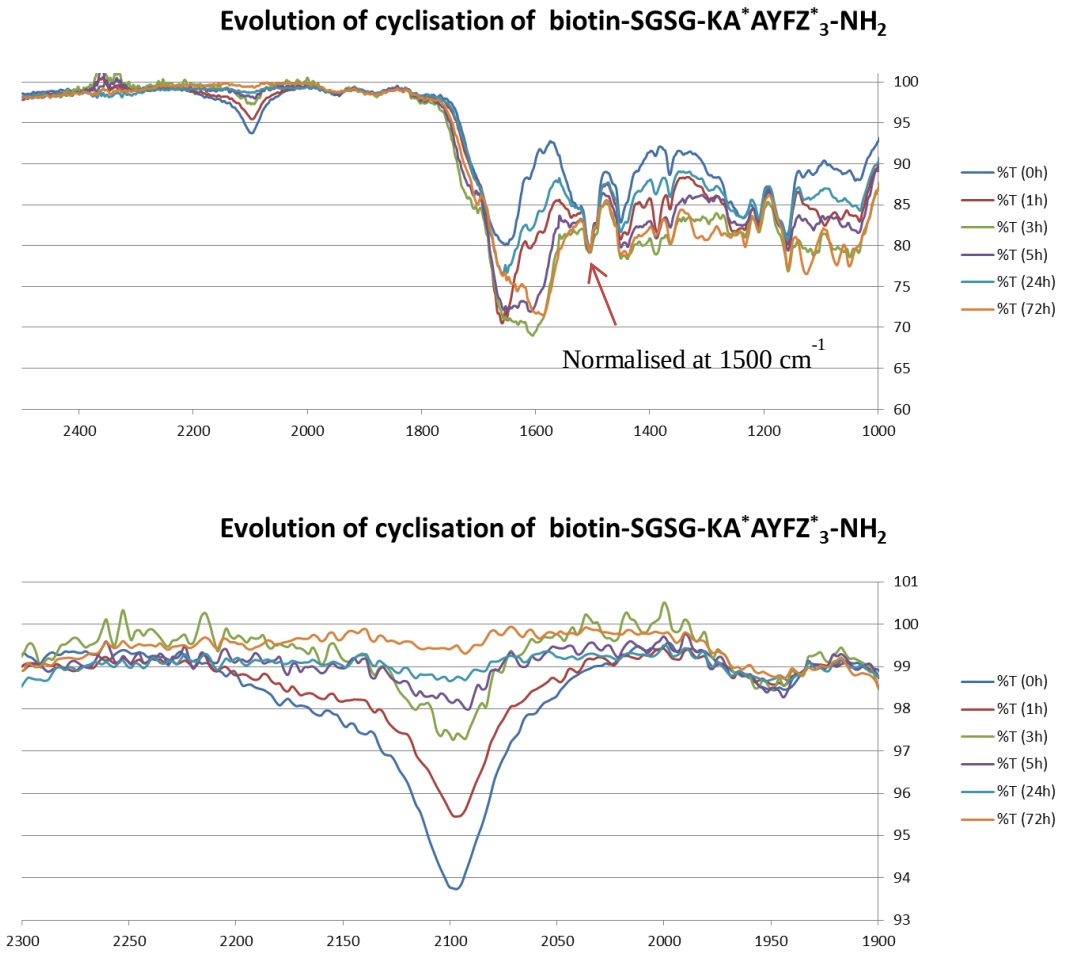

Figure 2.5-12. Conversion of **U13** (U)-Biotin-SGSG-KA*AYFZ*$_3$-NH_2 into its cyclic hybrid followed by IR. The baseline of individual IR spectra were calibrated to the baseline around the azide peak at 2100 cm-1 in the 1 h spectrum and peak intensities were normalised with respect to the 1500 cm^{-1} peak in the 1 h spectrum.

FTIR was performed on the resin displaying the peptoid-peptide hybrid **U13** (U)-Biotin-SGSG-KA*AYFZ*$_3$-NH_2 (Figure 2.5-12). Cyclisation of U13 was followed over time by IR at 1 h, 3 h, 5 h, 24 h and 72 h. The baseline of individual IR spectra were calibrated to the baseline around the azide peak at 2100 cm^{-1} in the 1 h spectrum and peak intensities were normalised with respect to the 1500 cm^{-1} peak in the 1 h spectrum. This represents a semi-quantitative method to estimate the progress of a reaction over time. With this method, it was estimated that the reaction carried out at room temperature had reached 33% of azide conversion after 1 h, 57% after 3 h, 79% after 5 h and 90% after 24 h.

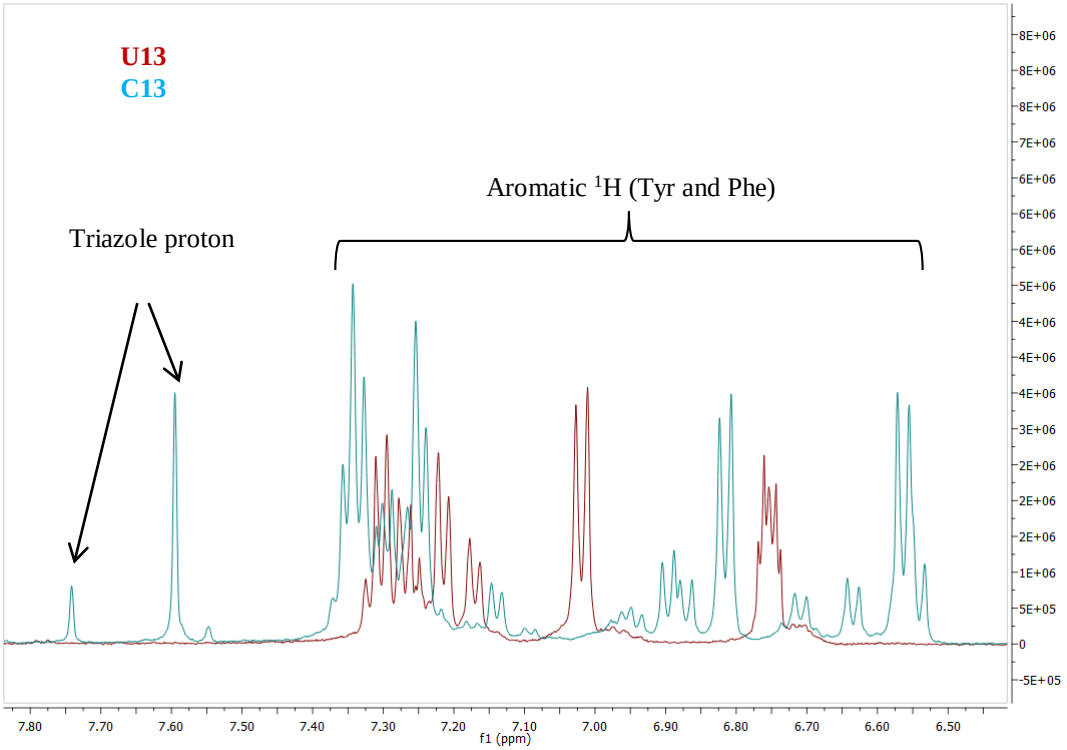

Figure 2.5-13. Overlaid ^{1}H NMR of **U13** (red) and **C13** (teal). Zoom-in region 7.85-6.40 ppm. NMR run in D_2O at 300K.

The hydrogen of a triazole in ^{1}H NMR is found around 7.5-8.5 ppm. Overlaid ^{1}H NMR spectra of purified **U13** and **C13** confirmed triazole formation (Figure 2.5-13) in **C13**. Two signals for triazole were observed. Initially thought to be rotamers, these peaks could also be due to the presence 1,4- and 1,5-regioisomers. Variable temperature NMR would confirm whether these triazole peaks are rotamers or a mix of regioisomers, but this was not performed at this time.

As discussed earlier (Section 2.5.3), side peaks eluting after the main product in the HPLC chromatograms of the acyclic hybrids were not always separable and were identified as their corresponding linear 1,4- and 1,5-triazole dimers (Scheme 2.5-3). There were also problems with regard to the purification of cyclic hybrids; side peaks co-eluted with the main product. MALDI experiments were carried out on two consecutive fractions containing mainly the cyclised desired product **C1** in the first fraction and mainly the unknown peak in the second fraction. MALDI spectra are shown in Figure 2.5-14, Figure 2.5-15 and Figure 2.5-16. Since the fractions contain overlapping peaks both spectra might be expected to contain ions from each peak; the

relative intensities suggest that $[M+H]^+$, $[M+Na]^+$, $[M+K]^+$ predominantly arise from peak 1 as the cyclic monomer and $[2M+H]^+$, $[2M+Na]^+$, $[2M+K]^+$ arise from peak 2 as the cyclic dimer.

While most hybrids reached a purity of approximately 90% or higher, some hybrids such as **C2**, **C18**, **C23**, **C6** and **C1** are below 70% purity after HPLC. They all have in common an *i* to *i*+3 spacing between the click building blocks. The lowest hybrid purity (**C2**, 42%) might be explained by the proximity of the alkyne and the azido-alkyl chain of $\mathbf{Z^*_5}$ which might induce an increased spatial torsion. However, click chemistry in solution phase of that same hybrid gave an excellent purity of 95.3%.

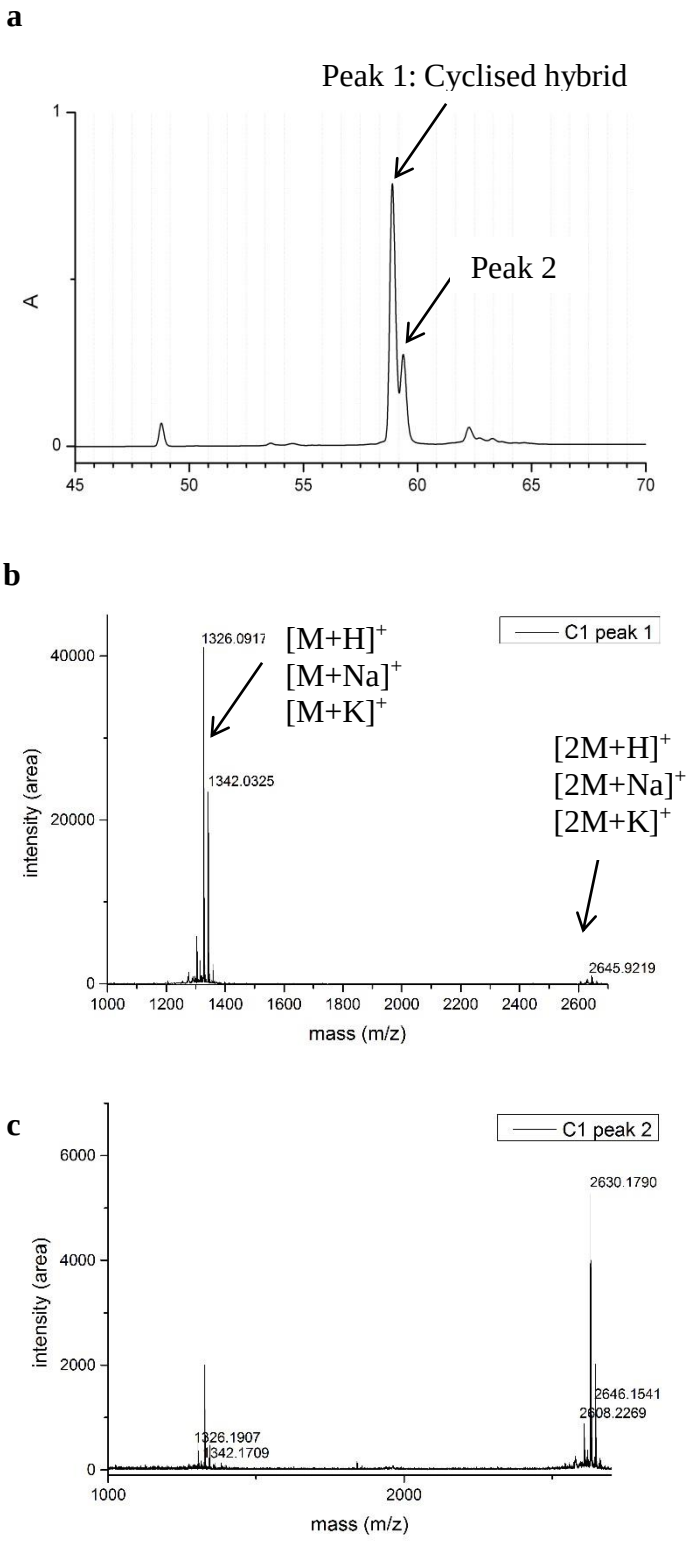

Figure 2.5-14. Identification of the peak eluting with cyclic hybrid from the on-bead cyclisation. (a) HPLC chromatogram of purified **C1** (C)-Biotin-SGSG-KAA*YFZ*$_5$-NH_2; (b) MALDI spectrum of peak 1; (c) MALDI spectrum of peak 2. Zoomed-in spectra are shown in Figure 2.5-15.

a

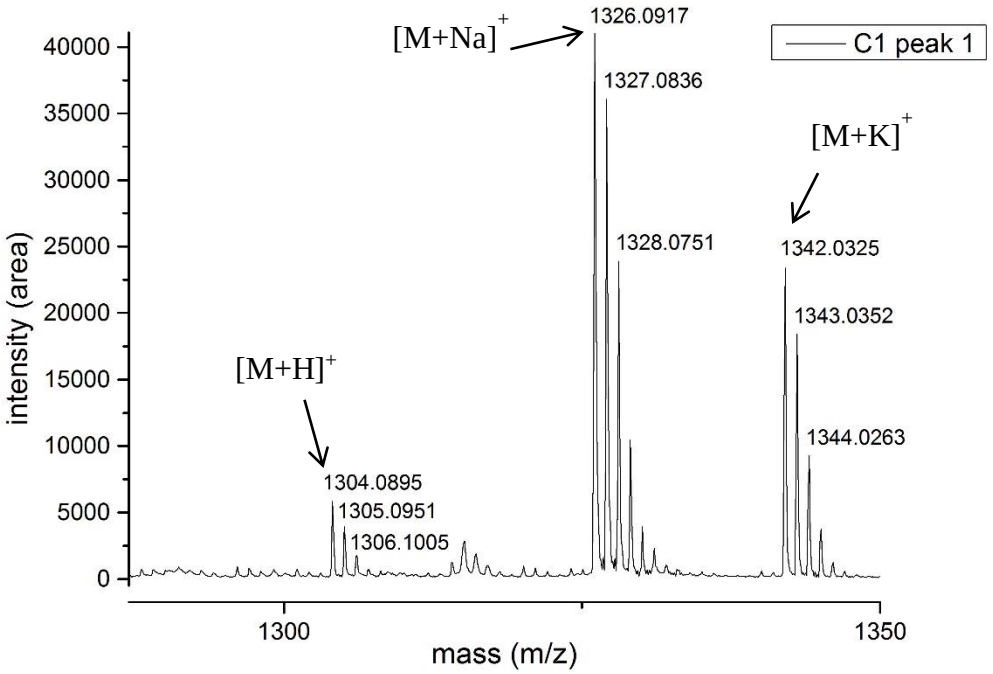

b

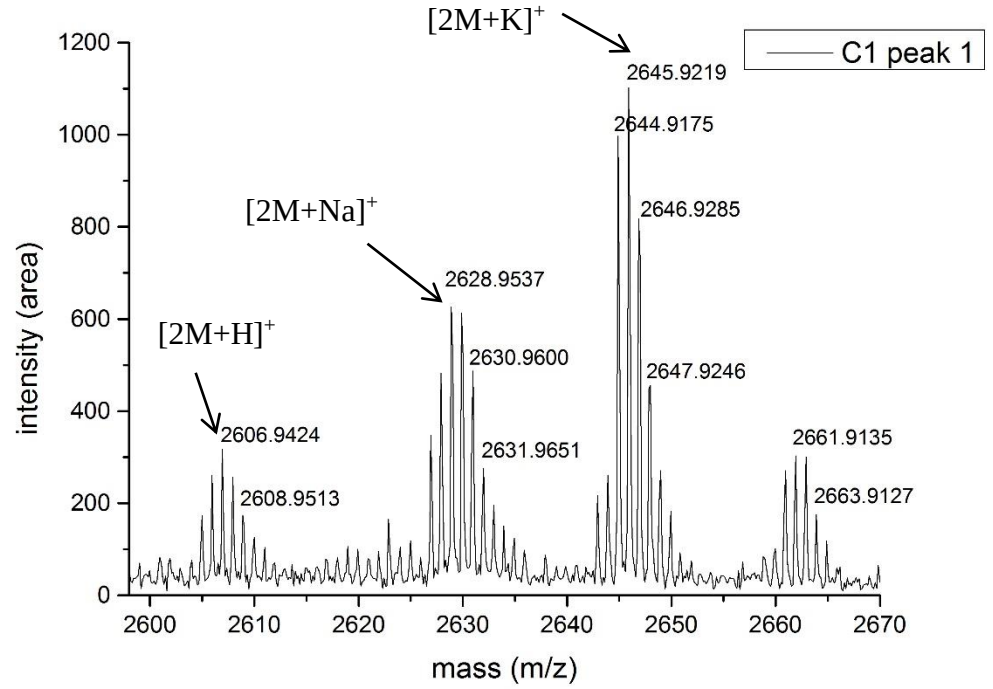

Figure 2.5-15. Identification of the peak eluting with the cyclic hybrid from on-bead cyclisation. (a) and (b) are zoomed-in MALDI spectra of peak 1 from the HPLC chromatogram of purified **C1** (C)-Biotin-SGSG-KAA*YFZ*$_5$-NH_2.

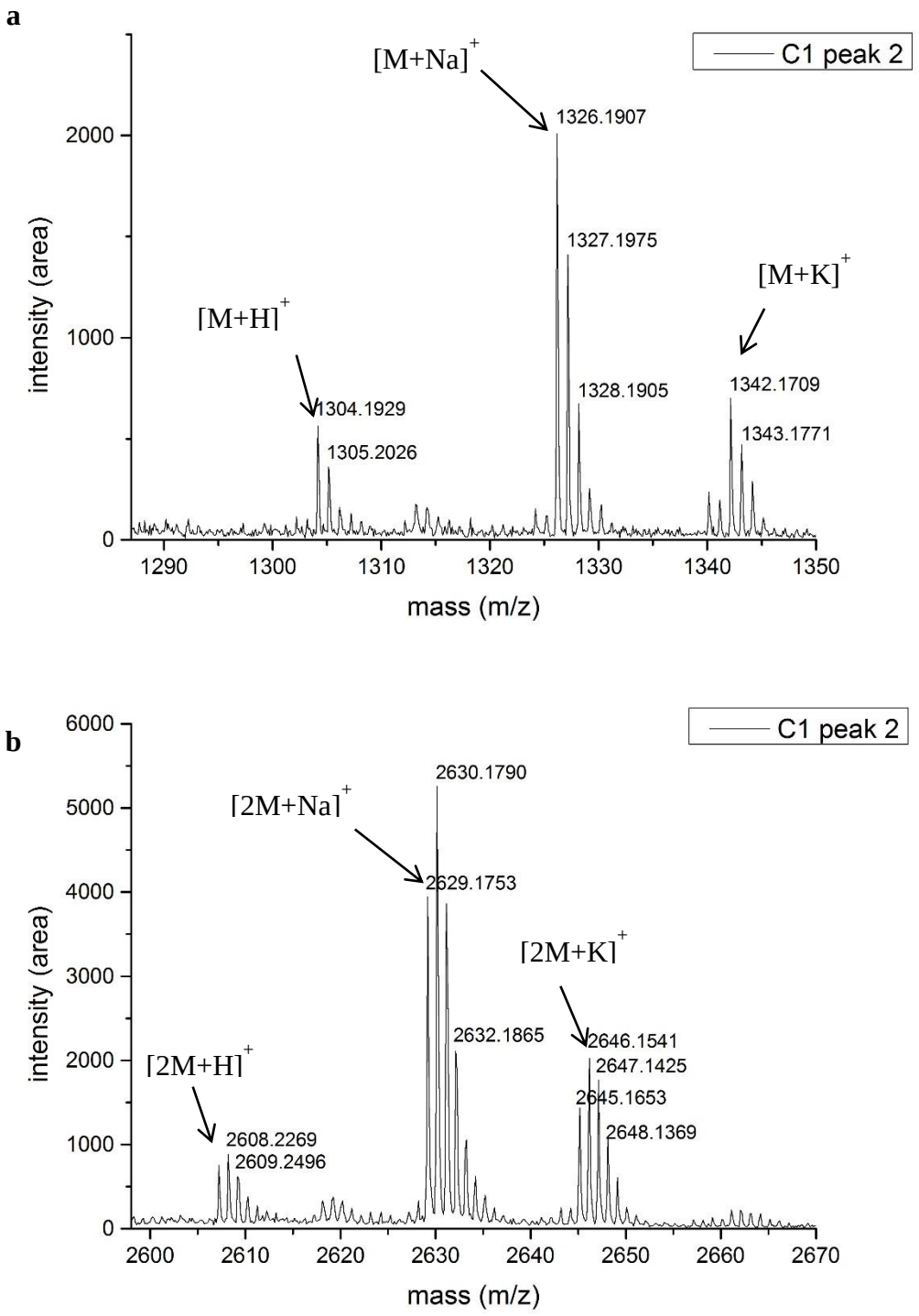

Figure 2.5-16. Identification of the peak eluting with the cyclic hybrid from on-bead cyclisation. (a) and (b) are zoomed-in MALDI spectra of peak 2 from the HPLC chromatogram of purified **C1**.

2.5.4.2 Off-bead synthesis

For off-bead cyclisation peptides were cleaved under standard conditions and purified by HPLC (Chapter 4.11.1) prior to CuAAC reaction in solution. Standard reaction conditions for the cycloaddition were used with $CuSO_4$, NaAsc and TBTA.[259] The cyclisation reaction did not require optimisation as the first conditions used gave 100% conversion of the starting material and high purity. Since cyclisation occurs in solution, it was assumed that the potential for intermolecular cyclisation was greater than on the resin. This was investigated by creating a set of ten-fold dilution experiments starting with a concentration of **U13** at 15.6 mM and decreasing to 15.6 µM.

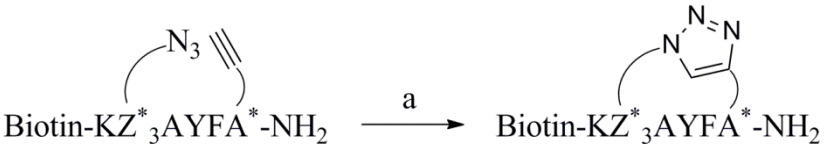

Scheme 2.5-4. Cycloaddition of peptoid-peptide hybrids in solution. (a) peptide (1 equiv.), $CuSO_4$ (0.1 equiv.), NaAsc (0.2 equiv.), TBTA (0.1 equiv.), *t*-BuOH:H_2O 2:1, 16 h, rt.

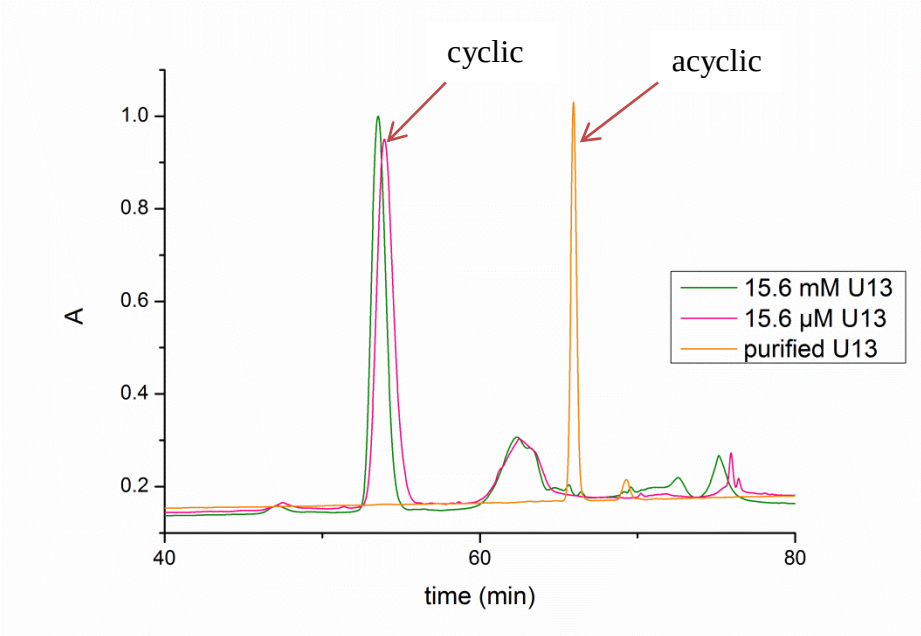

Figure 2.5-17. Cyclisation reaction in solution on hybrid **U13** (U)-Biotin-SGSG-KA*AYFZ*3-NH_2. Analytical HPLC experiments were carried out with method 4 (see Section 2.5.3); signal was detected at 215 nm.

The HPLC chromatograms corresponding to the dilution set did not reveal any significant changes in the reaction outcome with increased dilution over the range

tested. Even so, and to ensure that this observation was not just sample dependant, a final concentration of peptoid-peptide hybrids of 15.6 µM was chosen and used for cyclisation on other acyclic hybrids **C2**, **C3**, **C14**, **C18** and **C23**. Following the cyclisation reaction, another purification by HPLC was performed (Appendix 2). The retention times, peak areas of starting materials and products prior to HPLC, and purities of hybrids after HPLC are summarised in Table 2.5-3.

peptide	analytical t_R (min)	S.M. peak Area (%)	Product peak area (%)	Purity after HPLC[a] (%)	Purity after HPLC[b] (%)
C2 (C)-Biotin-SGSG-KAZ*$_5$YFA*-NH_2	59.8	1.4	51.6	95	42
C3 (C)-Biotin-SGSG-KA*AYFZ*$_5$-NH_2	54.6	1.5	71.7	100	95
C13 (C)-Biotin-SGSG-KA*AYFZ*$_3$-NH_2	53.5	0.0	59.4	100	85
C14 (C)-Ac-KAA*YFZ*$_5$-NH_2	56.2	0.0	52.3	100	91
C18 (C)-Ac-KAA*YFZ*$_3$-NH_2	53.7	0.1	41.8	99	67
C23 (C)-Ac-KAA*YFZ*$_4$-NH_2	53.0	0.9	44.7	92	58

Table 2.5-3. Retention times and purity of purified of a few cyclised hybrids in solution.
[a] : purity of corresponding hybrids cyclised in solution [15.6 µM in t-BuOH:H_2O, 2:1 (v/v)].
[b] : purity of corresponding hybrids cyclised on solid support.

The most striking observation about these HPLC chromatograms is the difference in purification achieved between the off-bead and the on-bead synthetic methods (Table 2.5-3). Indeed, hybrids cyclised in solution are much purer that the hybrids cyclised on-bead (Table 2.5-3) with a purity higher than 98% for most cyclisation reactions tested in solution. This is explained by the fact that in solution phase CuAAC, a first purification step was carried out prior to cyclisation and a second one after cyclisation,

while on solid phase CuAAC, the purification was performed after cyclisation (Figure 2.7-1). Having this first purification before the CuAAC reaction eliminates all potential CuAAC reaction on peptides with deleted sequences. Some of these cyclised peptides would also have a retention time similar to the one of the desired peptide, therefore making the separation more difficult.

2.6 Characterisation

2.6.1 Mass spectrometry

As previously shown in **Figure 2.5-14**, cyclisation of the acyclic peptoid-peptide hybrids raised the question whether dimers (Scheme 2.5-3) were present.

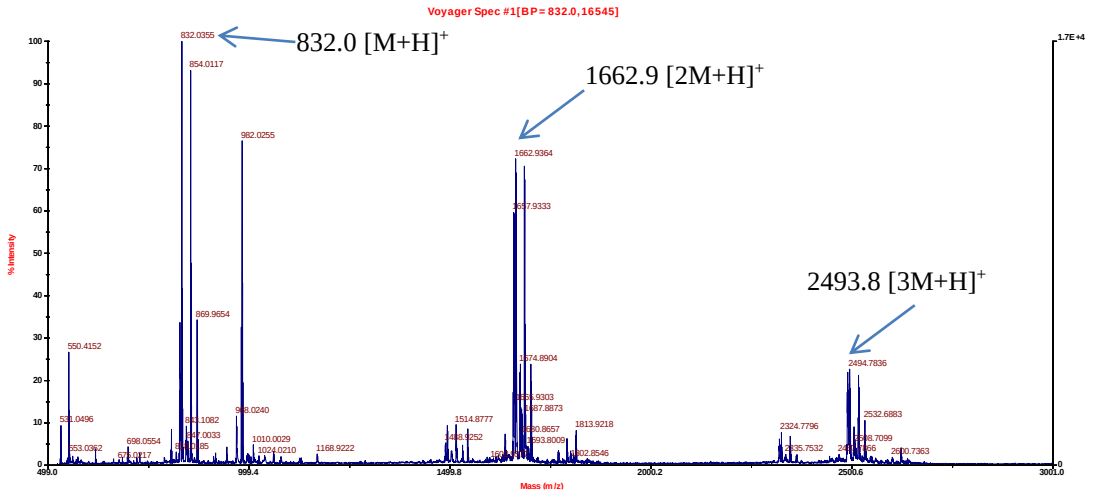

Figure 2.6-1. MALDI-ToF spectrum of **U17**. **Purity** 96%, ***m/z*** (MALDI-ToF, αCHCA) 832.0 $[M+H]^+$, 854.0 $[M+Na]^+$, 870.0 $[M+K]^+$, 1662.9 $[2M+H]^+$, 1684.9 $[2M+Na]^+$, 1700.8 $[2M+K]^+$, 2493.8 $[3M+H]^+$, 2515.7 $[3M+Na]^+$, 2531.7 $[3M+K]^+$

MALDI analysis mostly reveals singly charge species. Also, $[2M+H]^+$ or even $[3M+H]^+$ peaks from monomeric species can be observed as shown in Figure 2.6-1 in which **U17** (96% pure) displays 1M, 2M and 3M species (3M species for acetylated compounds only, out of scan range for biotinylated compounds). As mentioned in Section 2.5.3, preliminary MS experiments revealed the presence of linear dimers in the purified acyclic monomer hybrids, which brought more complexity to the identification of dimers. More spectrometry experiments such as MS-MS experiments

are therefore required. So far, IR studies and ^{1}H NMR carried out on **U13/C13** on resin (Section 2.5.4.1) and retention times observed by HPLC were sufficient to show that cyclisation did occur and MALDI experiments confirm the presence of the cyclised monomer. However, these are not sufficient to estimate or identify the dimer with absolute certainty.

2.6.2 Circular dichroism

CD is a useful technique to examine the secondary structure of protein or peptides (Figure 2.6-2).[260] In the presence of a chiral compound, the components of polarised light are absorbed differently. CD instruments measure that difference in absorbance, also called ellipticity, in degrees. For peptides, absorbance is usually observed between 180 nm and 260 nm, bands being essentially due peptide ponds.

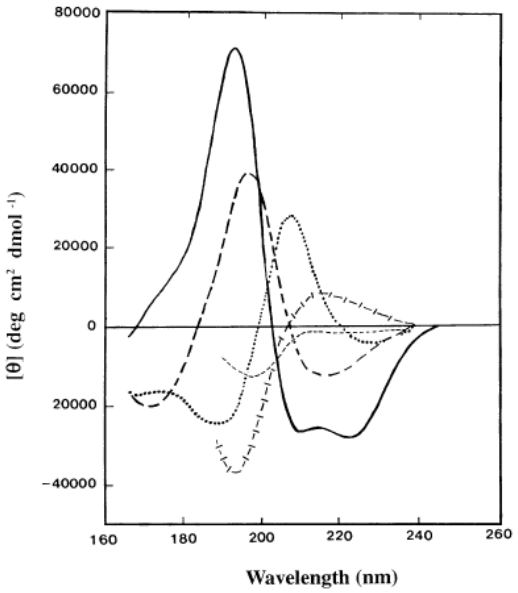

Figure 2.6-2. CD spectra with various types of secondary structures. Solid line, α-helix; long dashed line, anti-parallel β-sheet; dotted line, type I β-turn; cross dashed line, extended 3_1-helix or poly (Pro) II helix; short dashed line, irregular structure. Reproduced with permission.[260]

Solvents such as DMSO or DMF have to be avoided as they absorb strongly below 240 nm. Other solvent such as trifluoroethanol (TFE) can promote helix formation.[261]

In the Kirshenbaum laboratories, CD experiments were performed on their linear and cyclised peptoid (Figure 2.6-3).

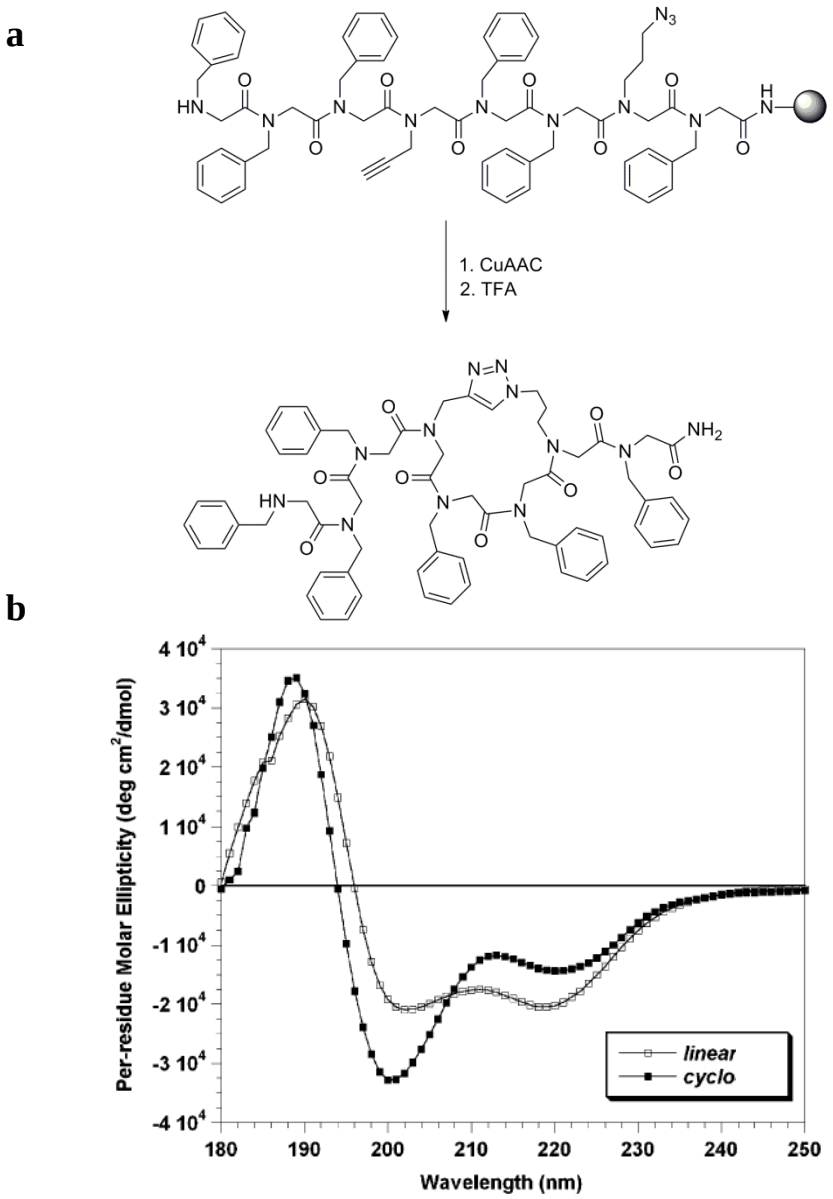

Figure 2.6-3. CuAAC on peptoids in the Kirshenbaum laboratories. (a) On-bead cyclisation of linear peptoid followed by TFA cleavage; (b) corresponding CD spectra. Final concentration of peptoid, 82 µM in H_2O. Experiments carried out at 25°C, 5 scans per run; 185 to 250 nm; scan rate of 1 nm s^{-1}. Bottom panel reproduced with permission.[232]

Samples of all hybrids were submitted to circular dichroism (CD) experiments, at a final concentration of 82 µM in HPLC grade H_2O and analysed using a CD spectrometer with conditions similar to those used in the Kirshenbaum laboratories.[232] Instead of acetonitrile, used in the Kirshenbaum laboratories, H_2O was used since the

hybrids are highly soluble in H_2O. This also avoids any risk of absorption by the solvent. Prior to any further analysis of the CD spectra, the background (H_2O) CD spectrum was substracted from the sample spectrum. The offset was chosen at 250 nm as this where there is the minimum absorption.

CD measurements were carried out on the purified hybrids; spectra are summarised in Figure 2.6-4.

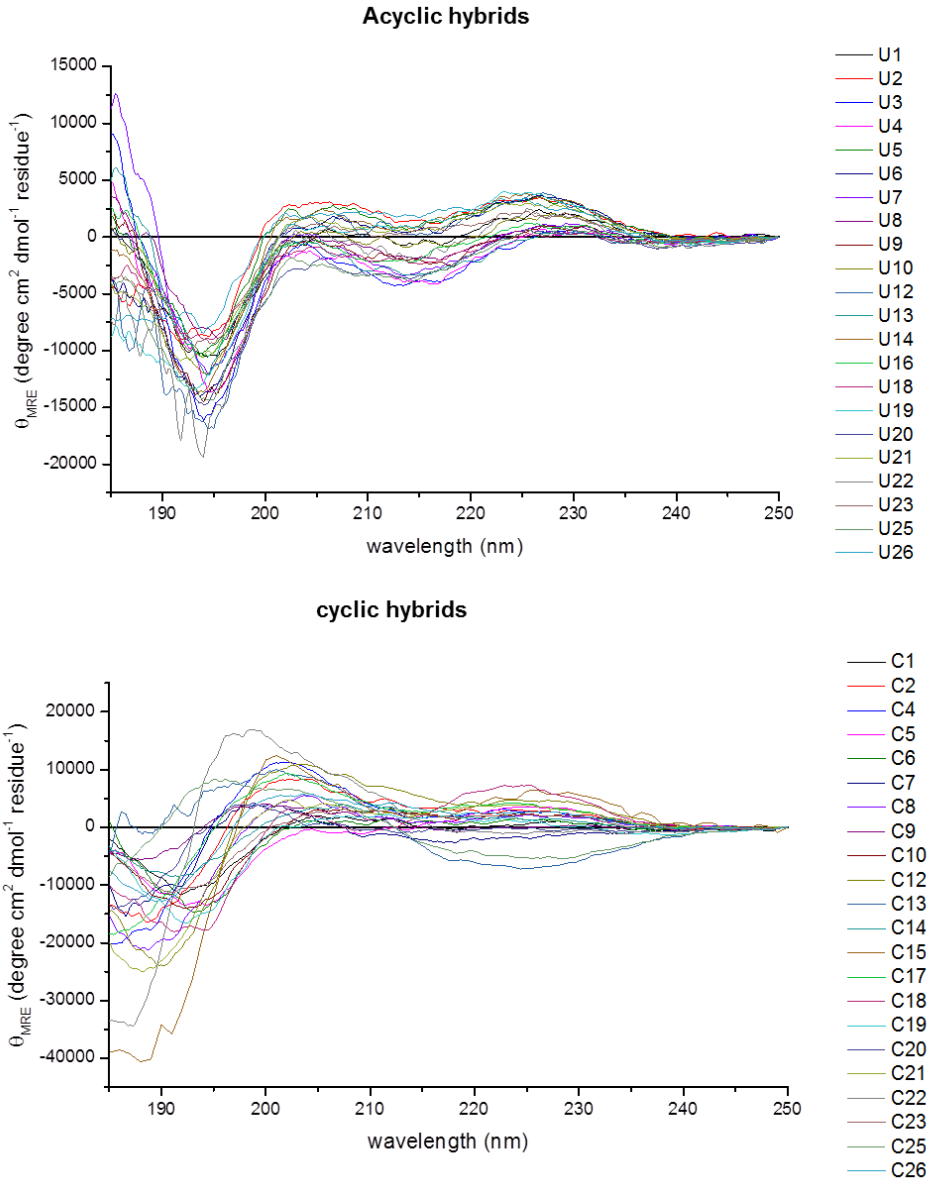

Figure 2.6-4. CD experiments on acyclic hybrids (top panel) and cyclic hybrids (bottom panel). Final concentration of hybrid, 82 µM in H_2O. Experiments carried out at 25°C, 5 scans per run; 185 to 250 nm; scan rate of 1 nm s^{-1}.

As expected for a series of short peptides, the acyclic hybrid spectra are all very similar, with a minimum at 195 nm and 215 nm, and a maximum at 205 and 225 nm. It is important to note that substraction of the background CD spectra was conducted with an offset at 250 nm. However, if the CD scan range had been carried out up to 260 nm, the overlay would have been better, and the shift observed on **U** hybrid spectra would not have been as significant.

For better clarity cyclic hybrid spectra can be arranged according to their common minima and maxima as shown in Figure 2.6-5.

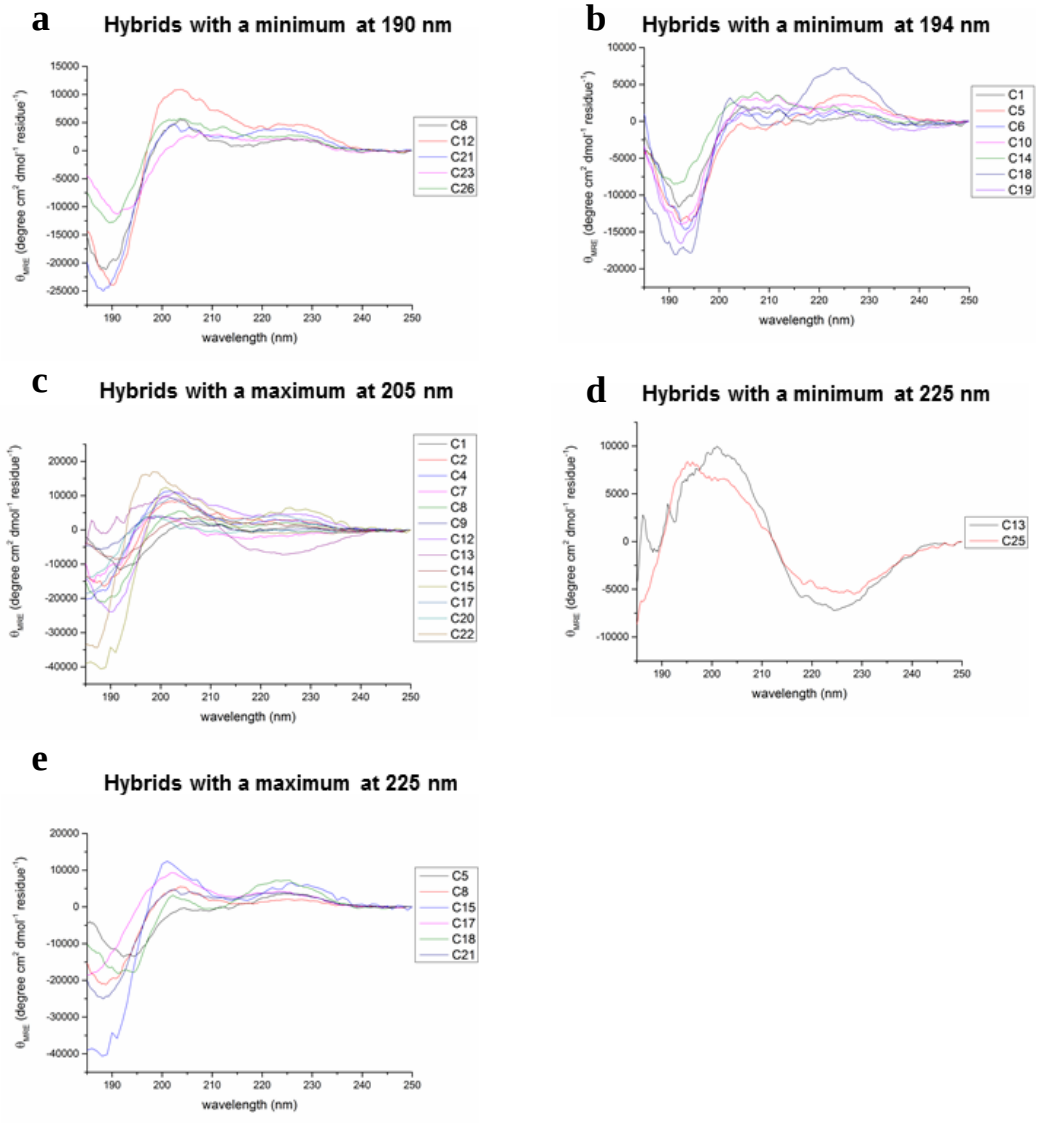

Figure 2.6-5. CD spectra of cyclic hybrids according to their positive or negative bands. (a) negative band at 190 nm; (b) negative band at 194 nm; (c) maximum at 205 nm; (d) negative band at 225 nm; (e) positive band at 225 nm; Final concentration of hybrid, 82 µM in H_2O. Experiments carried out at 25°C, 5 scans per run; 185 to 250 nm; scan rate of 1 nm s^{-1}.

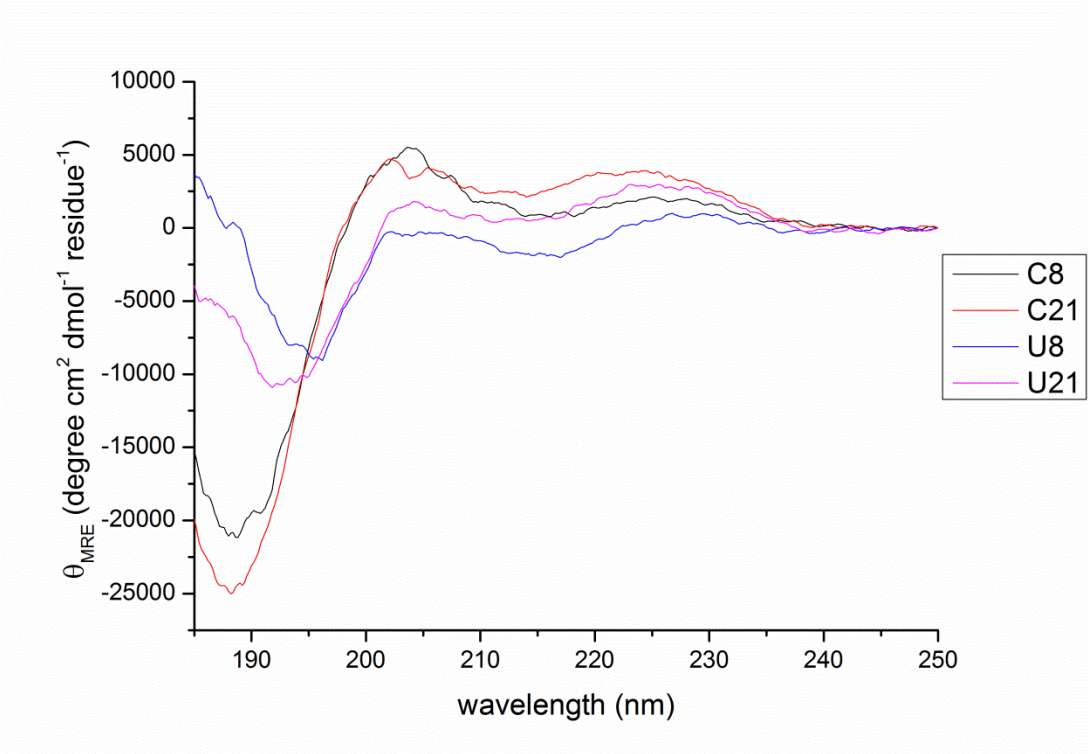

Figure 2.6-6. CD experiments on acyclic biotinylated hybrid **U8**, cyclic hybrid **C8** and the corresponding acetylated hybrids **U21**/**C21**. Final concentration of hybrid, 82 µM in H_2O. Experiments carried out at 25°C, 5 scans per run; 185 to 250 nm; scan rate of 1 nm s^{-1}.

By overlaying CD spectra of the same hybrid sequence but in its acyclic, cyclic, acetylated or biotinylated form, spectra of (**U**/**C**)**8**/**21** (Figure 2.6-6), (**U**/**C**)**7**/**20** and (**U**/**C**)**10**/**23** suggest that N-capping, whether acetylated or biotinylated, has no effect on the secondary structure. However, these pairs show a clear structural change between the uncyclised and the cyclised form. Indeed, while the CD spectra for **U8** and **U21** display a negative band in the 190-195 nm region and two weak positive bands at 205-210 nm and 220-225 nm, **C8** and **C21** have a stronger negative band shifted below 190 nm as well as slightly stronger positive bands at 205-210 nm and 220-225 nm. Similarly, the **U7**/**U20** and **C7**/**C20** pairs behave like the **U8**/**U21** and **C8**/**C21** pairs, respectively. It is interesting to note, that these hybrids (**U**/**C**)**7**/**20** ($KA^*AYFZ^*_4$) and (**U**/**C**)**8**/**21** ($K\ Z^*_4AYFA^*$) bear the $\mathbf{Z^*_4}$ monomer with an *i* to *i+4* spacing, $\mathbf{A^*}$ and $\mathbf{Z^*_4}$ have switched positions. In this case, switching $\mathbf{Z^*_4}$ with $\mathbf{A^*}$ had no effect. However, this phenomenon was not observed in other pairs.

(U/C)10/23 also display some interesting features. Negative bands at 190-195 nm and positive bands at 200-205 nm and 220-230 nm were observed but the intensities were stronger for the cyclic hybrids which may suggest that whatever the secondary structure is, it is enhanced by cyclisation. A similar trend was observed for **(U/C)5/18.**

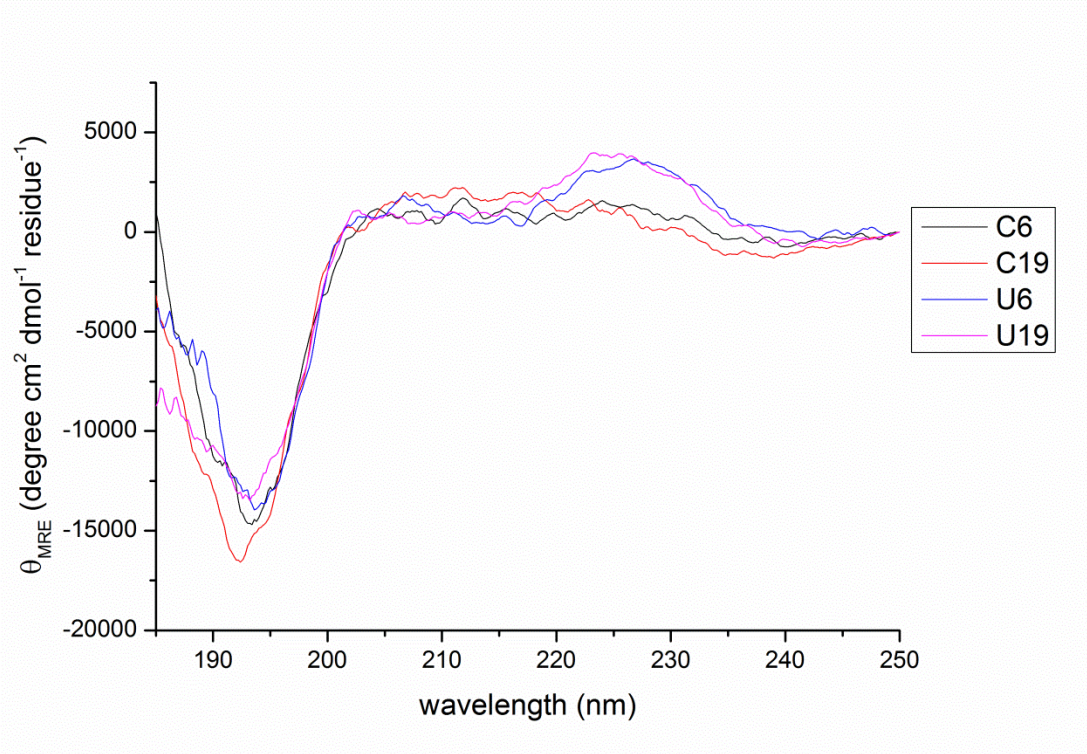

Figure 2.6-7. CD experiments on acyclic biotinylated hybrid **U6**, cyclic hybrid **C6** and the corresponding acetylated hybrids **U19/C19**. Final concentration of hybrid, 82 µM in H_2O. Experiments carried out at 25°C, 5 scans per run; 185 to 250 nm; scan rate of 1 nm s^{-1}.

Other pairs such as **(U/C)1/14** or **(U/C)6/19** (Figure 2.6-7) did not show any difference in structure between their uncylised and cyclized hybrids.

Altogether, based on these CD data, the effects of changing the position or the length of Z^* monomers on the structure cannot be predicted.

Szewkuk *et al*. have reported characteristic CD spectra of cyclic β-peptides with type I and II β-bend conformations.[262] They have studied fragments of the β2-chain of HLA-DP, 4 to 9 residue peptides, also including 2 cyclic analogues. Peptides were classed into two main groups (Figure 2.6-8); (1) the type II β-bend conformation displays a strong negative band below 190 nm, a positive band at 200-205 nm and very

weak bands at 220-230 nm (not always observed); (2) the type I β-bend conformation displays a negative band at 190-195 nm and a weak negative shoulder at 205-220 nm although the shoulder could be seen as two distinct negative bands at 200-205 nm and near 220 nm.

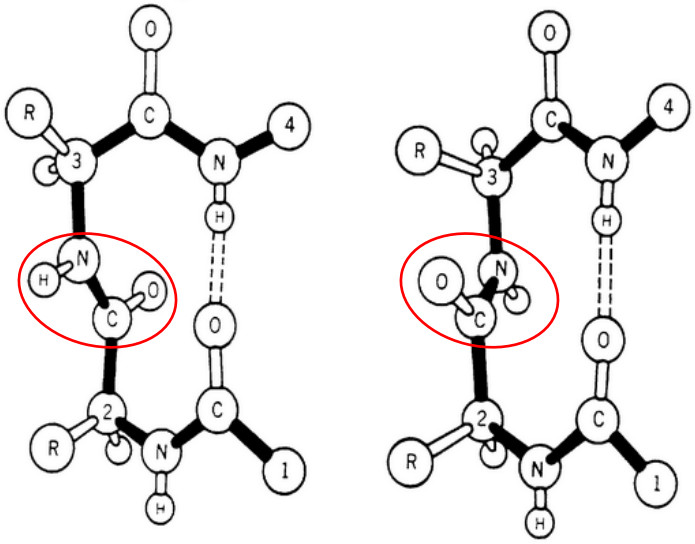

β-I type β-II type

Figure 2.6-8. Structure of β-I and β-II conformation.[263]

Overall, except for **C13**, **C17**, **C25**, all acyclic and cyclic hybrids have a minimum at 185-195 nm and maxima at 200-205 nm and 220-230 nm. Relating this to the known literature, the hybrids might have a type II β-bend conformation. **C17** was not selected as potentially having a type II β-bend conformation since the minimum near 190-195 nm was not observed.

C13 and **C25** CD spectra (Figure 2.6-5) are quite different from the others. With a positive band at 195-205 nm and negative band at 220-230 nm, an equilibrium could exist between type II β-bend conformation and type I β-bend conformation for **C13** and **C25** samples. However, CD is usually not sufficient and other structural data would be needed to confirm these hypotheses.

2.6.3 Protease resistance

Molecules with triazoles incorporated have often shown greater proteasomal degradation resistance; thus the protease resistance of **U13**, **U26**, **C13** and **C26** was analysed in collaboration with Dr. Catherine Botting (St Andrews University). To identify digestion products, samples were digested with trypsin which which specifically cleaves at the carbonyl sides of lysine and arginine. Possible fragments are shown in Figure 2.6-9.

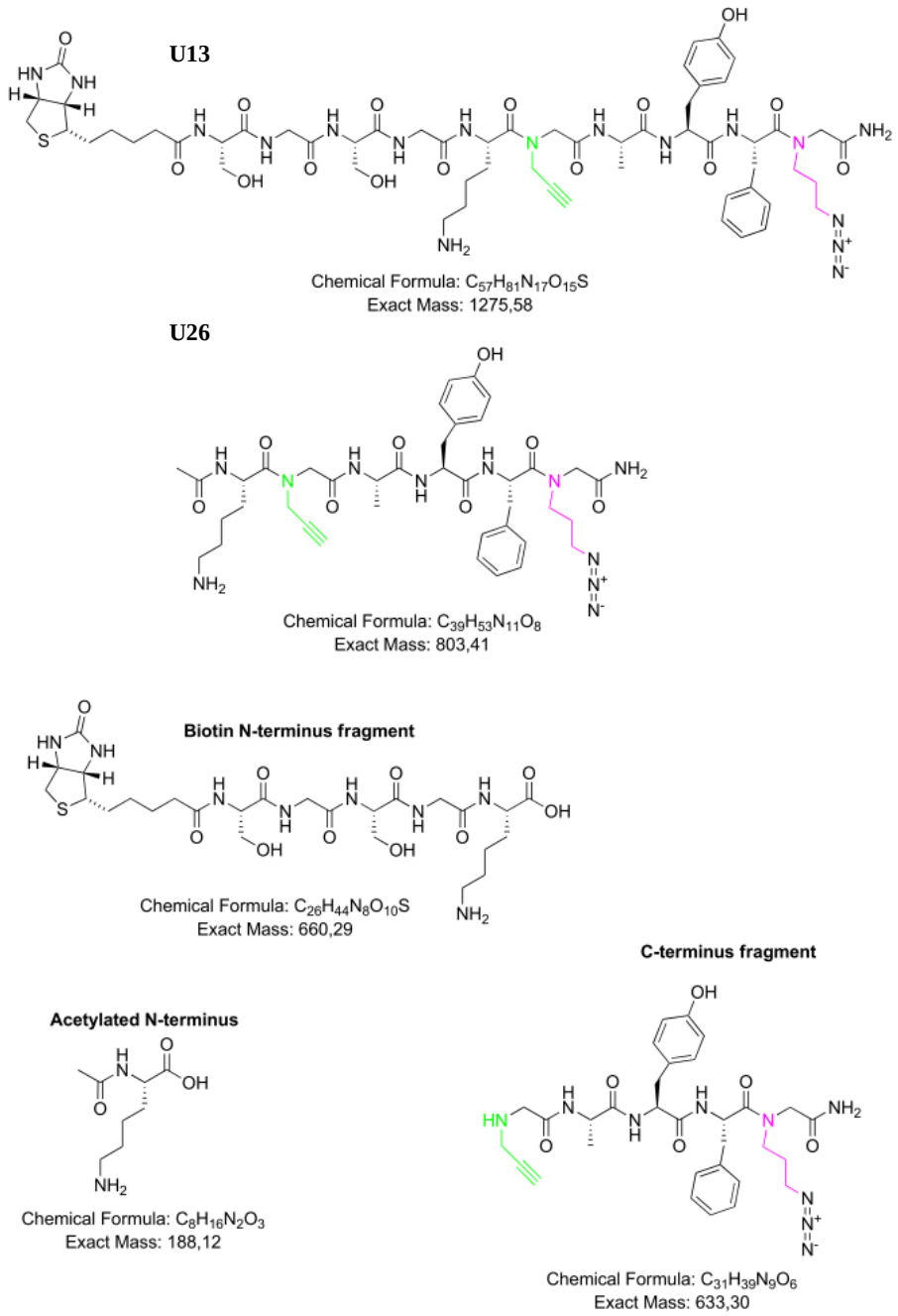

Figure 2.6-9. Undigested linear peptoid-peptide hybrids **U13**, **U26** and corresponding trypsin fragments.

Untreated samples as well as digested samples were analysed by ESI-MS. Peaks observed are detailed in Table 2.6-1.

Compound	Found mass
U13 (undigested)	1276.6 $[M+H]^+$, 660.8 $[2M+2Na]^{2+}$, 649.83 $[2M+Na+H]^{2+}$
U13 (digested)	1276.6 $[M+H]^+$, **661.1**, **656.1**
C13 (undigested)	1276.6 $[M+H]^+$, 1298.6 $[M+Na]^+$, 660.8 $[2M+2Na]^{2+}$, 649.83 $[2M+Na+H]^{2+}$
C13 (digested)	1276.6 $[M+H]^+$, 1298.6 $[M+Na]^+$, **661.1**, 660.8 $[2M+2Na]^{2+}$, 649.83 $[2M+Na+H]^{2+}$
U26 (undigested)	804.4 $[M+H]^+$
U26 (digested)	804.4 $[M+H]^+$, **634.1**, **656.1**
C26 (undigested)	804.4 $[M+H]^+$, 826.5 $[M+Na]^+$, 842.4 $[M+K]^+$,
C26 (digested)	804.4 $[M+H]^+$, 826.1 $[M+Na]^+$, 842.1 $[M+K]^+$, **634.1**, **656.1**
Biotin N-terminus fragment	**661.1** $[M+H]^+$
Acetylated N-terminus fragment	Expected 211.1 $[M+Na]^+$, 227.11 $[M+K]^+$, Essentially not seen
C-terminus fragment	**634.1** $[M+H]^+$, **656.1** $[M+Na]^+$

Table 2.6-1. Signals observed for undigested and digested trypsin products in mass spectrometry (ESI-MS). In bold are the masses corresponding to digestion fragments.

Digestion products were observed at 661.1 ($[M+H]^+$) for the biotin N-terminus fragment and at 634.1 ($[M+H]^+$), 656.1 ($[M+Na]^+$) for C-terminus fragment. The acetylated N-terminus fragment was not observed. Digestion products of **C13** were observed to be more complex (Figure 2.6-10) as the C-terminus cleavage fragment at 661.1 (single charge) overlapped with the signal at 660.8 representing $[2M+2Na]^{2+}$. However, when compared to the undigested product of the cyclised hybrid **C13**, the isotopic pattern in the spectrum of the digested product was distorted, therefore suggesting the presence of the digestion peak at 661.1 (Figure 2.6-11).

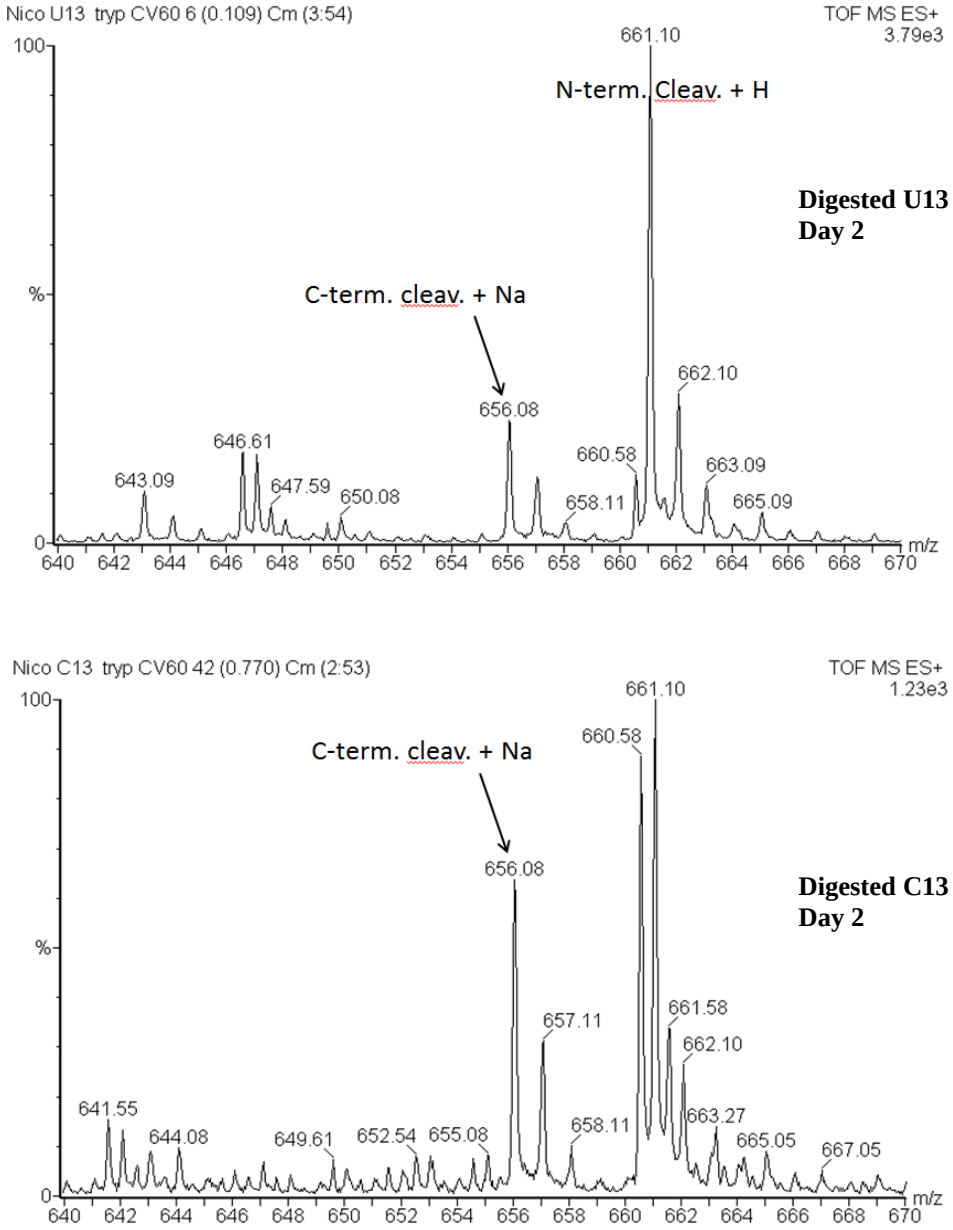

Figure 2.6-10. ESI-MS spectra of digestion products of linear (top) and cyclised (bottom) biotin-SGSG-KA*AYFZ*$_3$ (**U13**/**C13**), zoom at 656 (*m/z*). A solution of the biotinylated hybrids **U13** and **C13** (20 µL; 1.0 mg in 500 µL H_2O) was diluted with a solution of ammonium bicarbonate (20 µL, 50 mM) and trypsin was added (1 µg). Samples were incubated at 37°C for 1 day. Then a further aliquot of trypsin (4 µg) was added to samples on the third day, and mixture incubated for 4 days at 37°C. On the seventh day, a final aliquot of trypsin (20 µg) was added and the solution incubated for another 16 h at 37°C. Samples were analysed by ESI-MS on day 2, 7 and 8.

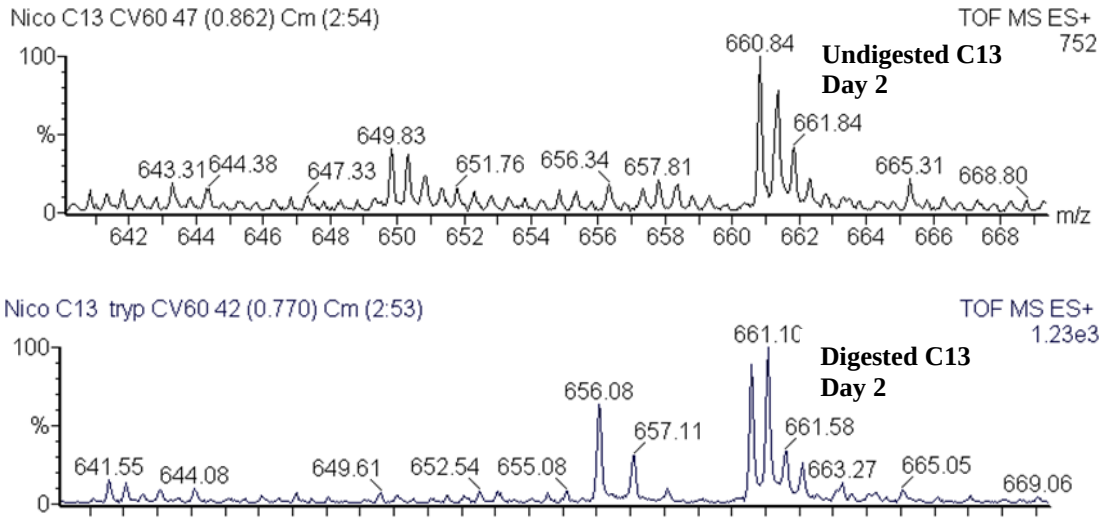

Figure 2.6-11. ESI-MS spectra of biotinylated hybrid **C13** for the identification of digestion product; zoom at 661.0 (*m/z*). A solution of the biotinylated hybrid **C13** (20 µL; 1.0 mg in 500 µL H_2O) was diluted with a solution of ammonium bicarbonate (20 µL, 50 mM) and trypsin was added (1 µg). Samples were incubated at 37°C for 1 day. Then a further aliquot of trypsin (4 µg) was added to samples on the third day, and mixture incubated for 4 days at 37°C. On the seventh day, a final aliquot of trypsin (20 µg) was added and the solution incubated for another 16 h at 37°C. Samples were analysed by ESI-MS on day 2, 7 and 8.

Resistance to protease was evaluated through a series of trypsin additions at different times on samples of **U13**, **C13**, **U26**, **C26** (Figure 2.6-10 to Figure 2.6-13).

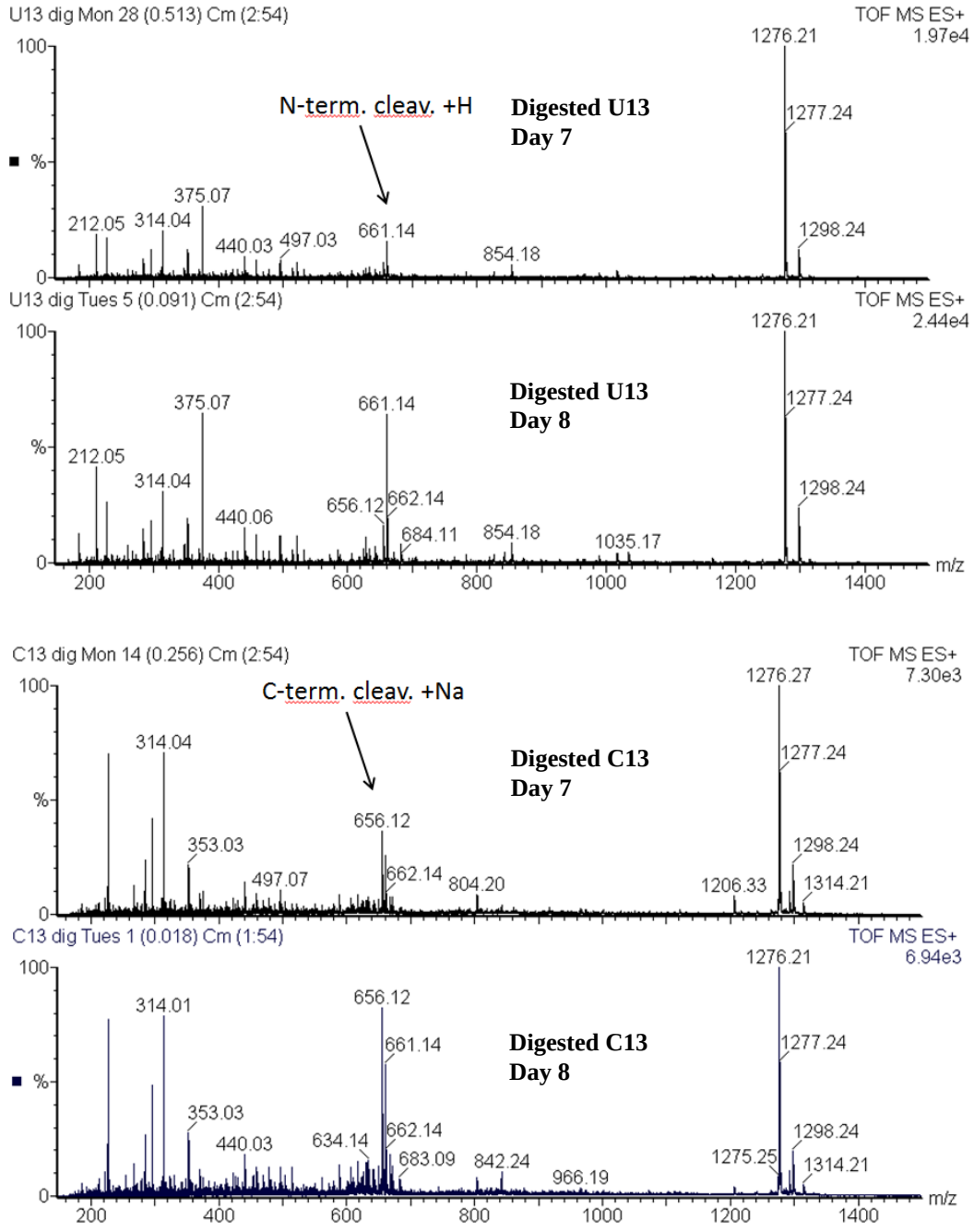

Figure 2.6-12. ESI-MS spectra corresponding to later stages of the trypsin digest experiment performed on biotinylated hybrids **U13** (top panels) and **C13** (bottom panels). Solutions of **U13** and **C13** (20 µL; 1.0 mg in 500 µL H_2O) were diluted with a solution of ammonium bicarbonate (20 µL, 50 mM) and trypsin was added (1 µg). Samples were incubated at 37°C for 1 day. Then a further aliquot of trypsin (4 µg) was added to samples on the third day, and mixture incubated for 4 days at 37°C. On the seventh day, a final aliquot of trypsin (20 µg) was added and the solution incubated for another 16 h at 37°C. Samples were analysed by ESI-MS on day 2, 7 and 8.

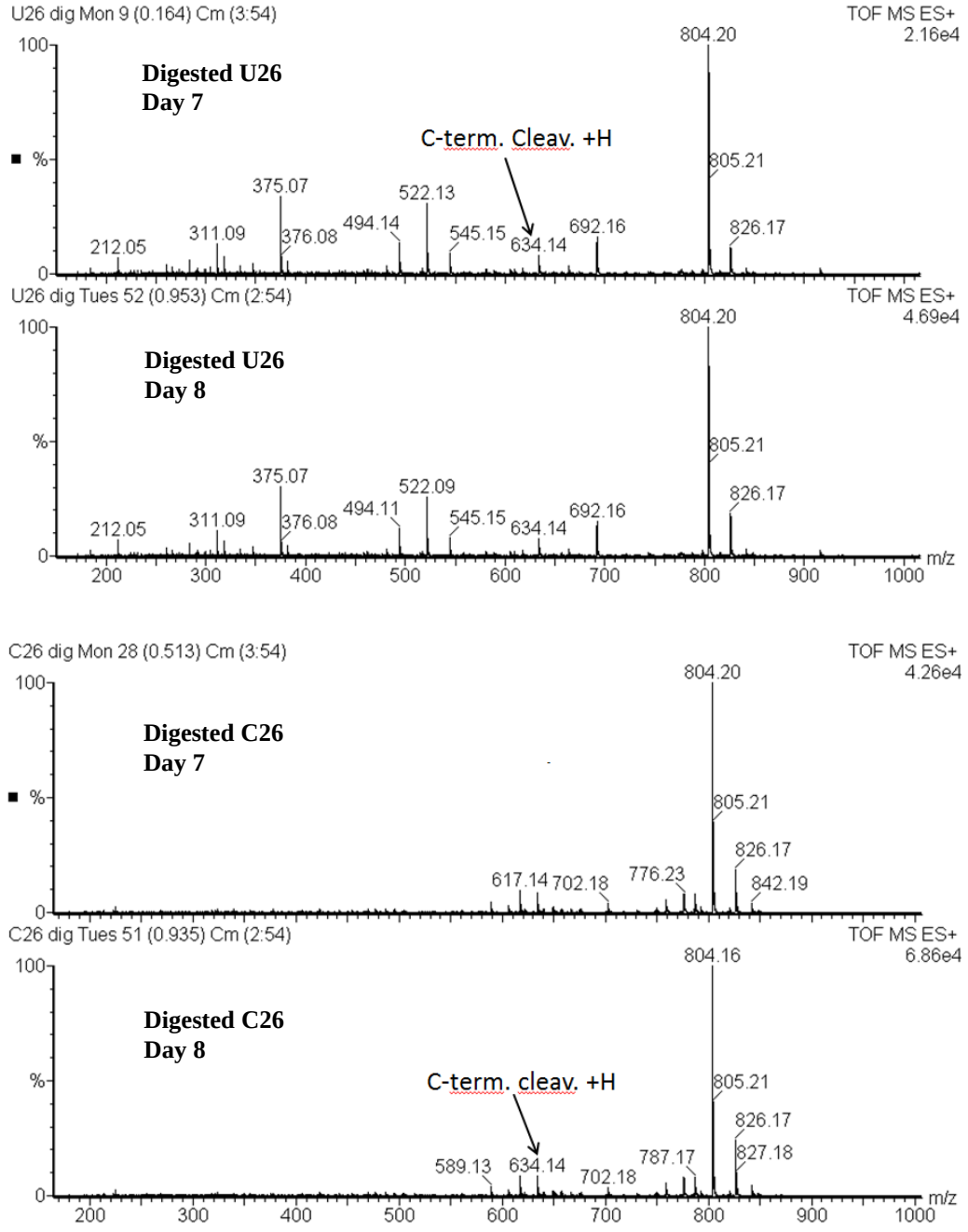

Figure 2.6-13. ESI-MS spectra corresponding to later stages of the trypsin digest experiment performed on acetylated hybrid **U26** (top panels) and biotinylated hybrid **C26** (bottom panels). Solutions of **U26** and **C26** (20 µL; 1.0 mg in 500 µL H_2O) were diluted with a solution of ammonium bicarbonate (20 µL, 50 mM) and trypsin was added (1 µg). Samples were incubated at 37°C for 1 day. Then a further aliquot of trypsin (4 µg) was added to samples on the third day, and mixture incubated for 4 days at 37°C. On the seventh day, a final aliquot of trypsin (20 µg) was added and the solution incubated for another 16 h at 37°C. Samples were analysed by ESI-MS on day 2, 7 and 8.

The last trypsinisation experiment analysed on day 8 for biotinylated **U13** and **C13** showed an increase in the relative percentage of C-terminal cleavage fragment observed compared to the samples analysed on day 7. The same experiments were

carried out on acetylated **U26** and **C26.** However, no increase in the percentage of cleavage fragments was observed. Thus for species **U/C13** or **U/C26**, there is no noticeable difference in the ratio of cleavage fragment percentage relative to the percentage of the parent ion between the linear and cyclised hybrids, suggesting a similar resistance between the linear and the cyclised hybrid. Since Trypsin does not cleave a Lys-Pro bond, it may be that the effect of trypsin with regard to the building blocks is greatly reduced. It would be interesting to check this effect by carrying this experiment on peptoid-peptide hybrids such as **U18** or **C18** (Ac-KAA*YFZ$^{*}{}_{3}$-NH_2) where the peptoid building block is one amino acid further away from lysine. It would also be interesting to conduct an experiment where the lysine lies between the peptoid monomers.

2.7 Conclusion

We have successfully developed *N*-propargylated glycine and *N*-azidoalkyl glycine building blocks. These stable units are suitable for Fmoc SPPS and the monomer based approach employed avoids the use of volatile hazardous azide intermediates. We have successfully incorporated these building blocks into peptides to generate peptoid-peptide hybrids and further cyclised them by CuAAC. We have applied the method to a library of peptoid-peptide hybrids, based on a truncated version of peptide KCCYFETHMPRH which was shown to bind MDM2 and inhibit MDM2-mediated ubiquitination of p53 *in vitro* in Chapter 1. As shown by experimental data, triazole formation is possible either on-resin or off-resin, which offer great flexibility. CuAAC reactions could be followed either by HPLC or by IR. The second HPLC purification performed following CuAAC in solution on the hybrids provided cleaner cyclic monomer (Figure 2.7-1). Triazole formation was also confirmed by preliminary ^{1}H NMR, and the resultant hybrid species were characterised by HPLC and MALDI-ToF. The acyclic hybrids have been shown to have similar secondary structure from circular dichroism experiments. Cyclic hybrids had different structures; cyclic hybrids had a significant change in their CD spectrum suggesting some form of β-turn. Protease resistance experiments on some of the hybrids have shown that cyclic hybrids are of comparable resistantance to their linear parent hybrids.

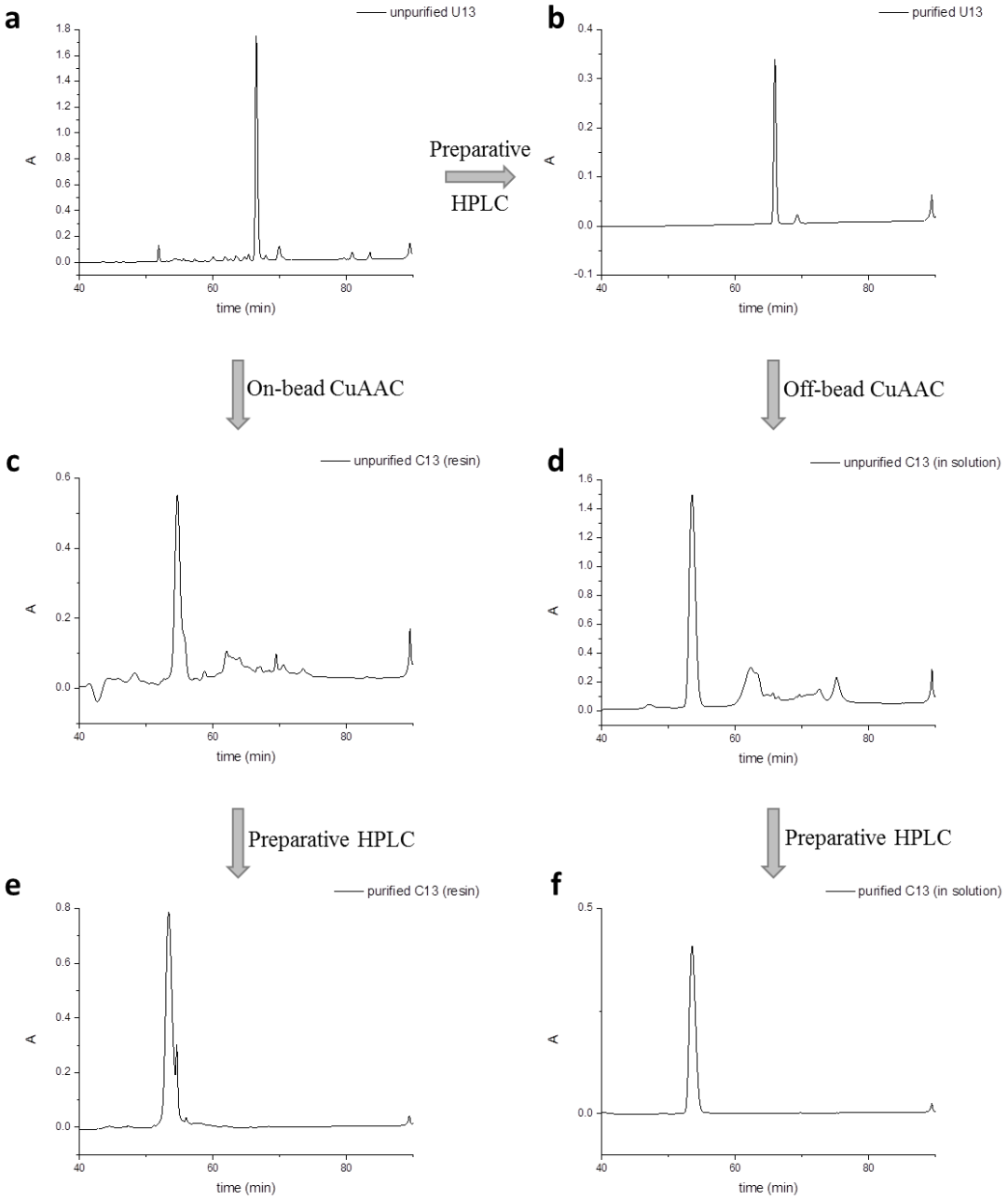

Figure 2.7-1. HPLC chromatograms of Biotin-SGSG-KA*AYFZ*$_3$-NH_2 in its linear or cyclised form (zoom on the 40-90 min region). **(a)** unpurified linear peptoid-peptide hybrid; **(b)** purified linear peptoid-peptide hybrid; **(c)** unpurified peptoid-peptide hybrid cyclised on solid support; **(d)** unpurified peptoid-peptide hybrid cyclised in solution phase; **(e)** HPLC-purified peptoid-peptide hybrid cyclised on solid support; **(f)** HPLC-purified peptoid-peptide hybrid cyclised in solution phase.

CHAPTER 3

Conclusion

The overall aims of this thesis the development of new peptide-based inhibitors for the MDM2-mediated ubiquitination of p53.

To this end, MDM2 and MDM4 RING fragments were cloned in pTrcHisB plasmid, the histidine-tagged proteins were expressed and purified on Ni-NTA beads. A library of 12-mer Phage-based peptides was used in phage display. The phage DNA of isolated colonies from the third and fourth round amplification of phage display were purified and sent for sequencing. In total, 109 sequences were successfully obtained and several peptides were identified as potential ligands for MDM2. The peptide sequences were aligned using ClustalW2 and two consensus sequences were observed, KCC and K(I/V/L)(W/V). The peptide sequences were also submitted to a BLAST search in the *Homo sapiens* database to evaluate possible correlations with cancer-linked proteins. Further assays including ELISA assays and pulldown assays were used to assess their binding towards MDM2 and the ubiquitination assay was used to assess their activity against the MDM2-dependant degradation of p53 *in vitro*. One peptide in particular, KCCYFETHMPRH, showed excellent binding of MDM2 and MDM4 and good activity in the ubiquitination assay. In order to test the selectivity of this peptide for the MDM2 family, cloning of the BRCA1 RING domain res. 1-304 was attempted. Unfortunately, the BRCA1 DNA insert failed to ligate with the plasmid. Instead commercially available plasmid with ligated BRCA1 res. 1-103 was used. Following successful expression and purification of BRCA1 res.1-103, the peptide KCCYFETHMPRH was tested against the protein and showed no binding towards it which confirms selectivity for the MDM family. This initial lead peptide was then developed further through testing alanine-mutated and truncated peptide variants. ELISA assays and ubiquitination assay *in vitro* suggested that the full-length peptide, KCCYFETHMPRH, is required but that mutation of the last histidine into an alanine increased significantly the ability of the peptide to prevent the MDM2-mediated ubiquitination of p53. However the lead peptide failed to show any binding in cell-based assays, a phenomenon that is quite common with peptides. We concluded that the design of peptidomimetics based on this peptide might increase its life time or cell permeability for a better activity in cells.

To achieve the synthesis of a new class of peptidomimetics which might incorporate *N*-alkylated peptoid building blocks for CuAAC coupling, syntheses of *N*-propargylated glycine and *N*-azidoalkyl glycine building blocks with variable lengths of side chain were successfully developed. These stable units are suitable for Fmoc SPPS and the monomer (rather than sub-monomer) based approach towards these peptoid building blocks employed avoids the use of volatile hazardous azide intermediates. These peptoid building blocks were successfully incorporated into peptides to generate peptoid-peptide hybrids which could then be cyclised by CuAAC. The method was applied to a library of peptoid-peptide hybrids, based on a truncated version of the peptide KCCYFETHMPRH which had been shown to bind MDM2 and inhibit MDM2-mediated ubiquitination of p53 *in vitro*. As shown by experimental data, triazole formation is possible either on-resin or off-resin, which offers great flexibility. CuAAC reactions could be followed either by changes in the retention time in the HPLC chromatograms or by the loss of the azide peak in the IR spectrum, and triazole formation was confirmed through observation of appropriate peaks in the ^{1}H NMR of the cyclic hybrid.

HPLC was performed for both on-bead and off-bead cyclisation. In this study, it was found that the second HPLC purification performed following off-bead CuAAC cyclisation on the hybrids provided cleaner cyclic monomer.

The hybrid peptoid-peptide species were characterised by MALDI-ToF and circular dichroism (CD). The acyclic hybrids have been shown to have similar secondary structure from circular dichroism experiments. Cyclic hybrids had different structures; cyclic hybrids had a significant change in their CD spectrum suggesting some form of β-turn. Protease resistance experiments on a few hybrids have shown that cyclic hybrids are as resistant as their linear parent hybrids.

In future work, the hybrids synthesised will be tested for their activity towards the ubiquitination of p53 *in vitro.* CuAAC will also be applied to a longer peptoid-peptide hybrid based more closely on the original peptide. Thus far, there is no indication where KCCYFETHMPRH binds to MDM2 and more detailed structural data is therefore required to allow further development of this interesting lead. Additional data such as Fluorescence Polarisation (FP) assay, Surface plasmon resonance (SPR)

assay and thermal shift assay may be required and would give new information on the kinetics and thermodynamics on the peptide-protein interaction

With the increasing interest in triazole formation and peptidomimetics, the creation of force fields for the computational modelling of such triazoles could be a powerful tool for the design of new peptidomimetics bearing triazole and help at the prediction of their secondary structure. Once the surface between the peptide lead and MDM2 is known, the stapled motifs could be overlapped to match this interaction and optimise the peptidomimetic accordingly. To this end, more rigid stapling motifs could be used; this could be done with the incorporation of one or several aromatic rings, alkenes or alkynes in the bridge.

Finally, we anticipate that this method might have more widespread application, including peptides with known activity. For example, several peptidomimetics mimic p53 peptides (Section 2.3.1.4). By replacing two of the non-interacting amino acids in the p53 peptides by the building blocks, the method could be applied and compared to the original p53 peptide and to the other peptidomimetics. This way we might gain enhanced protease resistance as well as novel structural features. Indeed while β-turn was observed for the peptoid-peptide hybrids, it would be interesting to develop peptidomimetics of p53 with the method described in this thesis and see if α-helicity could be maintained.

CHAPTER 4

Experimental

4.3 General microbiological techniques

All general chemicals and reagents were purchased from Sigma or BDH unless otherwise stated. All microbiological techniques were carried out using sterile apparatus and media under aseptic conditions.

4.3.1 Maintaining bacterial cultures

Bacterial cultures were grown in Luria-Bertani (LB) medium unless otherwise stated in an incubator-shaker maintained at 37°C, 200 rpm. Suitable sterile containers were used to allow for adequate aeration. If required, selective antibiotics were added to the LB medium at the following final concentrations: 100 µg mL^{-1} ampicillin or 20 µg mL^{-1} tetracycline.

Luria-Bertani (LB) medium:
LB medium (25 g, Miller) was dissolved in distilled water (1 L) and sterilised by autoclaving at 121°C for 15-20 min.

Final concentrations of each component: 1% (w/v) Tryptone, 0.5% (w/v) Yeast extract, 1% (w/v) NaCl

LB-agar plates were prepared by pouring LB-agar that was liquefied by heating (and subsequently cooled to about 40°C) into Petri dishes (Sterilin). If required, antibiotic was added to the liquefied LB-agar before pouring into the Petri dishes. The agar was then cooled until it solidified, and the plates were dried at 37°C for up to 1 h prior to use.

LB Agar:

LB-Agar (40 g, Miller) was dissolved in distilled water (1 L) and sterilised by autoclaving at 121°C for 15-20 min.

Final concentrations of each component: 1% (w/v) Tryptone, 0.5% (w/v) Yeast extract, 1% (w/v) NaCl, 1.5% (w/v) Agar

4.3.2 Glycerol stocks

Glycerol stocks were prepared by adding sterile glycerol (200 µL) to bacterial culture (800 µL) in a cryotube (Nunc). The stocks were mixed by gentle agitation, snap frozen in liquid nitrogen and stored at -80°C.

4.3.3 Transforming bacterial cells

Plasmid DNA (50-250 ng) was mixed with an aliquot of freshly thawed competent cells (30 µL) and incubated for 30 min on ice. The cells were then heat shocked at 42ºC for 45 seconds and cooled on ice for 2 min. LB medium without antibiotics (0.5 mL) was added and the mixture was incubated at 37ºC for 90 min with shaking. Aliquots (25 µL and 50 µL) were plated onto LB-agar plates containing the appropriate antibiotic and incubated overnight at 37ºC.

4.4 General molecular biology techniques

4.4.1 RNA extraction and RT-PCR

HCT116 cells in 10 cm plates were grown and scraped into ice-cold PBS (1 mL). The total RNA was extracted using the RNeasy Mini kit (Qiagen) according to the manufacturer's instructions (DTT used instead of β-mercaptoethanol). RNA was eluted in nuclease-free water (50 µL) and was reverse transcribed using the Omniscript RT Kit (Qiagen) in two steps as described below:

Reverse Transcription:

RNA extract (0.45 µL; 1.1 µg μL^{-1}) was diluted with nuclease-free water (to 7 µL) and heated at 65°C for 5 min to denature secondary structures. The RNA was then cooled on ice for 1 min, mixed with RT master mix (13 µL) and incubated at 37°C for 1 h. The cDNA freshly obtained could either be used immediately or stored at -20°C.

RT Master Mix:

2 µL RT Buffer (10X), 2 µL dNTP (5 mM), 0.2 µL oligo dT primer (0.5 mg mL^{-1}), 0.2 µL RNase inhibitor (40 U μL^{-1}), 2 µL DTT (100 mM), 1 µL Omniscript RT, 5.6 µL Nuclease-free water.

PCR:

PCR was performed with the cDNA template using PCR Master Mix (Rovalab) as described below. Primer sequences for BRCA1 are shown in Table 4.4-1.

target	Primer sequence (5'-3')	Product size
BRCA1 res. 1-103	Forward: GGAGTTGATCAAGGAACCTGTC Reverse: CTCGTACTTTCTTGTAGGCTCC	309 bp

Table 4.4-1. RT-PCR primer for BRCA1 cDNA template

PCR reactions:

25 µL pfu Master Mix (2X), 5 µL cDNA template, 0.35 µL Forward primer (100 µM), 0.35 µL Reverse primer (100 µM), 5 µL band doctor (5X), 14.3 µL Nuclease-free water.

Thermal cycling conditions:

1. 95°C for 2 min, 2. 95°C for 30 sec, 3. 62°C for 30 sec, 4. 72°C for 3 min, 5. Repeat steps 2-4 for 30 cycles, 6. 72°C for 10 min, 7. Hold at 4°C.

6X Gel loading dye was added to each sample, and the entire volume loaded on a 1.5% agarose gel and DNA bands observed under UV.

4.4.2 Plasmid DNA amplification, extraction and quantification

A single bacterial colony collected from an LB-Agar plate was added into LB medium (20 mL) containing a selective antibiotic and incubated overnight at 37ºC with shaking (200 rpm). This culture was then diluted into LB medium (500 mL) with the required antibiotic and again incubated overnight. Cells were collected by centrifuging at 6000 g for 20 min at 4ºC and plasmid DNA extracted using the Qiagen HiSpeed Maxi-prep kit according to the manufacturer's instructions. DNA was eluted in nuclease-free water (0.5 mL) and stored at -20ºC. DNA was quantified using a NanoDrop ND-1000 spectrophotometer against a nuclease-free water blank.

4.4.3 Agarose gel electrophoresis of DNA

1.5% agarose gels were prepared as required by dissolving electrophoresis-grade agarose (Invitrogen) in 1X TAE and then allowing the dissolved agarose to solidify by cooling. The intercalating dye ethidium bromide was added to the agarose solution at a final concentration of 0.5 μg mL^{-1} immediately prior to pouring. DNA samples were mixed with 6X DNA loading dye at a 5:1 ratio of sample:dye and loaded onto the agarose gel, which was then run at 100 V for approximately 1 h.

1X TAE Buffer:

Tris (40 mM), EDTA (1 mM), Adjust pH to 8 with glacial acetic acid

6X DNA Loading Dye:

bromophenol blue [0.25% (w/v)], xylene cyanol [0.25% (v/v)], glycerol [15% (v/v)]

4.4.4 DNA sequencing

DNA sequencing was carried out using the BigDye Terminator v3.1 Cycle Sequencing Kit (Applied Biosystems) essentially according to the manufacturer's instructions. The sequencing primers used for sequencing MDM4 and BRCA1 are listed in Table 4.4-2. All primers were purchased from Sigma Genosys unless stated otherwise. PCR reactions were set up as described below using each sequencing primer individually.

Sequencing PCR:

Sequencing reactions were set up as follows: 2 µL Big Dye v3.1, 2 µL Big Dye buffer (5X), 200 ng DNA template, 1 µL sequencing primer (3.2 M stock), Nuclease-free water to 10 µL.

Thermal cycling conditions were:

1. 96°C for 1 min, 2. 96°C for 10 sec, 3. 50°C for 5 sec, 4. 60°C for 4 min, 5. Repeat steps 2-4 for 24 cycles, 6. Hold at 4°C.

Following PCR, EDTA (2.5 µL of 125 mM stock prepared in nuclease-free water) and 100% ethanol (30 µL) were added to each reaction mix. The mix was briefly vortexed and incubated for 15 min at room temperature. Samples were centrifuged at 16000 g for 20 min at room temperature and the supernatant was gently removed. The samples were further centrifuged for 15 sec and any remaining liquid was discarded. The DNA pellet (which may or may not be visible) was rinsed with ethanol (30 µL; 70% aq) and centrifuged at 16000 g for 5 min at 4°C, following which the ethanol was gently removed. Again, the samples were further centrifuged at 16000 g for 15 sec at 4°C and any remaining liquid was removed. Finally, the pellet was air dried for 10-15 min and submitted for sequence analysis.

4.4.5 Cloning

All primers were purchased from Sigma Genosys.

Cloning using restriction enzymes (RE) was performed as follows: PCR amplification of the desired insert flanked by RE sites; RE digestion of insert and vector; and ligation of double-digested vector and insert.

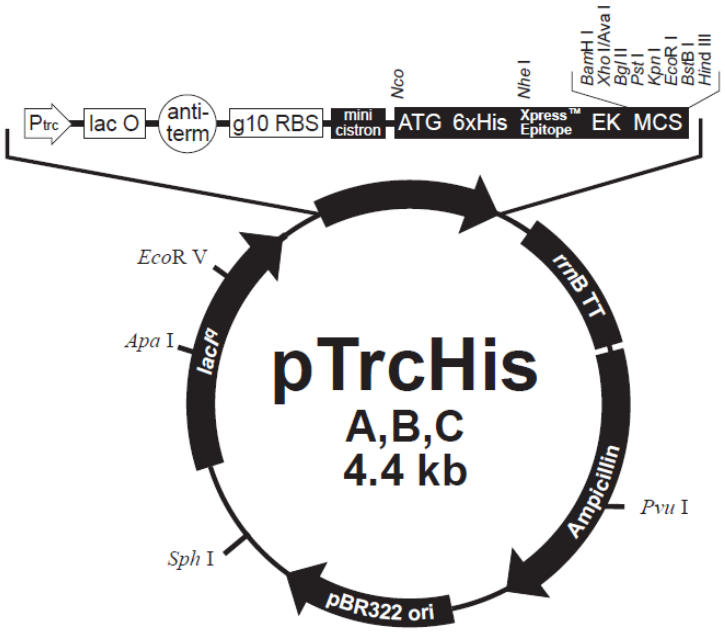

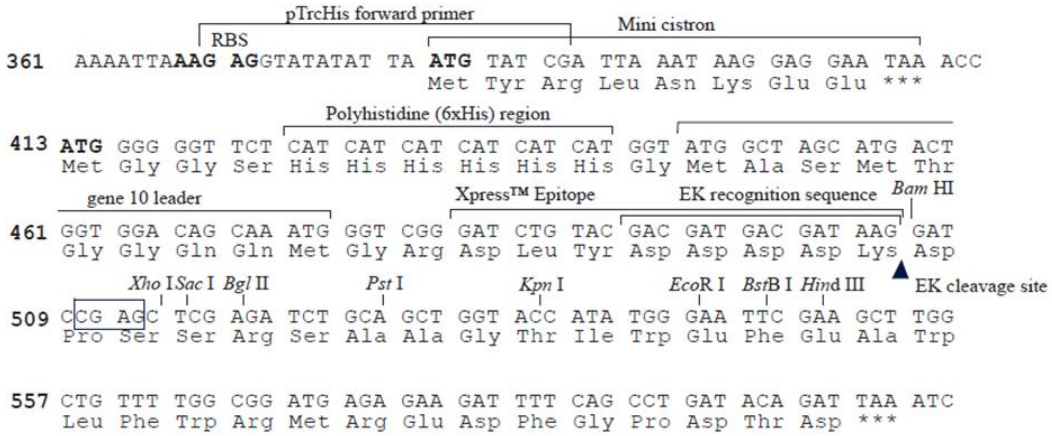

Figure 4.4-1. pTrcHis B map and multiple cloning site (MCS).

Amplification of the desired gene by PCR:

A suitable template (cDNA or plasmid DNA) was used to amplify the desired gene. Primers were designed so that different RE sites were incorporated into the 5' and 3' end of the insert. A list of primers with RE sites used for cloning is given in Table 4.4-2. Additionally, Table 4.4-3 lists the recognition sequences of the RE's used and the sites they cleave.

PCR reaction mix:

Reactions were set up as follows:

25 µL Pfu Master Mix (2X), 5 µL Band Doctor (supplied with Pfu Master Mix), 50 ng Template DNA, 0.25 µL Forward Primer (100 M stock), 0.25 µL Reverse Primer (100 M stock), Nuclease-free water to 50 µL.

Thermal cycling conditions:

1. 95°C for 15 min, 2. 94°C for 30 sec, 3. 55°C for 30 sec, 4. 72°C for 1 min, 5. Repeat steps 2-4 for 24 cycles, 6. 72°C for 5 min, 7. Hold at 4°C.

Cloned gene	Vector	tag	Primers sequences (5'-3')
MDM2 res.396-491	pTrcHis B	N-term 6x His	Forward: GACGTATCGTCGGATCCACAGC CATCAACTTCTAGTAGC Reverse: GCACTTCGGAATTCCTAGGGGA AATAAGTTAGCAC
MDM2 res.396-479	pTrcHis B	N-term 6x His	Forward: GACGTATCGTCGGATCCACAGC CATCAACTTCTAGTAGC Reverse: GCACTTCGGAATTCCTATCTACA TACTGGGCAGGGC
MDM4 res.395-490	pTrcHis B	N-term 6x His	Forward: GACGTATCGTCGGATCCATTGG ATTTGGCTCACAGTTCTG Reverse: GCACTTCGGAATTCCTATGCTAT AAAAACCTTAATAACCAGC
MDM4 res.395-478	pTrcHis B	N-term 6x His	Forward: GACGTATCGTCGGATCCATTGG ATTTGGCTCACAGTTCTG Reverse: GCACTTCGGAATTCCTACTTGC AAATAGGGCATGAAGCC
BRCA1 res.1-103	pTrcHis B	N-term 6x His	Forward: GACGTATCGTCGGATCCAATGG ATTTATCTGCTCTTCGCG Reverse: GCGCTGCGGAATTC**CTACTA**GT TTGCATACTCCAAACCTGTGTC

Table 4.4-2. Primers used for cloning

Restriction Enzyme	Recognition sequence (5'-3') (/ : cleavage site)
EcoRI	G/AATTC
BamHI	G/GATCC

Table 4.4-3. Recognition sequence of used Restriction Enzymes (RE).

Following PCR, the amplified DNA was cleaned up using a Qiagen PCR Clean-up Kit, and eluted in nuclease-free water (30 µL). An aliquot of the insert (2 µL) was loaded on a 1% agarose gel to check for adequate amplification.

Restriction Digest of vector and insert

Double digests were set up for the vector and insert as indicated below, using REs purchased from New England Biolabs (NEB). NEB buffers were used, and double digest conditions were as recommended by the supplier:

50 µL PCR product (insert), 6 µL NEB Buffer, 0.5 µL BSA (100X), 1 µL RE 1, 1 µL RE 2

The vector into which the desired gene was to be cloned was digested as follows: vector (15 µL; 90 ng μL^{-1}) was diluted in nuclease-free water (45 µL), and buffer, Bovin Albumin Serum (BSA) (Sigma) and RE's were added as above. Single digest controls were used to ensure that each enzyme could function efficiently under the reaction conditions used.

Double digests were carried out at 37°C for 90 min following which the samples were incubated at 65°C for 10 min to deactivate the REs.

Following the double digest, the entire digestion mix was loaded onto a 1% agarose (w/v) gel, and single bands corresponding to the double-digested vector and double digested insert (viewed under UV) were excised and purified using the Qiagen Gel Extraction Kit according to the manufacturer's instructions. Purified DNA was eluted in nuclease-free water (30 µL).

Ligation of double-digested vector and insert:

Ligation of the double-digested gel-extracted insert and vector was carried out using T4 DNA ligase (Promega) according to the manufacturer's instructions. The amount of insert to be added to the vector was calculated using the formula:

$$ng_{insert} = \frac{ng_{vector} \times kbp_{insert}}{kbp_{vector}} \times ratio\ \frac{insert}{vector}$$

Equation 4.4-1. Formula of the insert mass to add on the plasmid for a given molar ratio. pTrHis ~ 4.4 kbp; MDM4 res.396-491 insert ~ 317 bp; MDM4 res.396-479 ~ 281 bp.

Both 1:1 and 3:1 molar ratios of insert:vector were tested. A vector only control (no insert) was used to check for re-ligation of the vector alone.

Ligation reactions:

2.5 µL vector (8 ng μL^{-1}), x µL Insert (8 ng μL^{-1}) where x is calculated from Equation 4.4-1, 1 µL Ligase buffer (10X), 1 µL T4 DNA Ligase, Nuclease-free water to 10 µL.

Reactions were incubated overnight at 4°C. Competent DH5α cells were transformed with the ligation reaction mixtures and streaked out on LB-Agar plates containing selective antibiotics if required. Single colonies were picked and cultures were grown. After isolation of the plasmid DNA using the Qiagen Mini-prep Kit, a PCR was carried out using the extracted plasmid DNA to check for the presence of the insert in the selected clones. Positive clones were sequenced to verify that the insert was cloned in frame with tags on the vector (if present), and had no mutations. When the plasmid had sticky ends and re-ligated readily even in the absence of the insert, the double-digested vector was dephosphorylated at the 5' end immediately after RE digestion (before gel extraction) as outlined below.

Dephosphorylation of 5' ends:

Reactions were set up as follows:

0.5 U Calf Intestinal Alkaline Phosphatase (CIAP; Promega)/ pmol of 5' ends, 10 µL CIAP buffer (10X), 68.5 µL double-digested vector (2-4 µg), Nuclease-free water to 100 µL.

$$\text{pmol of } 5'\text{ends} = \frac{\text{amount of DNA (µg)}}{\text{size plasmid (kbp)}} \text{ x } \frac{1000}{660} \text{ x } 2$$

with 660: average molecular weight of a base pair

and factor 2 since 2 dephosphorylated ends per plasmid DNA

The reaction mix was incubated at 37°C for 15 min and then incubated at 56°C for 15 min. Further CIAP (0.5 U per pmol of 5' ends) was added and the above incubations repeated. EDTA (pH 8.0; 2 µL of 0.5 M) was added and the mix incubated at 65°C for 20 min. The entire dephosphorylated DNA mix was loaded onto a 1% agarose gel (w/v). To aid in visualising the DNA, the fluorescent intercalating dye ethidium bromide was added to the agarose solution at a final concentration of 0.5 µg/ml

immediately prior to pouring. A single band corresponding to the dephosphorylated double-digested vector (viewed under UV) was excised and purified using the Qiagen Gel Extraction Kit according to the manufacturer's instructions. Purified DNA was eluted in nuclease-free water (30 µL). This DNA was then used to set up a ligation reaction with double-digested insert as described above.

4.5 General biochemical techniques

4.5.1 Protein quantification

Protein concentration was estimated by using the using Bradford's reagent (Bio-Rad) as indicated, according to the manufacturer's instructions. Briefly, four BSA standards were prepared (0.2 to 1 mg mL^{-1}). The protein dye reagent (5X) provided was diluted by five and aliquots (200 µL) were pipetted into wells, one well for each standard, blank and protein solution. An aliquot (1 µL) of each solution to be tested was added to wells and the plate read at 595 nm using the Victor 3 plate reader (Perkin Elmer).
An alternative method used to measure protein concentration was BSA titration on a western blot. Aliquots of dilution sets of a protein (15 µL; 1:10, 2:10, 5:10, 7:10) and BSA standards (15 µL; 0.125 to 2 mg mL^{-1}) were run by western blotting, stained using Coomassie blue and compared by band intensity to provide an estimate of protein concentration.

4.5.2 SDS-PAGE

Polyacrylamide gels were prepared using the recipes listed above as described by Laemmli[264] using the Bio-Rad Mini-Protean kit. The separating gel was poured first, and overlaid with water to even out the upper surface of the separating gel. After polymerisation of the separating gel, the water was removed and the stacking gel was cast. Prior to loading, samples were mixed with a volume of 2X sample buffer at 1:1 ratio of sample to buffer. The mix was then heated for 3 minutes at 95ºC, and loaded onto the gel. Pre-stained protein standards (Fermentas) were loaded as size markers. Gels were run at 150 V for about 1 h in 1X running buffer, until the dye front reached the bottom of the gel.

10% separating gel

Reagent	Final conc.
H_2O	as required
30% acrylamide mix	10%
1.5 M Tris (pH 8.8)	0.39 M
10% (w/v) SDS	0.1%
10% (w/v) APS	0.1%
TEMED (v/v)	0.04%

12% separating gel

Reagent	Final conc.
H_2O	as required
30% acrylamide mix	12%
1.5 M Tris (pH 8.8)	0.39 M
10% (w/v) SDS	0.1%
10% (w/v) APS	0.1%
TEMED (v/v)	0.04%

5% stacking gel

Reagent	Final conc.
H_2O	as required
30% acrylamide mix	5%
1.5 M Tris (pH 6.8)	0.13 M
10% (w/v) SDS	0.1%
10% (w/v) APS	0.1%
TEMED (v/v)	0.1%

1X running Buffer

192 mM glycine
25 mM Tris
0.1% (w/v) SDS

2X Sample Buffer

300 mM Tris (pH 6.8)
5% (w/v) SDS
25% (v/v) glycerol
400 mM DTT
A few grains of bromophenol blue
Mix, aliquot and store at -20°C

4.5.3 Coomassie staining of SDS-PAGE gels

To visualise proteins by Coomassie brilliant blue staining, SDS-PAGE gels were stained with Coomassie blue stain for 30 min. Stained gels were then destained as required (from 30 min to overnight), washed in water and dried using a heated vacuum gel dryer (Gel Master Model 1426, Welch Rietschle Thomas).

Stain:

Methanol [50% (v/v)], Glacial acetic acid [10% (v/v)], Coomassie brilliant blue R-250 [0.2% (w/v)]

Destain:

Methanol [7.5% (v/v)], Glacial acetic acid [10% (v/v)]

4.5.4 Western Blotting

Proteins separated by SDS-PAGE were transferred onto 0.2 µm nitrocellulose membranes (Protran, Schleicher & Schuell Biosciences) using Bio-Rad transfer apparatus. The transfer was carried out in tanks containing transfer buffer and an ice pack at 120 V for 1 h, or 15 V overnight. Following the transfer, membranes were washed in phosphate-buffered saline (PBS) containing Tween-20 [0.1% (v/v)] (PBS-T) (3 x 5 min). The membrane was then blocked using blocking solution [5% (w/v) semi-skimmed milk powder (Marvel) in PBS-T] for 1 h, and was then incubated with the primary antibody (see Table 4.5-1) in blocking solution for 1 h at room temperature or overnight at 4ºC. The membrane was then washed with PBS-T (3 x 5 min) and incubated with horse radish peroxidase (HRP) conjugated secondary antibody [Dako Cytomation; used at 1:2000 dilution in blocking solution] for 1 h at room temperature. The membrane was again washed with PBS-T (3 x 5 min). Blots were overlaid with a mixture of enhanced chemiluminescence (ECL) solutions I and II at a 1:1 ratio (mixed immediately prior to use) for 2 min, dried and exposed to Hyperfilm ECL (Amersham) or X-Ray film (SLS) for the required period and finally developed using a Konica Medical Film Processor (Model SRX-101A).

1X Transfer Buffer:

Glycine (192 mM), Tris (25 mM), Methanol [20% (v/v)]

ECL Solution I:

Tris (100 mM, pH 8.5)**,** Luminol (2.5 mM), p-Coumaric acid (0.4 mM)

ECL Solution II:

Tris (100 mM, pH 8.5), H_2O_2 [0.02% (v/v)]

The primary antibodies used in this thesis are reported in Table 4.5-1.

Antibody for	type	name	supplier	dilution
p53	Mouse monoclonal	DO-1	Gift from B.Vojtesek	1:2000
MDM2	Mouse monoclonal	4B2	Gift from B.Vojtesek	1:2000
MDM2	Mouse monoclonal	2A10	Gift from B.Vojtesek	1:2000

Table 4.5-1. List of primary antibodies used for western Blotting.

4.6 Cell culture

4.6.1 Cell lines

Frozen cells were recovered by warming to 37ºC and transferring into a sterile culture dish containing fresh pre-warmed medium. The medium was replaced with fresh medium the following day.

Cells were incubated at the recommended temperature and humidity in incubators. The cell lines used are listed in Table 4.6-1. Media and supplements were stored at 4ºC and heated to 37ºC in a water bath prior to use.

Cell line	Origin	Growth conditions	Culture Media	Media supplements
H1299	Human (non-small cell lung carcinoma)	5% CO_2, 37ºC	RPMI-1640	10% (v/v) FBS, 1% (v/v) P/S
HCT116	Human (colorectal carcinoma)	5% CO_2, 37ºC	McCoy	10% (v/v) FBS, 1% (v/v) P/S

RPMI: Roswell Park Memorial Institute (Gibco)
FBS: Fetal Bovine Serum (Autogen Bioclear)
P/S: Penicillin/Streptomycin mix (Invitrogen)

Table 4.6-1. Cell lines used with growth conditions and appropriate media.

4.6.2 Cell splitting

Cells cultures were split at about 100% confluence (as often as required) into sterile tissue culture plates at a 1:10 dilution in fresh medium. To do so, the medium was discarded and the cells were washed in sterile PBS. Trypsin-EDTA (Invitrogen) was added (2 mL for a 10 mL culture dish) and the cells were incubated for 5 minutes at 37°C. Fresh culture medium (8 mL for a 10 mL culture dish) was added to deactivate the trypsin-EDTA, the cells were mixed by pipetting, and the required volume (1 mL for a 1:10 dilution) was plated onto a new culture dish containing pre-warmed fresh medium.

4.6.3 Transfection of DNA

H1299 cells were transfected at approximately 70-80% confluence with MDM2 DNA (0.4 µg; from Magda Maslon), Attractene (12 µL; Qiagen) in RPMI medium (300 µL; without antibiotic and FBS) according to the manufacturer's instructions and harvested 24 h post transfection.

4.6.4 Cell harvesting

At the time of harvesting the cells were placed on ice, following which the medium was discarded. The cells were rinsed with ice-cold PBS (1 mL/well for a 6-well plate and 10 mL for a 10 cm plate) and then harvested in further ice-cold PBS (1 mL) using a cell scraper. In some cases, cells in 10 cm plates were scraped directly into lysis buffer (1 mL; see below). Harvested cells were transferred to a microfuge tube and centrifuged at 2500 g for 5 min at 4ºC. The supernatant was discarded, and the cell pellet was either snap-frozen in liquid nitrogen (and then stored at -80ºC) or immediately lysed using the appropriate lysis buffer.

4.6.5 Mammalian Cell lysis

Lysis buffer was added to the harvested cell pellet (400 µL for a 10 cm plate). Samples were mixed thoroughly, incubated on ice for 20 min, and then centrifuged at 16000 g for 15 min at 4ºC. The supernatant (lysate) was transferred to a fresh tube, snap-frozen in liquid nitrogen and stored at -80ºC or used immediately.

0.1% Triton Lysis Buffer:

HEPES (50 mM, pH 7.5), Triton X-100 [0.1% (v/v)], NaCl (150 mM), NaF (10 mM), DTT (2 mM), EDTA (0.1 mM), protease inhibitor mix (1X)

Protease Inhibitor Mix (10X stock):

leupeptin (200 µg mL^{-1}), aprotinin (10 µg mL^{-1}), pepstatin (20 µg mL^{-1}), benzamidine (10 mM), soybean trypsin inhibitor (100 µg mL^{-1}), pefabloc (20 mM), EDTA (10 mM).

4.7 Protein expression and purification

4.7.1 Protein expression and lysis.

Bacterial expression plasmids containing the required gene insert were transformed into either BL21(AI) or BL21(DE3) cells as required and streaked onto LB-Agar plates. A single colony was picked from the LB-Agar plate, inoculated into LB (50 mL; with antibiotic if required) and incubated overnight in shaker at 37°C, 200 rpm. The following day, the 50 mL culture was diluted with fresh LB (to 1 L; with selective antibiotic if required) and incubated at 37°C until the OD_{600} was 0.4 (mid-Log phase). At this stage the inducing agent (0.5 mM IPTG or 0.2% L-arabinose based on chosen *E. coli* cells and plasmid) was added and the cultures incubated for 2-3 h in a shaker at room temperature or 37°C. Following induction, the cells were centrifuged at 6000 g for 20 min at 4°C and the supernatant was discarded.

The induced *E. coli* cell pellets were snap-frozen directly in liquid nitrogen. The following day, the required lysis buffer was added (10-15 mL per pellet from 500 mL culture) and the cells resuspended by pipetting. After 30 min incubation on ice, the cells were snap-frozen in liquid nitrogen and quickly thawed. The freeze-thaw cycle was repeated, after which the cells were sonicated using a Soniprep 150 sonicator (Sanyo; 3 x 15 sec at amplitude 5-10 µm with 15 sec incubations on ice in between). The sonicated samples were centrifuged at 16000 g for 15 min at 4°C and the supernatant (lysate) was collected.

His-purification Lysis Buffer:

Tris (20 mM, pH 8.0), NaCl (300 mM), NP-40 [0.3% (v/v)], Imidazole (20 mM), Lysozyme (1 mg mL^{-1}; fresh), protease inhibitor mix (1X)

GST-purification Lysis Buffer:

Tris (20 mM, pH 8.0), NaCl (150 mM), NP-40 [0.1% (v/v)], lysozyme (1 mg mL^{-1}; fresh), DTT (2 mM), protease inhibitor mix (1X)

4.7.2 Purification of His-tagged proteins

E.coli lysate was mixed with Ni^{2+}-NTA agarose beads (1 mL; 50% slurry, Qiagen) washed with lysis buffer (1 x 5 mL; beads centrifuged at 2000 rpm for 3 min at 4°C) and incubated for 1 h at 4°C on a spinning table. The mix was transferred to a 10 mL disposable column (MoBiTec) and allowed to empty by gravity, following which the beads were washed with Lysis buffer (2 x 5 mL) and Wash Buffer (3 x 5 mL). Next, Elution Buffer (5 mL) was added to the beads and incubated for 30 min at 4°C on a spinning table. The eluate was collected in fractions and stored at -80°C. If required, proteins were concentrated using Amicon Ultra columns (Millipore).

Lysis Buffer:

Tris (20 mM, pH 8.0), NaCl (150 mM), NP-40 [0.1% (v/v)], Glycerol [10% (v/v)], $MgCl_2$ (10 mM), Imidazole (20 mM)

Wash Buffer:

Imidazole, (40 mM; in Lysis buffer)

Elution Buffer:

Imidazole (150 mM; in Lysis buffer)

4.7.3 Purification of GST-tagged proteins

E. coli lysate from a 1 L culture was mixed with glutathione-sepharose 4B beads (1 mL; 50% slurry, Amersham GE) washed with Wash Buffer I (1 x 5 mL; beads centrifuged for 2000 rpm for 3 min at 4°C) and incubated for 1 h at 4°C on a spinning table. The mix was transferred to a 10 mL disposable column (MoBiTec) and allowed to empty by gravity, after which the beads were washed Wash Buffer I (5 x 5 mL). Next, Elution Buffer (5 mL) was added to the beads and incubated for 30 min at 4°C on a rotating table. The eluate was collected into fractions and stored at -80°C.

Wash Buffer I:

Tris (20 mM, pH 8.0), NaCl (150 mM), EDTA (1 mM), NP40 [0.5% (v/v)], Benzamidine (2 mM), DTT (2 mM), NaF (10 mM)

Wash Buffer II:

reduced glutathione Wash Buffer II (50 mM, pH 8.0)

Elution Buffer:

glycerol [10% (v/v)], NaCl (0.2 M), EDTA (0.1 mM), Triton X-100 [0.2% (v/v)], HEPES (25 mM, pH 8.0), DTT (1 mM), protease inhibitor mix (1X)

4.8 Binding assays

4.8.1 Peptide affinity chromatography (pull-down)

H1299 cells were grown in 10 cm dishes as required and lysed in 0.1% Triton (v/v) lysis buffer (1 mL) as described in Section 4.6. The cell lysate was collected and treated with avidin (20 µg mL^{-1}; Sigma) at for 30 min on ice followed by centrifugation at 16000 g for 5 min at 4°C. The supernatant was collected and was pre-cleared using sepharose-4B beads (200 µL of 50% slurry per lysate from 10 cm plate; beads were washed three times in PBS prior to use) for 1 h at 4°C with gentle shaking. Samples were centrifuged at 500 g for 3 min at 4°C to pellet the beads, supernatant (avidin-treated pre-cleared lysate) was collected and total protein levels quantified by Bradford assay. Alternatively, purified protein could be used instead of cell lysate.

In parallel, peptide affinity columns were prepared using Mobicol column jackets (MoBiTec; fitted with 35 µm pore-size lower filters) as follows: of streptavidin-agarose beads (20 µL; 50% slurry, Invitrogen) was added to each empty column jacket and washed with Buffer W (3 x 300 µL). After washing, the column outlet was sealed using the plug supplied and enough biotinylated peptide in PBS (about 2.5 µg of peptide in 200 µL PBS) to saturate the streptavidin-agarose was added and incubated with the beads for 1 h at room temperature on a rotating table. Then, the column was then allowed to empty by gravity and washed with Buffer W (3 x 300 µL) to remove any unbound peptide. The column was sealed again using the plug supplied and avidin-treated pre-cleared lysate (or purified protein) prepared as described above was then added to the peptide column (0.2 mg lysate or 20 ng protein per column; if required the total volume was made up to at least 200 µL with 0.1% Triton lysis buffer to aid in mixing) and incubated with the resin for 1 h at room temperature on a spinning

table. Once again, the column was allowed to empty by gravity, and then washed with PBS containing 0.2% Triton X-100 (v/v) (4 x 300 µL) and with Buffer W (2 x 300 µL). Next, Buffer W (200 µL) was added to the column and the resin emptied into a microfuge tube by removing the lower filter using a hooked needle. The tubes were centrifuged at 500 g for 3 min at room temperature to pellet the resin, and the supernatant was discarded. Bound proteins were eluted by heating in SDS 2X sample buffer supplemented with 100 mM DTT (40 µL) for three times 5 min at 85°C, shaking the tube between each period. Beads were centrifuged at 500 g for 3 min at room temperature and the supernatant was transferred to a new tube and stored at -20°C. Eluates (15-20 µL) were run out on 12% acrylamide SDS-PAGE gel and transferred to nitrocellulose and immunoblotted as required.

Buffer W:

Tris (100 mM; pH 8.0), NaCl (150 mM), EDTA (1 mM)

4.8.2 Protein-coated normalisation ELISA

Dilution sets of proteins were coated onto a white 96-well plate (Fisher) in $NaHCO_3$ buffer (50 µL; pH 8.6; 0.1 M aq.) at 4°C overnight. The following day wells were washed with PBS containing 0.1% Tween-20 (v/v; PBS-T) (3 x 200 µL) and non-reactive sites blocked using PBS containing 3% BSA (w/v; PBS-BSA) (200 µL) for 1 h at room temperature. Next, the wells were incubated with primary antibody diluted in PBS-BSA (50 µL per well; 1:2000 dilution) for 1 h at room temperature. The wells were washed with PBS-T (3 x 200 µL), and then incubated with an appropriate secondary antibody diluted in of PBS-BSA (50 µL per well; 1:2000 dilution) for 1 h at room temperature. Following further washing with PBS-T (3 x 200 µL), binding was detected by electrochemical luminescence (50 µL ECL mix per well) and was quantified using a Fluoroskan Ascent FL apparatus (Labsystems).

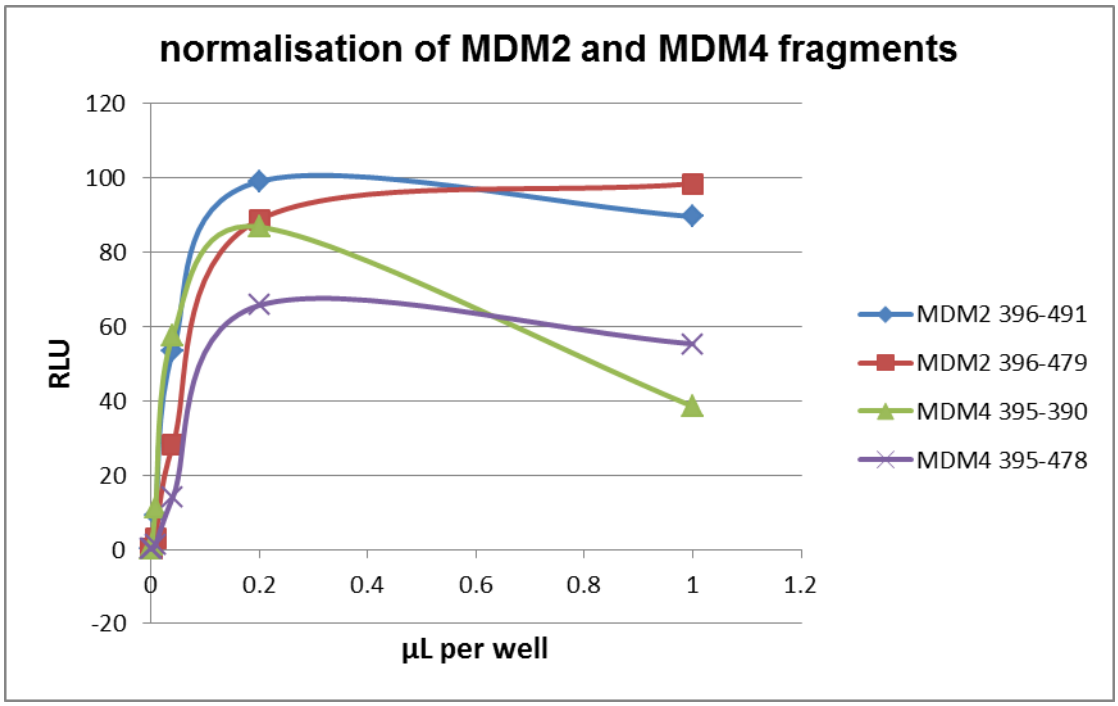

Figure 4.8-1. ELISA of dilution series of MDM2 and MDM4 fragments. MDM4 res. 395-478 has been chosen as the reference with a volume of 0.2 µL per well with a relative intensity of 65. The volumes per well of the other proteins correspond to the volumes giving this same intensity. Detection after addition of ECL with luminescence read on plate reader and analysed with the Fluoroskan Ascent software.

4.8.3 Protein-display ELISA

Purified protein (25-100 ng according to normalisation) was coated onto a white 96-well plate (Fisher) in $NaHCO_3$ buffer (50 µL; pH 8.6; 0.1 M aq.) at 4°C overnight. The following day wells were washed with PBS-T (3 x 200 µL) and non-reactive sites blocked using PBS-BSA (200 µL) for 1 h at room temperature. Biotinylated peptides (2.5 µg per well; Mimotopes) were added for 1 hour incubation at room temperature. Next, the wells were washed with PBS-T (3 x 200 µL) and incubated with HRP-linked streptavidin diluted in PBS-BSA (50 µL per well; 1:2000 dilution) for 1 h at room temperature. The wells were once again washed with PBS-T (3 x 200 µL). Finally, binding was detected by electrochemical luminescence (50 µL ECL mix per well) and was quantified using a Fluoroskan Ascent FL apparatus (Labsystems).

4.8.4 Peptide-display ELISA

Streptavidin (1 µg per well) was coated onto a white 96-well plate (Fisher) in PBS (50 µL) overnight at 37°C without shaking. The following day wells were washed with PBS-T (3 x 200 µL) and incubated with biotinylated peptide in PBS (5 µg in 50 µL) for 1 h at room temperature. The wells were washed again with PBS-T (3 x 200 µL) and non-reactive sites blocked using PBS-BSA (200 µL) for 1 h at room temperature. Solution phase calibration curves for the His-tagged proteins (Section 4.8.2) were used to determine standard luminescence outputs in RLU. His-tagged proteins (according to protein normalisation) in PBS (50 µL) were added to the wells and incubated for 1 h at room temperature. Next, the wells were washed with PBS-T (3 x 200 µL) and incubated with anti-His antibody (Novagen) diluted in PBS-BSA (50 µL per well; 1:2000 dilution) for 1 h at room temperature. The wells were once again washed with PBS-T (3 x 200 µL), and then incubated with HRP-conjugated rabbit anti-mouse antibody diluted in PBS-BSA (50 µL per well; 1:2000 dilution) for 1 h at room temperature. Following further washing with PBS-T (3 x 200 µL), binding was detected by electrochemical luminescence (50 µL ECL mix per well) and was quantified using a Fluoroskan Ascent FL apparatus (Labsystems).

4.9 Activity assay

4.9.1 *In vitro* ubiquitination assay

Reactions contained Hepes (25 mM, pH 8.0), $MgCl_2$ (6 mM), Triton X-100 [0.05% (v/v)], DTT (0.5 mM), ATP (3 mM, benzamidine (1 mM), ubiquitin (10 µM), creatine phosphate (10 mM), creatine kinase (10 µg mL^{-1}), E1 (UBE1; 100 nM), E2 (UbcH5a; 1 µM), p53 (23 nM), in the presence or absence of biotinylated peptides. GST-MDM2 (20 nM) was added last. After an incubation of 15 min at 30°C, reactions were stopped by adding 2x sample buffer with DTT (0.2 M) and heated for 5 min at 95°C. Samples were run on a 10- or 12-well Novex 4-12 % gel with MOPS running buffer. Immunoblotting was carried out with DO1 (1:2000 dilution) primary antibody and rabbit anti-mouse (1:2000 dilution) secondary antibody.

Master mix for 16 tubes:

366 µL H_2O, 10 µL HEPES (1 M, pH 8.0), 2.4 µL $MgCl_2$ (1 M), 2 µL Triton X-100 [10% (v/v)], 0.2 µL DTT (1 M), 6 µL ATP (0.2 M), 0.4 µL benzamidine (1 M), 3.2 µL ubiquitin (10 mg mL^{-1}).

4.10 Phage display

4.10.1 Panning

His-tagged MDM2 RING res. 396-491 (60 ng) and His-tagged MDM2 RING res. 396-479 (60 ng) in $NaHCO_3$ (0.1 M, pH 8.6) were coated into separate wells of a 96-well plate and incubated overnight at 4°C. Next, the solution was removed and the wells were incubated with a blocking buffer (200 µL; 5 mg mL^{-1} BSA in 0.1 M $NaHCO_3$) for 1 hour at room temperature. The blocking buffer was then removed and the well was washed with 0.1% TBS-T [6 x 200 µL; 50 mM Tris-HCl, pH 7.5, 150 mM NaCl, 0.1% (v/v) Tween 20]. An aliquot of the phage library Ph.D.-12™ (New England Biolabs) diluted in TBS-T (10 µL in 100 µL; ~2.7 10^9 phage) was added to each well and incubated for 1 hour at room temperature. Non-binding phage were discarded and the well was washed with TBS-T (6 x 200 µL). A non-specific elution buffer (100 µL; 0.2 M glycine-HCl, 1 mg mL^{-1} BSA) or an ATP-specific elution buffer (100 µL; 1 mM ATP, 3 mM $MgCl_2$) was added to the bound phage and incubated for 10 minutes at room temperature. The eluate was then transferred into a tube [and neutralized with Tris-HCl (15 µL; 1 M, pH 9.1) for the non-specific eluate]. Meanwhile a 3 mL culture of *E. coli* ER2738 (New England Biolabs) in LB medium with tetracycline (1:1000) at 37°C was incubated with shaking overnight. Next day, the culture was diluted (1:100) in LB medium and each eluate was then amplified by incubation with shaking (200 rpm) for 4.5 h at 37°C. The cultures were centrifuged at 10 000 rpm for 10 min at 4°C. The supernatant was collected and centrifuged at 10 000 rpm for 10 min at 4°C. The upper 80% of the supernatant was added to a solution of PEG/NaCl [20% (w/v) PEG-8000, 2.5 M NaCl] with 6:1 ratio (v/v) and the phage was allowed to precipitate overnight at 4°C. The precipitate was centrifuged at 13200 rpm for 15 min at 4°C, followed by removal of the supernatant and re-suspension in TBS (1 mL). Re-precipitation with PEG/NaCl for 1 h followed by centrifugation at

13200 rpm for 5 min at 4°C, removal of the supernatant as described above and re-suspension in TBS (200 µL) afforded the amplified eluate.

This panning procedure was repeated another three times using the freshly amplified eluate. The third and fourth round eluates were titered on IPTG/X-gal/LB agar plates for DNA sequencing.

4.10.2 Phage titering

LB/IPTG/Xgal plates (200 mL LB agar, 200 µL IPTG/Xgal mix, one plate for each required dilution) were prepared and pre-warmed at 37°C. While a culture of ER2738 in LB was grown (until OD_{600} ~ 0.5), 10-fold dilutions of phage eluate in LB were prepared. Aliquots (10 µL) of these were transferred to tubes of culture (200 µL) and quickly vortexed. After 5 min, the phage/ER2738 culture mix was transferred into pre-warmed melted Agarose Top (3 mL, 45°C), vortexed and immediately poured onto the previously made LB/IPTG/Xgal plates. The plates were allowed to cool for 5 min and incubated overnight at 37°C. Plates with blue plaques were observed.

IPTG/Xgal mix:
1.25 g IPTG, 1 g Xgal, 25 mL DMF.

4.10.3 Phage sequencing

Plates with around 100 blue plaques were chosen for phage sequencing. Single blue plaques were picked with a sterile pipette tip and transferred to tubes with diluted ER2738 culture (1 mL, 1:100 dilution of overnight grown culture) and incubated with shaking at 200 rpm for 4 h at 37°C. Cultures were centrifuged at 13200 rpm for 30 sec at 4°C and the supernatant collected. PEG/NaCl (200 µL) was added to an aliquot of the supernatant (500 µL), inverted and the mix was left for 10 min at room temperature. After centrifugation at 13200 rpm for 10 min at 4°C, the supernatant was removed followed by re-suspension of the pellets in iodide buffer (100 µL) and ethanol (250 µL) and the mixture was left for 10 min at room temperature. The precipitated Phage DNA was centrifuged at 13200 rpm for 10 min at 4°C and the supernatant discarded.

Pellets were washed with ethanol (500 µL; 70% aq) and air dried. Pellets were finally suspended in TE buffer (30 µL), and sent for sequencing.

Iodide-containing buffer:
Tris-HCl (10 mM, pH 8.0), EDTA (1 mM), NaI (4 M)

TE buffer:
Tris-HCl (10 mM, pH 8.0), EDTA (1 mM)

4.11 General chemical techniques

All solvents and reagents were obtained from commercial suppliers and used without purification, unless otherwise stated.

Thin-layer chromatography (TLC) was carried out using silica gel 60 F250 plates. TLC plates were visualised by ultra-violet light (254 nm) and/or with potassium permanganate staining (1.5 g of $KMnO_4$, 10 g K_2CO_3, and 1.25 mL 10% NaOH in 200 mL water). Column chromatography was carried out on Silica gel 60 (mesh 0.040-0.063 mm) (Merck).

^{1}H NMR spectra were recorded in the solvents indicated at 298 K on Bruker AVA400 or AVA500 spectrometers operating at 400 and 500 MHz, respectively.

^{13}C NMR spectra were recorded in the solvents indicated at 298 K on Bruker ARX- AVA400 or AVA500 spectrometers operating at 100.6 and 126 MHz, respectively. Chemical shifts for proton and carbon spectra are reported on the δ scale in ppm and were referenced to residual non-deuterated solvent. All coupling constants (J values) were measured in Hz.

Infrared (IR) spectra were obtained on a Shimadzu IRAffinity-1. All samples were recorded neat and frequencies are reported in cm^{-1} and only frequencies corresponding to significant functional groups are reported.

Matrix assisted laser desorption ionisation-time of flight (MALDI-TOF) mass spectra were performed using an Applied Biosystems Voyager-DE™ STR instrument

and analysed with the Voyager Instrument Control Panel software. α-Cyano-4-hydroxy-cinnamic acid (α-CHCA) was used as a matrix and positive ion mass spectra were reported.

High resolution mass spectrometry (HRMS) was recorded by the MS section of the University of Edinburgh on a Finnigan MAT 900 XLP high resolution, double-focussing mass spectrometer.

Microwave reactions were carried out using a Biotage Initiator instrument in sealed heavy-walled Pyrex tubes (vial caps and tubes; size 2 mL or 5 mL, Biotage AB).

Melting points (Mp) were determined using a Gallenkamp melting point apparatus.

High pressure liquid chromatography (HPLC) analyses were performed using the following eluents:
A: H_2O + 0.1% TFA;
B: MeCN + 0.1% TFA.

Analytical HPLC were performed on a Waters system (Agilant 1100 series degasser, Waters 600 controller, Waters 600 pump, Waters 486 detector, Waters 718 plus Autosampler, software Millenium[32]) with a Phenomenex Luna C18(2), 100 Å, 250 x 4.6 mm, 5µm column. HPLC grade eluents were employed, at a flow rate of 1 mL/min with samples filtered prior to injection. Detection was carried out at 214 nm.

Preparative HPLC purifications were performed on the same Waters system with a Phenomenex C18(2), 100 Å, 250 x 21.2 mm, 5 µm column, at a flow rate of 5 mL min^{-1}. Detection was carried out at 214 nm. Fractions were collected manually. The following gradients were used:

Analytical method (Method 4)

steps	Flow (mL min^{-1})	Time (min)	A (%)	B (%)
1	1	0.01	95	5
2	1	10	95	5
3	1	80	63	37
4	1	81	0	100
5	1	82	95	5
6	1	90	95	5
7	0	91	95	5

Preparative method (Method 4)

steps	Flow (mL min^{-1})	Time (min)	A (%)	B (%)
1	5	0.01	95	5
2	5	10	95	5
3	5	80	63	37
4	5	81	0	100
5	5	82	95	5
6	5	90	95	5
7	0	91	95	5

Table 4.11-1. Final methods for analytical and preparative HPLC. Solvent A: H_2O (0.1% TFA); solvent B: MeCN (0.1% TFA).

Circular dichroism (CD) experiments were carried out on a JASCO J-810 spectrometer equipped with Peltier controller JASCO PCT-4235 with the software spectra manager. Samples were diluted to a final concentration of 82 µM in HPLC grade H_2O (masses of hybrids and solvent precisely measured on an anti-static microbalance) and loaded into sealed quartz cells. Experiments were carried out at 25°C with 5 scans per run, from 185 to 250 nm with a scan rate of 1 nm s^{-1}. Cells (cuvettes) were handled with the greatest care to avoid any damage, such as scratches. Cells were washed with H_2O and ethanol and dried thoroughly with an air duster between runs. No bubbles should be present in the cell. Data processing was achieved using Spectra Manager. The background CD spectrum (H_2O) experiment was subtracted from the spectrum of each hybrid CD spectrum. Using Equation 4.11-1, ellipticity θ was converted into mean residual ellipticity θ_{MRE}.

$$\theta_{MRE} = \frac{\theta * 0.1 * Mw}{(n-1) * C * l}$$

Equation 4.11-1. Conversion of ellipticity θ into mean residual ellipticity θ_{MRE}, where $\boldsymbol{\theta}$ is ellipticity (in degrees), $\boldsymbol{Mw}$ is the molecular weight of the analysed compound, $\boldsymbol{n}$ is the number of residues, $\boldsymbol{C}$ is the final concentration (in mg/mL) and $\boldsymbol{l}$ is the cuvette length (in cm).

Protease resistance degradation experiments were carried out by Dr. Catherine Botting. Briefly, a solution of the biotinylated hybrid **U13** (20 µL; 1.0 mg in 500 µL

H_2O) was diluted with a solution of ammonium bicarbonate (20 µL, 50 mM) and trypsin was added (1 µg). Samples were incubated at 37°C for 1 day. Then a further aliquot of trypsin (4 µg) was added to samples on the third day, and mixture incubated for 4 days at 37°C. On the seventh day, a final aliquot of trypsin (20 µg) was added and the solution incubated for another 16 h at 37°C. Samples were analysed by ESI-MS on day 2, 7 and 8.

The analysis was also conducted for the biotinylated hybrid **C13** and the acetylated hybrids **U26** and **C26**.

4.11.1 General methods

Fmoc SPPS:

Generalities:

Peptoid-peptide hybrids were prepared on aminomethyl polystyrene resin crosslinked with 1% DVB (loading = 1.23 mmol/g) functionalised with a Rink amide linker. The functionalisation of the solid support is described in Section 4.11.3.1. The ratio of solvent-resin used for coupling washes was 10 mL of solvent for 1 g of dry resin. The resin must be swollen for 20 minutes at room temperature in DCM. Fmoc deprotection, final side-chain deprotection together with resin cleavage steps were carried out in solid phase extractor (SPE), polypropylene syringe equipped with a frit and a valve. Following wash volumes are given for 200 mg of resin.

Calculation of a theoretical loading:

Theoretical loading of a resin after a reaction is calculated using

$A = B*1000/[1000+B*(\text{difference of } M_w)]$

Equation 4.11-2. Calculation of theoretical loading. A = new theoretical loading (mmol/g), B = loading of starting resin (mmol/g), difference of M_w is the difference of Molecular weight between the product and the starting resin (g/mol)

Coupling of amino acids or building block monomers:

The Fmoc-protected monomer unit or amino acid (3 equiv., 0.1 M) and HOBt (3 equiv., 0.1 M) were dissolved in DMF. DIC (3 equiv., 0.1 M) was then added to the solution and the mixture was stirred for 10 minutes at room temperature. The solution was added to the Fmoc deprotected pre-swollen resin and the mixture was mixed for 3 h at room temperature or 30 min at 60°C under microwave radiation. The resin was then washed with DMF (3 x 2 mL) and DCM (3 x 2 mL). Coupling completion was monitored using the appropriate qualitative colorimetric tests (ninhydrin test for detection of primary amines and chloranil test for secondary amines). Coupling reactions were repeated until coupling completion.

Fmoc deprotection:

Fmoc deprotection was carried out by suspending the resin in 20% piperidine in DMF (2 mL) and shaking for 10 minutes. The resin was then filtered, washed with DMF (3 x 2 mL), DCM (3 x 2 mL). The treatment of the resin by 20% piperidine in DMF (2 mL) was repeated for another 10 minutes after which time the resin was washed with DMF (3 x 2 mL) and DCM (3 x 2 mL).

N-Acetylation capping:

When biotinylation of peptoid-peptide hybrid was not required, acetylation was carried out as follows. After the final Fmoc deprotection and washes with DMF (3 x 2 mL), DCM (3 x 2 mL) DMF (3 x 2 mL), A 50-fold molar excess of acetic anhydride and DIPEA was dissolved in DMF. The solution was added onto the resin and the reaction was left for 30 min at room temperature. N-Acetylation capping completion was monitored using the appropriate qualitative colorimetric tests.

TFA cleavage-deprotection and cold ether precipitation:

The resin containing the peptoid-peptide hybrids was washed with DMF (3 x 2 mL), DCM (3 x 2 mL), MeOH (3 x 2 mL), Et_2O (3 x 1.5 mL) and dried in vacuo. The resin was suspended in 2.5 mL of a mixture of TFA/TIS/H_2O (95: 2.5: 2.5) and stirred for 1 hour. After cleavage, the resin was filtered and washed with 5 mL of TFA. The TFA filtrates were collected and concentrated down to a volume of 1 mL. The concentrated

mixture was then added dropwised in a centrifuge tube containing cold Et_2O (12 mL). The precipitated peptoid-peptide hybrid was then sonicated and recovered by centrifugation. The solid was then washed with cold ether (12 mL) and centrifuged three times. After the last cycle of washes/centrifugation, Et_2O was removed, the peptoid-peptide hybrid was dried, redissolved in H_2O and lyophilised overnight.

Ninhydrin test:[256]

The test was carried out on a few resin beads with the addition of 3 drops of reagent A and 1 drop of reagent B. The mixture was heated at 100°C for 5 minutes. A blue solution indicated the presence of free amine on the resin while a yellow solution corresponded to the absence of free amine.

Preparation of ninhydrin reagents A and B:

Reagent A:

Solution 1: Reagent grade phenol (40 g, 0.43 mol) was added to absolute ethanol (10 mL) and the mixture was heated until complete dissolution of the phenol. Amberlite mixed-bed resin MB-3 (4 g) was added to the solution and stirred for 45 minutes and filtered.

Solution 2: KCN (65 mg, 1 mmol) was dissolved in water (100 mL). The KCN solution (2 mL) was diluted to 100 mL with freshly distilled. Amberlite mixed-bed resin MB-3 (4 g) was added, stirred for 45 minutes and filtered. Solutions 1 and 2 were mixed.

Reagent B:

Ninhydrin (2.5 g, 14 mmol) was dissolved in absolute ethanol (50 mL).

Chloranil test:[265]

The test was carried out on a few resin beads by the addition of 1 drop of solution A and 1 drop of solution B. The mixture was shaken at room temperature for 3 minutes. Dark green resin beads indicated free secondary amine group, whilst colourless resin beads correspond to no free secondary amine group.

Chloranil solutions A and B:

Solution A: 2% acetaldehyde in DMF

Solution B: 2% chloranil in DMF

Preparation of samples for MALDI-TOF-MS:

A solution of the compound (0.5 µL; approximately 0.01 M in HPLC solvent) was loaded onto the MALDI plate. An aliquot of the CHCA matrix solution (0.5 µL) was added on top of the compound and mixed up and down. The plate was allowed to dry at room temperature for 10 minutes prior to analysis.

α-CHCA matrix solution:
10 mg of α-CHCA dissolved in 1 mL of H_2O:MeCN 1:1 (v/v) with 0.1% TFA (v/v).

4.11.2 Synthesis of building blocks A^*, Z^*_3, Z^*_4 and Z^*_5

***tert*-Butyl 3-aminopropylcarbamate 85**

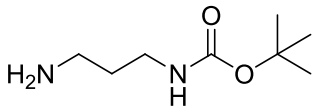

To a solution of propane-1,3-diamine **82** (24.3 g, 328 mmol) in DCM (600 mL) was added di-*tert*-butyl dicarbonate (8.94 g, 41.0 mmol) dropwise in DCM (300 mL) over 5 h at room temperature. After stirring for ~48 h at room temperature, DCM was evaporated and the residue was resuspended in water (100 mL) and extracted with DCM (3 × 100 mL). The combined organic layers were washed with brine (2 × 50 mL, sat aq), dried over $MgSO_4$ and concentrated *in vacuo* to give the carbamate **66** as a pale yellow oil (6.81 g, 96% yield). The product was used without further purification. **R_f** (EtOH:H_2O, 7:3) = 0.59; **IR** (neat, cm^{-1}) 3373 (NH), 1684 (C=O); **^{1}H NMR** (400 MHz, $CDCl_3$) δ 5.05 (1H, br s, N*H*), 3.15 (2H, br q, *J* = 6.6 Hz, C*H*$_2$NHCO), 2.70 (2H, t, *J* = 6.6 Hz, C*H*$_2$NH$_2$), 1.55 (2H, qn, *J* = 6.6 Hz, CH$_2$C*H*$_2$CH$_2$), 1.38 (9H, s, O*t*-Bu), 1.35 (2H, br s, N*H*$_2$); **^{13}C NMR** (101 MHz, $CDCl_3$) δ 156.21 (C), 78.98 (C), 39.69 (CH$_2$), 38.40 (CH$_2$), 33.47 (CH$_2$), 28.44 (3CH$_3$); ***m/z*** (ESI+) 175 ([M+H]$^+$, 88%).

The spectroscopic data is in good agreement with the literature.[266]

***tert*-Butyl 2-[3-(*tert*-butoxycarbonylamino)propylamino]acetate 88a**

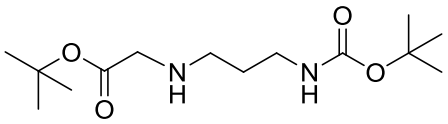

To a solution of *tert*-butyl 3-aminopropylcarbamate **85** (6.70 g, 38.5 mmol) in THF (200 mL) was added triethylamine (16.1 mL, 115 mmol) followed by a solution of *tert*-butyl 2-bromoacetate (7.50 g, 38.5 mmol) in THF (100 mL) dropwise over 2 h at room temperature. After stirring for ~18 h at room temperature, a colourless precipitate was removed by filtration and THF removed *in vacuo*. DCM (50 mL) was added and the mixture washed with brine (2 × 50 mL, sat aq). The organic phase was separated, dried over $MgSO_4$ and concentrated *in vacuo*. The product was purified by column chromatography (Hexane:EtOAc, 1:1 then EtOAc:MeOH, 95:5) to give the amino acetate **88a** as a pale yellow oil (5.98 g, 54%). $\mathbf{R_f}$ (EtOAc, 7:3) = 0.13; **IR** (neat, cm^{-1}) 3337 (NH), 1695 (C=O); **^{1}H NMR** (500 MHz, $CDCl_3$) δ 5.01 (1H, br s, N*H*), 3.28 (2H, s, C(O)CH_2NH), 3.23-3.18 (2H, m, CH_2CH_2NHC(O)), 2.65 (2H, t, *J* = 6.7 Hz, C(O)CH_2NHCH_2), 1.65 (2H, qn, *J* = 6.7 Hz, CH_2CH_2CH_2), 1.47 (9H, s, O*t*-Bu), 1.44 (9H, s, O*t*-Bu); **^{13}C NMR** (126 MHz, $CDCl_3$) δ 171.88 (C), 156.17 (C), 81.36 (C), 79.10 (C), 51.77 (CH_2), 47.38 (CH_2), 39.09 (CH_2), 30.10 (CH_2), 28.56 ($3CH_3$), 28.24 ($3CH_3$); ***m/z*** (ESI+) 311 ($[M+Na]^+$, 18%), 289 ($[M+H]^+$, 100), 233 (19.1); **HRMS** (ESI+) $[M+H]^+$ found 289.2122, $C_{14}H_{29}N_2O_4$ requires 289.2122.

The spectroscopic data is in good agreement with the literature.[267]

***tert*-Butyl 2-({[(9*H*-fluoren-9-yl)methoxy]carbonyl}[3-(*tert*-butoxycarbonylamino)propyl]amino)acetate 91**

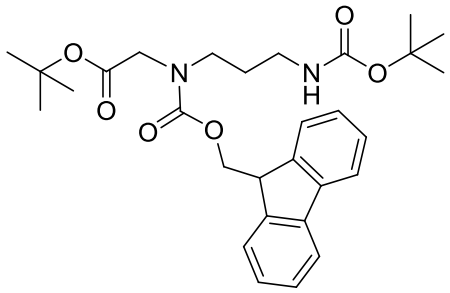

To a solution of *tert*-butyl 2-[3-(*tert*-butoxycarbonylamino)propylamino]acetate **88a** (4.80 g, 16.6 mmol) in DCM (100 mL) was added Fmoc-OSu (5.61 g, 16.6 mmol) and the mixture was stirred for ~18 h at room temperature. Water (50 mL) was added and the organic layer separated, washed with brine (2 × 50 mL, sat aq), dried over $MgSO_4$ and concentrated *in vacuo*. The product was purified by column chromatography (Hexane:EtOAc, 7:3) to give the Fmoc carbamate **91** as a colourless oil (8.00 g, 94%). **R_f** (Hexane:EtOAc, 7:3) = 0.29; **IR** (neat, cm^{-1}) 3347 (NH), 1742 (C=O), 1703 (C=O); In both the ^{1}H and ^{13}C NMR, two rotamers were observed (ratio 63$^{(*)}$:37); **^{1}H NMR** (500 MHz, $CDCl_3$) δ 7.78 and 7.77* (2H, d, *J* = 7.5 Hz, Ar*H*), 7.59 (2H, d, *J* = 7.5 Hz, Ar*H*), 7.41 (2H, t, *J* = 7.5 Hz, Ar*H*), 7.32 and 7.31* (2H, t, *J* =7.5 Hz, Ar*H*), 5.23 and 4.41* (1H, m, N*H*), 4.58* and 4.41 (2H, d, *J* = 5.6 Hz and 7.0 Hz, OCH_2CH), 4.25 and 4.22* (1H, t, *J* = 7.0 Hz, OCH_2CH), 3.85* and 3.84 (2H, s, C(O)CH_2N), 3.42* and 3.09 (2H, t, *J* = 6.2 Hz and 7.3 Hz, C(O)NCH_2CH_2), 3.15* and 2.91 (2H, dt, *J* = 6.2 Hz and 5.5 Hz, CH_2CH_2NH), 1.68* and 1.45 (2H, qn, *J* = 7.5 Hz, $CH_2CH_2CH_2$), 1.46 and 1.45 (18H, m, 2 × O*t*-Bu); **^{13}C NMR** (126 MHz, $CDCl_3$) δ 168.57 and 168.52* (C), 156.38, 156,09, 155.94, 155.68 (2C), 143.80 and 143.79* (2C), 141.20 and 141.10* (2C), 127.55* and 127.47 (2CH), 126.99 and 126.91* (2CH), 124.88* and 124.57 (2CH), 119.79* and 119.72 (2CH), 81.84* and 81.60 (C), 79.03 and 78.78* (C), 67.67* and 66.82 (CH_2), 49.93 and 49.51 (CH_2), 47.16* and 47.13 (CH), 45.92* and 45.74 (CH_2), 37.80 and 36.94* (CH_2), 28.38, 28.27, 28.22, 27.88 ($6CH_3$, CH_2); ***m/z*** (ESI+) 533.2 ([M+Na]$^+$, 100%), 477 (45.6), 421 (40.8); **HRMS** (ESI+) [M+Na]$^+$ found, 533.2623, $C_{29}H_{38}N_2NaO_6$ requires 533.2622.

2-({[(9*H*-Fluoren-9-yl)methoxy]carbonyl}(3-aminopropyl)amino)acetic acid hydrochloride 94

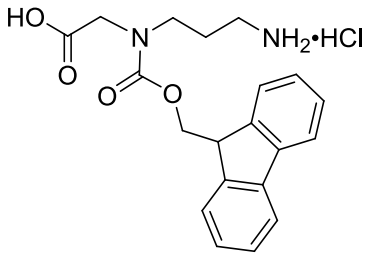

To *tert*-butyl 2-[{[(9*H*-fluoren-9-yl)methoxy]carbonyl}[3-(*tert*- butoxycarbonylamino) propyl]amino]acetate **91** (7.90 g, 15.5 mmol) was added 80% v/v TFA in DCM (160 mL) at room temperature. After stirring for ~18 h at room temperature, DCM and TFA were removed *in vacuo*. The product was re-dissolved in EtOAc (35 mL) and HCl in EtOAc [prepared by dropwise addition of AcCl (1.58 mL, 22.3 mmol) in EtOH (10 mL) at 0°C] added dropwise at 0°C. The colourless precipitate formed was isolated by filtration, washed with EtOAc (4 × 10 mL) and dried under vacuum to give the amine salt **94** as a colourless solid (5.48 g, 91%). **R_f** (EtOH:H_2O, 7:3) = 0.65; **mp** 158-159 °C; **IR** (neat, cm^{-1}) 1728 (C=O), 1697 (C=O), 1668 (C=O); In both the ^{1}H and ^{13}C NMR, two rotamers were observed (ratio 71$^{(*)}$:29); **^{1}H NMR** (500 MHz, D_2O) δ 7.32 and 7.17-7.13* (2H, d and m, *J* = 7.3 Hz, Ar*H*), 7.17-7.13 and 7.08-7.05* (2H, m, Ar*H*), 7.03-6.89 (4H, m, Ar*H*), 4.20 and 3.97* (2H, d, *J* = 3.6 Hz and 4.8 Hz, OC*H*$_2$CH), 3.68 and 3.56* (1H, t, *J* = 4.8 Hz, OCH$_2$C*H*), 3.51 and 3.28* (2H, s, C(O)C*H*$_2$N), 2.95 and 2.48 (2H, t, *J* = 6.8 Hz, NC*H*$_2$CH$_2$), 2.62* and 2.02 (1H, t, *J* = 7.8 Hz and 7.8 Hz, CH$_2$C*H*$_2$NH$_2$), 1.50* and 1.12 (2H, qn, *J* = 7.0 Hz and 7.8 Hz, CH$_2$C*H*$_2$CH$_2$); **^{13}C NMR** (126 MHz, D_2O) δ 173.17 and 172.87* (C), 156.89* and 156.82 (C), 143.54 and 143.26* (2C), 140.78 and 140.65* (2C), 127.44 and 127.37* (2CH), 127.05 and 126.86* (2CH), 124.31 (2CH), 119.64 and 119.57* (2CH), 67.05* and 66.60 (CH_2), 48.90 and 48.37* (CH_2), 46.47 and 46.37* (CH), 45.28* and 45.17 (CH_2), 36.64* and 36.44 (CH_2), 25.25 and 25.08* (CH_2); ***m/z*** (ESI+) 377 ($[M+Na]^+$, 100%), 355 ($[M+H]^+$, 17), 179 (31); **HRMS** (ESI+) $[M+Na]^+$ found 377.1459, $C_{20}H_{22}N_2NaO_4$ requires 377.1472.

2-({[(9*H*-Fluoren-9-yl)methoxy]carbonyl}(3-azidopropyl)amino)acetic acid 97

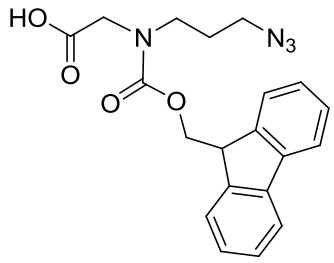

CAUTION: hazardous and explosive material, use azide with care.

To a solution of 2-({[(9*H*-fluoren-9-yl)methoxy]carbonyl}(3-aminopropyl)amino) acetic acid hydrochloride **94** (11.1 g, 28.1 mmol) in MeOH (500 mL) at room temperature was added sodium hydrogencarbonate (7.09 g, 84.4 mmol), copper (II) sulphate (0.450 g, 2.81 mmol) and imidazole-1-sulfonyl azide hydrochloride **100** (7.08 g, 33.8 mmol) portionwise. After stirring for ~18 h at room temperature, MeOH was evaporated, the residue was dissolved in DCM (30 mL) and washed with water (2 × 20 mL). The organic layer was separated, dried over $MgSO_4$ and concentrated *in vacuo*. The product was purified by column chromatography (from 0.1% AcOH in DCM:MeOH, 99:1, to 0.1% AcOH in DCM:MeOH, 90:10) and triturated with Et_2O/PE to give the azide **97** as a pale yellow solid (9.31 g, 24.48 mmol, 87%). $\mathbf{R_f}$ (0.1% AcOH in DCM:MeOH, 9:1) = 0.58; **mp** 86-87 °C; **IR** (neat, cm^{-1}) 2095 (N_3), 1734 (C=O), 1651 (C=O); In both the ^1H and ^{13}C NMR, two rotamers were observed (ratio 57$^{(*)}$:43); ^{1}**H NMR** (500 MHz, $CDCl_3$) δ 7.78* and 7.74 (2H, d, *J* = 7.5 Hz, Ar*H*), 7.58* and 7.54 (2H, d, *J* = 7.5 Hz, Ar*H*), 7.42* and 7.38 (2H, t, *J* = 7.5 Hz, Ar*H*), 7.34* and 7.29 (2H, t, *J* = 7.5 Hz and 7.1 Hz, Ar*H*), 4.63* and 4.48 (2H, d, *J* = 5.4 Hz and 6.2 Hz, OC*H*$_2$CH), 4.25* and 4.19 (1H, t, *J* = 5.4 Hz and 6.2 Hz, OCH$_2$C*H*), 3.95* and 3.87 (2H, s, C(O)C*H*$_2$N), 3.39 and 3.11* (2H, t, *J* = 6.8 Hz and 7.1 Hz, NC*H*$_2$CH$_2$), 3.32 and 3.00* (2H, t, *J* = 6.8 Hz, CH$_2$C*H*$_2$N$_3$), 1.79 and 1.48* (2H, qn, *J* = 6.8 Hz, CH$_2$C*H*$_2$CH$_2$); ^{13}**C NMR** (126 MHz, $CDCl_3$) δ 174.34 and 174.05* (C), 156.62* and 156.06 (C), 143.83* and 143.80 (2C), 141.48* and 141.40 (2C), 127.85* and 127.80 (2CH), 127.29* and 127.16 (2CH), 124.89 and 124.74* (2CH), 120.07 and 120.03* (2CH), 67.77 and 67.36* (CH_2), 49.45* and 49.00 (CH_2), 48.87 and 48.64* (CH_2), 47.29 (CH), 46.62 and 46.14* (CH_2), 27.52* and 27.45 (CH_2); ***m/z*** (ESI+) 403 ($[M+Na]^+$, 100%), 179 (31); **HRMS** (ESI+) $[M+Na]^+$ found 403.1381, $C_{20}H_{20}N_4NaO_4$ requires 403.1377.

***tert*-Butyl 4-aminobutylcarbamate 86**

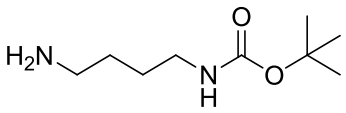

To a solution of butane-1,4-diamine **83** (24.2 g, 275 mmol) in DCM (600 mL) was added di-*tert*-butyl dicarbonate (9.99 g, 45.8 mmol) dropwise in DCM (300 mL) over 5 h at room temperature. After stirring for ~48 h at room temperature, DCM was evaporated and the residue was resuspended in water (100 mL) and extracted with DCM (3 × 100 mL). The combined organic layers were washed with brine (2 × 50 mL, sat aq), dried over $MgSO_4$ and concentrated *in vacuo* to give the carbamate **86** as a pale yellow oil (8.14 g, 95%). The product was used without further purification. **R_f** (EtOH:H_2O, 7:3) = 0.58; **IR** (neat, cm^{-1}) 3373 (NH_2), 1684 (C=O); **^{1}H NMR** (400 MHz, $CDCl_3$) δ 4.85 (1H, br s, N*H*), 3.05 (2H, br q, *J* = 6.5 Hz, C*H*$_2$NHC(O)), 2.64 (2H, t, *J* = 6.5 Hz, C*H*$_2$$NH_2$), 1.50-1,37 (4H, m, CH_2(C*H*$_2$)$_2$$CH_2$), 1.37 (9H, s, O*t*-Bu), 1.22 (2H, br s, N*H*$_2$); **^{13}C NMR** (101 MHz, $CDCl_3$) δ 156.06 (C), 78.92 (C), 41.82 (CH_2), 39.41 (CH_2), 30.91 (CH_2), 28.43 ($3CH_3$), 27.48 (CH_2); ***m/z*** (ESI+) 377 ($[2M+H]^+$, 9%), 189 ($[M+H]^+$, 100).

The spectroscopic data is in good agreement with the literature.[266]

***tert*-Butyl 2-[4-(*tert*-butoxycarbonylamino)butylamino]acetate 89a**

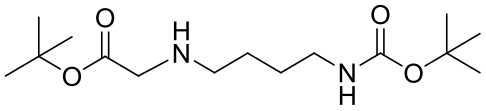

To a solution of *tert*-butyl 4-aminobutylcarbamate **86** (8.00 g, 42.5 mmol) in THF (200 mL) was added triethylamine (17.8 mL, 127 mmol) followed by a solution of *tert*-butyl 2-bromoacetate (8.29 g, 42.5 mmol) in THF (100 mL) dropwise over 2 h at room temperature. After stirring for ~18 h at room temperature, a colourless precipitate was removed by filtration and THF removed *in vacuo*. DCM (50 mL) was added and the mixture washed with brine (2 × 50 mL, sat aq). The organic phase was separated, dried over $MgSO_4$ and concentrated *in vacuo*. The product was purified by column chromatography (from Hexane:EtOAc, 1:1 to 100% EtOAc) to give the amino acetate **89a** as a pale yellow oil (6.59 g, 51%). $\mathbf{R_f}$ (EtOAc, 7:3) = 0.12; **IR** (neat, cm^{-1}) 3335 (NH), 1697 (C=O); ^{1}**H NMR** (500 MHz, $CDCl_3$) δ 4.84 (1H, s, N*H*), 3.22 (2H, s, C(O)CH_2NH), 3.08-3.03 (2H, m, CH_2CH_2NHC(O)), 2.54 (2H, t, *J* = 6.7 Hz, C(O)CH_2NHCH_2), 1.87 (1H, br s, CH_2NHCH_2), 1.50-1.42 (4H, m, $CH_2(CH_2)_2CH_2$), 1.40 (9H, s, O-*t*Bu), 1.37 (9H, s, O-*t*Bu); ^{13}**C NMR** (126 MHz, $CDCl_3$) δ 171.71 (C), 156.03 (C), 81.16 (C), 78.89 (C), 51.57 (CH_2), 49.03 (CH_2), 40.37 (CH_2), 28.42 ($3CH_3$), 28.10 ($3CH_3$), 27.72 (CH_2), 27.29 (CH_2); ***m/z*** (ESI+) 325 ($[M+Na]^+$, 33%), 303 ($[M+H]^+$, 100), 247 (17); **HRMS** (ESI+) $[M+H]^+$ found 303.2280, $C_{15}H_{31}N_2O_4$ requires 303.2278.

***tert*-Butyl 2-({[(9*H*-fluoren-9-yl)methoxy]carbonyl}[4-(*tert*-butoxycarbonylamino)butyl] amino)acetate 92**

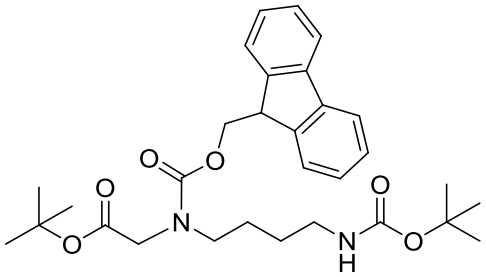

To a solution of *tert*-butyl 2-[4-(*tert*-butoxycarbonylamino)butylamino]acetate **89a** (5.00 g, 16.5 mmol) in DCM (50 mL) was added Fmoc-OSu (5.58 g, 16.5 mmol) and the mixture was stirred for ~18 h at room temperature. Water (50 mL) was added and the organic layer separated, washed with brine (2 × 50 mL, sat aq), dried over $MgSO_4$ and concentrated *in vacuo*. The product was purified by column chromatography (Hexane:EtOAc, 7:3) to give the Fmoc carbamate **92** as a colourless solid (7.90 g, 91%). **R_f** (Hexane:EtOAc, 7:3) = 0.30; **IR** (neat, cm^{-1}) 3364 (NH), 1742 (C=O), 1697 (C=O); In both the ^{1}H and ^{13}C NMR, two rotamers were observed (ratio 51:49); **^{1}H NMR** (400 MHz, DMSO) δ 7.92 and 7.90 (2H, d, *J* = 7.4 Hz, Ar*H*), 7.68-7.61 (2H, m, Ar*H*), 7.43 (2H, t, *J* = 7.4 Hz, Ar*H*), 7.35 and 7.32 (2H, t, *J* = 7.4 Hz, Ar*H*), 6.81-6.73 (1H, m, N*H*), 4.46 and 4.32 (2H, d, *J* = 5.6 Hz, OCH_2CH), 4.30 and 4.20 (1H, t, *J* = 7.3 Hz, OCH$_2$C*H*), 3.85 and 3.78 (2H, s, C(O)CH_2N), 3.22 and 2.96-2.89 (2H, t and m, *J* = 7.3 Hz, C(O)NCH_2CH$_2$), 2.96-2.89 and 2.82 (2H, m and br q, *J* = 5.6 Hz, CH$_2$CH_2NH), 1.47-1.05 (22H, m, 2 × O*t*-Bu, CH$_2$(CH_2)$_2$CH$_2$); **^{13}C NMR** (101 MHz, DMSO) δ 168.84 and 168.62 (C), 155.64-155.55, 155.47 and 155.28 (2C), 143.97 and 143.74 (2C), 140.90 and 140.72 (2C), 127.67 and 127.53 (2CH), 127.05 (2CH), 124.99 and 124.70 (2CH), 120.11 and 120.08 (2CH), 80.90 and 80.70 (C), 77.33 (C), 66.80 and 66.46 (CH_2), 49.39 and 48.89 (CH_2), 47.84 and 47.57 (CH_2), 46.78 and 46.65 (CH), 39.42 and 39.38 (CH_2), 28.25 ($3CH_3$), 27.68 and 27.67 ($3CH_3$), 26.72 and 26.67 (CH_2), 25.07 and 24.66 (CH_2); ***m/z*** (ESI+) 1071 ([2M+Na]$^+$, 72%), 547 ([M+Na]$^+$, 100), 492 (6); **HRMS** (ESI+) [M+Na]$^+$ found 547.2770, $C_{30}H_{40}N_2NaO_6$ requires 547.2779.

2-({[(9*H*-Fluoren-9-yl)methoxy]carbonyl}(4-aminobutyl)amino)acetic acid hydrochloride 95

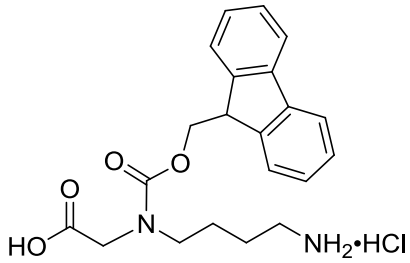

To *tert*-butyl 2-[{[(9*H*-fluoren-9-yl)methoxy]carbonyl}[4-(*tert*-butoxycarbonylamino) butyl]amino]acetate **92** (7.80 g, 14.9 mmol) was added 80% v/v TFA in DCM (160 mL) at room temperature. After stirring for ~18 h at room temperature, DCM and TFA were removed *in vacuo*. The product was re-dissolved in EtOAc (35 mL) and HCl in EtOAc [prepared by dropwise addition of AcCl (1.58 mL, 22.30 mmol) in EtOH (10 mL) at 0°C] added dropwise at 0°C. The colourless precipitate formed was isolated by filtration, washed with EtOAc (4 × 10 mL) and dried under vacuum to give the amine salt **95** as a colourless solid (5.42 g, 90%). $\mathbf{R_f}$ (EtOH:H_2O, 7:3) = 0.66; **mp** 183-184 °C; **IR** (neat, cm^{-1}), 1730 (C=O), 1668 (C=O); In both the ^1H and ^{13}C NMR, two rotamers were observed (ratio 62$^{(*)}$:38); **^{1}H NMR** (500 MHz, D_2O) δ 7.36 and 7.23* (2H, d, *J* = 7.3 Hz and 5.3 Hz, Ar*H*), 7.19 and 7.14* (2H, d, *J* = 7.3 Hz and 5.3 Hz, Ar*H*), 7.07-6.95 (4H, m, Ar*H*), 4.23 and 4.04* (2H, br s, OCH_2CH), 3.72 and 3.65* (1H, br s, OCH_2CH), 3.56 and 3.31* (2H, s, C(O)CH_2N), 2.91 and 2.47* (2H, t, *J* = 7.2 Hz, $CH_2NCH_2CH_2$), 2.69* and 2.40 (2H, t, *J* = 7.2 Hz, CH_2NH_2), 1.31* and 0.89 (2H, qn, *J* = 7.2 Hz, NCH_2CH_2), 1.18* and 0.74 (2H, qn, *J* = 7.2 Hz, C$H_2CH_2NH_2$); **^{13}C NMR** (126 MHz, D_2O) δ 173.57 and 173.23* (C), 157.26 and 156.96* (C), 143.80 and 143.60* (2C), 141.05 and 140.91* (2C), 127.63 (2CH), 127.21 and 127.14* (2CH), 124.53* and 124.49 (2CH), 119.83 (2CH), 67.14* and 66.52 (CH_2), 49.25 and 48.36* (CH_2), 47.74* and 47.68 (CH_2), 46.82 and 46.65* (CH), 39.03* and 38.94 (CH_2), 24.13 and 24.05* (CH_2), 23.88* and 23.71 (CH_2); ***m/z*** (ESI+) 413 ($[M-H+2Na]^+$, 38%), 391 ($[M+Na]^+$, 24), 369 ($[M+H]^+$, 100), 209 (52); **HRMS** (ESI+) $[M+H]^+$ found 369.1801, $C_{21}H_{25}N_2O_4$ requires 369.1809.

2-({[(9*H*-Fluoren-9-yl)methoxy]carbonyl}(4-azidobutyl)amino)acetic acid 98

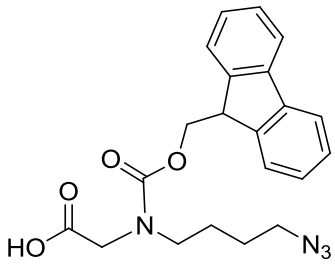

CAUTION: hazardous and explosive material, use azide with care.

To a solution of 2-({[(9*H*-fluoren-9-yl)methoxy]carbonyl}(4-aminobutyl)amino)acetic acid hydrochloride **95** (28.4 g, 70.3 mmol) in MeOH (1500 mL) at room temperature was added sodium hydrogencarbonate (17.7 g, 21.1 mmol), copper (II) sulphate (2.24 g, 14.0 mmol) and imidazole-1-sulfonyl azide hydrochloride **100** (17.7 g, 84.3 mmol) portionwise. After stirring for ~18 h at room temperature, MeOH was evaporated, the residue was dissolved in DCM (30 mL) and washed with water (2 × 20 mL). The organic layer was separated, dried over $MgSO_4$ and concentrated *in vacuo*. The product was purified by column chromatography (from 0.1% AcOH in DCM:MeOH, 99:1, to 0.1% AcOH in DCM:MeOH, 90:10) and triturated with Et_2O:Hexane to give the azide **98** as a pale yellow solid (22.4 g, 81%). **R_f** (0.1% AcOH in DCM:MeOH, 9:1) = 0.62; **mp** 91-92 °C; **IR** (neat, cm^{-1}) 2089 (N_3), 1741 (C=O), 1686 (C=O), 1651 (C=C); In both the ^1H and ^{13}C NMR, two rotamers were observed (ratio 57$^{(*)}$:43); **^1H NMR** (500 MHz, $CDCl_3$) δ 10.16 (1H, br s, COO*H*), 7.78* and 7.74* (2H, d, *J* = 7.5 Hz, Ar*H*), 7.58* and 7.54 (2H, d, *J* = 7.5 Hz, Ar*H*), 7.42* and 7.37 (2H, t, *J* = 7.5 Hz, Ar*H*), 7.34* and 7.29 (2H, t, *J* = 7.5 Hz, Ar*H*), 4.64* and 4.48 (2H, d, *J* = 5.3 Hz and 6.1 Hz, OCH_2), 4.25* and 4.20 (1H, t, *J* = 5.3 Hz and 6.1 Hz, OCH_2CH), 3.97* and 3.88 (2H, s, C(O)CH_2N), 3.38-3.32 and 3.06* (2H, m and t, *J* = 6.7 Hz, NCH_2CH_2), 3.32-3.27 and 3.11* (2H, m and t, *J* = 6.1 Hz, $CH_2CH_2N_3$), 1.59 and 1.31* (4H, m, $NCH_2(CH_2)_2CH_2$); **^{13}C NMR** (126 MHz, $CDCl_3$) δ 175.11 and 174.89* (C), 156.66* and 156.03 (C), 143.91* and 143.89 (2C), 141.53* and 141.44 (2C), 127.84* and 127.79 (2CH), 127.26* and 127.17 (2CH), 124.89 and 124.75* (2CH), 120.06 (2CH), 67.74 and 67.24* (CH_2), 51.18 and 51.08* (CH_2), 49.10* and 48.43 (CH_2), 48.28 and 48.08* (CH_2), 47.37* and 47.35 (CH), 26.07 and 26.01* (CH_2), 25.50* and 25.20 (CH_2); ***m/z*** (ESI+) 833 ($[2M-H+2Na]^+$, 28%), 811 ($[2M+Na]^+$, 24), 439 ($[M-H+2Na]^+$, 17), 417 ($[M+Na]^+$, 100), 395 ($[M+H]^+$, 13%), 179 (31); **HRMS** (ESI+) $[M+Na]^+$ found 417.1518, $C_{21}H_{22}N_4NaO_4$ requires 417.1533.

***tert*-Butyl 5-aminopentylcarbamate 87**

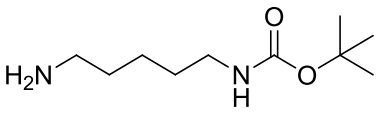

To a solution of pentane-1,5-diamine **84** (25.0 g, 245 mmol) in DCM (200 mL) was added di-*tert*-butyl dicarbonate (6.67 g, 30.6 mmol) dropwise in DCM (100 mL) over 5 h at room temperature. After stirring for ~48 h at room temperature, DCM was evaporated and the residue was resuspended in water (100 mL) and extracted with DCM (3 × 100 mL). The combined organic layers were washed with brine (2 × 50 mL, sat aq), dried over $MgSO_4$ and concentrated *in vacuo* to give the carbamate **87** as a pale yellow oil (5.81g, 94%). The product was used without further purification. **R_f** (EtOH:H_2O, 7:3) = 0.57; **IR** (neat, cm^{-1}) 3373 (NH_2), 1684 (C=O); **^{1}H NMR** (400 MHz, $CDCl_3$) δ 4.72 (1H, br s, N*H*), 3.05 (2H, br q, *J* = 6.4 Hz, CH_2NH), 2.62 (2H, t, *J* = 6.9 Hz, H_2NCH_2) 1.47-1.36 (4H, m, CH_2(CH_2)$_2$CH_2), 1.38 (s, 9H, O*t*-Bu); **^{13}C NMR** (101 MHz, $CDCl_3$) δ 156.06 (C), 78.94 (C), 42.07 (CH_2), 40.49 (CH_2), 33.40 (CH_2), 29.95 (CH_2), 28.43 (3CH_3), 24.08 (CH_2); ***m/z*** (ESI+) 225 ($[M+Na]^+$, 11%), 203 ($[M+H]^+$, 100%).

The spectroscopic data is in good agreement with the literature.[266]

***tert*-Butyl-2-[5-(*tert*-butoxycarbonylamino)pentylamino]acetate 90a**

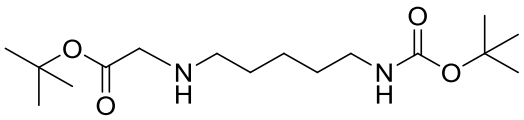

To a solution of *tert*-butyl 5-aminopentylcarbamate **87** (5.70 g, 28.2 mmol) in THF (200 mL) was added triethylamine (11.8 mL, 84.6 mmol) followed by a solution of *tert*-butyl 2-bromoacetate (5.50 g, 28.2 mmol) in THF (100 mL) dropwise over 2 h at room temperature. After stirring for ~18 h at room temperature, a colourless precipitate was removed by filtration and THF removed *in vacuo*. DCM (50 mL) was added and the mixture washed with brine (2 × 50 mL, sat aq). The organic phase was separated, dried over $MgSO_4$ and concentrated *in vacuo*. The product was purified by column chromatography (Hexane:EtOAc, 1:1 then EtOAc:MeOH, 95:5) to give the amino acetate **90a** as a pale yellow oil (5.50 g, 62%). $\mathbf{R_f}$ (EtOAc, 7:3) = 0.14; **IR** (neat, cm^{-1}) 3327 (NH), 1713 (C=O), 1697 (C=O); **^{1}H NMR** (500 MHz, $CDCl_3$) δ 4.81 (1H, br s, C(O)CH_2N*H*), 3.16 (2H, s, C(O)C*H*$_2$NH), 2.98 (2H, br q, *J* = 6.4 Hz, $CH_2C\mathit{H}_2$-NHC(O)), 2.47 (2H, t, *J* = 7.2 Hz, C(O)CH_2NHC*H*$_2$), 2.18 (1H, s, CH_2N*H*CH_2), 1.35-1.42 (4H, m, $CH_2C\mathit{H}_2CH_2C\mathit{H}_2CH_2$), 1.35 (9H, s, O-*t*Bu), 1.31 (9H, s, O-*t*Bu), 1.20-1.27 (2H, m, $(CH_2)_2C\mathit{H}_2(CH_2)_2$); **^{13}C NMR** (126 MHz, $CDCl_3$) δ 171.62 (C), 155.93 (C), 80.98 (C), 78.69 (C), 51.47 (CH_2), 49.18 (CH_2), 40.35 (CH_2), 29.91 (CH_2), 29.57 (CH_2), 28.32 ($3CH_3$), 27.99 ($3CH_3$), 24.34 (CH_2); ***m/z*** (ESI+) 339 ($[M+Na]^+$, 5%) 317 ($[M+H]^+$, 100%); **HRMS** (ESI+) $[M+H]^+$ found, 317.2433, $C_{16}H_{33}N_2O_4$ requires 317.2435.

***tert*-Butyl 2-[{[(9*H*-fluoren-9-yl)methoxy]carbonyl}[5-(*tert*-butoxycarbonylamino) pentyl]amino]acetate 93**

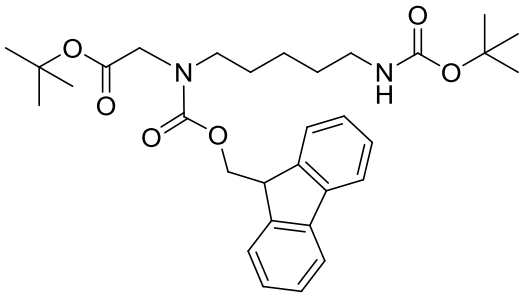

To a solution of *tert*-butyl 2-[5-(*tert*-butoxycarbonylamino)pentylamino]acetate **90a** (5.00 g, 15.8 mmol) in DCM (100 mL) was added Fmoc-OSu (5.33 g, 15.8 mmol) and the mixture stirred for ~18 h at room temperature. Water (50 mL) was added and the organic layer separated, washed with brine (2 × 50 mL, sat aq), dried over $MgSO_4$ and concentrated *in vacuo*. The product was purified by column chromatography (Hexane:EtOAc, 7:3) to give the Fmoc carbamate **93** as a colourless solid (7.5 g, 88%). **R_f** (Hexane:EtOAc, 7:3) = 0.31; **mp** 64.1 - 65.8 °C; **IR** (neat, cm^{-1}) 3368 (NH), 1744 (C=O), 1703 (C=O); In both the ^1H and ^{13}C NMR, two rotamers were observed (ratio 50:50); **^{1}H NMR** (500 MHz, $CDCl_3$) δ 7.77 and 7.76 (2H, d, *J* = 7.5 Hz, Ar*H*), 7.59 and 7.59 (2H, d, *J* = 7.5 Hz, Ar*H*), 7.40 (2H, t, *J* = 7.5 Hz, Ar*H*), 7.31 (2H, m, Ar*H*), 4.66 and 4.54 (1H, br s, N*H*), 4.53 and 4.39 (2H, d, *J* = 6.0 Hz and 7.1 Hz, OCH_2CH), 4.24 and 4.22 (1H, t, *J* = 6.0 Hz and 7.1 Hz, OCH_2CH), 3.87 and 3.84 (2H, s, C(O)CH_2N), 3.35 and 3.10 (2H, t, *J* = 7.3 Hz and 7.4 Hz, C(O)NCH_2CH_2), 3.14-3.05 (2H, m, CH_2CH_2NH), 1.60-1.30 (22H, m, 2 × O*t*-Bu, $CH_2CH_2CH_2CH_2CH_2$), 1.36-1.31 and 1.16-1.08 (2H, m, $(CH_2)_2CH_2(CH_2)_2$); **^{13}C NMR** (126 MHz, $CDCl_3$) δ 168.93 and 168.89 (C), 156.46 and 156.15 (C), 156.10, 156.04 (C), 144.12 and 144.08 (2C), 141.47 and 141.34 (2C), 127.75 and 127.70 (2CH), 127.14 and 127.13 (2CH), 125.19 and 124.86 (2CH), 120.02 and 119.99 (2CH), 81.95 and 81.75 (C), 79.14 and 79.03 (C), 67.81 and 67.12 (CH_2), 49.88 and 49.61 (CH_2), 48.70 and 48.32 (CH_2), 47.44 and 47.38 (CH), 40.40 (CH_2), 29.90 and 29.72 (CH_2), 28.52 and 28.51 ($3CH_3$), 28.15 ($3CH_3$), 28.03 and 27.62 (CH_2), 23.95 and 23.87 (CH_2); ***m/z*** (ESI+) 561 ($[M+Na]^+$, 100%), 505 (22); **HRMS** (ESI+) $[M+Na]^+$ found 561.2919, $C_{31}H_{42}N_2NaO_6$ requires 561.2935.

2-({[(9*H*-Fluoren-9-yl)methoxy]carbonyl}(5-aminopentyl)amino)acetic acid hydrochloride 96

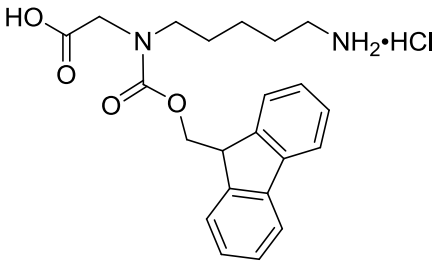

To *tert*-butyl 2-[{[(9*H*-fluoren-9-yl)methoxy]carbonyl}[5-(*tert*-butoxycarbonylamino) pentyl]amino]acetate **93** (7.40 g, 13.7 mmol) was added 80% v/v TFA in DCM (160 mL) at room temperature. After stirring for ~18 h at room temperature, DCM and TFA were removed *in vacuo*. The product was re-dissolved in EtOAc (35 mL) and HCl in EtOAc [prepared by dropwise addition of AcCl (1.46 mL, 20.6 mmol) in EtOH (10 mL) at 0°C] added dropwise at 0°C. The colourless precipitate formed was isolated by filtration, washed with EtOAc (4 × 10 mL) and dried under vacuum to give the amine salt **96** as a colourless solid (5.23 g, 91%). $\mathbf{R_f}$ (EtOH:H_2O, 7:3) = 0.66; **mp** 189-190 °C; **IR** (neat, cm^{-1}) 1719 (C=O), 1690 (C=O); In both the ^{1}H and ^{13}C NMR, two rotamers were observed (ratio 57$^{(*)}$:43); **^{1}H NMR** (400 MHz, D_2O) δ 7.59 and 7.55* (2H, d, *J* = 7.5 Hz, Ar*H*), 7.40 and 7.35* (2H, d, *J* = 7.5, Ar*H*), 7.25-7.12 (4H, m, Ar*H*), 4.48 and 4.37* (2H, d, *J* = 3.7 Hz and 4.2 Hz, OCH_2CH), 3.99 and 3.96* (1H, br s and t, *J* = 4.2 Hz, OCH$_2$C*H*), 3.58 and 3.24* (2H, s, C(O)CH_2N), 2.90* and 2.46 (2H, t, *J* = 7.1 Hz, NCH_2CH$_2$), 2.72* and 2.61 (2H, t, *J* = 7.6 Hz, CH$_2$CH_2NH$_2$), 1.38* and 1.16 (2H, qn, *J* = 7.6 Hz, C(O)NCH$_2$CH_2CH$_2$), 1.14* and 0.71 (2H, qn, *J* = 7.6 Hz, CH$_2$CH_2CH$_2$NH$_2$), 1.05-0.94* and 0.62-0.52 (2H, m, (CH$_2$)$_2$CH_2(CH$_2$)$_2$); **^{13}C NMR** (126 MHz, D_2O) δ 173.82 and 173.42* (C), 157.26 and 156.92* (C), 143.78 and 143.62* (2C), 141.01 and 140.90* (2C), 127.59 (2CH), 127.13 (2CH), 124.52 and 124.46 (2CH), 119.79 (2CH), 66.98* and 66.50 (CH_2), 49.20 and 48.29 (CH_2), 48.03 and 47.96* (CH_2), 46.77 and 46.71* (CH), 39.18* and 39.10 (CH_2), 26.58 and 26.35* (CH_2), 26.35 and 26.30* (CH_2), 22.63* and 22.56 (CH_2); ***m/z*** (ESI+) 427 ([M-H+2Na]$^+$, 12%), 383 ([M+H]$^+$, 16), 179 (24); **HRMS** (ESI+) [M+H]$^+$ found 383.1948, $C_{22}H_{27}N_2O_4$ requires 383.1965.

2-({[(9*H*-Fluoren-9-yl)methoxy]carbonyl}(5-azidopentyl)amino)acetic acid 99

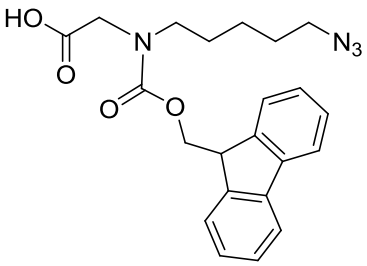

CAUTION: hazardous and explosive material, use azide with care.

To a solution of 2-({[(9*H*-fluoren-9-yl)methoxy]carbonyl}(5-aminopentyl)amino)acetic acid hydrochloride **96** (7.76 g, 18.5 mmol) in MeOH (500 mL) at room temperature was added sodium hydrogencarbonate (4.67 g, 55.6 mmol), copper (II) sulphate (0.591 g, 3.70 mmol) and imidazole-1-sulfonyl azide hydrochloride **100** (4.66 g, 22.2 mmol) portionwise. After stirring for ~18 h at room temperature, the solvent was evaporated and the residue was dissolved in DCM (300 mL) and washed with water (2 × 200 mL). The organic layer was separated, dried over $MgSO_4$ and concentrated *in vacuo*. The product was purified by column chromatography (from 0.1% AcOH in DCM:MeOH, 99:1, to 0.1% AcOH in DCM:MeOH, 90:10) and triturated with Et_2O:PE to give the azide **99** as a pale yellow solid (6.73 g, 89%). $\mathbf{R_f}$ (0.1% AcOH in DCM:MeOH, 9:1) = 0.64; **mp** 93-94 °C; **IR** (neat, cm^{-1}) 2089 (N_3), 1713 (C=O); In both the ^1H and ^{13}C NMR, two rotamers were observed (ratio 57$^{(*)}$:43); **^{1}H NMR** (500 MHz, $CDCl_3$) δ 7.77* and 7.74 (2H, d, *J* = 7.5 Hz, Ar*H*), 7.58* and 7.54 (2H, d, 7.5 Hz, Ar*H*), 7.41* and 7.37 (2H, t, *J* = 7.5 Hz, Ar*H*), 7.33* and 7.29 (2H, t, *J* = 7.5 Hz, Ar*H*), 4.58* and 4.46 (2H, d, *J* = 5.6 Hz and 6.1 Hz, OCH_2CH), 4.25* and 4.20 (1H, t, *J* = 5.6 Hz and 6.1 Hz, OCH$_2$C*H*), 3.98* and 3.88 (2H, s, C(O)CH_2N), 3.33 and 3.09* (2H, t, *J* = 7.2 Hz, NCH_2CH$_2$), 3.26 and 3.22* (2H, t, *J* = 7.2 Hz, CH_2N$_3$), 1.61 and 1.48* (2H, qn, *J* = 7.2 Hz, NCH$_2$CH_2), 1.54 and 1.32* (2H, qn, *J* = 7.2 Hz, CH_2CH$_2$N$_3$), 1.40-1.34 and 1.19-1.12* (2H, m, CH_2(CH$_2$)$_2$N$_3$); **^{13}C NMR** (101 MHz, $CDCl_3$) δ 175.03 and 174.76* (C), 156.76* and 156.01 (C), 143.95 (2C), 141.51* and 141.42 (2C), 128.00* and 127.78 (2CH), 127.21* and 127.16 (2CH), 124.94 and 124.82* (2CH), 120.05 (2CH), 67.74 and 67.40* (CH_2), 51.38 (CH_2), 49.23, 48.48, 48.70, 48.54 (2CH_2), 47.36 (CH), 28.64 (CH_2), 27.85* and 27.49 (CH_2), 23.92* and 23.89 (CH_2); ***m/z*** (ESI+) 431 ([M-H+2Na]$^+$, 28%), 431 ([M+Na]$^+$, 51), 409 ([M+H]$^+$, 9); **HRMS** (ESI+) [M+Na]$^+$ found 431.1672, $C_{22}H_{24}N_4NaO_4$ requires 431.1690.

***tert*-Butyl 2-(prop-2-ynylamino)acetate 104a**

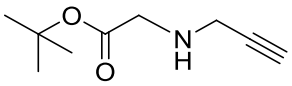

To a solution of propargylamine **101** (7.06 g, 128 mmol) in THF (200 mL) was added triethylamine (53.6 mL, 385 mmol) followed by *tert*-butyl 2-bromoacetate (25.0 g, 128 mmol) in THF (50 mL) dropwise over 2 h at room temperature. After stirring for ~18 h at room temperature, the colourless precipitate formed was removed by filtration, washed with THF (3 × 50 mL) and the residue was concentrated *in vacuo*. The product was purified by column chromatography (8:2 Hexane:EtOAc to 100% EtOAc) to give the propargyl amine **104a** as a yellow oil (9.51 g, 44%). $\mathbf{R_f}$ (DCM:MeOH, 9:1) = 0.63; **IR** (neat, cm^{-1}) 3298, 3267 (NH, ≡C−H), 2132 (w, C≡C), 1732 (C=O); **^{1}H NMR** (400 MHz, $CDCl_3$) δ 3.48 (2H, d, *J* = 2.4 Hz, C*H*$_2$C≡CH), 3.40 (2H, s, C(O)C*H*$_2$NH), 2.23 (1H, t, *J* = 2.4 Hz, CH$_2$C≡C*H*) 1.48 (9H, s, O*t*-Bu); **^{13}C NMR** (101 MHz, $CDCl_3$) δ 171.25 (C), 81.52 (C), 81.45 (C), 71.96 (CH), 50.21 (CH_2), 37.76 (CH_2), 28.23 ($3CH_3$); ***m/z*** (ESI+) 192 ($[M+Na]^+$, 100%); **HRMS** (ESI+) $[M+H]^+$ found 170.1176, $C_9H_{16}NO_2$ requires 170.1176.

***tert*-Butyl 2-({[(9*H*-fluoren-9-yl)methoxy]carbonyl}(prop-2-ynyl)amino)acetate 105**

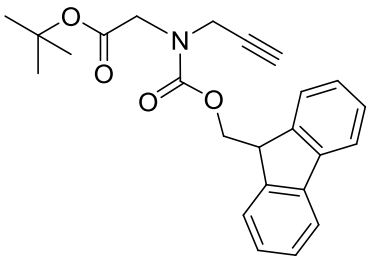

To a solution of *tert*-butyl 2-(prop-2-ynylamino)acetate **104a** (9.51 g, 55.9 mmol) in DCM (150 mL) was added Fmoc-OSu (18.9 g, 55.9 mmol). After stirring for ~18 h at room temperature, the colourless precipitate formed was removed by filtration and the resulting filtrate concentrated *in vacuo*. The product was purified by column chromatography (80:20 Hexane:EtOAc) to give the Fmoc carbamate **105** as a colourless solid (17.8 g, 81%). **R_f** (Hexane:EtOAc, 1:1) = 0.62; **mp** 79-80 °C; **IR** (neat, cm^{-1}) 3279 (≡C−H), 2123 (w, C≡C), 1744 (C=O), 1715 (C=O); Two rotamers were observed in the ^{1}H NMR and ^{13}C NMR spectra; In both the ^{1}H and ^{13}C NMR, two rotamers were observed (ratio 53$^{(*)}$:47); **^{1}H NMR** (400 MHz, $CDCl_3$) δ 7.78 (2H, d, *J* = 7.3 Hz, Ar*H*), 7.66 and 7.59* (2H, d, *J* = 7.3 Hz, Ar*H*), 7.42 (2H, t, *J* = 7.3 Hz, Ar*H*), 7.36-7.29 (2H, m, Ar*H*), 4.44 and 4.42* (2H, d, *J* = 7.1 Hz, OCH_2CH), 4.31* and 4.27 (2H, d, *J* = 2.4 Hz, CH_2≡CH), 4.31 and 4.25 (1H, m, OCH$_2$C*H*), 4.14 and 4.10* (2H, s, C(O)CH_2N), 2.33 and 2.30* (1H, t, *J* = 2.4 Hz, CH$_2$≡C*H*), 1.50 and 1.49* (9H, s, O*t*-Bu); **^{13}C NMR** (101 MHz, $CDCl_3$) δ 168.56 and 168.48* (C), 155.67* and 155.65 (C), 143.92 (2C), 141.41 and 141.37* (2C), 127.85 (2CH), 127.20 (2CH), 125.29 and 125.17* (2CH), 120.11 (2CH), 82.26* and 82.13 (C), 78.51 and 78.47* (C), 73.06* and 72.90 (CH), 68.40 and 68.37* (CH_2), 48.20 and 47.86* (CH_2), 47.30* and 47.19 (CH), 37.40* and 37.11 (CH_2), 28.19 ($3CH_3$); ***m/z*** (ESI+) 414 ([M+Na]$^+$, 100%); **HRMS** (ESI+) [M+Na]$^+$ found 414.1657, $C_{24}H_{25}NNaO_4$ requires 414.1676.

2-({[(9*H*-Fluoren-9-yl)methoxy]carbonyl}(prop-2-ynyl)amino)acetic acid 103

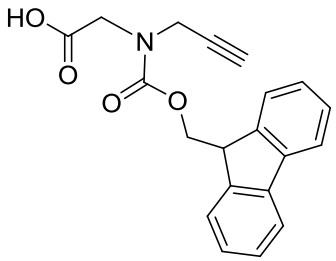

To *tert*-butyl 2-({[(9*H*-fluoren-9-yl)methoxy]carbonyl}(prop-2-ynyl)amino)acetate **105** was added 80% v/v TFA in DCM (160 mL). After stirring for ~18 h at room temperature, DCM and TFA were removed *in vacuo*. The product was purified by column chromatography (100% DCM to 10:90 MeOH:DCM) to give the acid **103** as a colourless solid (9.46 g, 62.0%). $\mathbf{R_f}$ (DCM) = 0.22; **mp** 106-108 °C; **IR** (neat, cm^{-1}) 3255 (≡C−H), 2117 (w, C≡C), 1734 (C=O), 1676 (C=O); In both the ^{1}H and ^{13}C NMR, two rotamers were observed (ratio 50:50);**^{1}H NMR** (500 MHz, $CDCl_3$) δ 9.39 (1H, br s, COO*H*), 7.79 and 7.74 (2H, d, *J* = 7.5 Hz, Ar*H*), 7.64 and 7.53 (2H, d, *J* = 7.5 Hz, Ar*H*), 7.42 and 7.38 (2H, t, *J* = 7.5 Hz, Ar*H*), 7.33 and 7.30 (2H, t, *J* = 7.5 Hz, Ar*H*), 4.50 and 4.48 (2H, d, *J* = 6.1 Hz and 7.1 Hz, OCH_2CH), 4.31 and 4.22 (1H, t, *J* = 7.1 Hz and 6.1 Hz, OCH_2CH), 4.29 and 4.09 (2H, s, $C(O)CH_2N$), 4.27 and 4.26 (2H, d, *J* = 2.2 Hz, CH_2C≡CH), 2.35 and 2.30 (1H, m, $CH_2C{\equiv}CH$) ; **^{13}C NMR** (126 MHz, $CDCl_3$) δ 174.97 (C), 155.78 and 155.49 (C), 143.75 (2C), 141.45 (2C), 127.94 and 127.88 (2CH), 127.26 and 127.22 (2CH), 125.23 and 124.85 (2CH), 120.18 and 120.14 (2CH), 77.93 and 77.90 (C), 73.65 and 73.56 (CH), 68.63 and 68.23 (CH_2), 47.32 and 46.60 (CH_2) 47.19 and 47.17 (CH), 37.34 and 37.22 (CH_2); ***m/z*** (ESI+) 358 ($[M+Na]^+$, 55%), 421 (100); **HRMS** (ESI+) $[M+Na]^+$ found 358.1036, $C_{20}H_{17}NO_4$ requires 358.1050.

Imidazole-1-sulfonyl Azide Hydrochloride 100

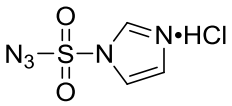

CAUTION: hazardous and explosive material, use azide with care.

Sulfuryl chloride (16.1 mL, 200 mmol) was added dropwise to an ice-cooled suspension of NaN_3 (13.0 g, 200 mmol) in MeCN (200 mL) and the mixture was stirred overnight at room temperature. Imidazole (25.9 g, 380 mmol) was added portion-wise to the ice-cooled mixture and the resulting slurry stirred for 3 h at room temperature. The mixture was diluted with EtOAc (400 mL), washed with H_2O (2 × 400 mL) then saturated aqueous $NaHCO_3$ (2 × 400 mL), dried over $MgSO_4$ and filtered. A solution of HCl in EtOH [obtained by the drop-wise addition of AcCl (21.3 mL, 300 mmol) to ice-cooled dry ethanol (75 mL)] was added drop-wise to the filtrate with stirring, the mixture chilled in an ice-bath, filtered and the filter cake washed with EtOAc (3 × 100 mL) to give azide **100** as colourless solid (26.5 g, 63%). **^{1}H NMR** (400 MHz, D_2O) δ 9.11 (1H, m, NC*H*N), 7.82 (1H, t, *J* = 1.8 Hz, SNC*H*CHN), 7.41 (1H, m, SNCHC*H*N); ***m/z*** (ESI+) 173.9 ([M+H]$^+$, 100%).

The spectroscopic data is in good agreement with the literature.[253]

4.11.3 Synthesis of peptoid-peptide hybrids

4.11.3.1 Synthesis of acyclic peptoid-peptide hybrids

Fmoc-Rink linker **106** (2.15 g, 4 mmol) was coupled to aminomethyl polystyrene resin **107** (1.08 g, 1.3 mmol) as described in Section 4.11.1. After coupling, the solid support was Fmoc deprotected using 20% piperidine in DMF to provide the functionalized resin **108**. Residues were then coupled to the functionalised resin as described in Section 4.11.1. Cleavage of acyclic peptoid-peptide hybrids was allowed using a TFA cocktail. Cleaved hybrids were precipitated in cold ether and lyophilised overnight. Acyclic hybrids were finally purified by HPLC using method on a preparative column Luna C18(2), lyophilised and further characterised by MALDI-ToF.

4.11.3.2 Solid support CuAAC

Copper iodide (13.0 equiv.), sodium ascorbate (7.0 equiv.) and lutidine (17.0 equiv.) were used. Masses and volumes were calculated based on the theoretical loading of the resin, 0.38 mmol/g

A General protocol for solid support CuAAC on the peptoid-peptide hybrid is the following:

Method A:

Copper iodide (9.4 mg, 0.50 mmol), sodium ascorbate (5.2 mg, 0.26 mmol) and lutidine (7.4 µL, 0.64 mmol) were added to the resin bearing **U13** (5 mg; theoretical loading: 0.38 mmol/g) in DMF (2.5 mL). The resin was shaken for 24 h at room temperature. The resin was filtered and washed with DMF: pyridine [5 x 2.5 mL; 7:3 (v/v)], DMF (3 x 2.5 mL) and DCM (3 x 2.5 mL). The peptoid-peptide hybrid **C13** was cleaved from the resin with TFA:TIS:H_2O (95:2.5:2.5, (v/v)) for 1 h at room temperature. The hybrid in TFA was concentrated, precipitated in cold Et_2O and filtered. The unpurified peptoid-peptide hybrid **C13** was solubilised in H_2O and lyophilised. HPLC was carried out (method in Section 4.11). The purified product was lyophilised and further characterised by MALDI-ToF.

4.11.3.3 Solution phase CuAAC

A General protocol for CuAAC in solution on the peptoid-peptide hybrid is the following:

Method B:

A solution of copper sulfate (12.5 mg, 0.078 mmol), sodium ascorbate (31.0 mg, 0.15 mmol) and TBTA (41.6 mg, 0.078 mmol) in *t*-BuOH:H_2O [50 mL; 2:1 (v/v)] was prepared. 50 µL of this solution was added to the purified peptoid-peptide hybride **U13** (1.0 mg, 0.8 µmol) in *t*-BuOH:H_2O [50 mL; 2:1 (v/v)]. The reaction mixture was stirred for 24 h at room temperature. The solvent was removed *in vacuo* and the reaction mixture was solubilised in H_2O and lyophilised. HPLC was finally carried out (method in Section 4.11). The purified product **C13** was lyophilised and further characterised by MALDI-ToF.

U1: (U)-Biotin-SGSG-KAA*YFZ$^*{}_5$-NH_2

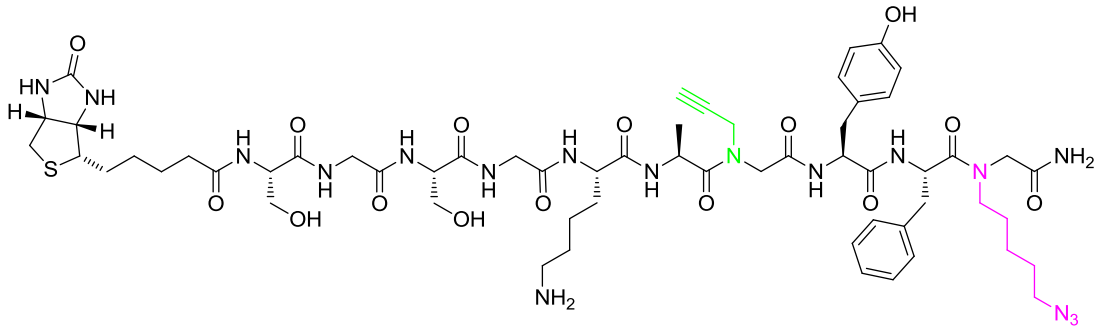

U1 was synthesised using general methods described in Section 4.11.1 and 4.11.3.1. **t_R** (Analytical, method 4) 69.9 min; **t_R** (preparative, method 4) 87.3 min; **purity** 99.7%, ***m/z*** (MALDI-ToF, αCHCA) 1304.0 $[M+H]^+$, 1326.0 $[M+Na]^+$, 1341.9 $[M+K]^+$, 2606.8 $[2M+H]^+$, 2628.7 $[2M+Na]^+$, 2644.7 $[2M+K]^+$.

U2: (U)-Biotin-SGSG-KAZ*$_5$YFA*-NH_2

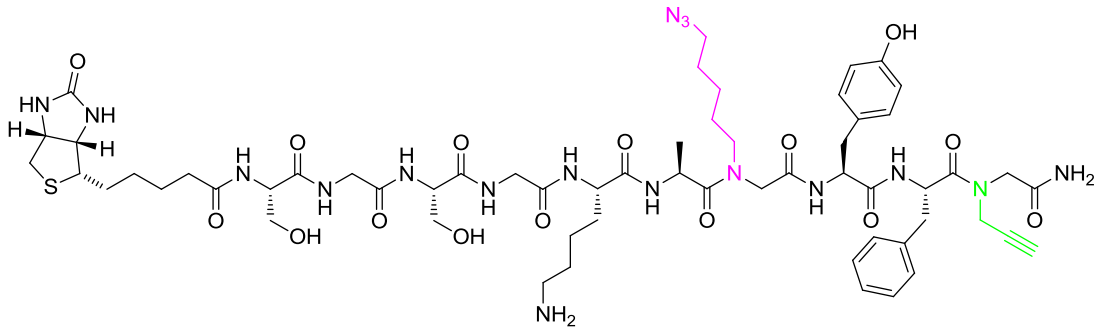

U2 was synthesised using general methods described in Section 4.11.1 and 4.11.3.1. t_R (Analytical, method 4) 72.0 min; t_R (preparative, method 4) 84.0 min; **purity** 96.9%, ***m/z*** (MALDI-ToF, αCHCA) 1304.5 $[M+H]^+$, 1326.5 $[M+Na]^+$, 1342.5 $[M+K]^+$, 2607.8 $[2M+H]^+$, 2629.8 $[2M+Na]^+$, 2645.7 $[2M+K]^+$.

U3: (U)-Biotin-SGSG-KA*AYFZ*$_5$-NH_2

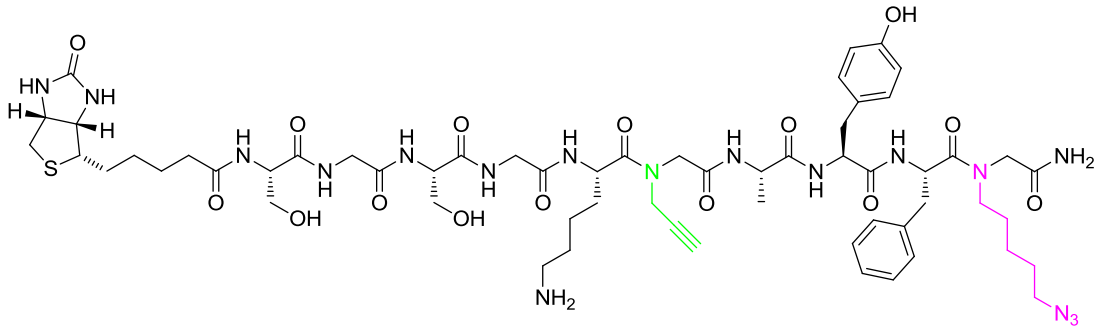

U3 was synthesised using general methods described in Section 4.11.1 and 4.11.3.1. t_R (Analytical, method 4) 74.2 min; t_R (preparative, method 4) 86.2 min; **purity** 89.3%, ***m/z*** (MALDI-ToF, αCHCA) 1304.5 $[M+H]^+$, 1326.5 $[M+Na]^+$, 1342.5 $[M+K]^+$, 2607.8 $[2M+H]^+$.

U4: (U)-Biotin-SGSG-KZ*$_5$AYFA*-NH_2

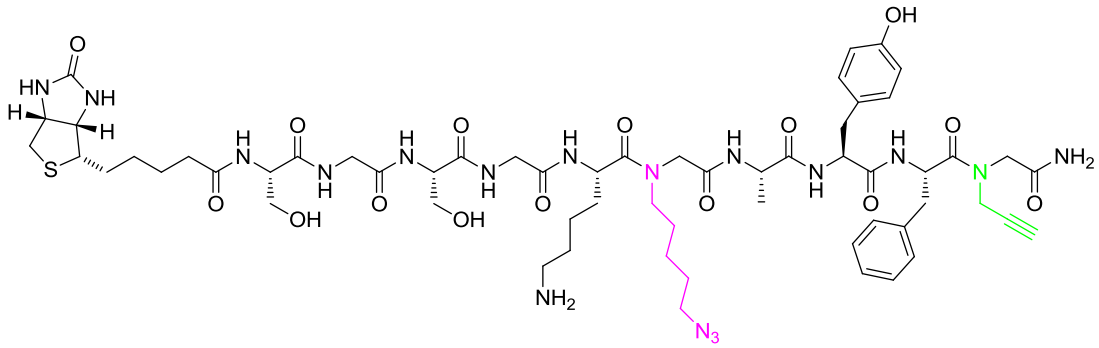

U4 was synthesised using general methods described in Section 4.11.1 and 4.11.3.1. t_R (Analytical, method 4) 70.0 min; t_R (preparative, method 4) 82.2 min; **purity** 99.1%, ***m/z*** (MALDI-ToF, αCHCA) 1304.3 $[M+H]^+$, 1326.2 $[M+Na]^+$, 1342.2 $[M+K]^+$, 2607.3 $[2M+H]^+$, 2629.3 $[2M+Na]^+$, 2645.3 $[2M+K]^+$.

U5: (U)-Biotin-SGSG-KAA*YFZ*$_3$-NH_2

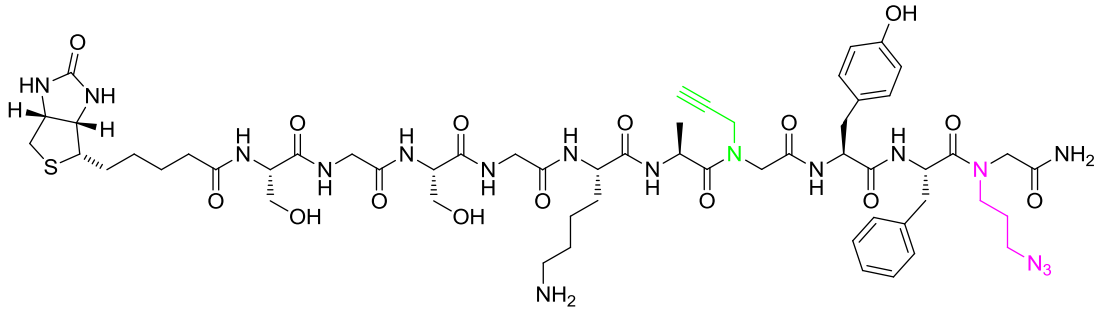

U5 was synthesised using general methods described in Section 4.11.1 and 4.11.3.1. t_R (Analytical, method 4) 67.3 min; t_R (preparative, method 4) 79.2 min; **purity** 92.4%, ***m/z*** (MALDI-ToF, αCHCA) 1276.5 $[M+H]^+$, 1298.5 $[M+Na]^+$, 1314.5 $[M+K]^+$, 2551.8 $[2M+H]^+$, 2573.8 $[2M+Na]^+$, 2589.8 $[2M+K]^+$.

U6: (U)-Biotin-SGSG-KAZ*$_3$YFA*-NH_2

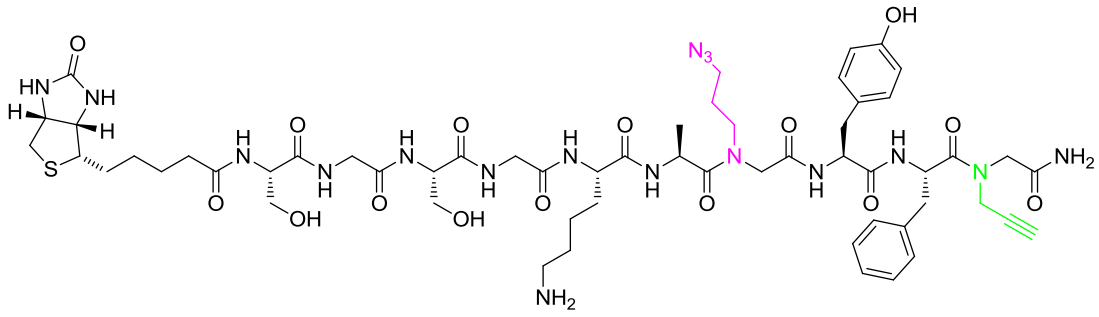

U6 was synthesised using general methods described in Section 4.11.1 and 4.11.3.1. t_R (Analytical, method 4) 65.9 min; t_R (preparative, method 4) 78.0 min; **purity** 90.8%, ***m/z*** (MALDI-ToF, αCHCA) 1276.5 $[M+H]^+$, 1298.4 $[M+Na]^+$, 1314.4 $[M+K]^+$, 2551.7 $[2M+H]^+$, 2573.7 $[2M+Na]^+$, 2589.7 $[2M+K]^+$.

U7: (U)-Biotin-SGSG-KA*AYFZ*$_4$-NH_2

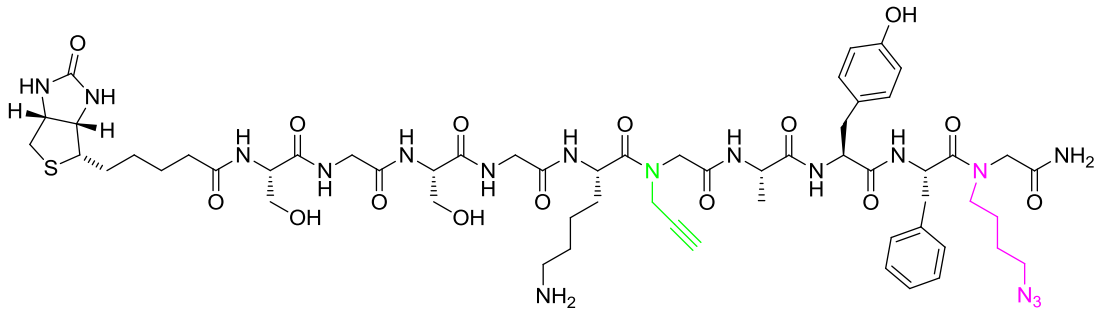

U7 was synthesised using general methods described in Section 4.11.1 and 4.11.3.1. t_R (Analytical, method 4) 69.3 min; t_R (preparative, method 4) 81.6 min; **purity** 97.5%, ***m/z*** (MALDI-ToF, αCHCA) 1290.2 $[M+H]^+$, 1312.1 $[M+Na]^+$, 1328.1 $[M+K]^+$, 2579.1 $[2M+H]^+$, 2601.0 $[2M+Na]^+$.

U8: (U)-Biotin-SGSG-KZ*$_4$AYFA*-NH_2

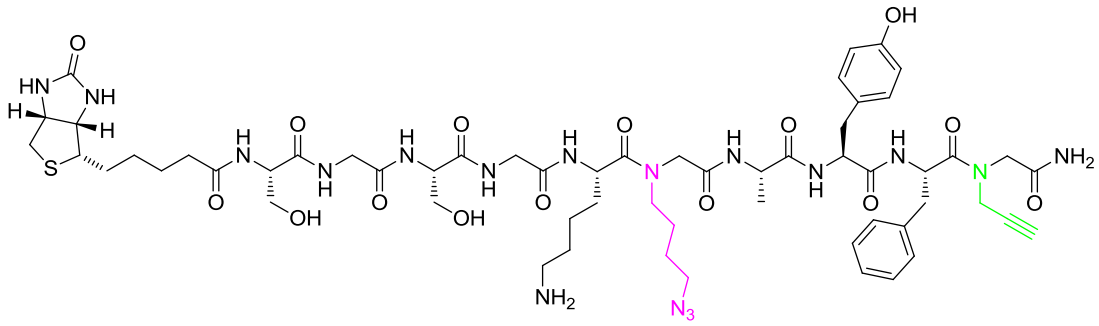

U8 was synthesised using general methods described in Section 4.11.1 and 4.11.3.1. t_R (Analytical, method 4) 66.8 min; t_R (preparative, method 4) 78.8 min; **purity** 92.9%, ***m/z*** (MALDI-ToF, αCHCA) 1289.9 $[M+H]^+$, 1311.8 $[M+Na]^+$, 1327.8 $[M+K]^+$, 2578.5 $[2M+H]^+$, 2600.5 $[2M+Na]^+$, 2616.4 $[2M+K]^+$.

U9: (U)-Biotin-SGSG-KZ*$_3$AYFA*-NH_2

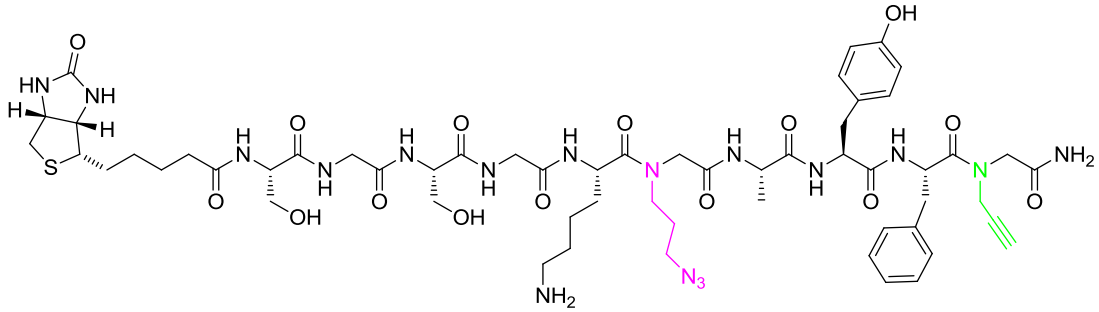

U9 was synthesised using general methods described in Section 4.11.1 and 4.11.3.1. t_R (Analytical, method 4) 63.8 min; t_R (preparative, method 4) 76.0 min; **purity** 93.8%, ***m/z*** (MALDI-ToF, αCHCA) 1276.1 $[M+H]^+$, 1298.1 $[M+Na]^+$, 1314.1 $[M+K]^+$, 2551.0 $[2M+H]^+$.

U10: (U)-Biotin-SGSG-KAA*YFZ$^{*}{}_{4}$-NH_2

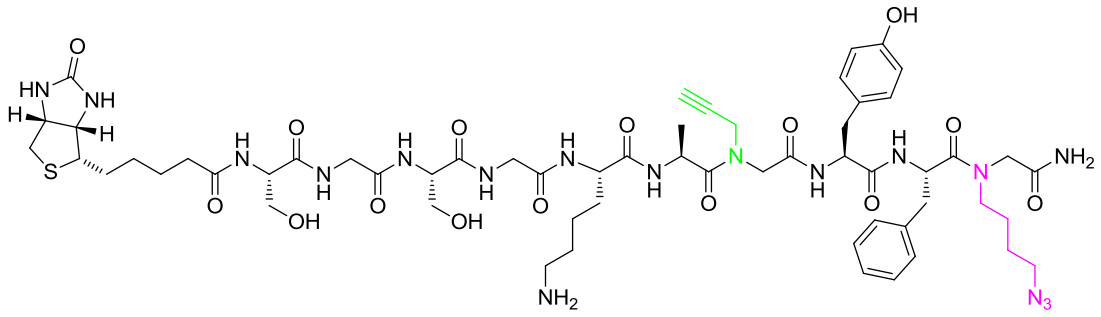

U10 was synthesised using general methods described in Section 4.11.1 and 4.11.3.1. t_R (Analytical, method 4) 70.4 min; t_R (preparative, method 4) 82.1 min; **purity** 89.9%, ***m/z*** (MALDI-ToF, αCHCA) 1290.2 $[M+H]^+$, 1312.2 $[M+Na]^+$, 1328.2 $[M+K]^+$, 2601.2 $[2M+Na]^+$, 2617.1 $[2M+K]^+$.

U12: (U)-Biotin-SGSG-KAZ$^{*}{}_{4}$YFA*-NH_2

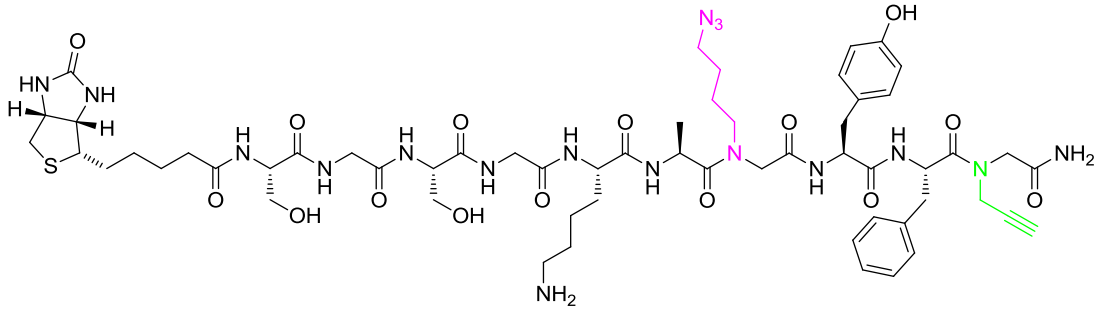

U12 was synthesised using general methods described in Section 4.11.1 and 4.11.3.1. t_R (Analytical, method 4) 68.6 min; t_R (preparative, method 4) 80.5 min; **purity** 91.9%, ***m/z*** (MALDI-ToF, αCHCA) 1290.2 $[M+H]^+$, 1312.2 $[M+Na]^+$, 1328.2 $[M+K]^+$, 2579.2 $[2M+H]^+$, 2601.2 $[2M+Na]^+$, 2617.1 $[2M+K]^+$.

U13: (U)-Biotin-SGSG-KA*AYFZ*$_3$-NH_2

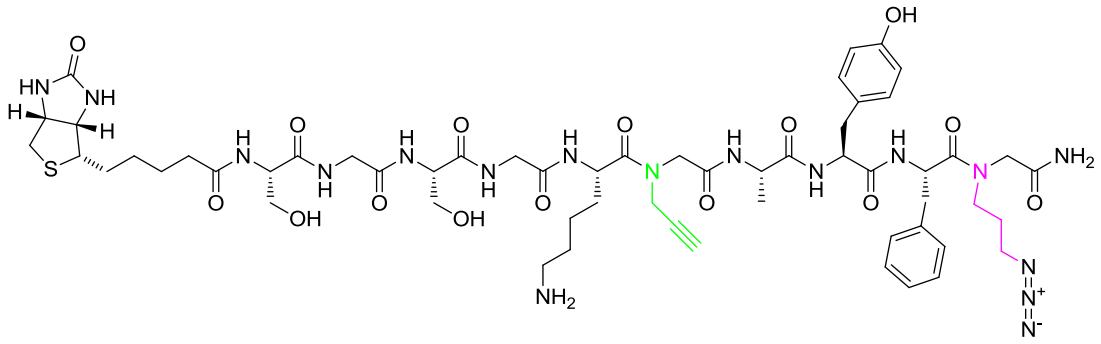

U13 was synthesised using general methods described in Section 4.11.1 and 4.11.3.1. t_R (Analytical, method 4) 65.9 min; t_R (preparative, method 4) 78.3 min; **purity** 94.4%, ***m/z*** (MALDI-ToF, αCHCA) 1275.9 $[M+H]^+$, 2550.6 $[2M+H]^+$.

U14: (U)-Ac-KAA*YFZ*$_5$-NH_2

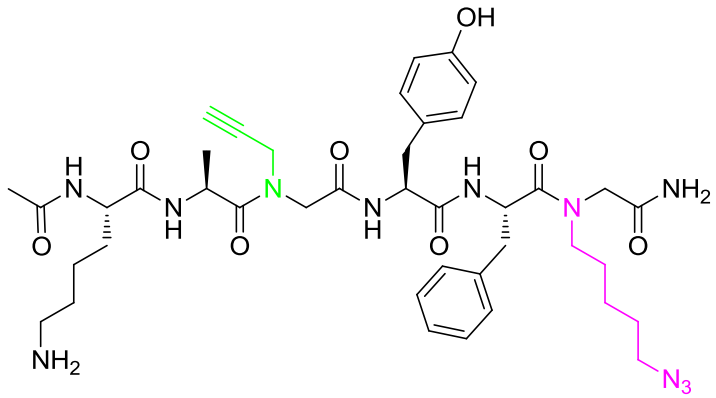

U14 was synthesised using general methods described in Section 4.11.1 and 4.11.3.1. t_R (Analytical, method 4) 74.7 min; t_R (preparative, method 4) 89.4 min; **purity** 95.9%, ***m/z*** (MALDI-ToF, αCHCA) 832.4 $[M+H]^+$, 854.4 $[M+Na]^+$, 870.4 $[M+K]^+$, 1663.8 $[2M+H]^+$, 1685.7 $[2M+Na]^+$, 1701.7 $[2M+K]^+$, 2495.1 $[3M+H]^+$, 2517.0 $[3M+Na]^+$, 2533.0 $[3M+K]^+$.

U15: (U)-Ac-KAZ*$_5$YFA*-NH_2

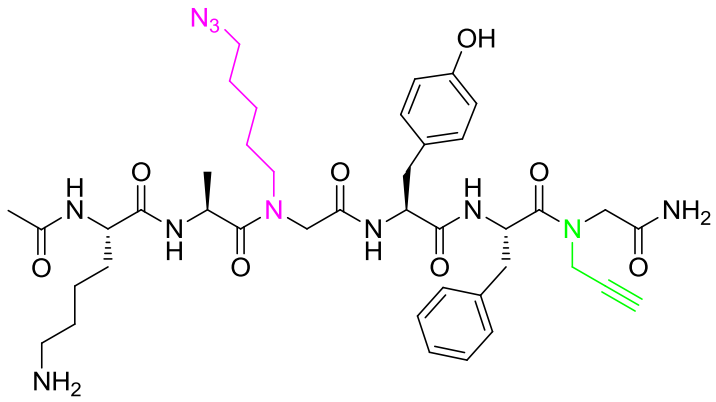

U15 was synthesised using general methods described in Section 4.11.1 and 4.11.3.1. t_R (Analytical, method 4) 72.4 min; t_R (preparative, method 4) 87.1 min; **purity** 96.0%, ***m/z*** (MALDI-ToF, αCHCA) 832.3 $[M+H]^+$, 854.2 $[M+Na]^+$, 870.2 $[M+K]^+$, 1663.4 $[2M+H]^+$, 1685.3 $[2M+Na]^+$, 1701.3 $[2M+K]^+$, 2494.5 $[3M+H]^+$, 2516.4 $[3M+Na]^+$, 2532.4 $[3M+K]^+$.

U16: (U)-Ac-KA*AYFZ*$_5$-NH_2

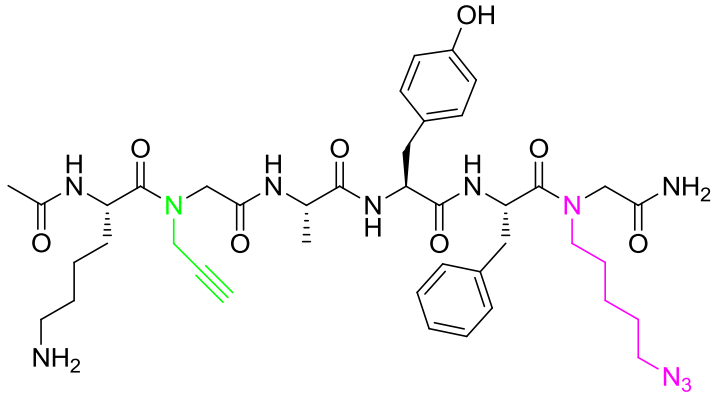

U16 was synthesised using general methods described in Section 4.11.1 and 4.11.3.1. t_R (Analytical, method 4) 73.4 min; t_R (preparative, method 4) 86.8 min; **purity** 71.6%, ***m/z*** (MALDI-ToF, αCHCA) 832.4 $[M+H]^+$, 854.4 $[M+Na]^+$, 870.4 $[M+K]^+$, 1663.7 $[2M+H]^+$, 1685.7 $[2M+Na]^+$, 1701.6 $[2M+K]^+$, 2495.9 $[3M+H]^+$, 2517.6 $[3M+Na]^+$.

U17: (U)-Ac-KZ*$_5$AYFA*-NH_2

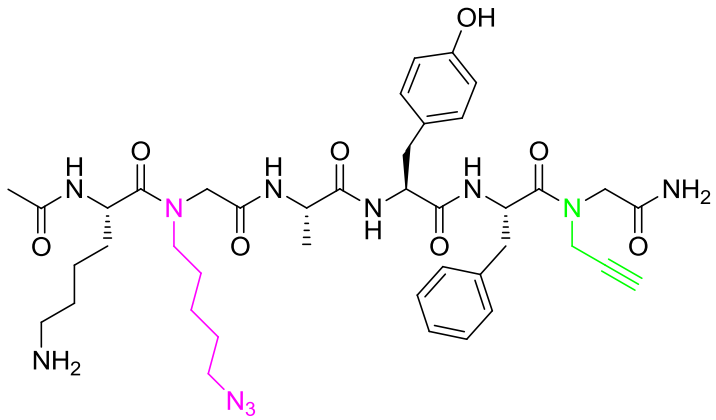

U17 was synthesised using general methods described in Section 4.11.1 and 4.11.3.1. t_R (Analytical, method 4) 70.1 min; t_R (preparative, method 4) 83.9 min; **purity** 96.2%, ***m/z*** (MALDI-ToF, αCHCA) 832.0 $[M+H]^+$, 854.0 $[M+Na]^+$, 870.0 $[M+K]^+$, 1662.9 $[2M+H]^+$, 1684.9 $[2M+Na]^+$, 1700.8 $[2M+K]^+$, 2493.8 $[3M+H]^+$, 2515.7 $[3M+Na]^+$, 2531.7 $[3M+K]^+$.

U18: (U)-Ac-KAA*YFZ*$_3$-NH_2

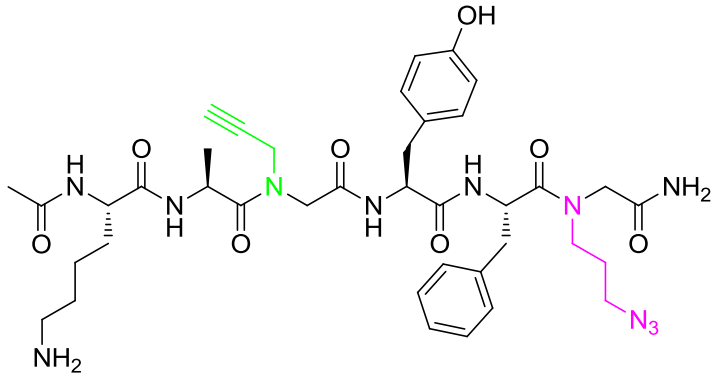

U18 was synthesised using general methods described in Section 4.11.1 and 4.11.3.1. t_R (Analytical, method 4) 66.2 min; t_R (preparative, method 4) 79.7 min; **purity** 83.4%, ***m/z*** (MALDI-ToF, αCHCA) 804.0 $[M+H]^+$, 826.4 $[M+Na]^+$, 842.4 $[M+K]^+$, 1607.8 $[2M+H]^+$, 1628.8 $[2M+Na]^+$, 1644.8 $[2M+K]^+$, 2409.7 $[3M+H]^+$, 2431.7 $[3M+Na]^+$, 2447.6 $[3M+K]^+$.

U19: (U)-Ac-KAZ*$_3$YFA*-NH_2

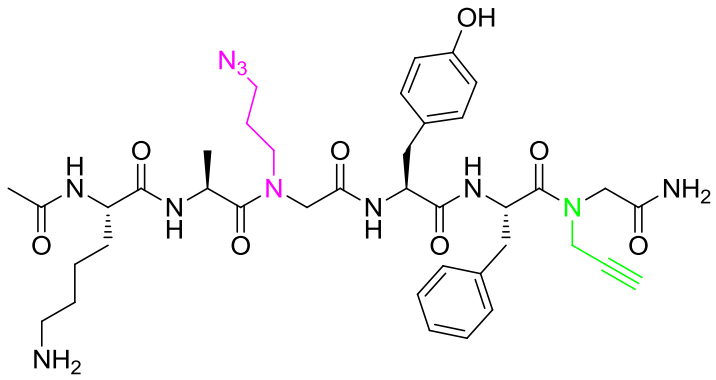

U19 was synthesised using general methods described in Section 4.11.1 and 4.11.3.1. t_R (Analytical, method 4) 65.0 min; t_R (preparative, method 4) 78.3 min; **purity** 84.4%, ***m/z*** (MALDI-ToF, αCHCA) 804.2 $[M+H]^+$, 826.0 $[M+Na]^+$, 841.9 $[M+K]^+$, 1607.3 $[2M+H]^+$, 1629.3 $[2M+Na]^+$, 1645.3 $[2M+K]^+$, 410.4 $[3M+H]^+$, 2432.4 $[3M+Na]^+$, 2448.3 $[3M+K]^+$.

U20: (U)-Ac-KA*AYFZ*$_4$-NH_2

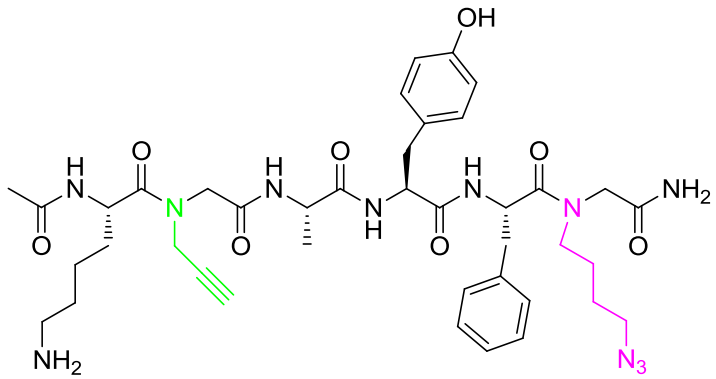

U20 was synthesised using general methods described in Section 4.11.1 and 4.11.3.1. t_R (Analytical, method 4) 68.1 min; t_R (preparative, method 4) 82.6 min; **purity** 68.0%, ***m/z*** (MALDI-ToF, αCHCA) 818.7 $[M+H]^+$, 840.7 $[M+Na]^+$, 856.7 $[M+K]^+$, 1636.3 $[2M+H]^+$, 1658.3 $[2M+Na]^+$, 1674.3 $[2M+K]^+$, 2452.8 $[3M+H]^+$, 2475.8 $[3M+Na]^+$, 2491.8 $[3M+K]^+$.

U21: (U)-Ac-KZ*$_4$AYFA*-NH_2

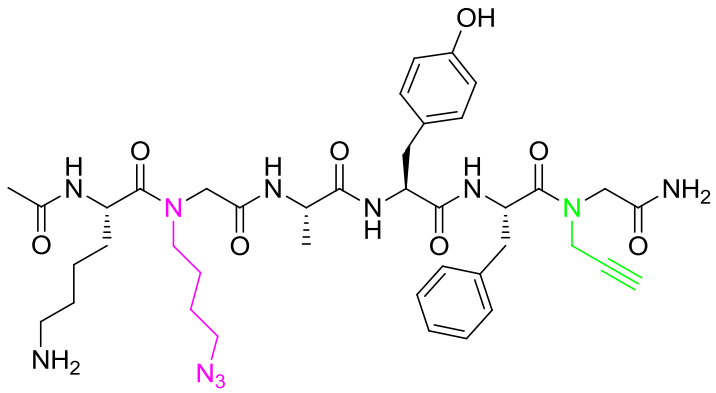

U21 was synthesised using general methods described in Section 4.11.1 and 4.11.3.1. t_R (Analytical, method 4) 66.2 min; t_R (preparative, method 4) 80.0 min; **purity** 82.3%, ***m/z*** (MALDI-ToF, αCHCA) 818.2 $[M+H]^+$, 840.2 $[M+Na]^+$, 856.1 $[M+K]^+$, 1635.2 $[2M+H]^+$, 1657.2 $[2M+Na]^+$, 1673.1 $[2M+K]^+$, 2452.3 $[3M+H]^+$, 2474.2 $[3M+Na]^+$, 2490.1 $[3M+K]^+$.

U22: (U)-Ac-KZ*$_3$AYFA*-NH_2

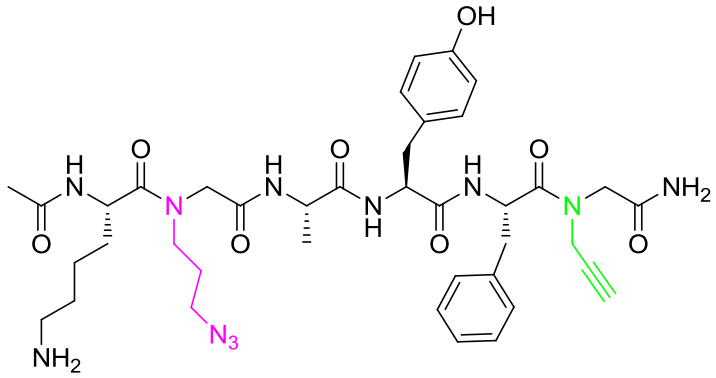

U22 was synthesised using general methods described in Section 4.11.1 and 4.11.3.1. t_R (Analytical, method 4) 62.8 min; t_R (preparative, method 4) 76.7 min; **purity** 91.4%, ***m/z*** (MALDI-ToF, αCHCA) 803.6 $[M+H]^+$, 826.6 $[M+Na]^+$, 842.6 $[M+K]^+$, 1608.1 $[2M+H]^+$, 1630.1 $[2M+Na]^+$, 1646.1 $[2M+K]^+$, 2411.6 $[3M+H]^+$, 2433.6 $[3M+Na]^+$, 2449.6 $[3M+K]^+$.

U23: (U)-Ac-KAA*YFZ*$_4$-NH_2

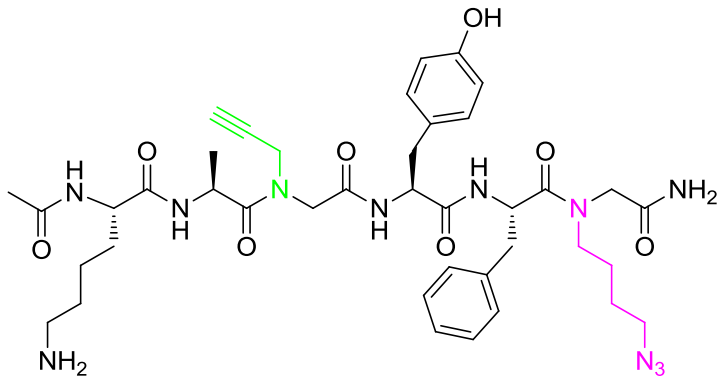

U23 was synthesised using general methods described in Section 4.11.1 and 4.11.3.1. t_R (Analytical, method 4) 70.2 min; t_R (preparative, method 4) 84.5 min; **purity** 79.5%, ***m/z*** (MALDI-ToF, αCHCA) 818.7 $[M+H]^+$, 840.7 $[M+Na]^+$, 856.7 $[M+K]^+$, 1636.3 $[2M+H]^+$, 1658.3 $[2M+Na]^+$, 1674.3 $[2M+K]^+$, 2452.9 $[3M+H]^+$, 2475.8 $[3M+Na]^+$, 2491.8 $[3M+K]^+$.

U25: (U)-Ac-KAZ*$_4$YFA*-NH_2

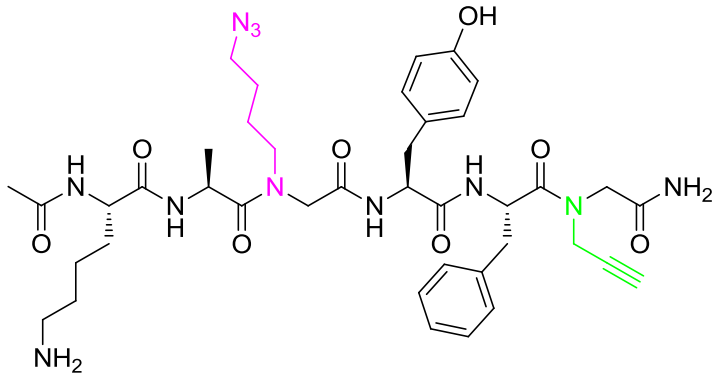

U25 was synthesised using general methods described in Section 4.11.1 and 4.11.3.1. t_R (Analytical, method 4) 64.4 min; t_R (preparative, method 4) 79.0 min; **purity** 69.4%, ***m/z*** (MALDI-ToF, αCHCA) 818.7 $[M+H]^+$, 840.7 $[M+Na]^+$, 856.7 $[M+K]^+$, 1636.3 $[2M+H]^+$, 1658.3 $[2M+Na]^+$, 1674.3 $[2M+K]^+$, 2452.8 $[3M+H]^+$, 2475.8 $[3M+Na]^+$, 2491.8 $[3M+K]^+$ $[3M+K]^+$.

U26: (U)-Ac-KA*AYFZ*$_3$-NH_2

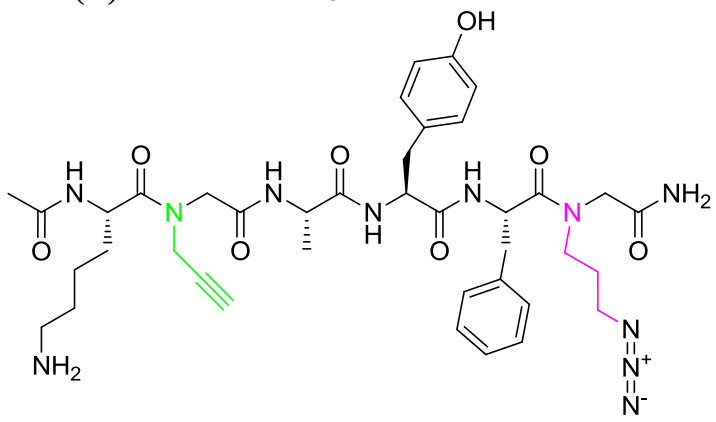

U26 was synthesised using general methods described in Section 4.11.1 and 4.11.3.1. t_R (Analytical, method 4) 68.3 min; t_R (preparative, method 4) 82.5 min; **purity** 77.2%, ***m/z*** (MALDI-ToF, αCHCA) 804.5 $[M+H]^+$, 826.0 $[M+Na]^+$, 841.9 $[M+K]^+$, 1606.9 $[2M+H]^+$, 1629.7 $[2M+Na]^+$, 1645.7 $[2M+K]^+$, 2411.1 $[3M+H]^+$, 2433.0 $[3M+Na]^+$, 2449.0 $[3M+K]^+$.

C1: (C)-Biotin-SGSG-KAA*YFZ*$_5$-NH_2

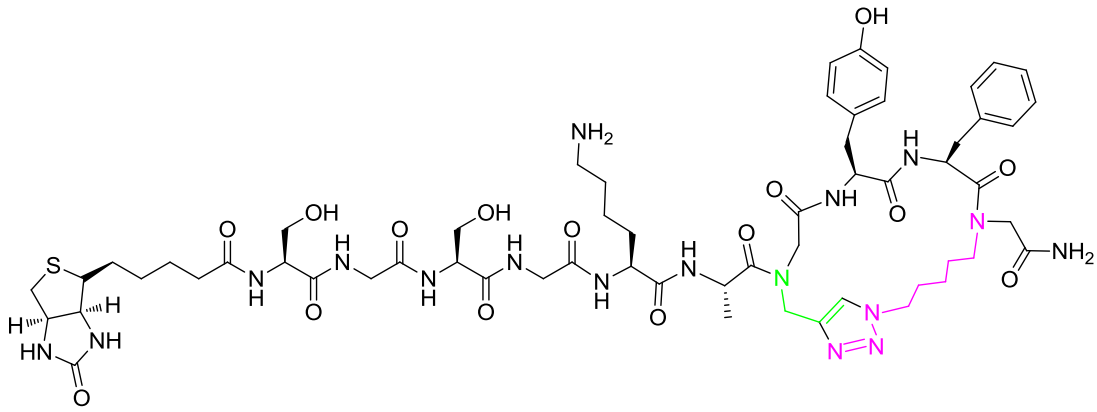

C1 was synthesised from **U1** attached on the Rink amide resin using Method A described in Section 4.11.3.2.

t_R (Analytical, method 4) 58.9 min; t_R (preparative, method 4) 73.3 min; **purity** 60.8%, ***m/z*** (MALDI-ToF, αCHCA) 1304.4 $[M+H]^+$, 1326.5 $[M+Na]^+$, 1342.3 $[M+K]^+$, 2607.5 $[2M+H]^+$, 2629.5 $[2M+Na]^+$, 2645.4 $[2M+K]^+$.

C2: (C)-Biotin-SGSG-KAZ*$_5$YFA*-NH_2

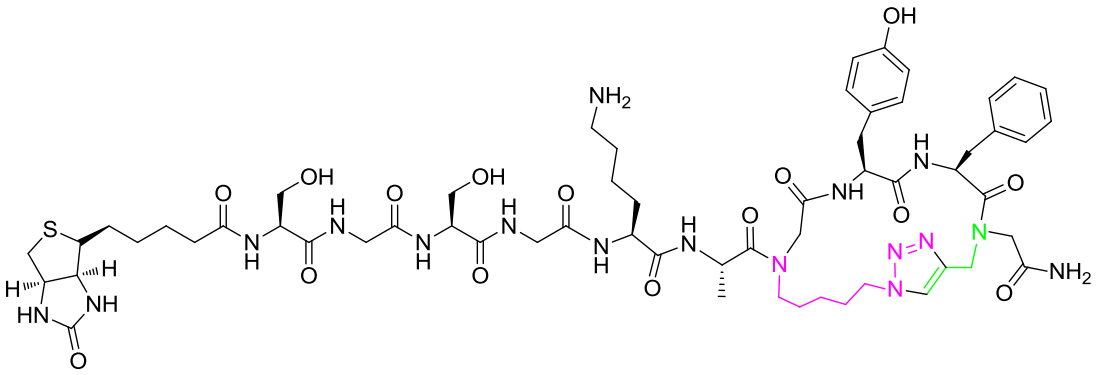

C2 was synthesised from **U2** attached on the Rink amide resin using Method A described in Section 4.11.3.2. Alternatively, **C2** was also synthesised in solution from purified **U2** using method B as described in Section 4.11.3.3.

t_R (Analytical, method 4) 58.8 min; **t_R** (preparative, method 4) 73.8 min; **purity (Method A)** 41.9%, **purity (Method B)** 95.3%, ***m/z*** (MALDI-ToF, αCHCA) 1304.1 $[M+H]^+$, 1326.1 $[M+Na]^+$, 1342.0 $[M+K]^+$.

C3: (C)-Biotin-SGSG-KA*AYFZ$^{*}{}_{5}$-NH$_2$

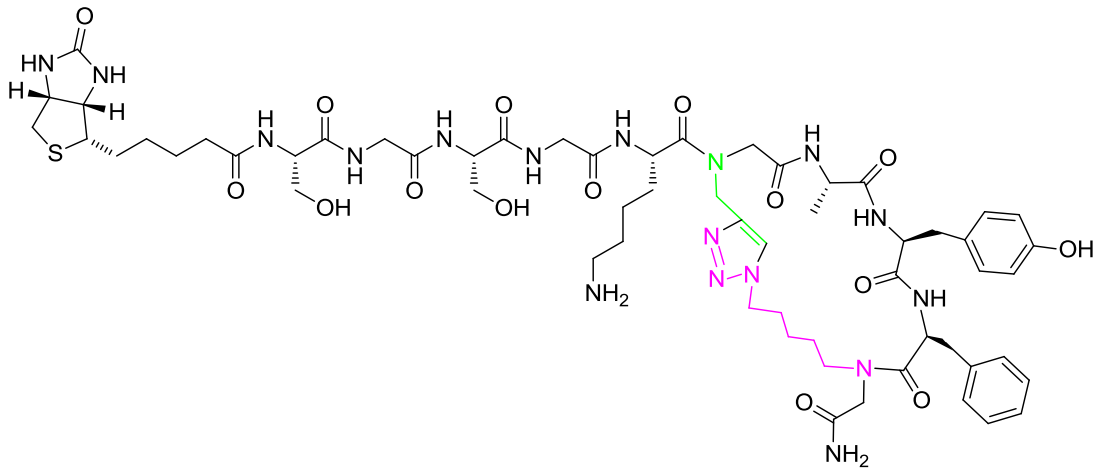

C3 was synthesised from **U3** attached on the Rink amide resin using Method A described in Section 4.11.3.2. Alternatively, **C3** was also synthesised in solution from purified **U3** using method B as described in Section 4.11.3.3.

t$_R$ (Analytical, method 4) 54.3 min; **t$_R$** (preparative, method 4) 69.2 min; **purity (Method A)** 94.8%, **purity (Method B)** 100.0%, ***m/z*** (MALDI-ToF, αCHCA) 1304.5 $[M+H]^+$, 1326.4 $[M+Na]^+$, 1342.4 $[M+K]^+$, 2607.7 $[2M+H]^+$, 2629.7 $[2M+Na]^+$, 2645.6 $[2M+K]^+$.

C4: (C)-Biotin-SGSG-KZ$^{*}{}_{5}$AYFA*-NH$_2$

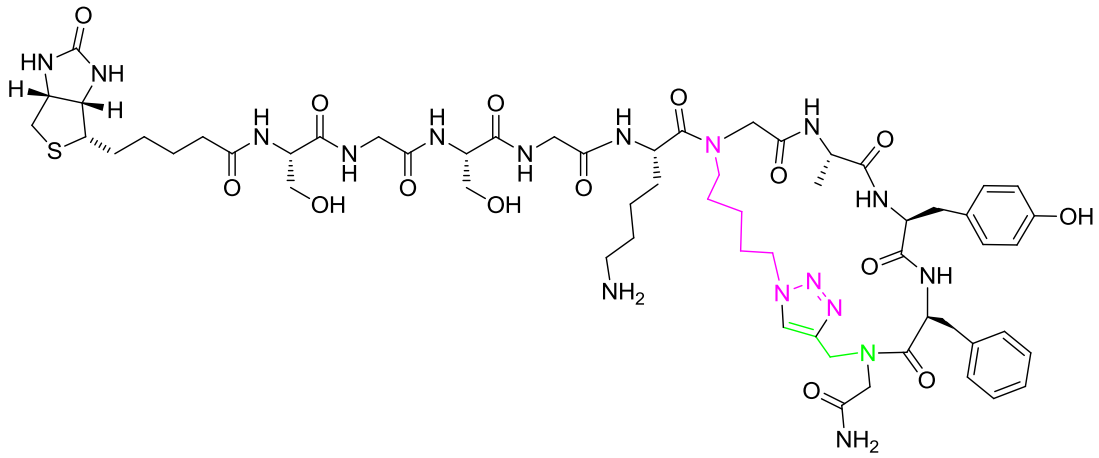

C4 was synthesised from **U4** attached on the Rink amide resin using Method A described in Section 4.11.3.2.

t$_R$ (Analytical, method 4) 53.6 min; **t$_R$** (preparative, method 4) 65.4 min; **purity** 86.1%, ***m/z*** (MALDI-ToF, αCHCA) 1304.5 $[M+H]^+$, 1326.4 $[M+Na]^+$, 1342.4 $[M+K]^+$.

C5: (C)-Biotin-SGSG-KAA*YFZ*$_3$-NH_2

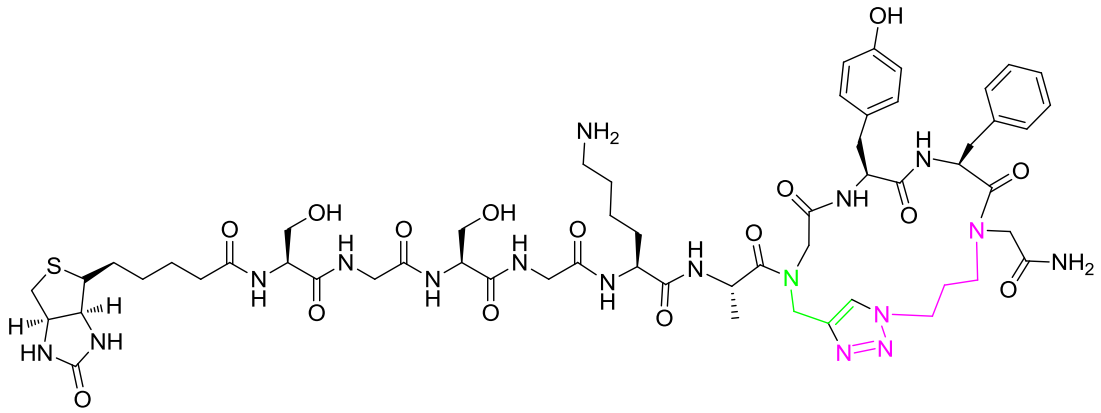

C5 was synthesised from **U5** attached on the Rink amide resin using Method A described in Section 4.11.3.2.

t_R (Analytical, method 4) 56.0 min; **t_R** (preparative, method 4) 68.0 min; **purity** 69.5%, ***m/z*** (MALDI-ToF, αCHCA) 1276.6 $[M+H]^+$, 1298.6 $[M+Na]^+$, 1314.6 $[M+K]^+$, 2552.0 $[2M+H]^+$, 2574.0 $[2M+Na]^+$, 2589.9 $[2M+K]^+$.

C6: (C)-Biotin-SGSG-KAZ*$_3$YFA*-NH_2

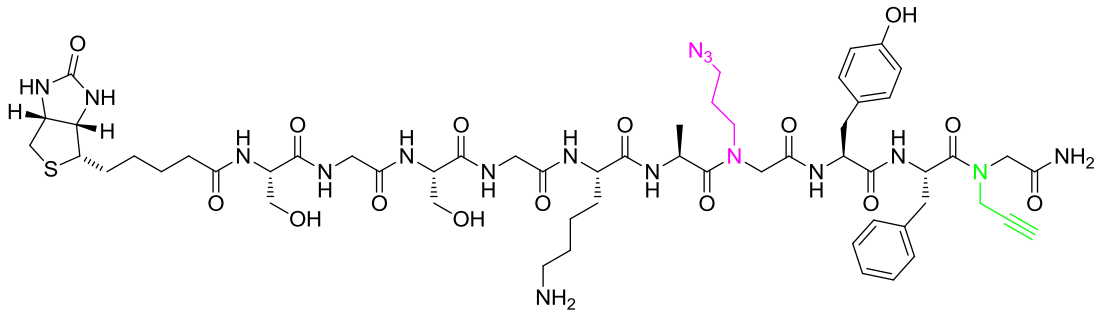

C6 was synthesised from **U6** attached on the Rink amide resin using Method A described in Section 4.11.3.2.

t_R (Analytical, method 4) 57.7 min; **t_R** (preparative, method 4) 69.3 min; **purity** 69.0%, ***m/z*** (MALDI-ToF, αCHCA) 1276.5 $[M+H]^+$, 1298.5 $[M+Na]^+$, 1314.5 $[M+K]^+$, 2551.7 $[2M+H]^+$, 2573.7 $[2M+Na]^+$, 2589.7 $[2M+K]^+$.

C7: (C)-Biotin-SGSG-KA*AYFZ*$_4$-NH_2

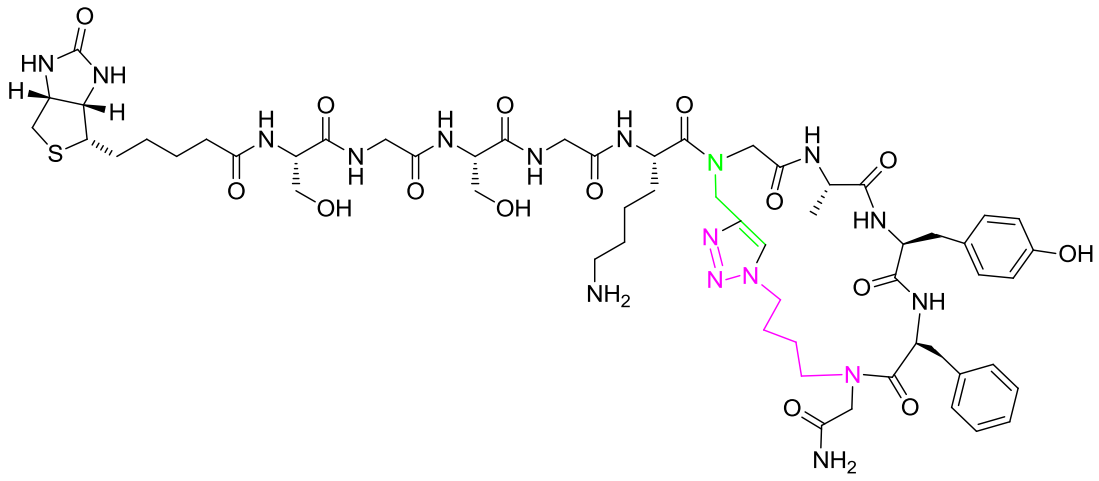

C7 was synthesised from **U7** attached on the Rink amide resin using Method A described in Section 4.11.3.2.

$\mathbf{t_R}$ (Analytical, method 4) 55.1 min; $\mathbf{t_R}$ (preparative, method 4) 67.0 min; **purity** 91.5%, ***m/z*** (MALDI-ToF, αCHCA) 1290.1 $[M+H]^+$, 1312.1 $[M+Na]^+$, 1328.1 $[M+K]^+$.

C8: (C)-Biotin-SGSG-KZ*$_4$AYFA*-NH_2

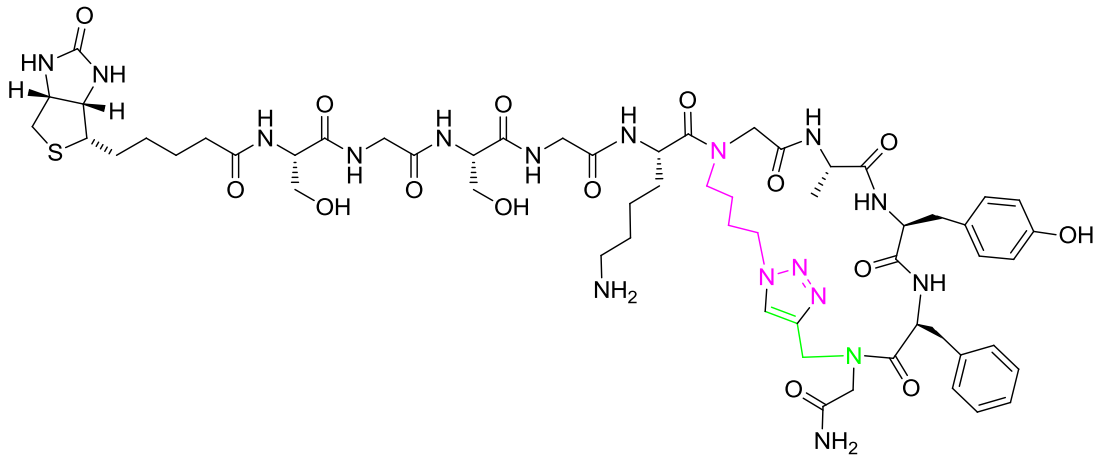

C8 was synthesised from **U8** attached on the Rink amide resin using Method A described in Section 4.11.3.2. $\mathbf{t_R}$ (Analytical, method 4) 57.1 min; $\mathbf{t_R}$ (preparative, method 4) 69.0 min; **purity** 77.9%, ***m/z*** (MALDI-ToF, αCHCA) 1290.0 $[M+H]^+$, 1312.0 $[M+Na]^+$, 1328.0 $[M+K]^+$.

C9: (C)-Biotin-SGSG-KZ*$_3$AYFA*-NH_2

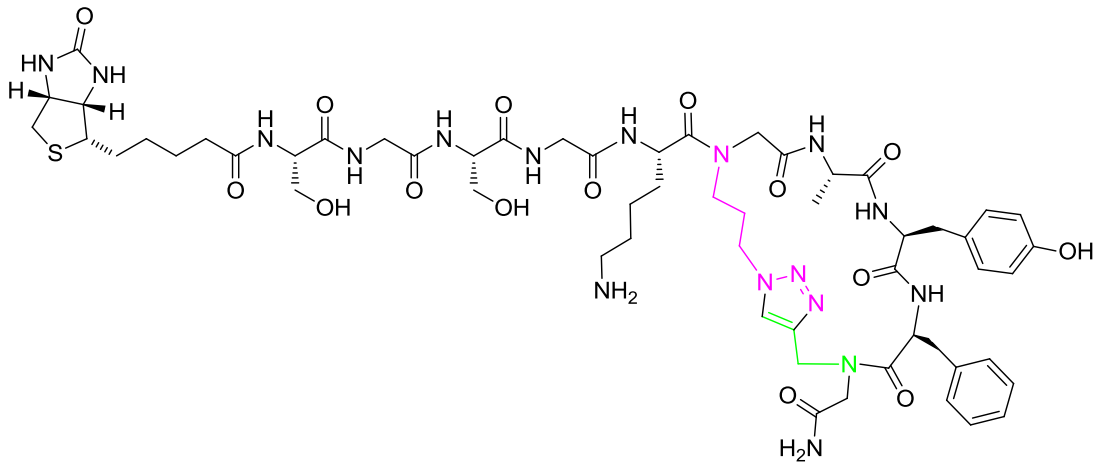

C9 was synthesised from **U9** attached on the Rink amide resin using Method A described in Section 4.11.3.2.

t_R (Analytical, method 4) 54.5 min; **t_R** (preparative, method 4) 65.1 min; **purity** 74.3%, ***m/z*** (MALDI-ToF, αCHCA) 1276.2 $[M+H]^+$, 1298.2 $[M+Na]^+$, 1314.1 $[M+K]^+$.

C10: (C)-Biotin-SGSG-KAA*YFZ*$_4$-NH_2

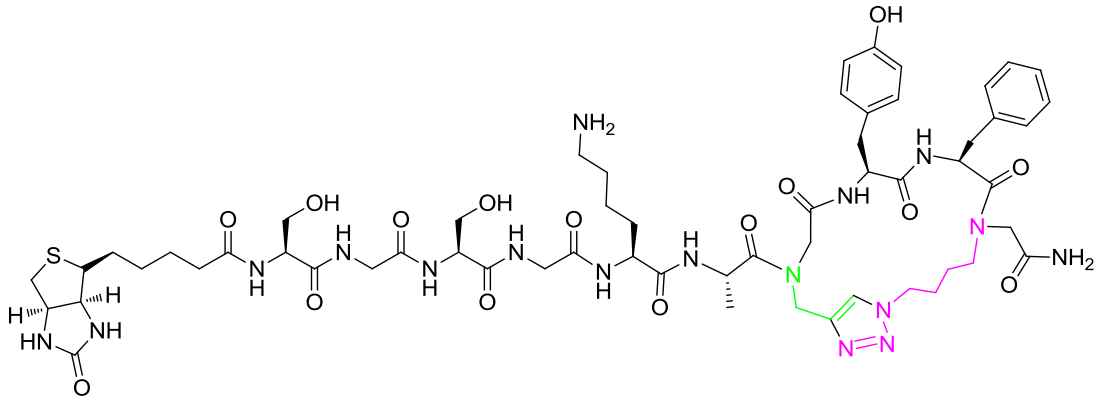

C10 was synthesised from **U10** attached on the Rink amide resin using Method A described in Section 4.11.3.2.

t_R (Analytical, method 4) 56.4 min; **t_R** (preparative, method 4) 68.3 min; **purity** 87.5%, ***m/z*** (MALDI-ToF, αCHCA) 1290.2 $[M+H]^+$, 1312.2 $[M+Na]^+$, 1328.2 $[M+K]^+$.

C12: (C)-Biotin-SGSG-KAZ*$_4$YFA*-NH_2

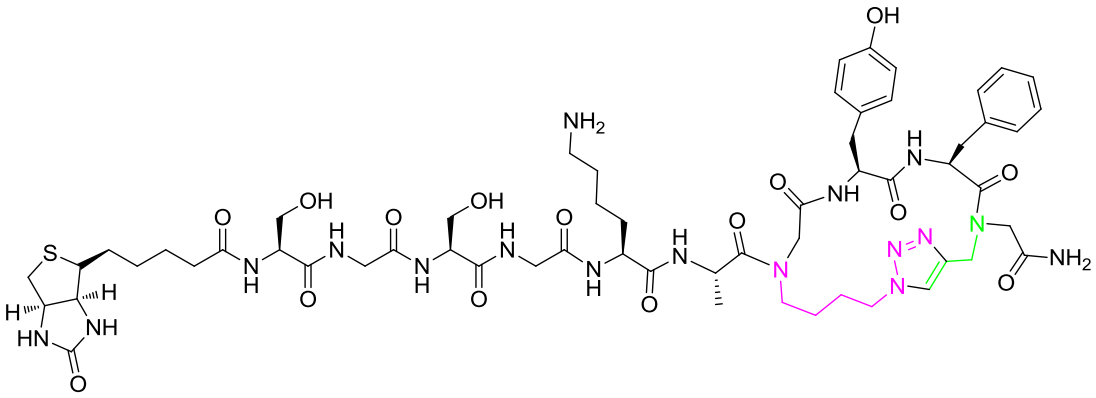

C12 was synthesised from **U12** attached on the Rink amide resin using Method A described in Section 4.11.3.2. t_R (Analytical, method 4) 57.3 min; t_R (preparative, method 4) 69.1 min; **purity** 83.7%, ***m/z*** (MALDI-ToF, αCHCA) 1290.2 $[M+H]^+$, 1312.2 $[M+Na]^+$, 1328.1 $[M+K]^+$.

C13: (C)-Biotin-SGSG-KA*AYFZ*$_3$-NH_2

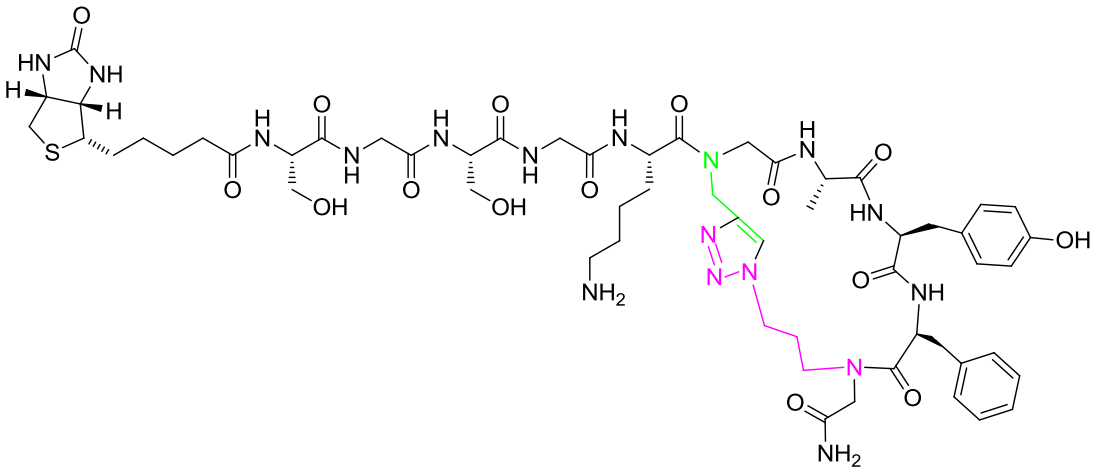

C13 was synthesised from **U13** attached on the Rink amide resin using Method A described in Section 4.11.3.2. Alternatively, **C13** was also synthesised in solution from purified **U13** using method B as described in Section 4.11.3.3.

t_R (Analytical, method 4) 53.4 min; t_R (preparative, method 4) 65.0 min; **purity (Method A)** 85.4%, **purity (Method B)** 99.9%, ***m/z*** (MALDI-ToF, αCHCA) 1276.0 $[M+H]^+$, 1298.0 $[M+Na]^+$, 1314.0 $[M+K]^+$.

C14: (C)-Ac-KAA*YFZ$^{*}{}_{5}$-NH_2

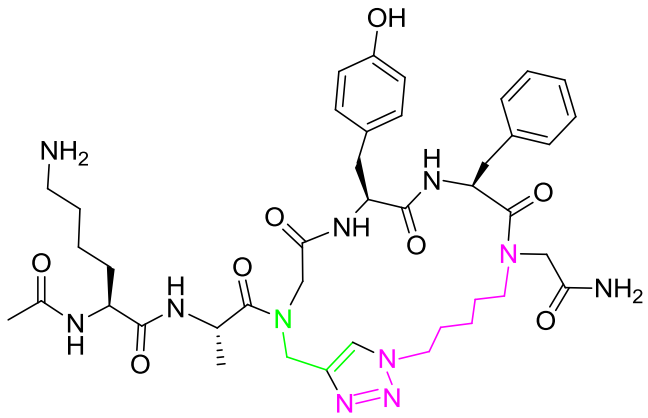

C14 was synthesised from **U14** attached on the Rink amide resin using Method A described in Section 4.11.3.2. Alternatively, **C14** was also synthesised in solution from purified **U14** using method B as described in Section 4.11.3.3.

t_R (Analytical, method 4) 55.6 min; **t_R** (preparative, method 4) 69.8 min; **purity (Method A)** 90.5%, **purity (Method B)** 100.0%, ***m/z*** (MALDI-ToF, αCHCA) 832.5 $[M+H]^+$, 854.4 $[M+Na]^+$, 870.4 $[M+K]^+$.

C15: (C)-Ac-KAZ$^{*}{}_{5}$YFA*-NH_2

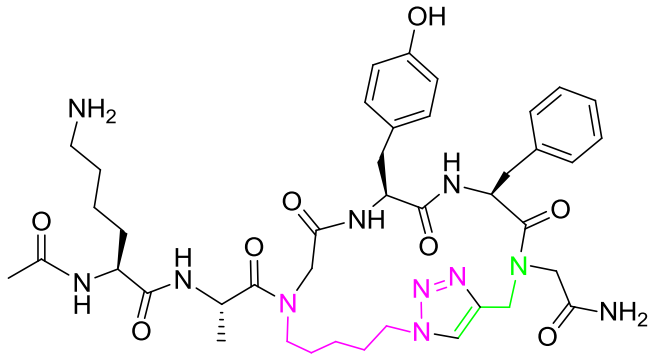

C15 was synthesised from **U15** attached on the Rink amide resin using Method A described in Section 4.11.3.2.

t_R (Analytical, method 4) 57.1 min; **t_R** (preparative, method 4) 71.5 min; **purity** 85.0%, ***m/z*** (MALDI-ToF, αCHCA) 832.3 $[M+H]^+$, 854.3 $[M+Na]^+$, 870.2 $[M+K]^+$, 1663.3 $[2M+H]^+$, 1685.3 $[2M+Na]^+$, 1701.3 $[2M+K]^+$.

C16: (C)-Ac-KA*AYFZ*$_5$-NH_2

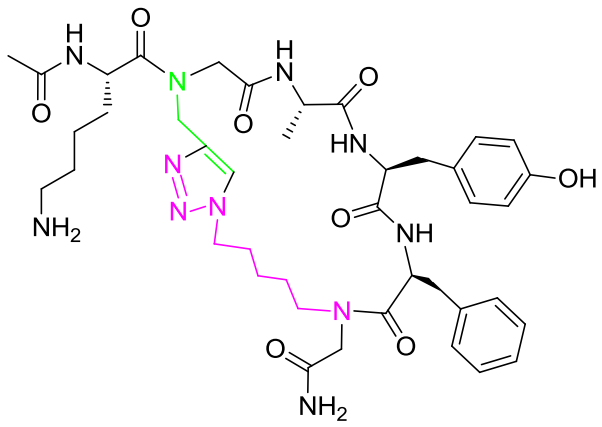

C16 was synthesised from **U16** attached on the Rink amide resin using Method A described in Section 4.11.3.2.

t_R (Analytical, method 4) 50.0 min; **t_R** (preparative, method 4) 63.7 min; **purity** 96.6%, ***m/z*** (MALDI-ToF, αCHCA) 832.3 $[M+H]^+$, 854.1 $[M+Na]^+$, 870.1 $[M+K]^+$, 1663.3 $[2M+H]^+$, 1685.3 $[2M+Na]^+$, 1701.3 $[2M+K]^+$.

C17: (C)-Ac-KZ*$_5$AYFA*-NH_2

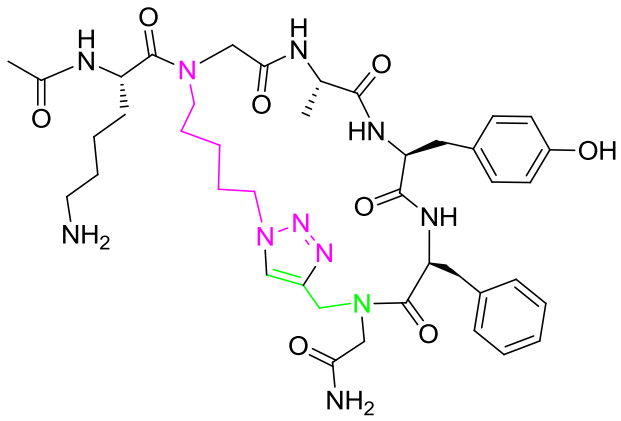

C17 was synthesised from **U17** attached on the Rink amide resin using Method A described in Section 4.11.3.2.

t_R (Analytical, method 4) 50.4 min; **t_R** (preparative, method 4) 63.8 min; **purity** 93.1%, ***m/z*** (MALDI-ToF, αCHCA) 832.3 $[M+H]^+$, 854.2 $[M+Na]^+$, 870.2 $[M+K]^+$.

C18: (C)-Ac-KAA*YFZ$^{*}{}_{3}$-NH$_2$

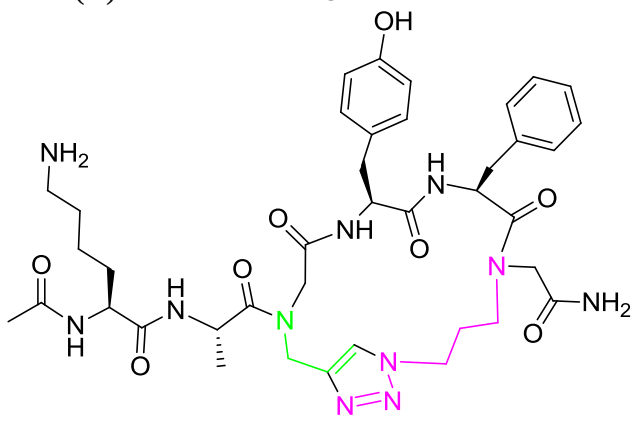

C18 was synthesised from **U18** attached on the Rink amide resin using Method A described in Section 4.11.3.2. Alternatively, **C18** was also synthesised in solution from purified **U18** using method B as described in Section 4.11.3.3.

t$_R$ (Analytical, method 4) 55.9 min; **t$_R$** (preparative, method 4) 65.4 min; **purity (Method A)** 66.6%, **purity (Method B)** 98.8%, ***m/z*** (MALDI-ToF, αCHCA) 804.2 $[M+H]^+$, 826.4 $[M+Na]^+$, 842.4 $[M+K]^+$, 1607.7 $[2M+H]^+$, 1629.3 $[2M+Na]^+$, 1645.2 $[2M+K]^+$

C19: (C)-Ac-KAZ$^{*}{}_{3}$YFA*-NH$_2$

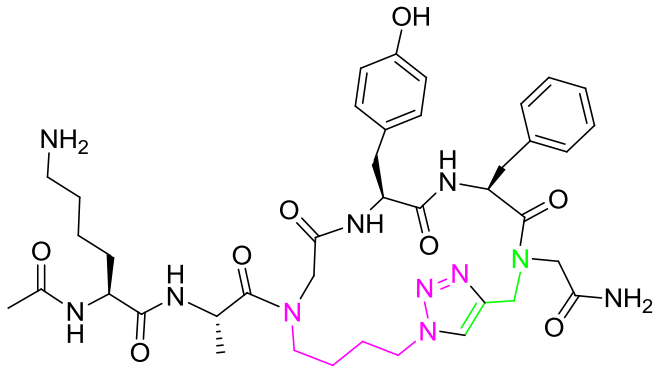

C19 was synthesised from **U19** attached on the Rink amide resin using Method A described in Section 4.11.3.2.

t$_R$ (Analytical, method 4) 53.5 min; **t$_R$** (preparative, method 4) 67.2 min; **purity** 96.9%, ***m/z*** (MALDI-ToF, αCHCA) 804.7 $[M+H]^+$, 826.7 $[M+Na]^+$, 842.7 $[M+K]^+$, 1606.3 $[2M+H]^+$, 1628.23$[2M+Na]^+$, 1644.3 $[2M+K]^+$.

C20: (C)-Ac-KA*AYFZ*$_4$-NH$_2$

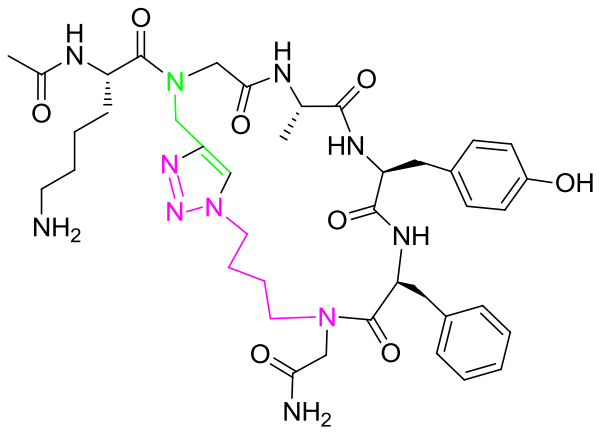

C20 was synthesised from **U20** attached on the Rink amide resin using Method A described in Section 4.11.3.2.

t$_R$ (Analytical, method 4) 50.9 min; **t$_R$** (preparative, method 4) 64.6 min; **purity** 93.2%, ***m/z*** (MALDI-ToF, αCHCA) 818.7 $[M+H]^+$, 840.8 $[M+Na]^+$, 856.7 $[M+K]^+$.

C21: (C)-Ac-KZ*$_4$AYFA*-NH$_2$

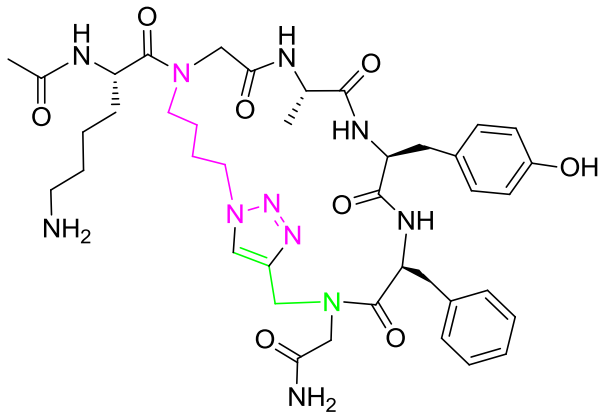

C21 was synthesised from **U21** attached on the Rink amide resin using Method A described in Section 4.11.3.2.

t$_R$ (Analytical, method 4) 53.6 min; **t$_R$** (preparative, method 4) 66.9 min; **purity** 92.0%, ***m/z*** (MALDI-ToF, αCHCA) 818.6 $[M+H]^+$, 840.6 $[M+Na]^+$, 856.6 $[M+K]^+$.

C22: (C)-Ac-KZ*$_3$AYFA*-NH_2

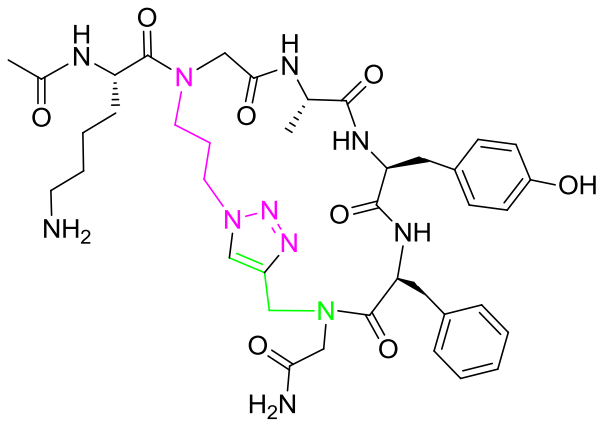

C22 was synthesised from **U22** attached on the Rink amide resin using Method A described in Section 4.11.3.2.

t_R (Analytical, method 4) 50.6 min; **t_R** (preparative, method 4) 63.3 min; **purity** 98.7%, ***m/z*** (MALDI-ToF, αCHCA) 804.7 $[M+H]^+$, 826.7 $[M+Na]^+$, 842.7 $[M+K]^+$, 1606.2 $[2M+H]^+$ $]^+$, 1628.2 $[2M+Na]^+$, 1644.2 $[2M+K]^+$.

C23: (C)-Ac-KAA*YFZ$^{*}{}_{4}$-NH$_2$

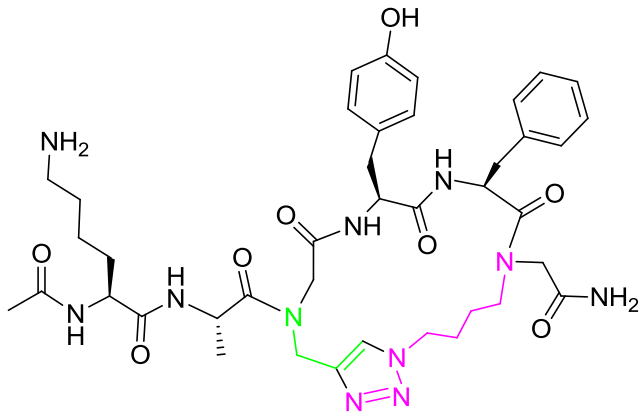

C23 was synthesised from **U23** attached on the Rink amide resin using Method A described in Section 4.11.3.2. Alternatively, **C23** was also synthesised in solution from purified **U23** using method B as described in Section 4.11.3.3.

t$_R$ (Analytical, method 4) 52.7 min; **t$_R$** (preparative, method 4) 66.0 min; **purity (Method A)** 57.6%, **purity (Method B)** 91.9%, ***m/z*** (MALDI-ToF, αCHCA) 818.7 $[M+H]^+$, 840.8 $[M+Na]^+$, 856.7 $[M+K]^+$, 1634.3 $[2M+H]^+$, 1656.3 $[2M+Na]^+$, 1672.3 $[2M+K]^+$.

C25: (C)-Ac-KAZ$^{*}{}_{4}$YFA*-NH$_2$

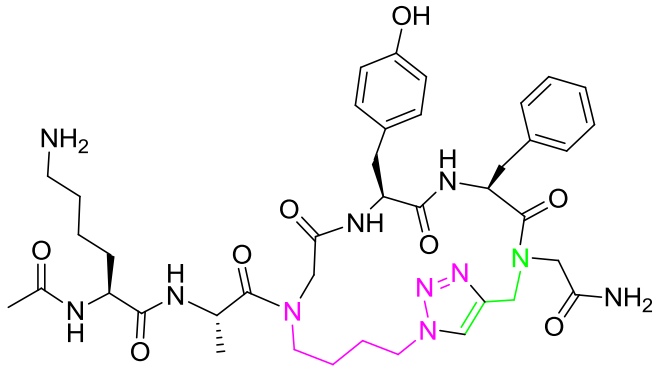

C25 was synthesised from **U25** attached on the Rink amide resin using Method A described in Section 4.11.3.2.

t$_R$ (Analytical, method 4) 47.5 min; **t$_R$** (preparative, method 4) 61.3 min; **purity** 99.5%, ***m/z*** (MALDI-ToF, αCHCA) 818.7 $[M+H]^+$, 840.7 $[M+Na]^+$, 856.7 $[M+K]^+$, 1634.2 $[2M+H]^+$, 1656.2 $[2M+Na]^+$, 1672.2 $[2M+K]^+$.

C26: (C)-Ac-KA*AYFZ*$_3$-NH_2

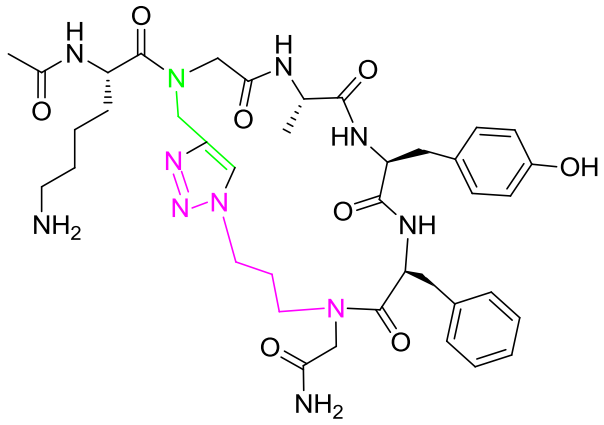

C26 was synthesised from **U26** attached on the Rink amide resin using Method A described in Section 4.11.3.2.

t_R (Analytical, method 4) 53.2 min; **t_R** (preparative, method 4) 67.4 min; **purity** 95.0%, ***m/z*** (MALDI-ToF, αCHCA) 804.5 $[M+H]^+$, 826.7 $[M+Na]^+$, 842.7 $[M+K]^+$, 1607.4 $[2M+H]^+$.

CHAPTER 5

References

(1) Brooke, N. M.; Holland, P. W. H. *Curr. Opin. Genet. Dev.* **2003**, *13*, 599.
(2) CRUK *http://info.cancerresearchuk.org/cancerstats/keyfacts/* **2008**.
(3) Fearon, E. R.; Vogelstein, B. *Cell* **1990**, *61*, 759.
(4) Compagni, A.; Christofori, G. *Br. J. Cancer* **2000**, *83*, 1.
(5) Braun, P.; Gingras, A. C. *Proteomics* **2012**, *12*, 1478.
(6) Pommier, Y.; Cherfils, J. *Trends Pharmacol. Sci.* **2005**, *26*, 138.
(7) Neduva, V.; Russell, R. B. *Curr. Opin. Biotechnol.* **2006**, *17*, 465.
(8) Neduva, V.; Linding, R.; Su-Angrand, I.; Stark, A.; de, M. F.; Gibson, T. J.; Lewis, J.; Serrano, L.; Russell, R. B. *PLoS. Biol.* **2005**, *3*, e405.
(9) Fry, D. C. *Pept. Sci.* **2006**, *84*, 535.
(10) Eyrisch, S.; Helms, V. *J.Med.Chem.* **2007**, *50*, 3457.
(11) Neduva, V.; Russell, R. B. *FEBS Lett.* **2005**, *579*, 3342.
(12) Dyson, H. J.; Wright, P. E. *Nature Reviews Molecular Cell Biology* **2005**, *6*, 197.
(13) Bogan, A. A.; Thorn, K. S. *J. Mol. Biol.* **1998**, *280*, 1.
(14) Joshi, M.; Vargas, C.; Boisguerin, P.; Diehl, A.; Krause, G.; Schmieder, P.; Moelling, K.; Hagen, V.; Schade, M.; Oschkinat, H. *Angew.Chem.Int.Ed Engl.* **2006**, *45*, 3790.
(15) Yaffe, M. B. *Nat. Rev. Mol. Cell Biol.* **2002**, *3*, 177.
(16) Mayer, B. J. *J. Cell Sci.* **2001**, *114*, 1253.
(17) Nicholson, J.; Scherl, A.; Way, L.; Blackburn, E. A.; Walkinshaw, M. D.; Ball, K. L.; Hupp, T. R. *Cellular Signalling* **2014**, *26*, 1243.
(18) Linzer, D. I.; Levine, A. J. *Cell* **1979**, *17*, 43.
(19) Deleo, A. B.; Jay, G.; Appella, E.; Dubois, G. C.; Law, L. W.; Old, L. J. *Proceedings of the National Academy of Sciences of the United States of America* **1979**, *76*, 2420.
(20) Lane, D. P.; Crawford, L. V. *Nature* **1979**, *278*, 261.
(21) Oren, M.; Levine, A. J. *Proceedings of the National Academy of Sciences of the United States of America-Biological Sciences* **1983**, *80*, 56.
(22) Levine, A. J.; Momand, J.; Finlay, C. A. *Nature* **1991**, *351*, 453.
(23) Hollstein, M.; Sidransky, D.; Vogelstein, B.; Harris, C. C. *Science* **1991**, *253*, 49.
(24) Nigro, J. M.; Baker, S. J.; Preisinger, A. C.; Jessup, J. M.; Hostetter, R.; Cleary, K.; Bigner, S. H.; Davidson, N.; Baylin, S.; Devilee, P.; Glover, T.; Collins, F. S.; Weston, A.; Modali, R.; Harris, C. C.; Vogelstein, B. *Nature* **1989**, *342*, 705.
(25) Tsai, Y. C.; Nichols, P. W.; Hiti, A. L.; Williams, Z.; Skinner, D. G.; Jones, P. A. *Cancer Research* **1990**, *50*, 44.
(26) Atkin, N. B.; Baker, M. C. *Cancer Genet. Cytogenet.* **1989**, *37*, 229.
(27) Yano, T.; Linehan, M.; Anglard, P.; Lerman, M. I.; Daniel, L. N.; Stein, C. A.; Robertson, C. N.; Larocca, R.; Zbar, B. *J. Natl. Cancer Inst.* **1989**, *81*, 518.
(28) Hjortsberg, L.; Rubio-Nevado, J. M.; Hamroun, D.; Claustre, M.; Béroud, C.; Soussi, T. *The p53 Mutation HandBook* **2008**.
(29) Chen, X.; Ko, L. J.; Jayaraman, L.; Prives, C. *Genes Dev.* **1996**, *10*, 2438.
(30) Donehower, L. A.; Harvey, M.; Slagle, B. L.; McArthur, M. J.; Montgomery, C. A.; Butel, J. S.; Bradley, A. *Nature* **1992**, *356*, 215.
(31) Li, F. P.; Fraumeni, J. F. *Annals of Internal Medicine* **1969**, *71*, 747.

(32) Malkin, D.; Li, F. P.; Strong, L. C.; Fraumeni, J. F.; Nelson, C. E.; Kim, D. H.; Kassel, J.; Gryka, M. A.; Bischoff, F. Z.; Tainsky, M. A.; Friend, S. H. *Science* **1990**, *250*, 1233.
(33) Oliner, J. D.; Kinzler, K. W.; Meltzer, P. S.; George, D. L.; Vogelstein, B. *Nature* **1992**, *358*, 80.
(34) Momand, J.; Jung, D.; Wilczynski, S.; Niland, J. *Nucleic Acids Res.* **1998**, *26*, 3453.
(35) Giaccia, A. J.; Kastan, M. B. *Genes Dev.* **1998**, *12*, 2973.
(36) Amundson, S. A.; Myers, T. G.; Fornace, A. J. *Oncogene* **1998**, *17*, 3287.
(37) Helton, E. S.; Chen, X. B. *J. Cell. Biochem.* **2007**, *100*, 883.
(38) Maltzman, W.; Czyzyk, L. *Molecular and Cellular Biology* **1984**, *4*, 1689.
(39) Maki, C. G.; Howley, P. M. *Molecular and Cellular Biology* **1997**, *17*, 355.
(40) Candeias, M. M.; Malbert-Colas, L.; Powell, D. J.; Daskalogianni, C.; Maslon, M. M.; Naski, N.; Bourougaa, K.; Calvo, F.; Fahraeus, R. *Nat.Cell Biol.* **2008**, *10*, 1098.
(41) Jones, S. N.; Roe, A. E.; Donehower, L. A.; Bradley, A. *Nature* **1995**, *378*, 206.
(42) Montes de Oca, L. R.; Wagner, D. S.; Lozano, G. *Nature* **1995**, *378*, 203.
(43) Harris, S. L.; Levine, A. J. *Oncogene* **2005**, *24*, 2899.
(44) Walerych, D.; Kudla, G.; Gutkowska, M.; Wawrzynow, B.; Muller, L.; King, F. W.; Helwak, A.; Boros, J.; Zylicz, A.; Zylicz, M. *J. Biol. Chem.* **2004**, *279*, 48836.
(45) Veprintsev, D. B.; Freund, S. M. V.; Andreeva, A.; Rutledge, S. E.; Tidow, H.; Canadillas, J. M. P.; Blair, C. M.; Fersht, A. R. *Proceedings of the National Academy of Sciences of the United States of America* **2006**, *103*, 2115.
(46) Weinberg, R. L.; Veprintsev, D. B.; Fersht, A. R. *J. Mol. Biol.* **2004**, *341*, 1145.
(47) Levine, A. J.; Hu, W.; Feng, Z. *Cell Death Differ.* **2006**, *13*, 1027.
(48) Braithwaite, A. W.; Del Sal, G.; Lu, X. *Cell Death Differ.* **2006**, *13*, 984.
(49) Brooks, C. L.; Gu, W. *Mol. Cell* **2006**, *21*, 307.
(50) Kubbutat, M. H. G.; Ludwig, R. L.; Ashcroft, M.; Vousden, K. H. *Molecular and Cellular Biology* **1998**, *18*, 5690.
(51) Lai, Z.; Ferry, K. V.; Diamond, M. A.; Wee, K. E.; Kim, Y. B.; Ma, J.; Yang, T.; Benfield, P. A.; Copeland, R. A.; Auger, K. R. *J.Biol.Chem.* **2001**, *276*, 31357.
(52) Grossman, S. R.; Deato, M. E.; Brignone, C.; Chan, H. M.; Kung, A. L.; Tagami, H.; Nakatani, Y.; Livingston, D. M. *Science* **2003**, *300*, 342.
(53) Zhu, Q. Z.; Yao, J. H.; Wani, G.; Wani, M. A.; Wani, A. A. *J. Biol. Chem.* **2001**, *276*, 29695.
(54) Shaulsky, G.; Goldfinger, N.; Tosky, M. S.; Levine, A. J.; Rotter, V. *Oncogene* **1991**, *6*, 2055.
(55) Stommel, J. M.; Marchenko, N. D.; Jimenez, G. S.; Moll, U. M.; Hope, T. J.; Wahl, G. M. *EMBO J.* **1999**, *18*, 1660.
(56) Daujat, S.; Neel, H.; Piette, J. *Trends Genet.* **2001**, *17*, 459.
(57) Boyd, S. D.; Tsai, K. Y.; Jacks, T. *Nat.Cell Biol.* **2000**, *2*, 563.
(58) Xirodimas, D. P.; Stephen, C. W.; Lane, D. P. *Exp. Cell Res.* **2001**, *270*, 66.
(59) Esser, C.; Scheffner, M.; Hohfeld, J. *J. Biol. Chem.* **2005**, *280*, 27443.

(60) Fakharzadeh, S. S.; Trusko, S. P.; George, D. L. *EMBO J.* **1991**, *10*, 1565.
(61) Cahilly-Snyder, L.; Yang-Feng, T.; Francke, U.; George, D. L. *Somat. Cell Mol. Genet.* **1987**, *13*, 235.
(62) Barak, Y.; Gottlieb, E.; Juvengershon, T.; Oren, M. *Genes Dev.* **1994**, *8*, 1739.
(63) Saucedo, L. J.; Myers, C. D.; Perry, M. E. *J. Biol. Chem.* **1999**, *274*, 8161.
(64) Perry, M. E.; Mendrysa, S. M.; Saucedo, L. J.; Tannous, P.; Holubar, M. *J. Biol. Chem.* **2000**, *275*, 5733.
(65) Bartel, F.; Taubert, H.; Harris, L. C. *Cancer Cell* **2002**, *2*, 9.
(66) Lane, D. P.; Cheok, C. F.; Brown, C.; Madhumalar, A.; Ghadessy, F. J.; Verma, C. *Cell Cycle* **2010**, *9*, 540.
(67) Marechal, V.; Elenbaas, B.; Taneyhill, L.; Piette, J.; Mechali, M.; Nicolas, J. C.; Levine, A. J.; Moreau, J. *Oncogene* **1997**, *14*, 1427.
(68) Momand, J.; Zambetti, G. P.; Olson, D. C.; George, D.; Levine, A. J. *Cell* **1992**, *69*, 1237.
(69) Roth, J.; Dobbelstein, M.; Freedman, D. A.; Shenk, T.; Levine, A. J. *EMBO J.* **1998**, *17*, 554.
(70) Marechal, V.; Elenbaas, B.; Piette, J.; Nicolas, J. C.; Levine, A. J. *Mol. Cell Biol.* **1994**, *14*, 7414.
(71) Yu, G. W.; Rudiger, S.; Veprintsev, D.; Freund, S.; Fernandez-Fernandez, M. R.; Fersht, A. R. *Proc.Natl.Acad.Sci U.S.A* **2006**, *103*, 1227.
(72) Wallace, M.; Worrall, E.; Pettersson, S.; Hupp, T. R.; Ball, K. L. *Mol. Cell* **2006**, *23*, 251.
(73) Shimizu, H.; Burch, L. R.; Smith, A. J.; Dornan, D.; Wallace, M.; Ball, K. L.; Hupp, T. R. *J.Biol.Chem.* **2002**, *277*, 28446.
(74) Wawrzynow, B.; Pettersson, S.; Zylicz, A.; Bramham, J.; Worrall, E.; Hupp, T. R.; Ball, K. L. *J.Biol.Chem.* **2009**, *284*, 11517.
(75) Honda, R.; Yasuda, H. *Oncogene* **2000**, *19*, 1473.
(76) Meek, D. W.; Knippschild, U. *Mol. Cancer Res.* **2003**, *1*, 1017.
(77) Kostic, M.; Matt, T.; Martinez-Yamout, M. A.; Dyson, H. J.; Wright, P. E. *J.Mol.Biol.* **2006**, *363*, 433.
(78) Oliner, J. D.; Pietenpol, J. A.; Thiagalingam, S.; Gyuris, J.; Kinzler, K. W.; Vogelstein, B. *Nature* **1993**, *362*, 857.
(79) Wu, X.; Bayle, J. H.; Olson, D.; Levine, A. J. *Genes Dev.* **1993**, *7*, 1126.
(80) Wang, Q.; Yang, Y.; Wang, L.; Zhang, P. Z.; Yu, L. *Biochem.Biophys.Res.Commun.* **2008**, *374*, 437.
(81) Khosravi, R.; Maya, R.; Gottlieb, T.; Oren, M.; Shiloh, Y.; Shkedy, D. *Proceedings of the National Academy of Sciences of the United States of America* **1999**, *96*, 14973.
(82) Mayo, L. D.; Turchi, J. J.; Berberich, S. J. *Cancer Research* **1997**, *57*, 5013.
(83) Weber, H. O.; Ludwig, R. L.; Morrison, D.; Kotlyarov, A.; Gaestel, M.; Vousden, K. H. *Oncogene* **2005**, *24*, 1965.
(84) Zhang, T. T.; Prives, C. *J. Biol. Chem.* **2001**, *276*, 29702.
(85) Goldberg, Z.; Vogt Sionov, R.; Berger, M.; Zwang, Y.; Perets, R.; Van Etten, R. A.; Oren, M.; Taya, Y.; Haupt, Y. *EMBO J.* **2002**, *21*, 3715.
(86) Zhou, B. H. P.; Liao, Y.; Xia, W. Y.; Zou, Y. Y.; Spohn, B.; Hung, M. C. *Nat. Cell Biol.* **2001**, *3*, 973.

(87) Mayo, L. D.; Donner, D. B. *Proceedings of the National Academy of Sciences of the United States of America* **2001**, *98*, 11598.
(88) Miyauchi, Y.; Yogosawa, S.; Honda, R.; Nishida, T.; Yasuda, H. *J. Biol. Chem.* **2002**, *277*, 50131.
(89) Buschmann, T.; Fuchs, S. Y.; Lee, C.-G.; Pan, Z.-Q.; Ronai, Z. e. *Cell* **2000**, *101*, 753.
(90) Ganguli, G.; Wasylyk, B. *Molecular Cancer Research* **2003**, *1*, 1027.
(91) Iwakuma, T.; Lozano, G. *Mol. Cancer Res.* **2003**, *1*, 993.
(92) Tao, W.; Levine, A. J. *Proc.Natl.Acad.Sci U.S.A* **1999**, *96*, 3077.
(93) Xirodimas, D.; Saville, M. K.; Edling, C.; Lane, D. P.; Lain, S. *Oncogene* **2001**, *20*, 4972.
(94) Lohrum, M. A. E.; Ludwig, R. L.; Kubbutat, M. H. G.; Hanlon, M.; Vousden, K. H. *Cancer Cell* **2003**, *3*, 577.
(95) Chen, D. L.; Li, M. Y.; Luo, J. Y.; Gu, W. *J. Biol. Chem.* **2003**, *278*, 13595.
(96) Johnson-Pais, T.; Degnin, C.; Thayer, M. J. *Proceedings of the National Academy of Sciences of the United States of America* **2001**, *98*, 2211.
(97) Loughran, O.; La Thangue, N. B. *Molecular and Cellular Biology* **2000**, *20*, 2186.
(98) Kussie, P. H.; Gorina, S.; Marechal, V.; Elenbaas, B.; Moreau, J.; Levine, A. J.; Pavletich, N. P. *Science* **1996**, *274*, 948.
(99) Vassilev, L. T.; Vu, B. T.; Graves, B.; Carvajal, D.; Podlaski, F.; Filipovic, Z.; Kong, N.; Kammlott, U.; Lukacs, C.; Klein, C.; Fotouhi, N.; Liu, E. A. *Science* **2004**, *303*, 844.
(100) Hershko, A.; Leshinsky, E.; Ganoth, D.; Heller, H. *Proceedings of the National Academy of Sciences of the United States of America-Biological Sciences* **1984**, *81*, 1619.
(101) Jentsch, S.; Seufert, W.; Hauser, H. P. *Biochim. Biophys. Acta* **1991**, *1089*, 127.
(102) Handleygearhart, P. M.; Stephen, A. G.; Trauschazar, J. S.; Ciechanover, A.; Schwartz, A. L. *J. Biol. Chem.* **1994**, *269*, 33171.
(103) Zheng, N.; Wang, P.; Jeffrey, P. D.; Pavletich, N. P. *Cell* **2000**, *102*, 533.
(104) Huang, L.; Kinnucan, E.; Wang, G. L.; Beaudenon, S.; Howley, P. M.; Huibregtse, J. M.; Pavletich, N. P. *Science* **1999**, *286*, 1321.
(105) Weissman, A. M. *Nat. Rev. Mol. Cell Biol.* **2001**, *2*, 169.
(106) Borden, K. L. B.; Freemont, P. S. *Curr. Opin. Struct. Biol.* **1996**, *6*, 395.
(107) Hashizume, R.; Fukuda, M.; Maeda, I.; Nishikawa, H.; Oyake, D.; Yabuki, Y.; Ogata, F.; Ohta, T. *J. Biol. Chem.* **2001**, *276*, 14537.
(108) Koegl, M.; Hoppe, T.; Schlenker, S.; Ulrich, H. D.; Mayer, T. U.; Jentsch, S. *Cell* **1999**, *96*, 635.
(109) Hicke, L. *Nature Reviews Molecular Cell Biology* **2001**, *2*, 195.
(110) Finley, D.; Sadis, S.; Monia, B. P.; Boucher, P.; Ecker, D. J.; Crooke, S. T.; Chau, V. *Molecular and Cellular Biology* **1994**, *14*, 5501.
(111) Deng, L.; Wang, C.; Spencer, E.; Yang, L. Y.; Braun, A.; You, J. X.; Slaughter, C.; Pickart, C.; Chen, Z. J. *Cell* **2000**, *103*, 351.
(112) Hoege, C.; Pfander, B.; Moldovan, G. L.; Pyrowolakis, G.; Jentsch, S. *Nature* **2002**, *419*, 135.
(113) Komander, D. *Biochem. Soc. Trans.* **2009**, *37*, 937.

(114) Li, M. Y.; Chen, D. L.; Shiloh, A.; Luo, J. Y.; Nikolaev, A. Y.; Qin, J.; Gu, W. *Nature* **2002**, *416*, 648.
(115) Li, M. Y.; Brooks, C. L.; Kon, N.; Gu, W. *Molecular Cell* **2004**, *13*, 879.
(116) Yeh, E. T. H.; Gong, L. M.; Kamitani, T. *Gene* **2000**, *248*, 1.
(117) Rodriguez, M. S.; Desterro, J. M. P.; Lain, S.; Midgley, C. A.; Lane, D. P.; Hay, R. T. *EMBO J.* **1999**, *18*, 6455.
(118) Xirodimas, D. P.; Saville, M. K.; Bourdon, J. C.; Hay, R. T.; Lane, D. P. *Cell* **2004**, *118*, 83.
(119) Watson, I. R.; Li, B. K.; Roche, O.; Blanch, A.; Ohh, M.; Irwin, M. S. *Oncogene* **2010**, *29*, 297.
(120) Elenbaas, B.; Dobbelstein, M.; Roth, J.; Shenk, T.; Levine, A. J. *Mol. Med.* **1996**, *2*, 439.
(121) Saville, M. K.; Sparks, A.; Xirodimas, D. P.; Wardrop, J.; Stevenson, L. F.; Bourdon, J. C.; Woods, Y. L.; Lane, D. P. *J.Biol.Chem.* **2004**, *279*, 42169.
(122) Fang, S.; Jensen, J. P.; Ludwig, R. L.; Vousden, K. H.; Weissman, A. M. *J.Biol.Chem.* **2000**, *275*, 8945.
(123) Uldrijan, S.; Pannekoek, W. J.; Vousden, K. H. *EMBO J.* **2007**, *26*, 102.
(124) Tanimura, S.; Ohtsuka, S.; Mitsui, K.; Shirouzu, K.; Yoshimura, A.; Ohtsubo, M. *FEBS Lett.* **1999**, *447*, 5.
(125) Linke, K.; Mace, P. D.; Smith, C. A.; Vaux, D. L.; Silke, J.; Day, C. L. *Cell Death.Differ.* **2008**.
(126) Badciong, J. C.; Haas, A. L. *J.Biol.Chem.* **2002**, *277*, 49668.
(127) Linares, L. K.; Hengstermann, A.; Ciechanover, A.; Muller, S.; Scheffner, M. *Proc.Natl.Acad.Sci U.S.A* **2003**, *100*, 12009.
(128) Marine, J. C.; Jochemsen, A. G. *Biochem.Biophys.Res.Commun.* **2005**, *331*, 750.
(129) Finch, R. A.; Donoviel, D. B.; Potter, D.; Shi, M.; Fan, A.; Freed, D. D.; Wang, C. Y.; Zambrowicz, B. P.; Ramirez-Solis, R.; Sands, A. T.; Zhang, N. *Cancer Res.* **2002**, *62*, 3221.
(130) Marine, J.-C. W.; Dyer, M. A.; Jochemsen, A. G. *J. Cell Sci.* **2007**, *120*, 371.
(131) Pan, Y.; Chen, J. *Mol. Cell Biol.* **2003**, *23*, 5113.
(132) Bykov, V. J. N.; Selivanova, G.; Wiman, K. G. *European Journal of Cancer* **2003**, *39*, 1828.
(133) Wang, Z.; Sun, Y. *Transl. Oncol.* **2010**, *3*, 1.
(134) Hu, B.; Gilkes, D. M.; Chen, J. *Cancer Res.* **2007**, *67*, 8810.
(135) Fischer, P. M. *Int.J.Pept.Res.Ther.* **2006**, *12*, 3.
(136) McCoy, M. A.; Gesell, J. J.; Senior, M. M.; Wyss, D. F. *Proceedings of the National Academy of Sciences of the United States of America* **2003**, *100*, 1645.
(137) Fry, D. C.; Emerson, S. D.; Palme, S.; Vu, B. T.; Liu, C. M.; Podlaski, F. *J. Biomol. NMR* **2004**, *30*, 163.
(138) Uhrinova, S.; Uhrin, D.; Powers, H.; Watt, K.; Zheleva, D.; Fischer, P.; McInnes, C.; Barlow, P. N. *J. Mol. Biol.* **2005**, *350*, 587.
(139) Vu, B.; Wovkulich, P.; Pizzolato, G.; Lovey, A.; Ding, Q.; Jiang, N.; Liu, J. J.; Zhao, C.; Glenn, K.; Wen, Y.; Tovar, C.; Packman, K.; Vassilev, L.; Graves, B. *ACS Med. Chem. Lett.* **2013**.
(140) Shangary, S.; Qin, D. G.; McEachern, D.; Liu, M. L.; Miller, R. S.; Qiu, S.; Nikolovska-Coleska, Z.; Ding, K.; Wang, G. P.; Chen, J. Y.; Bernard, D.;

Zhang, J.; Lu, Y. P.; Gu, Q. Y.; Shah, R. B.; Pienta, K. J.; Ling, X. L.; Kang, S. M.; Guo, M.; Sun, Y.; Yang, D. J.; Wang, S. M. *Proceedings of the National Academy of Sciences of the United States of America* **2008**, *105*, 3933.

(141) Hardcastle, I. R.; Ahmed, S. U.; Atkins, H.; Calvert, A. H.; Curtin, N. J.; Farnie, G.; Golding, B. T.; Griffin, R. J.; Guyenne, S.; Hutton, C.; Kallbad, P.; Kemp, S. J.; Kitching, M. S.; Newell, D. R.; Norbedo, S.; Northen, J. S.; Reid, R. J.; Saravanan, K.; Willems, H. M. G.; Lunec, J. *Bioorg. Med. Chem. Lett.* **2005**, *15*, 1515.

(142) Grasberger, B. L.; Lu, T. B.; Schubert, C.; Parks, D. J.; Carver, T. E.; Koblish, H. K.; Cummings, M. D.; LaFrance, L. V.; Milkiewicz, K. L.; Calvo, R. R.; Maguire, D.; Lattanze, J.; Franks, C. F.; Zhao, S. Y.; Ramachandren, K.; Bylebyl, G. R.; Zhang, M.; Manthey, C. L.; Petrella, E. C.; Pantoliano, M. W.; Deckman, I. C.; Spurlino, J. C.; Maroney, A. C.; Tomczuk, B. E.; Molloy, C. J.; Bone, R. F. *J. Med. Chem.* **2005**, *48*, 909.

(143) Yin, H.; Lee, G. I.; Park, H. S.; Payne, G. A.; Rodriguez, J. M.; Sebti, S. M.; Hamilton, A. D. *Angewandte Chemie-International Edition* **2005**, *44*, 2704.

(144) Watson, A. F.; Liu, J. F.; Bennaceur, K.; Drummond, C. J.; Endicott, J. A.; Golding, B. T.; Griffin, R. J.; Haggerty, K.; Lu, X. H.; McDonnell, J. M.; Newell, D. R.; Noble, M. E. M.; Revill, C. H.; Riedinger, C.; Xu, Q.; Zhao, Y.; Lunec, J.; Hardcastle, I. R. *Bioorg. Med. Chem. Lett.* **2011**, *21*, 5916.

(145) Stoll, R.; Renner, C.; Hansen, S.; Palme, S.; Klein, C.; Belling, A.; Zeslawski, W.; Kamionka, M.; Rehm, T.; Muhlhahn, P.; Schumacher, R.; Hesse, F.; Kaluza, B.; Voelter, W.; Engh, R. A.; Holak, T. A. *Biochemistry* **2001**, *40*, 336.

(146) Ding, K.; Lu, Y.; Nikolovska-Coleska, Z.; Wang, G.; Qiu, S.; Shangary, S.; Gao, W.; Qin, D.; Stuckey, J.; Krajewski, K.; Roller, P. P.; Wang, S. *J.Med.Chem.* **2006**, *49*, 3432.

(147) Zhao, Y.; Liu, L.; Sun, W.; Lu, J.; McEachern, D.; Li, X.; Yu, S.; Bernard, D.; Ochsenbein, P.; Ferey, V.; Carry, J.-C.; Deschamps, J. R.; Sun, D.; Wang, S. *J. Am. Chem. Soc.* **2013**, *135*, 7223.

(148) Ding, Q.; Zhang, Z.; Liu, J.-J.; Jiang, N.; Zhang, J.; Ross, T. M.; Chu, X.-J.; Bartkovitz, D.; Podlaski, F.; Janson, C.; Tovar, C.; Filipovic, Z. M.; Higgins, B.; Glenn, K.; Packman, K.; Vassilev, L. T.; Graves, B. *J. Med. Chem.* **2013**, *56*, 5979.

(149) Ohgami, T.; Kato, K.; Kobayashi, H.; Sonoda, K.; Inoue, T.; Yamaguchi, S.; Yoneda, T.; Wake, N. *Cancer Sci.* **2010**, *101*, 1387.

(150) Zheng, T. S.; Wang, J. B.; Song, X. A.; Meng, X. Z.; Pan, S. H.; Jiang, H. C.; Liu, L. X. *J. Cancer Res. Clin. Oncol.* **2010**, *136*, 1597.

(151) Jin, L. H.; Tabe, Y.; Kojima, K.; Zhou, Y. X.; Pittaluga, S.; Konopleva, M.; Miida, T.; Raffeld, M. *Cancer Lett.* **2010**, *299*, 161.

(152) Pazgier, M.; Liu, M.; Zou, G.; Yuan, W.; Li, C.; Li, C.; Li, J.; Monbo, J.; Zella, D.; Tarasov, S. G.; Lu, W. *Proc.Natl.Acad.Sci.U.S.A* **2009**, *106*, 4665.

(153) Popowicz, G. M.; Czarna, A.; Holak, T. A. *Cell Cycle* **2008**, *7*, 2441.

(154) Kallen, J.; Goepfert, A.; Blechschmidt, A.; Izaac, A.; Geiser, M.; Tavares, G.; Ramage, P.; Furet, P.; Masuya, K.; Lisztwan, J. *J.Biol.Chem.* **2009**, *284*, 8812.

(155) Reed, D.; Shen, Y.; Shelat, A. A.; Arnold, L. A.; Ferreira, A. M.; Zhu, F.; Mills, N.; Smithson, D. C.; Regni, C. A.; Bashford, D.; Cicero, S. A.; Schulman, B. A.; Jochemsen, A. G.; Guy, R. K.; Dyer, M. A. *J.Biol.Chem.* **2010**, *285*, 10786.
(156) Sasiela, C. A.; Stewart, D. H.; Kitagaki, J.; Safiran, Y. J.; Yang, Y. L.; Weissman, A. M.; Oberoi, P.; Davydov, I. V.; Goncharova, E.; Beutler, J. A.; McMahon, J. B.; O'Keefe, B. R. *J. Biomol. Screening* **2008**, *13*, 229.
(157) Murray, M. F.; Jurewicz, A. J.; Martin, J. D.; Ho, T. F.; Zhang, H.; Johanson, K. O.; Kirkpatrick, R. B.; Ma, J. H.; Lor, L. A.; Thrall, S. H.; Schwartz, B. *J. Biomol. Screening* **2007**, *12*, 1050.
(158) Lai, Z. H.; Yang, T.; Kim, Y. B.; Sielecki, T. M.; Diamond, M. A.; Strack, P.; Rolfe, M.; Caligiuri, M.; Benfield, P. A.; Auger, K. R.; Copeland, R. A. *Proceedings of the National Academy of Sciences of the United States of America* **2002**, *99*, 14734.
(159) Yang, Y.; Ludwig, R. L.; Jensen, J. P.; Pierre, S. A.; Medaglia, M. V.; Davydov, I. V.; Safiran, Y. J.; Oberoi, P.; Kenten, J. H.; Phillips, A. C.; Weissman, A. M.; Vousden, K. H. *Cancer Cell* **2005**, *7*, 547.
(160) Narayan, V. *Molecular, Genetic and Population Health Sciences thesis and dissertation collection* **2011**.
(161) Katz, B. A. *Biochemistry* **1995**, *34*, 15421.
(162) Smith, G. P.; Petrenko, V. A. *Chem. Rev.* **1997**, *97*, 391.
(163) Petitjean, N. **2008**.
(164) Dornan, D.; Shimizu, H.; Burch, L.; Smith, A. J.; Hupp, T. R. *Mol. Cell Biol.* **2003**, *23*, 8846.
(165) Tao, P.; Wang, R.; Lai, L. *Molecular modeling annual* **1999**, *5*, 189.
(166) Murray, E.; McKenna, E. O.; Burch, L. R.; Dillon, J.; Langridge-Smith, P.; Kolch, W.; Pitt, A.; Hupp, T. R. *Biochemistry* **2007**, *46*, 13742.
(167) Flexner, C. *Nat. Rev. Drug Discov.* **2007**, *6*, 959.
(168) Reichert, J. *Peptide Therapeutics Foundation* **2010**, 1.
(169) Craik, D. J.; Fairlie, D. P.; Liras, S.; Price, D. *Chemical Biology & Drug Design* **2013**, *81*, 136.
(170) Marr, A. K.; Gooderham, W. J.; Hancock, R. E. W. *Curr. Opin. Pharmacol.* **2006**, *6*, 468.
(171) Fox, J. L. *Nat Biotech* **2013**, *31*, 379.
(172) Salamat-Miller, N.; Johnston, T. P. *Int. J. Pharm.* **2005**, *294*, 201.
(173) Goodwin, D.; Simerska, P.; Toth, I. *Current Medicinal Chemistry* **2012**, *19*, 4451.
(174) Killian, B. J.; Kravitz, J. Y.; Somani, S.; Dasgupta, P.; Pang, Y. P.; Gilson, M. K. *J. Mol. Biol.* **2009**, *389*, 315.
(175) Ho, B. K.; Dill, K. A. *Plos Comput. Biol.* **2006**, *2*, 228.
(176) Koslover, E. F.; Wales, D. J. *J. Chem. Phys.* **2007**, *127*.
(177) Campbell, F.; Plante, J. P.; Edwards, T. A.; Warriner, S. L.; Wilson, A. J. *Org. Biomol. Chem.* **2010**, *8*, 2344.
(178) Zhan, C. Y.; Zhao, L.; Wei, X. L.; Wu, X. J.; Chen, X. S.; Yuan, W. R.; Lu, W. Y.; Pazgier, M. *J. Med. Chem.* **2012**, *55*, 6237.
(179) Cheng, R. P.; Gellman, S. H.; DeGrado, W. F. *Chem. Rev.* **2001**, *101*, 3219.
(180) Tamilarasu, N.; Huq, I.; Rana, T. M. *Bioorg. Med. Chem. Lett.* **2001**, *11*, 505.

(181) Peretto, I.; Sanchez-Martin, R. M.; Wang, X. H.; Ellard, J.; Mittoo, S.; Bradley, M. *Chem. Commun.* **2003**, 2312.
(182) Boeglin, D.; Cantel, S.; Martinez, J.; Fehrentz, J. A. *Tetrahedron Lett.* **2003**, *44*, 459.
(183) Paik, S.; White, E. H. *Tetrahedron* **1996**, *52*, 5303.
(184) Yang, K. W.; Golich, F. C.; Sigdel, T. K.; Crowder, M. W. *Bioorg. Med. Chem. Lett.* **2005**, *15*, 5150.
(185) Yang, K. W.; Brandt, J. J.; Chatwood, L. L.; Crowder, M. W. *Bioorg. Med. Chem. Lett.* **2000**, *10*, 1085.
(186) Freeman, N. S.; Hurevich, M.; Gilon, C. *Tetrahedron* **2009**, *65*, 1737.
(187) Brik, A.; Alexandratos, J.; Lin, Y. C.; Elder, J. H.; Olson, A. J.; Wlodawer, A.; Goodsell, D. S.; Wong, C. H. *Chembiochem* **2005**, *6*, 1167.
(188) Bock, V. D.; Speijer, D.; Hiemstra, H.; van Maarseveen, J. H. *Org. Biomol. Chem.* **2007**, *5*, 971.
(189) Roy, O.; Faure, S.; Thery, V.; Didierjean, C.; Taillefumier, C. *Org. Lett.* **2008**, *10*, 921.
(190) Vaz, B.; Brunsveld, L. *Org. Biomol. Chem.* **2008**, *6*, 2988.
(191) Shin, S. B.; Yoo, B.; Todaro, L. J.; Kirshenbaum, K. *J.Am.Chem.Soc.* **2007**, *129*, 3218.
(192) Ovadia, O.; Linde, Y.; Haskell-Luevano, C.; Dirain, M. L.; Sheynis, T.; Jelinek, R.; Gilon, C.; Hoffman, A. *Biorg. Med. Chem.* **2010**, *18*, 580.
(193) Dekker, F. J.; de Mol, N. J.; Liskamp, R. M. J. *J. Pept. Sci.* **2010**, *16*, 322.
(194) Caporale, A.; Schievano, E.; Peggion, E. *J. Pept. Sci.* **2010**, *16*, 480.
(195) Olsen, C. A.; Ziegler, H. L.; Nielsen, H. M.; Frimodt-Moller, N.; Jaroszewski, J. W.; Franzyk, H. *Chembiochem* **2010**, *11*, 1356.
(196) Aguilar, M. I.; Purcell, A. W.; Devi, R.; Lew, R.; Rossjohn, J.; Smith, A. I.; Perlmutter, P. *Org. Biomol. Chem.* **2007**, *5*, 2884.
(197) Hjelmgaard, T.; Faure, S.; Caumes, C.; De Santis, E.; Edwards, A. A.; Taillefumier, C. *Org. Lett.* **2009**, *11*, 4100.
(198) Phelan, J. C.; Skelton, N. J.; Braisted, A. C.; McDowell, R. S. *J. Am. Chem. Soc.* **1997**, *119*, 455.
(199) Scholtz, J. M.; Qian, H.; Robbins, V. H.; Baldwin, R. L. *Biochemistry* **1993**, *32*, 9668.
(200) Jackson, D. Y.; King, D. S.; Chmielewski, J.; Singh, S.; Schultz, P. G. *J. Am. Chem. Soc.* **1991**, *113*, 9391.
(201) Albert, J. S.; Hamilton, A. D. *Biochemistry* **1995**, *34*, 984.
(202) Ruan, F. Q.; Chen, Y. Q.; Hopkins, P. B. *J. Am. Chem. Soc.* **1990**, *112*, 9403.
(203) Ghadiri, M. R.; Fernholz, A. K. *J. Am. Chem. Soc.* **1990**, *112*, 9633.
(204) Blackwell, H. E.; Grubbs, R. H. *Angewandte Chemie-International Edition* **1998**, *37*, 3281.
(205) Schafmeister, C. E.; Po, J.; Verdine, G. L. *J. Am. Chem. Soc.* **2000**, *122*, 5891.
(206) Baek, S.; Kutchukian, P. S.; Verdine, G. L.; Huber, R.; Holak, T. A.; Lee, K. W.; Popowicz, G. M. *J. Am. Chem. Soc.* **2012**, *134*, 103.
(207) Kim, Y. W.; Kutchukian, P. S.; Verdine, G. L. *Org. Lett.* **2010**, *12*, 3046.
(208) Walensky, L. D.; Kung, A. L.; Escher, I.; Malia, T. J.; Barbuto, S.; Wright, R. D.; Wagner, G.; Verdine, G. L.; Korsmeyer, S. J. *Science* **2004**, *305*, 1466.

(209) Hamy, F.; Felder, E. R.; Heizmann, G.; Lazdins, J.; AboulEla, F.; Varani, G.; Karn, J.; Klimkait, T. *Proceedings of the National Academy of Sciences of the United States of America* **1997**, *94*, 3548.
(210) Comegna, D.; Benincasa, M.; Gennaro, R.; Izzo, I.; De Riccardis, F. *Biorg. Med. Chem.* **2010**, *18*, 2010.
(211) Nnanabu, E.; Burgess, K. *Org. Lett.* **2006**, *8*, 1259.
(212) Olsen, C. A.; Montero, A.; Leman, L. J.; Ghadiri, M. R. *ACS Med. Chem. Lett.* **2012**, *3*, 749.
(213) Dijkgraaf, I.; Kruijtzer, J. A. W.; Frielink, C.; Soede, A. C.; Hilbers, H. W.; Oyen, W. J. G.; Corstens, F. H. M.; Liskamp, R. M. J.; Boerman, O. C. *Nucl. Med. Biol.* **2006**, *33*, 953.
(214) Fowler, S. A.; Stacy, D. M.; Blackwell, H. E. *Org. Lett.* **2008**, *10*, 2329.
(215) Liu, F.; Stephen, A. G.; Waheed, A. A.; Freed, E. O.; Fisher, R. J.; Burke, T. R. *Bioorg. Med. Chem. Lett.* **2010**, *20*, 318.
(216) Kolb, H. C.; Finn, M. G.; Sharpless, K. B. *Angewandte Chemie-International Edition* **2001**, *40*, 2004.
(217) Rostovtsev, V. V.; Green, L. G.; Fokin, V. V.; Sharpless, K. B. *Angewandte Chemie-International Edition* **2002**, *41*, 2596.
(218) Tornøe, C. W.; Christensen, C.; Meldal, M. *The Journal of Organic Chemistry* **2002**, *67*, 3057.
(219) Huisgen, R. *Angewandte Chemie International Edition in English* **1963**, *2*, 633.
(220) Isobe, H.; Fujino, T.; Yamazaki, N.; Guillot-Nieckowski, M.; Nakamura, E. *Org. Lett.* **2008**, *10*, 3729.
(221) Rodionov, V. O.; Presolski, S. I.; Gardinier, S.; Lim, Y.-H.; Finn, M. G. *J. Am. Chem. Soc.* **2007**, *129*, 12696.
(222) Hong, V.; Steinmetz, N. F.; Manchester, M.; Finn, M. G. *Bioconjugate Chem.* **2010**, *21*, 1912.
(223) Chan, T. R.; Hilgraf, R.; Sharpless, K. B.; Fokin, V. V. *Org. Lett.* **2004**, *6*, 2853.
(224) Baskin, J. M.; Prescher, J. A.; Laughlin, S. T.; Agard, N. J.; Chang, P. V.; Miller, I. A.; Lo, A.; Codelli, J. A.; Bertozzi, C. R. *Proc. Natl. Acad. Sci. U. S. A.* **2007**, *104*, 16793.
(225) Abedin, M. J.; Liepold, L.; Suci, P.; Young, M.; Douglas, T. *J. Am. Chem. Soc.* **2009**, *131*, 4346.
(226) Aucagne, V.; Hanni, K. D.; Leigh, D. A.; Lusby, P. J.; Walker, D. B. *J. Am. Chem. Soc.* **2006**, *128*, 2186.
(227) Morvan, F.; Meyer, A.; Pourceau, G.; Vidal, S.; Chevolot, Y.; Souteyrand, E.; Vasseur, J. J. *Nucleic Acids Symp. Ser.* **2008**, 47.
(228) Hayashi, K.; Moriya, M.; Sakamoto, W.; Yogo, T. *Chem. Mater.* **2009**, *21*, 1318.
(229) Srinivasan, R.; Tan, L. P.; Wu, H.; Yang, P. Y.; Kalesh, K. A.; Yao, S. Q. *Org. Biomol. Chem.* **2009**, *7*, 1821.
(230) Manetsch, R.; Krasinski, A.; Radic, Z.; Raushel, J.; Taylor, P.; Sharpless, K. B.; Kolb, H. C. *J. Am. Chem. Soc.* **2004**, *126*, 12809.
(231) Mocharla, V. P.; Colasson, B.; Lee, L. V.; Roper, S.; Sharpless, K. B.; Wong, C. H.; Kolb, H. C. *Angewandte Chemie-International Edition* **2005**, *44*, 116.

(232) Holub, J. M.; Jang, H.; Kirshenbaum, K. *Org.Lett.* **2007**, *9*, 3275.
(233) Gueell, I.; Micalo, L.; Cano, L.; Badosa, E.; Ferre, R.; Montesinos, E.; Bardaji, E.; Feliu, L.; Planas, M. *Peptides* **2012**, *33*, 9.
(234) Valverde, I. E.; Lecaille, F.; Lalmanach, G.; Aucagne, V.; Delmas, A. F. *Angewandte Chemie-International Edition* **2012**, *51*, 718.
(235) Bock, V. D.; Perciaccante, R.; Jansen, T. P.; Hiemstra, H.; van Maarseveen, J. H. *Org. Lett.* **2006**, *8*, 919.
(236) Samarasimhareddy, M.; Hemantha, H. P.; Sureshbabu, V. V. *Tetrahedron Lett.* **2012**, *53*, 3104.
(237) Cantel, S.; Isaad, A. L. C.; Scrima, M.; Levy, J. J.; DiMarchi, R. D.; Rovero, P.; Halperin, J. A.; D'Ursi, A. M.; Papini, A. M.; Chorev, M. *J. Org. Chem.* **2008**, *73*, 5663.
(238) Isaad, A. L.; Papini, A. M.; Chorev, M.; Rovero, P. *J. Pept. Sci.* **2009**, *15*, 451.
(239) Isaad, A. L. C.; Barbetti, F.; Rovero, P.; D'Ursi, A. M.; Chelli, M.; Chorev, M.; Papini, A. M. *Eur. J. Org. Chem.* **2008**, 5308.
(240) Jacobsen, O.; Maekawa, H.; Ge, N. H.; Gorbitz, C. H.; Rongved, P.; Ottersen, O. P.; miry-Moghaddam, M.; Klaveness, J. *J. Org. Chem.* **2011**, *76*, 1228.
(241) Kritzer, J. A.; Lear, J. D.; Hodsdon, M. E.; Schepartz, A. *J. Am. Chem. Soc.* **2004**, *126*, 9468.
(242) Duncan, S. J.; Gruschow, S.; Williams, D. H.; McNicholas, C.; Purewal, R.; Hajek, M.; Gerlitz, M.; Martin, S.; Wrigley, S. K.; Moore, M. *J. Am. Chem. Soc.* **2001**, *123*, 554.
(243) Harker, E. A.; Schepartz, A. *Chembiochem* **2009**, *10*, 990.
(244) Hayashi, R.; Wang, D.; Hara, T.; Iera, J. A.; Durell, S. R.; Appella, D. H. *Bioorg.Med.Chem.* **2009**, *17*, 7884.
(245) Liu, M.; Li, C.; Pazgier, M.; Li, C. Q.; Mao, Y. B.; Lv, Y. F.; Gu, B.; Wei, G.; Yuan, W. R.; Zhan, C. Y.; Lu, W. Y. *Proceedings of the National Academy of Sciences of the United States of America* **2010**, *107*, 14321.
(246) Bernal, F.; Wade, M.; Godes, M.; Davis, T. N.; Whitehead, D. G.; Kung, A. L.; Wahl, G. M.; Walensky, L. D. *Cancer Cell* **2010**, *18*, 411.
(247) Madden, M. M.; Muppidi, A.; Li, Z.; Li, X.; Chen, J.; Lin, Q. *Bioorg.Med.Chem.Lett.* **2011**, *21*, 1472.
(248) Hu, Y.; Li, X.; Sebti, S. M.; Chen, J.; Cai, J. *Bioorg.Med.Chem.Lett.* **2011**, *21*, 1469.
(249) Fasan, R.; Dias, R. L. A.; Moehle, K.; Zerbe, O.; Vrijbloed, J. W.; Obrecht, D.; Robinson, J. A. *Angewandte Chemie-International Edition* **2004**, *43*, 2109.
(250) Zuckermann, R. N.; Kerr, J. M.; Kent, S. B. H.; Moos, W. H. *J. Am. Chem. Soc.* **1992**, *114*, 10646.
(251) Unciti-Broceta, A.; Diezmann, F.; Ou-Yang, C. Y.; Fara, M. A.; Bradley, M. *Bioorg.Med.Chem.* **2009**, *17*, 959.
(252) Cavender, C. J.; Shiner, V. J. *The Journal of Organic Chemistry* **1972**, *37*, 3567.
(253) Goddard-Borger, E. D.; Stick, R. V. *Org. Lett.* **2007**, *9*, 3797.
(254) Norgren, A. S.; Budke, C.; Majer, Z.; Heggemann, C.; Koop, T.; Sewald, N. *Synthesis-Stuttgart* **2009**, 488.

(255) Chan, W. C.; White, P. D. *Oxford University Press* **2000**.
(256) Kaiser, E.; Colescot.Rl; Bossinge.Cd; Cook, P. I. *Anal. Biochem.* **1970**, *34*, 595.
(257) Torres, O.; Yuksel, D.; Bernardina, M.; Kumar, K.; Bong, D. *Chembiochem* **2008**, *9*, 1701.
(258) Jang, H.; Fafarman, A.; Holub, J. M.; Kirshenbaum, K. *Org. Lett.* **2005**, *7*, 1951.
(259) Landi, F.; Johansson, C. M.; Campopiano, D. J.; Hulme, A. N. *Org. Biomol. Chem.* **2010**, *8*, 56.
(260) Kelly, S. M.; Jess, T. J.; Price, N. C. *Biochim. Biophys. Acta, Proteins Proteomics* **2005**, *1751*, 119.
(261) Buck, M. *Q. Rev. Biophys.* **1998**, *31*, 297.
(262) Szewczuk, Z.; Wilczynski, A.; Stefanowicz, P.; Fedorowicz, W.; Siemion, I. Z.; Wieczorek, Z. *Mol. Immunol.* **1999**, *36*, 525.
(263) Richardson, J. S. *Adv. Protein Chem.* **1981**, *34*, 339.
(264) Laemmli, U. K. *Nature* **1970**, *227*, 680.
(265) Vojkovsky, T. *Peptide Res.* **1995**, *8*, 236.
(266) Muller, D.; Zeltser, I.; Bitan, G.; Gilon, C. *J. Org. Chem.* **1997**, *62*, 411.
(267) Shibata, N.; Das, B. K.; Honjo, H.; Takeuchi, Y. *J. Chem. Soc., Perkin Trans. 1* **2001**, 1605.

CHAPTER 6

Appendices

Permissions for reuse of figures/tables/illustrations in the thesis.

- **Figure 1.1-3**

  License number: 3290380901205 (Copyright Clearance Center)
  Licensed content title: Intrinsically unstructured proteins and their functions
  Licensed content author: H. Jane Dyson, Peter E. Wright
  Licensed content date: Mar 1, 2005

- **Figure 1.1-8. Bottom panel**

  License number: 3290400351090 (Copyright Clearance Center)
  Licensed content title: Solution Structure of the Hdm2 C2H2C4 RING, a Domain Criticalfor Ubiquitination of p53
  Licensed content author: Milka Kostic, Theresia Matt, Maria A. Martinez-Yamout, H. Jane Dyson, Peter E. Wright
  Licensed content date: Oct 20, 2006

- **Figure 1.1-2**

  License Number: 3290371098153 (Copyright Clearance Center)
  Licensed content title: History of protein–protein interactions: From egg-white tocomplex networks
  Licensed content author: Pascal Braun, Anne-Claude Gingras
  Licensed content date: Jun 19, 2012

- **Figure 1.1-7**

  License number: 3290390433487 (Copyright Clearance Center)
  Licensed content title: MDM2: life without p53
  Licensed content author: Sylvain Daujat, Henry Neel, Jacques Piette
  Licensed content date: Aug 1, 2001

- **Figure 1.1-6**

  License Number: 3290390134887 (Copyright Clearance Center)
  Licensed content title: The p53 pathway: positive and negative feedback loops
  Licensed content author: Sandra L Harris, Arnold J Levine
  Licensed content date: Dec 31, 1969

- **Figure 2.3-15**
- **Figure 2.3-22**

- **Figure 2.6-2**
  License number: 3291380558598 (Copyright Clearance Center)
  Licensed content title How to study proteins by circular dichroism
  Licensed content author: Sharon M. Kelly,Thomas J. Jess,Nicholas C. Price
  Licensed content date: 10 August 2005

- **Figure 2.6-3**
- **Figure 2.6-8**

6.7 Appendix 1: peptoid-peptide building blocks ($^{1}H/^{13}C$)

6.7.1 A*

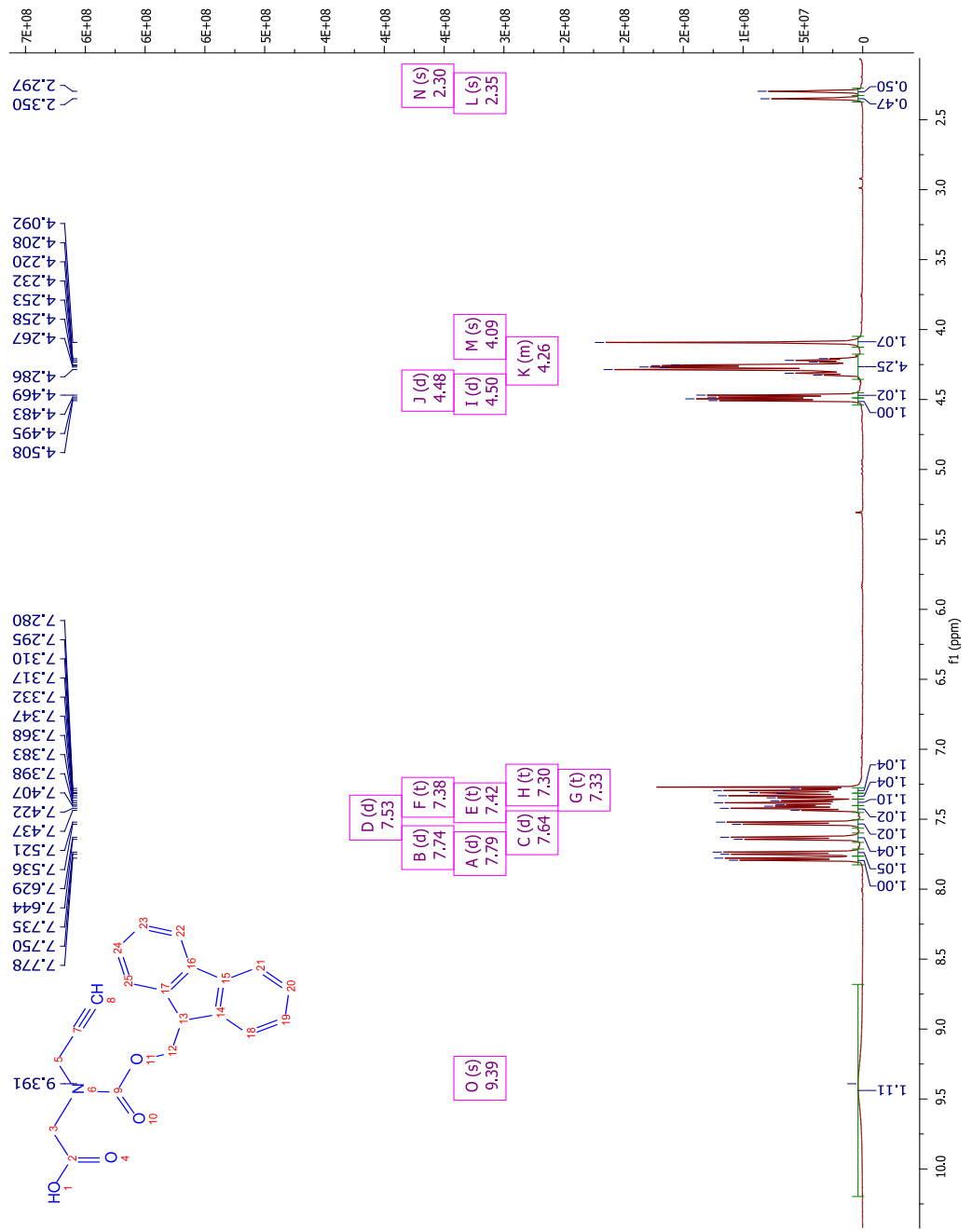

^{1}H

^{13}C

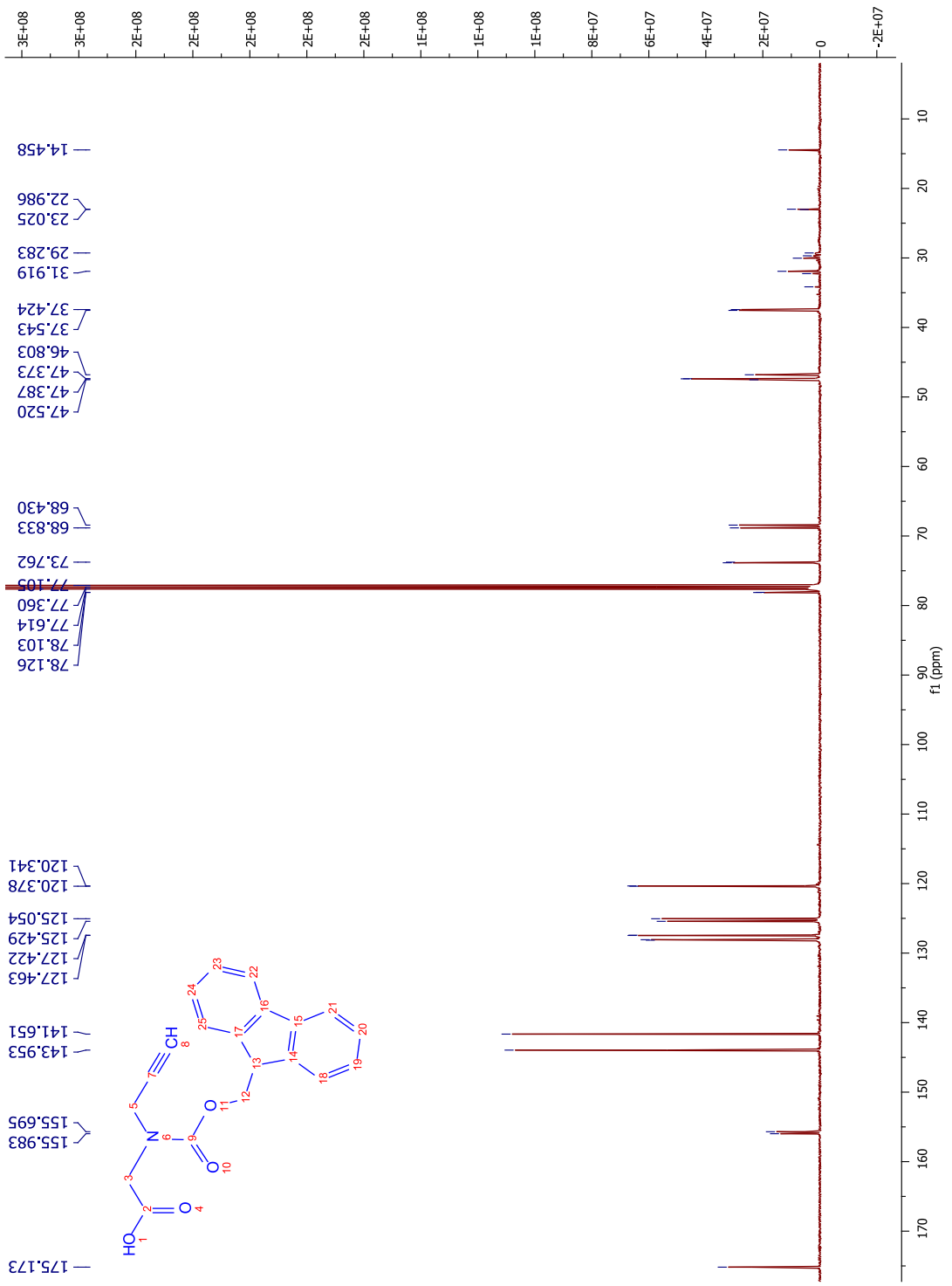
175.173
155.983
155.695
143.953
141.651
127.463
127.422
125.429
125.054
120.378
120.341
78.126
78.103
77.614
77.360
77.105
73.762
68.833
68.430
47.520
47.387
47.373
46.803
37.543
37.424
31.919
29.283
23.025
22.986
14.458
f1 (ppm)

13C-DEPT135

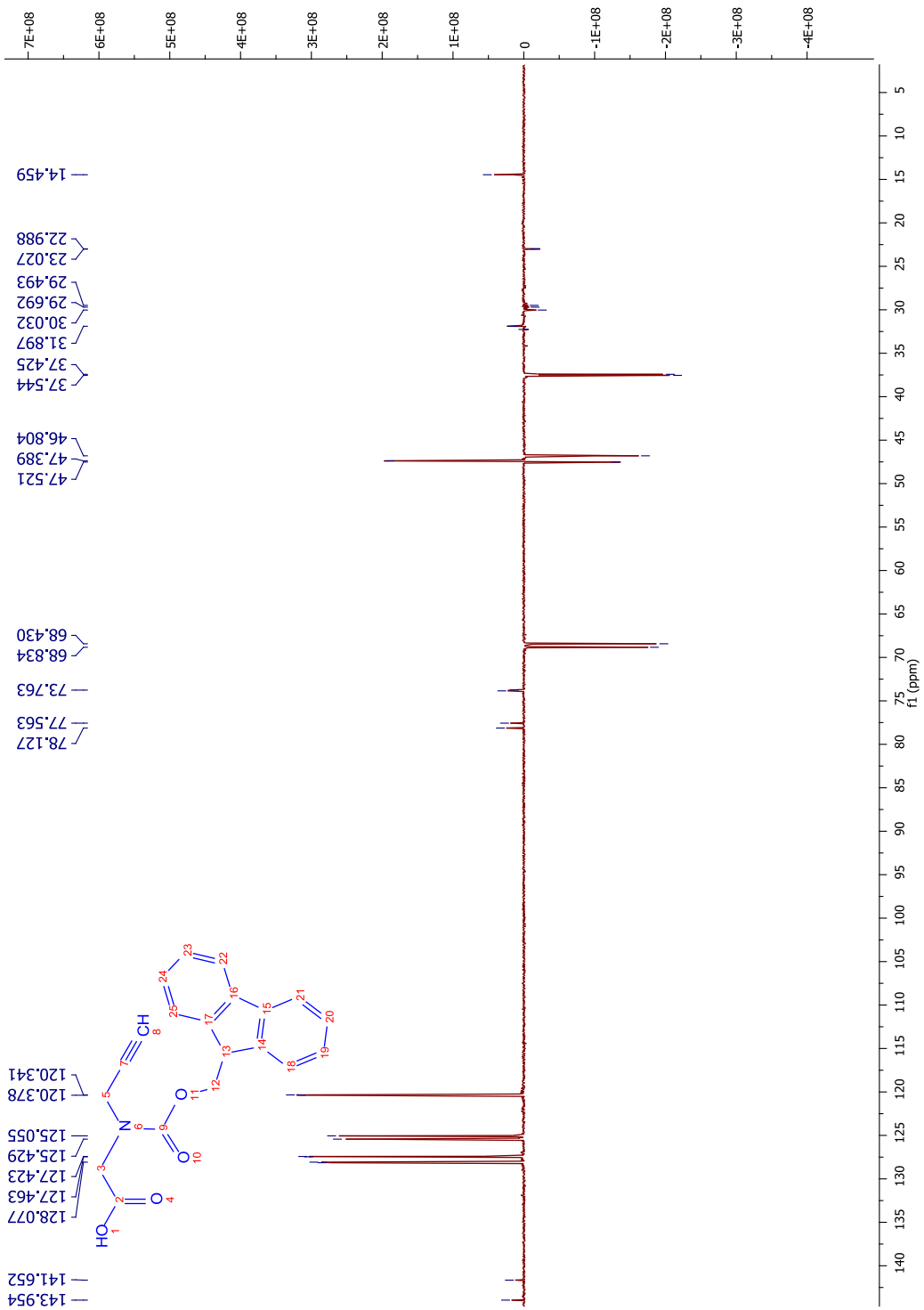
14.459
22.988
23.027
29.493
29.692
30.032
31.897
37.425
37.544
46.804
47.389
47.521
68.430
68.834
73.763
77.563
78.127
120.341
120.378
125.055
125.429
127.423
127.463
128.077
141.652
143.954
f1 (ppm)

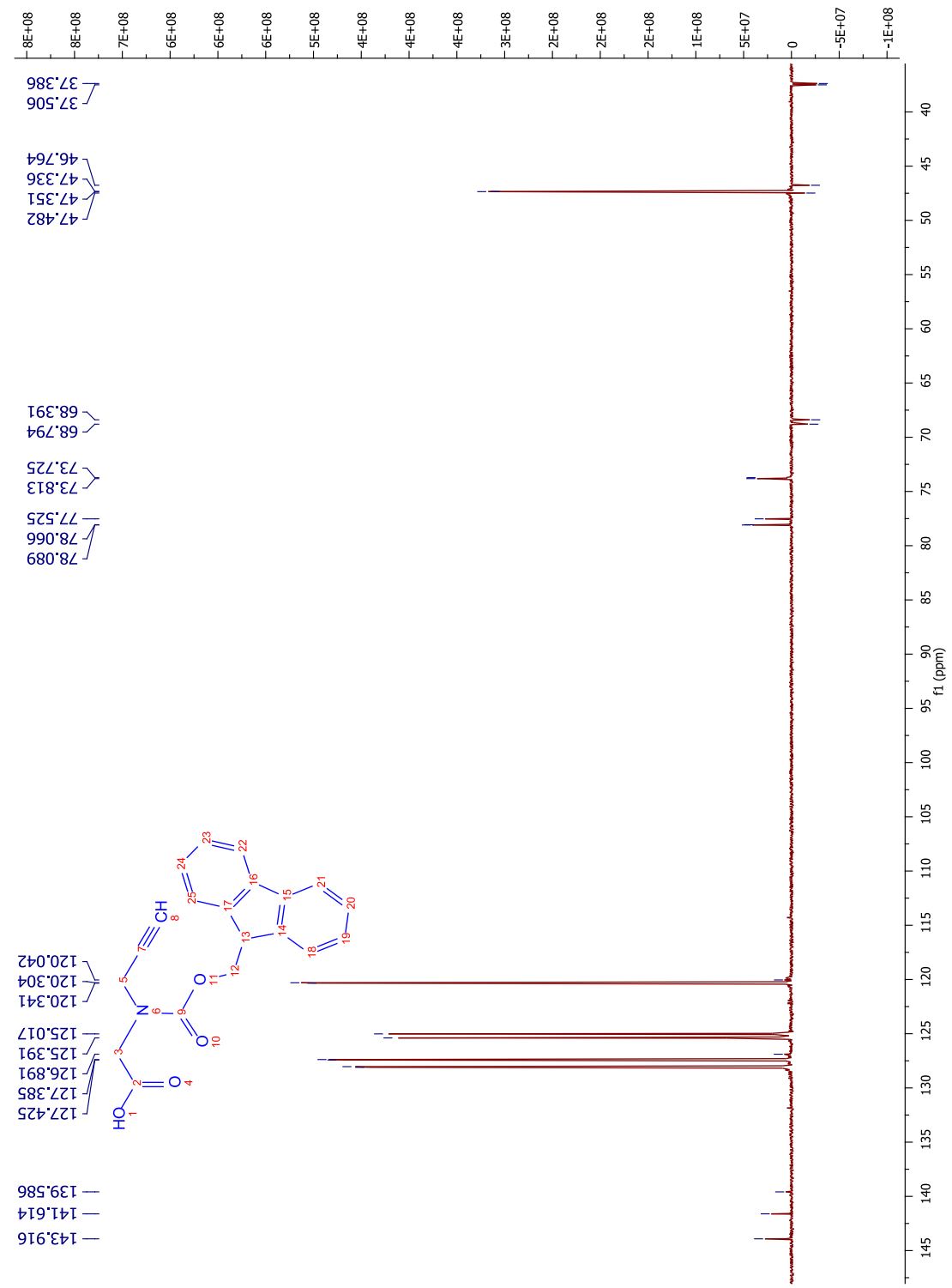
143.916
141.614
139.586
127.425
127.385
126.891
125.391
125.017
120.341
120.304
120.042
78.089
78.066
77.525
73.813
73.725
68.794
68.391
47.482
47.351
47.336
46.764
37.506
37.386
f1 (ppm)

^{13}C-DEPT90

6.7.2 Z^*_3

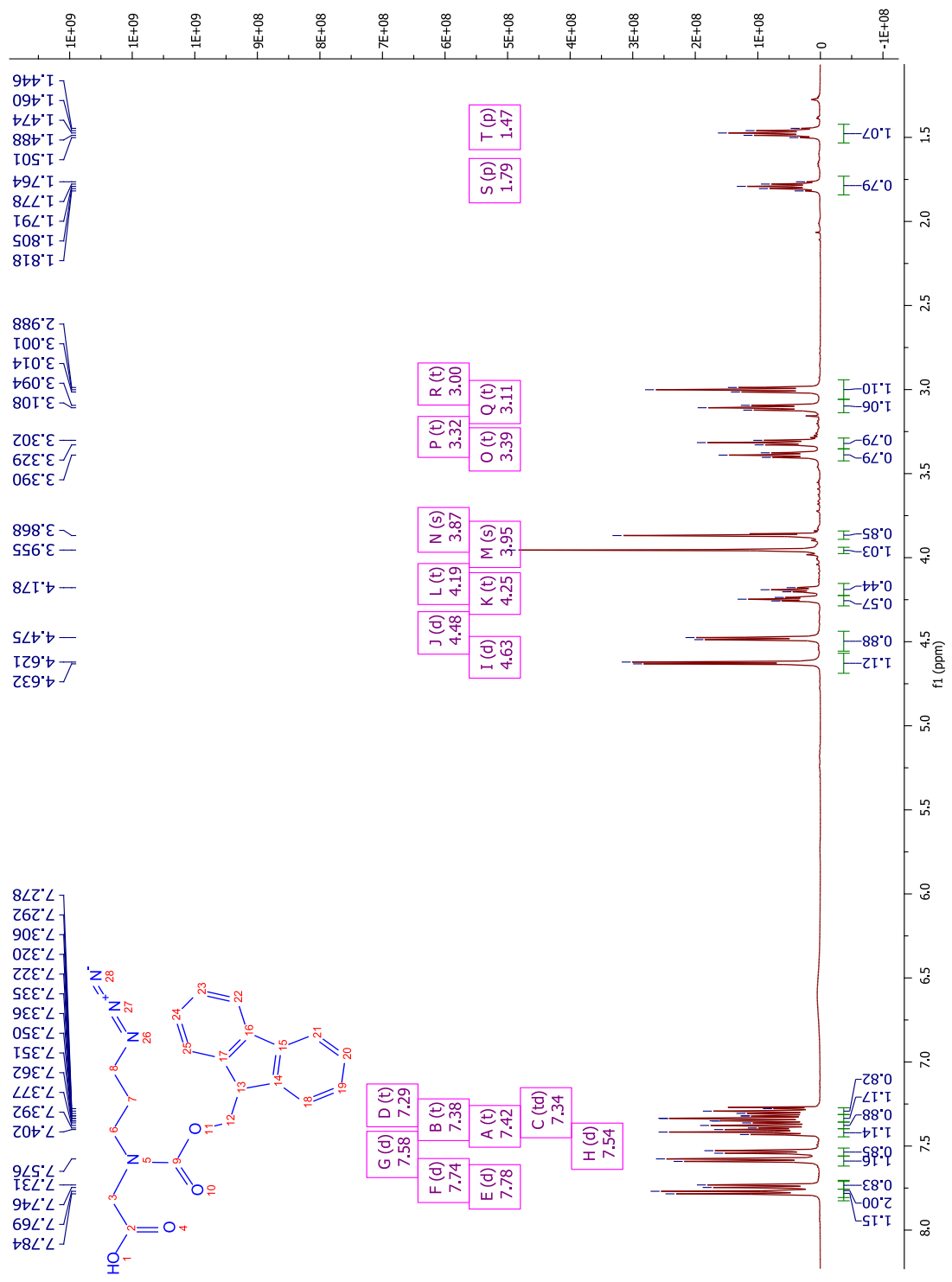
A (t) 7.42
B (t) 7.38
C (td) 7.34
D (t) 7.29
E (d) 7.78
F (d) 7.74
G (d) 7.58
H (d) 7.54
I (d) 4.63
J (d) 4.48
K (t) 4.25
L (t) 4.19
M (s) 3.95
N (s) 3.87
O (t) 3.39
P (t) 3.32
Q (t) 3.11
R (t) 3.00
S (p) 1.79
T (p) 1.47
f1 (ppm)

^1H

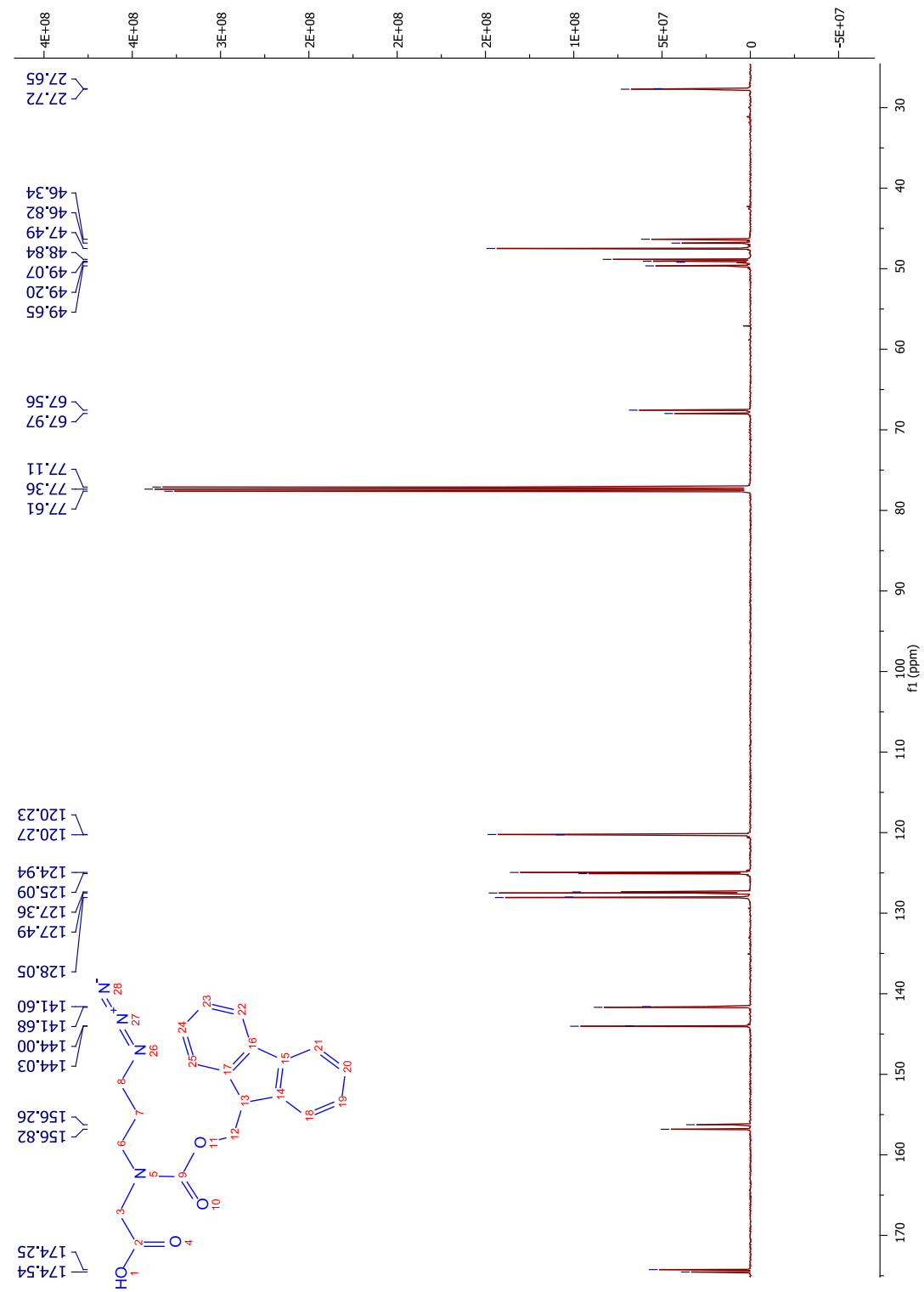
13C
174.54
174.25
156.82
156.26
144.03
144.00
141.68
141.60
128.05
127.49
127.36
125.09
124.94
120.27
120.23
77.61
77.36
77.11
67.97
67.56
49.65
49.20
49.07
48.84
47.49
46.82
46.34
27.72
27.65
f1 (ppm)

^{13}C-DEPT135

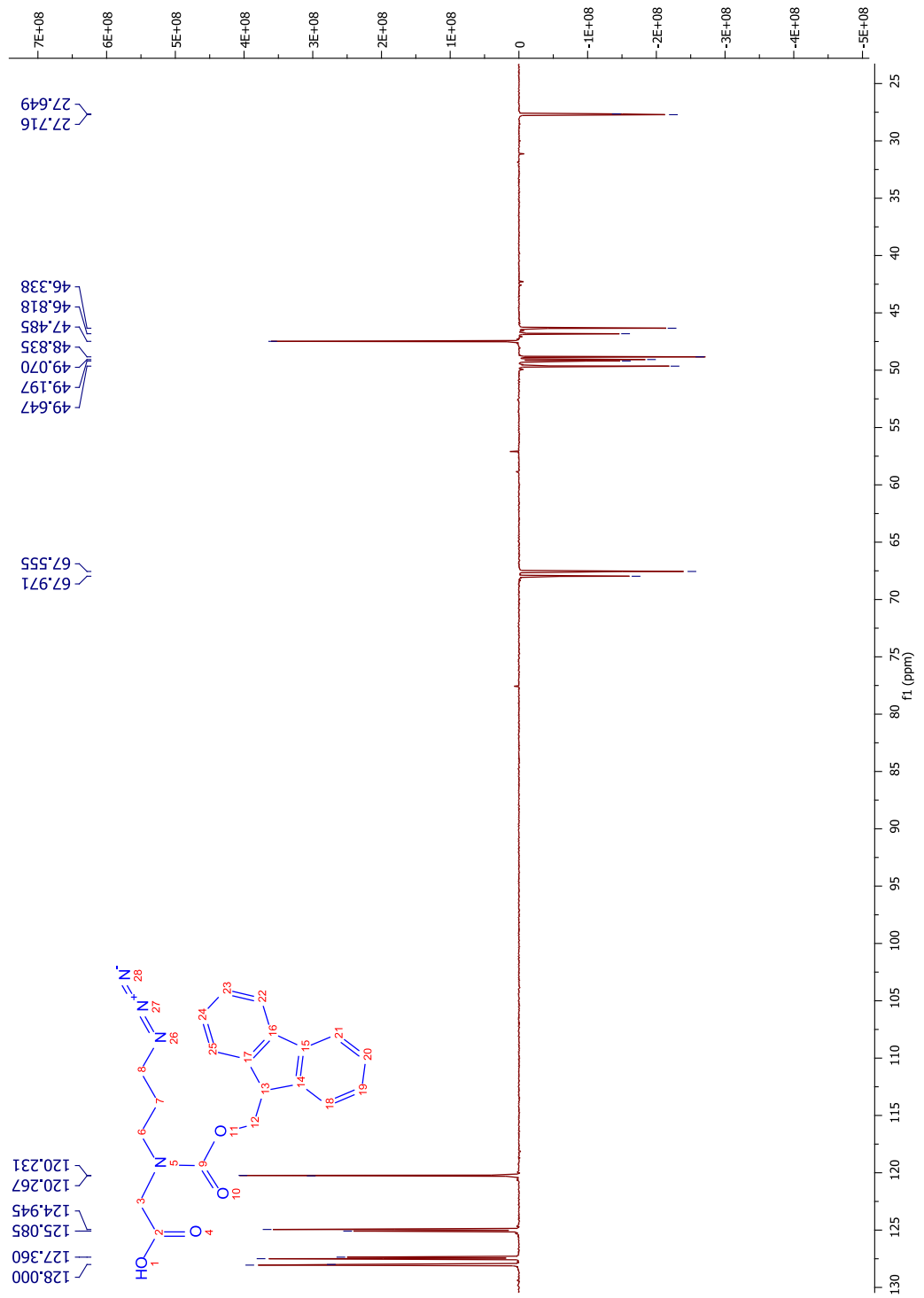
128.000
127.360
125.085
124.945
120.267
120.231
67.971
67.555
49.647
49.197
49.070
48.835
47.485
46.818
46.338
27.716
27.649
f1 (ppm)

^{13}C-DEPT90

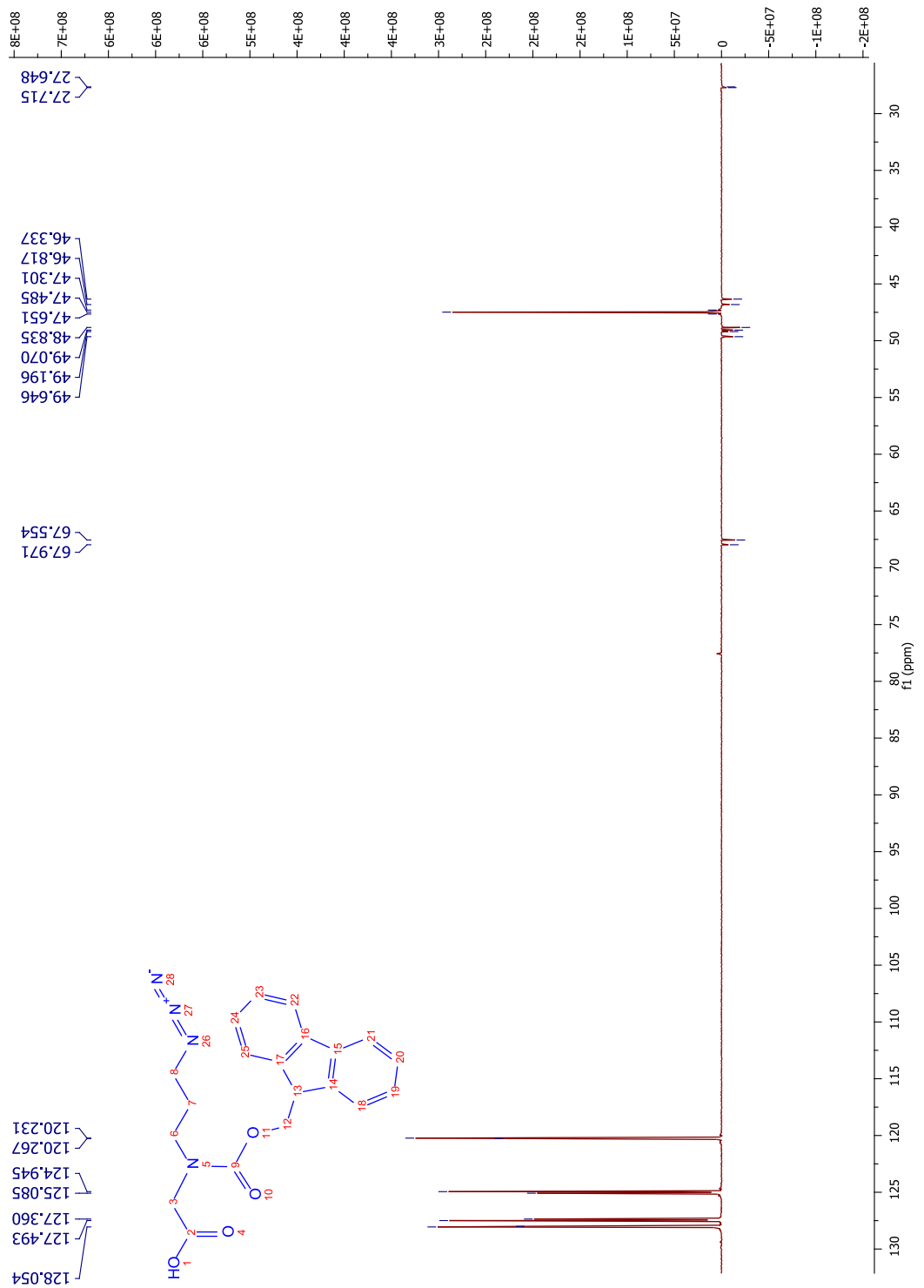
27.648
27.715
46.337
46.817
47.301
47.485
47.651
48.835
49.070
49.196
49.646
67.554
67.971
120.231
120.267
124.945
125.085
127.360
127.493
128.054
f1 (ppm)

6.7.3 Z^*_4

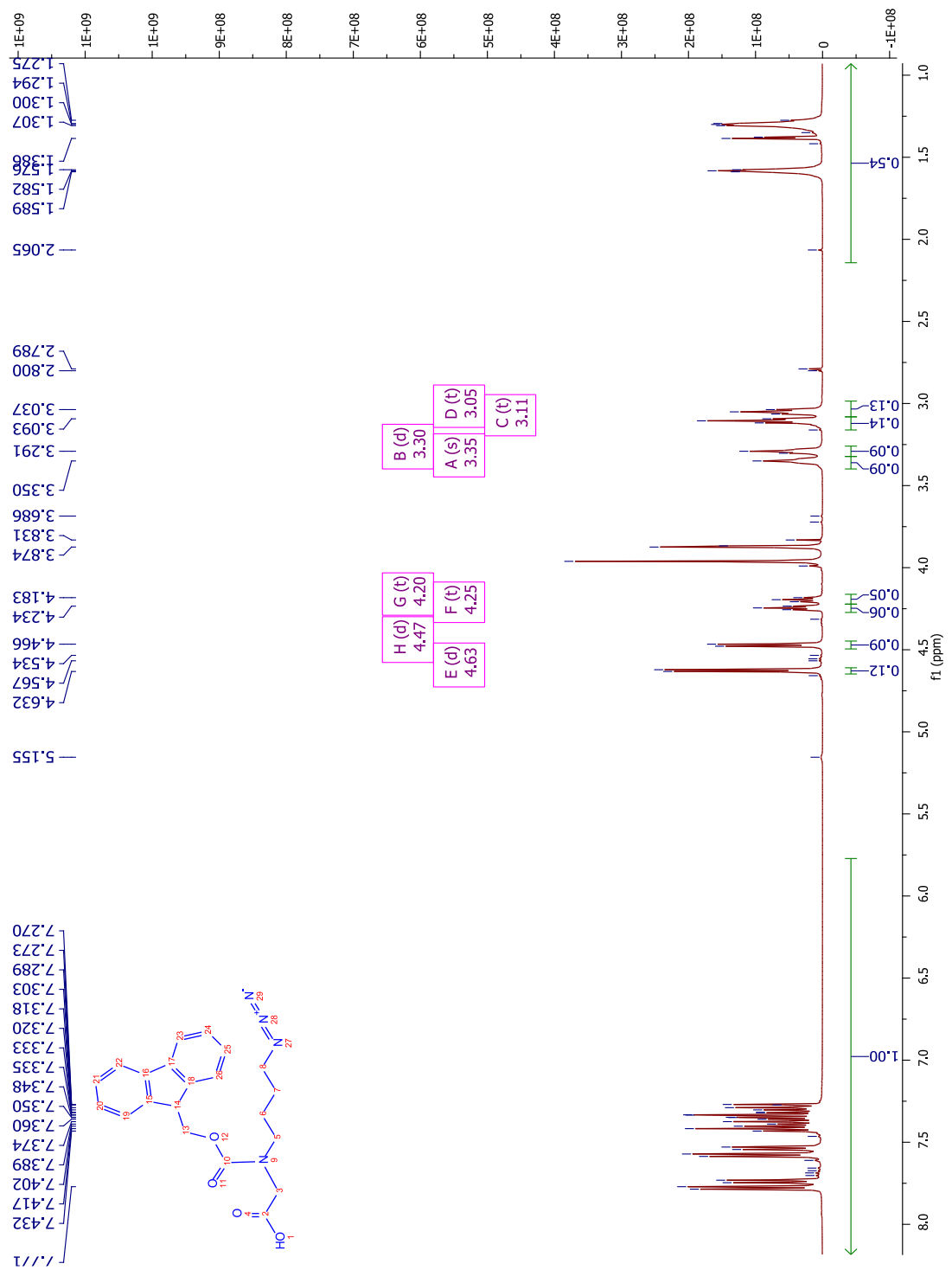

^1H

^{13}C

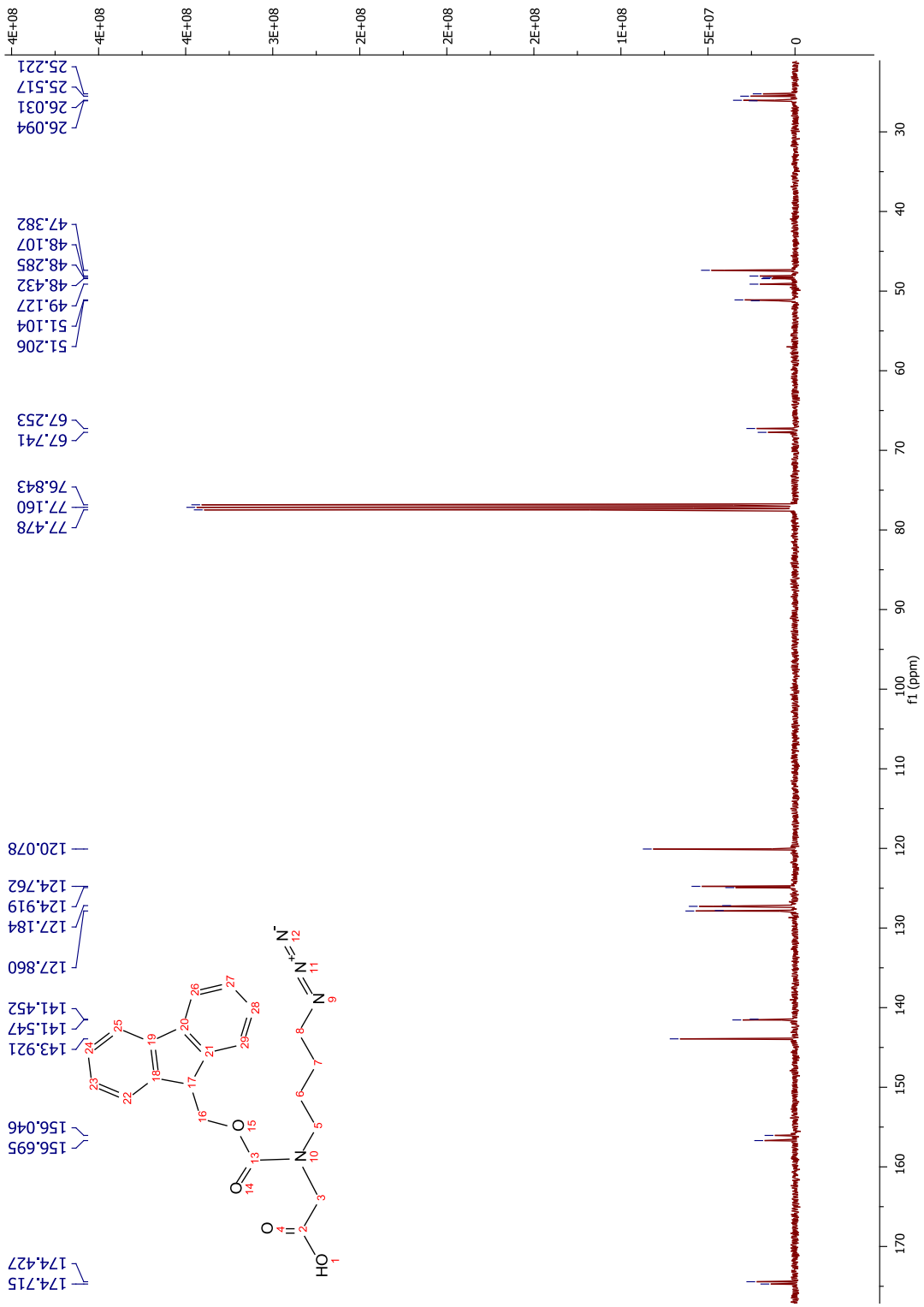
174.715
174.427
156.695
156.046
143.921
141.547
141.452
127.860
127.184
124.919
124.762
120.078
77.478
77.160
76.843
67.741
67.253
51.206
51.104
49.127
48.432
48.285
48.107
47.382
26.094
26.031
25.517
25.221
f1 (ppm)

^{13}C-DEPT90

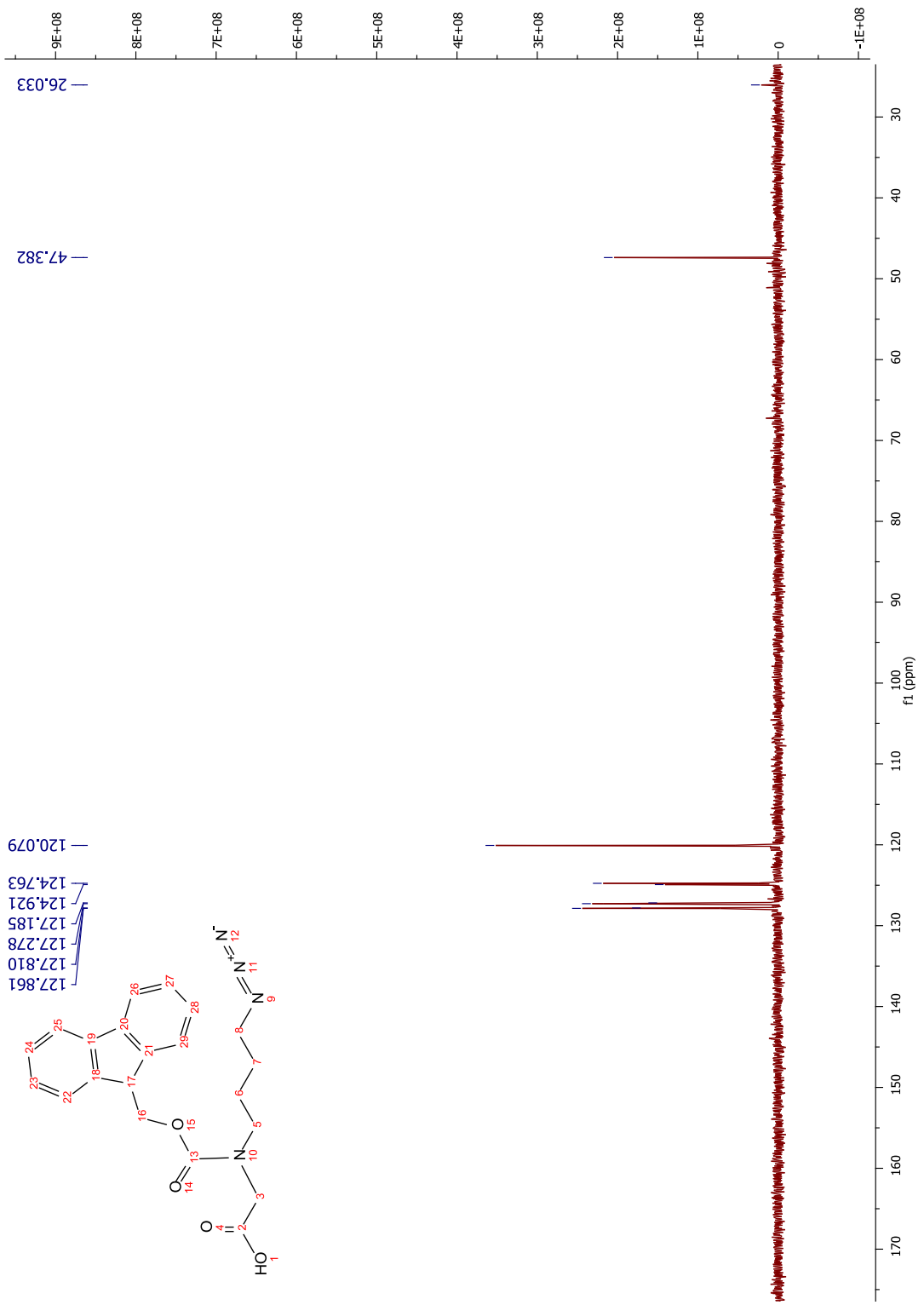
26.033
47.382
120.079
124.763
124.921
127.185
127.278
127.810
127.861
f1 (ppm)

^{13}C-DEPT135

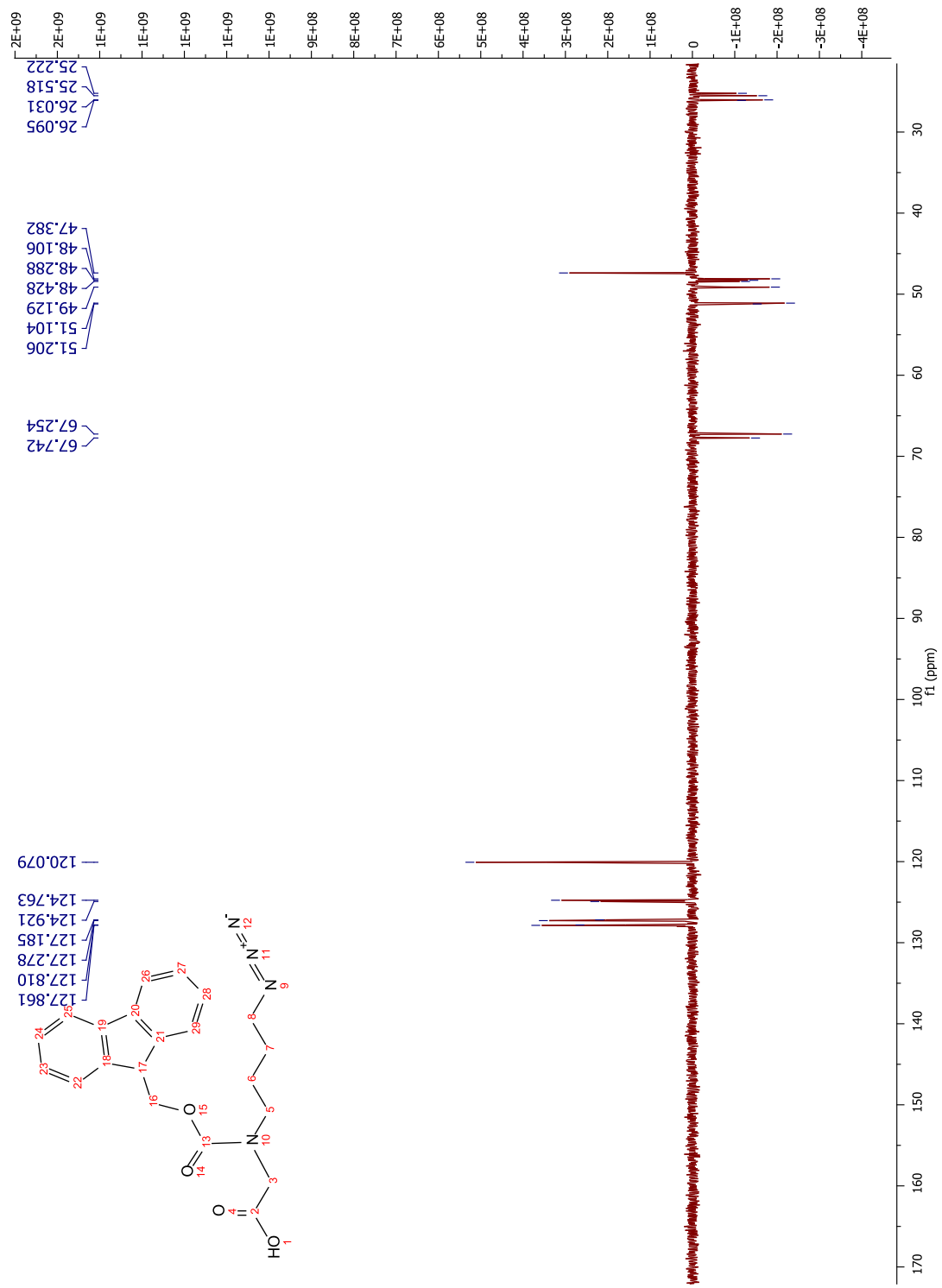
25.222
25.518
26.031
26.095
47.382
48.106
48.288
48.428
49.129
51.104
51.206
67.254
67.742
120.079
124.763
124.921
127.185
127.278
127.810
127.861
f1 (ppm)

6.7.4 Z^*_5

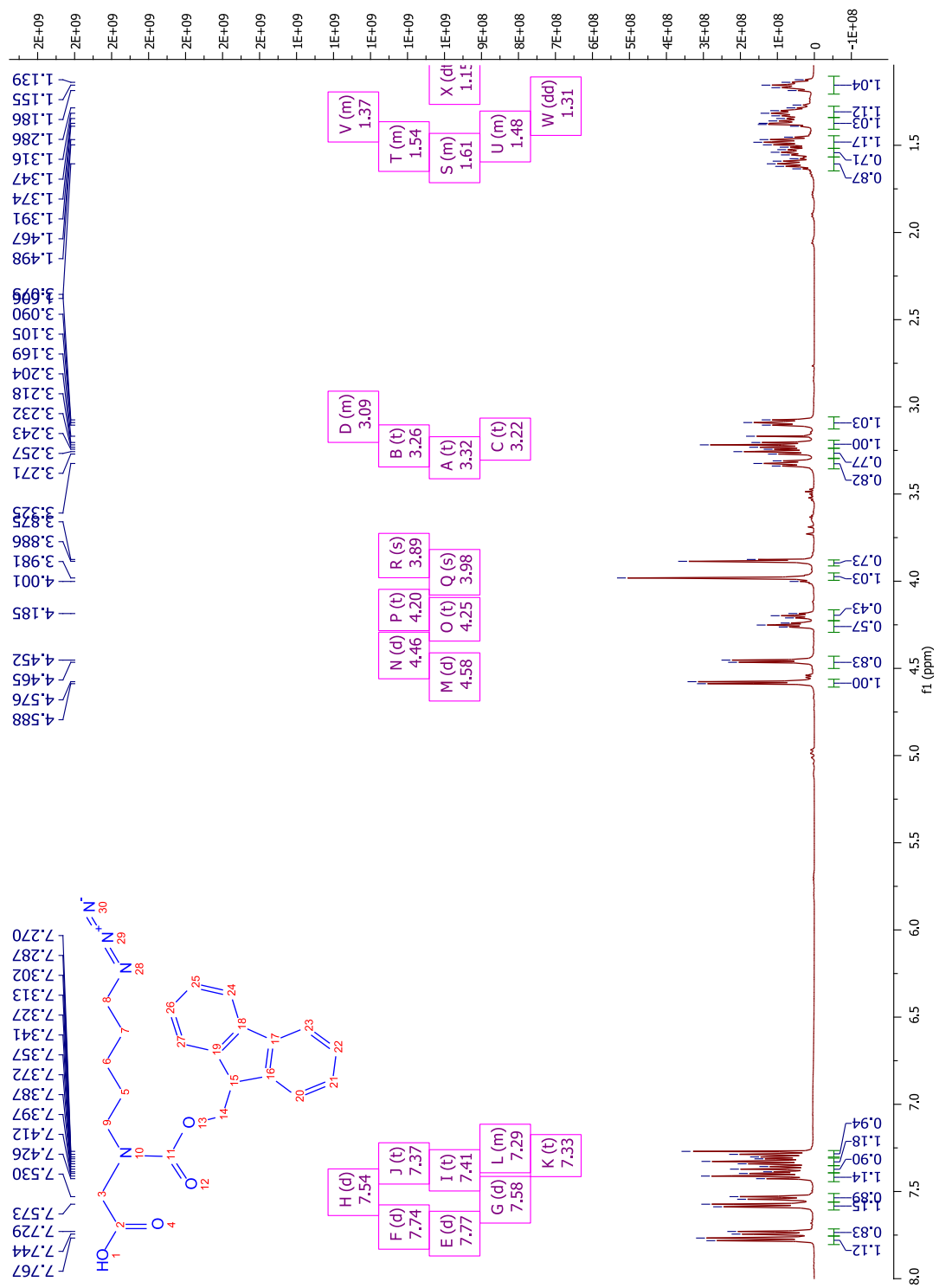

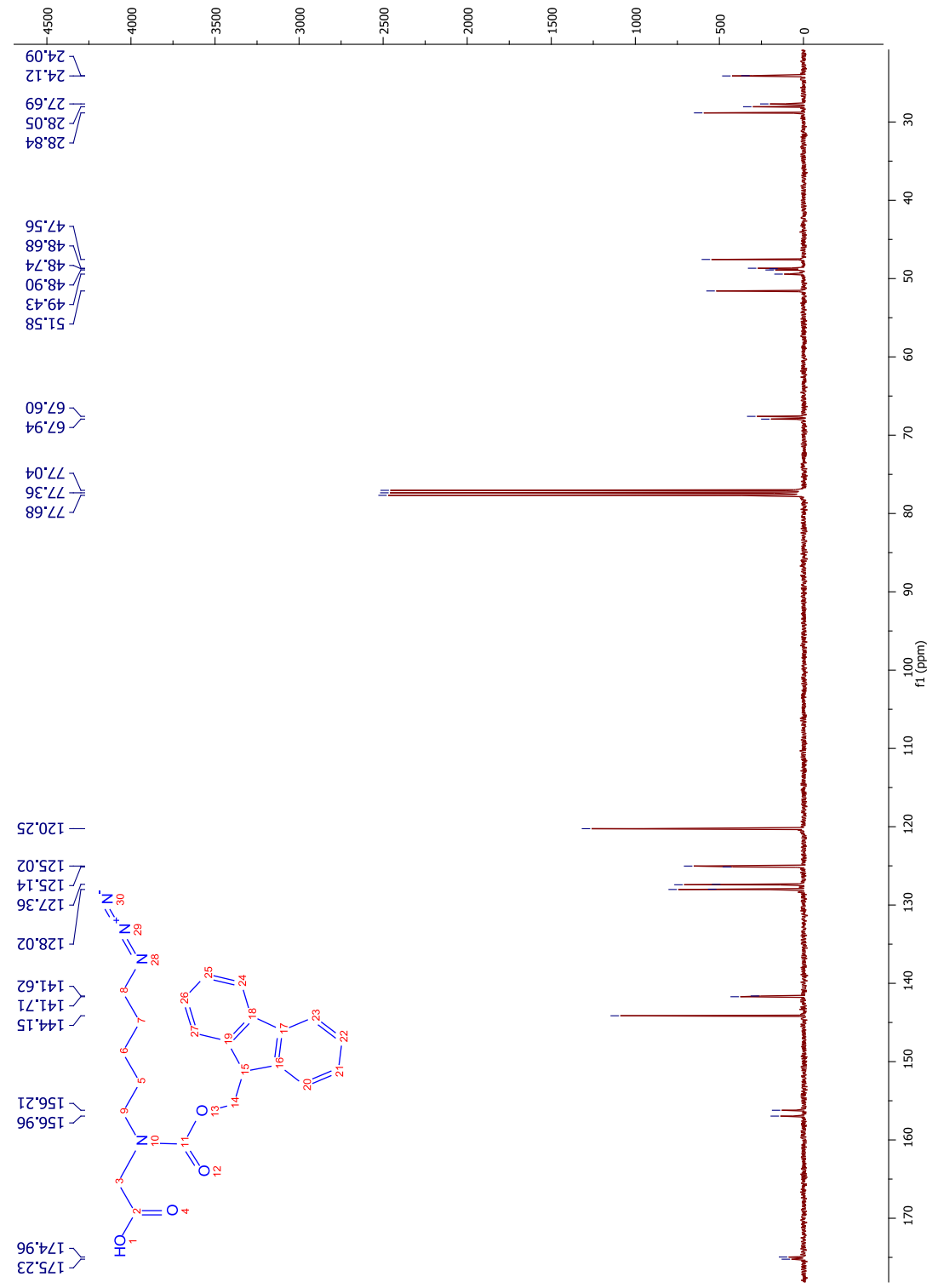
175.23
174.96
156.96
156.21
144.15
141.71
141.62
128.02
127.36
125.14
125.02
120.25
77.68
77.36
77.04
67.94
67.60
51.58
49.43
48.90
48.74
48.68
47.56
28.84
28.05
27.69
24.12
24.09
f1 (ppm)

^{13}C

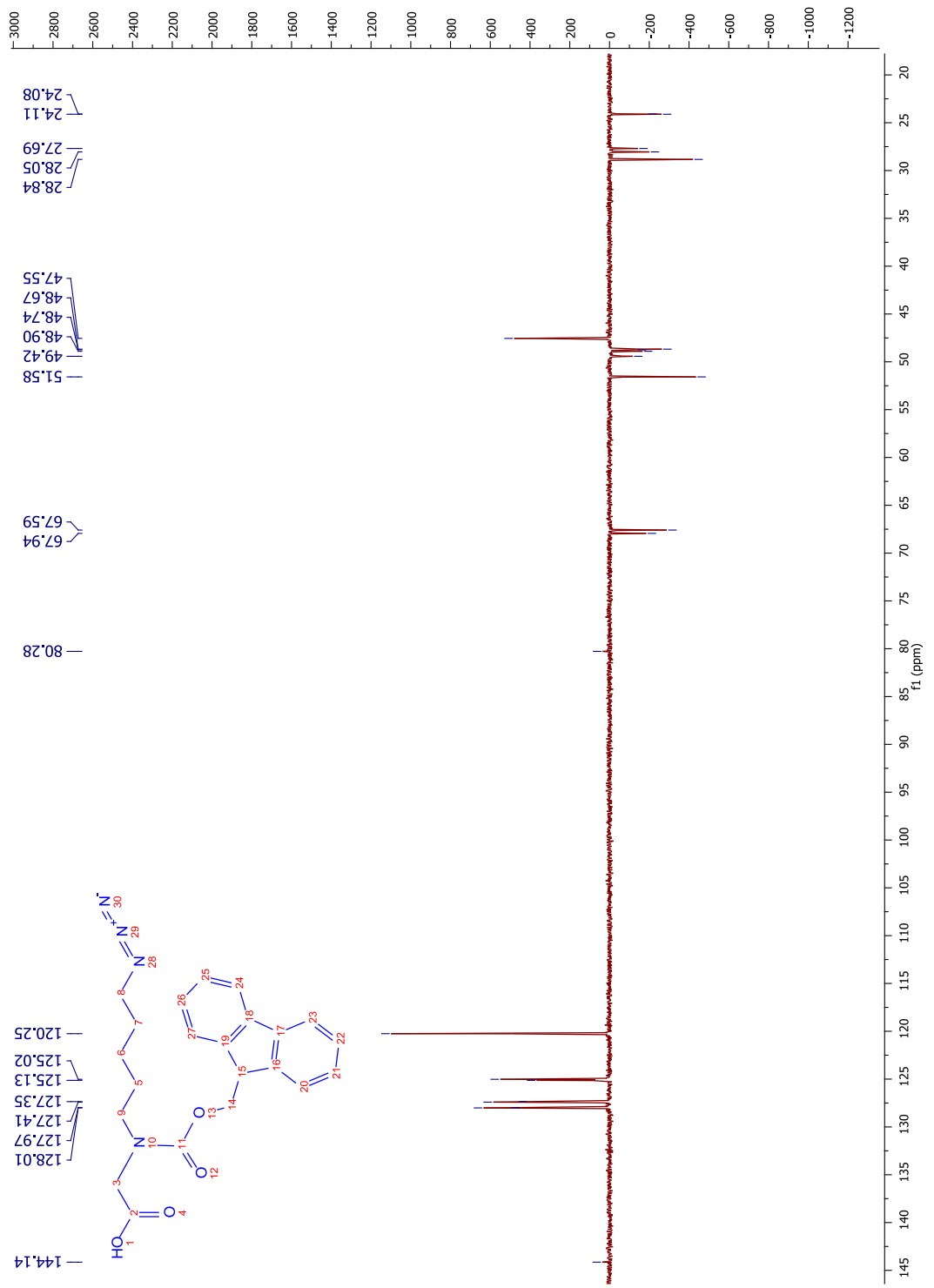
144.14
128.01
127.97
127.41
127.35
125.13
125.02
120.25
80.28
67.94
67.59
51.58
49.42
48.90
48.74
48.67
47.55
28.84
28.05
27.69
24.11
24.08
f1 (ppm)

^{13}C-DEPT135

^{13}C-DEPT90

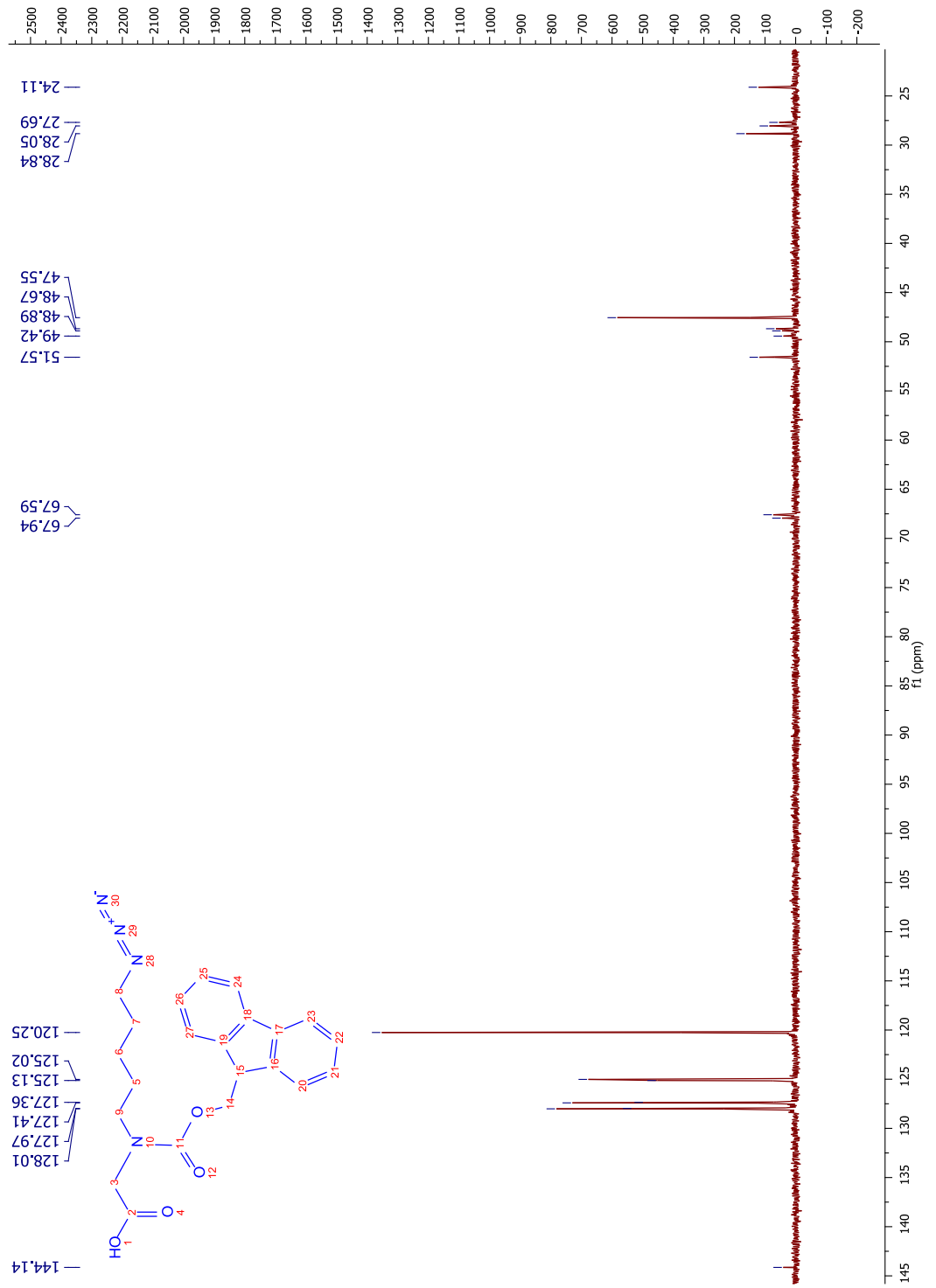
144.14
128.01
127.97
127.41
127.36
125.13
125.02
120.25
67.94
67.59
51.57
49.42
48.89
48.67
47.55
28.84
28.05
27.69
24.11
f1 (ppm)

6.8 Appendix 2: linear and cyclised peptoid-peptide hybrids

U1: (U)-Biotin-SGSG-KAA*YFZ$^{*}{}_{5}$-NH_2

U2: (U)-Biotin-SGSG-KAZ$^{*}{}_{5}$YFA*-NH_2

U3: (U)-Biotin-SGSG-KA*AYFZ$^{*}{}_{5}$-NH_2

U4: (U)-Biotin-SGSG-KZ$^{*}{}_{5}$AYFA*-NH_2

U5: (U)-Biotin-SGSG-KAA*YFZ$^{*}{}_{3}$-NH_2

U6: (U)-Biotin-SGSG-KAZ$^{*}{}_{3}$YFA*-NH_2

U7: (U)-Biotin-SGSG-KA*AYFZ$^{*}{}_{4}$-NH_2

U8: (U)-Biotin-SGSG-KZ$^{*}{}_{4}$AYFA*-NH_2

U9: (U)-Biotin-SGSG-KZ$^{*}{}_{3}$AYFA*-NH_2

U10:(U)-Biotin-SGSG-KAA*YFZ$^{*}{}_{4}$-NH_2

U12:(U)-Biotin-SGSG-KAZ$^{*}{}_{4}$YFA*-NH_2

U13:(U)-Biotin-SGSG-KA*AYFZ$^{*}{}_{3}$-NH_2

U14: (U)-Ac-KAA*YFZ$^{*}{}_{5}$-NH_2

U15: (U)-Ac-KAZ$^{*}{}_{5}$YFA*-NH_2

U16: (U)-Ac-KA*AYFZ$^{*}{}_{5}$-NH_2

U17: (U)-Ac-KZ$^{*}{}_{5}$AYFA*-NH_2

U18: (U)-Ac-KAA*YFZ$^{*}{}_{3}$-NH_2

U19: (U)-Ac-KAZ$^{*}{}_{3}$YFA*-NH_2

U20: (U)-Ac-KA*AYFZ$^{*}{}_{4}$-NH_2

U21: (U)-Ac-KZ$^{*}{}_{4}$AYFA*-NH_2

U22: (U)-Ac-KZ$^{*}{}_{3}$AYFA*-NH_2

U23: (U)-Ac-KAA*YFZ$^{*}{}_{4}$-NH_2

U25: (U)-Ac-KAZ$^{*}{}_{4}$YFA*-NH_2

U26: (U)-Ac-KA*AYFZ$^{*}{}_{3}$-NH_2

C1: (C)-Biotin-SGSG-KAA*YFZ$^{*}{}_{5}$-NH_2

C2: (C)-Biotin-SGSG-KAZ$^{*}{}_{5}$YFA*-NH_2

C3: (C)-Biotin-SGSG-KA*AYFZ$^{*}{}_{5}$-NH_2

C4: (C)-Biotin-SGSG-KZ$^{*}{}_{5}$AYFA*-NH_2

C5: (C)-Biotin-SGSG-KAA*YFZ$^{*}{}_{3}$-NH_2

C6: (C)-Biotin-SGSG-KAZ$^{*}{}_{3}$YFA*-NH_2

C7: (C)-Biotin-SGSG-KA*AYFZ$^{*}{}_{4}$-NH_2

C8: (C)-Biotin-SGSG-KZ$^{*}{}_{4}$AYFA*-NH_2

C9: (C)-Biotin-SGSG-KZ$^{*}{}_{3}$AYFA*-NH_2

C10: (C)-Biotin-SGSG-KAA*YFZ$^{*}{}_{4}$-NH_2

C12: (C)-Biotin-SGSG-KAZ$^{*}{}_{4}$YFA*-NH_2

C13: C)-Biotin-SGSG-KA*AYFZ$^{*}{}_{3}$-NH_2

C14: (C)-Ac-KAA*YFZ$^{*}{}_{5}$-NH_2

C15:(C)-Ac-KAZ$^{*}{}_{5}$YFA*-NH_2

C16: (C)-Ac-KA*AYFZ$^{*}{}_{5}$-NH_2

C17: (C)-Ac-KZ$^{*}{}_{5}$AYFA*-NH_2

C18: (C)-Ac-KAA*YFZ$^{*}{}_{3}$-NH_2

C19: (C)-Ac-KAZ$^{*}{}_{3}$YFA*-NH_2

C20: (C)-Ac-KA*AYFZ$^{*}{}_{4}$-NH_2

C21: (C)-Ac-KZ$^{*}{}_{4}$AYFA*-NH_2

C22: (C)-Ac-KZ$^{*}{}_{3}$AYFA*-NH_2

C23: (C)-Ac-KAA*YFZ$^{*}{}_{4}$-NH_2

C25: (C)-Ac-KAZ$^{*}{}_{4}$YFA*-NH_2

C26: (C)-Ac-KA*AYFZ$^{*}{}_{3}$-NH_2

6.8.1 Optimisation conditions for on-bead CuAAC

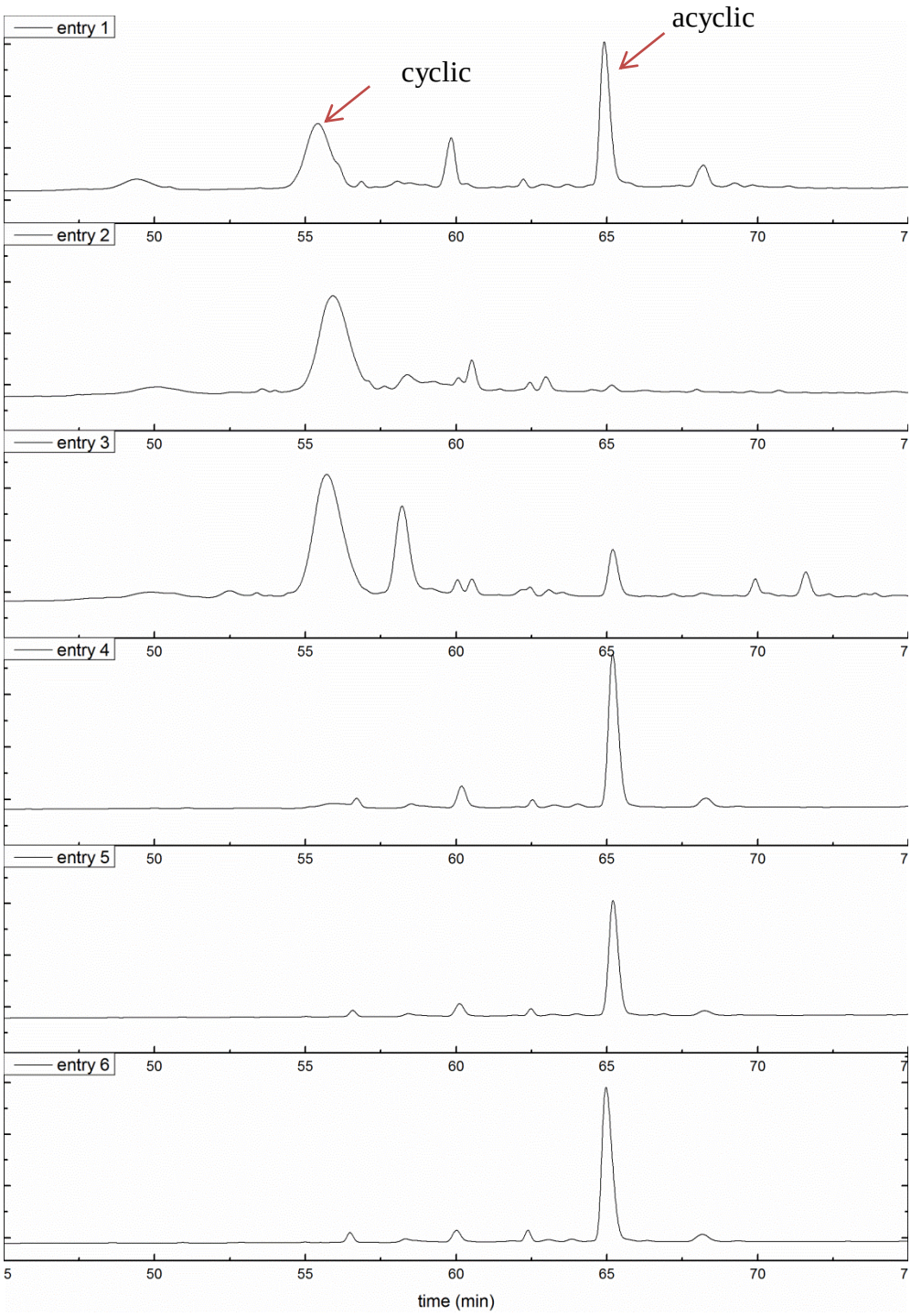

Figure 6.8-1. HPLC chromatograms (zoom 45-75 min) of reaction conditions **entry 1-6** (for 16 h, rt). Analytical HPLC experiments were carried out with method 4; signal was detected at 215 nm.

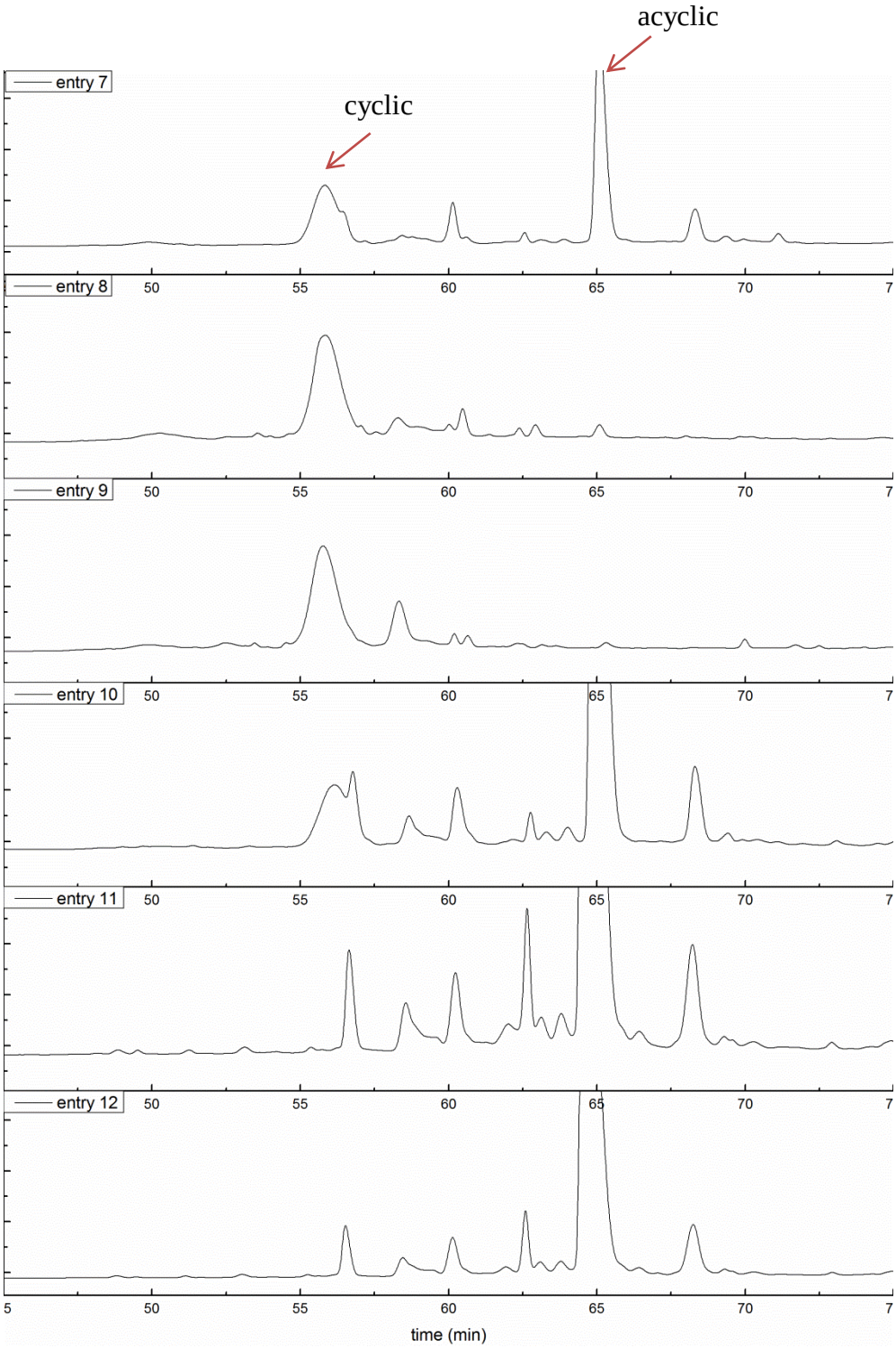

Figure 6.8-2. HPLC chromatograms (zoom 45-75 min) of reaction conditions **entry 7-12** (for 72 h, rt). Analytical HPLC experiments were carried out with method 4; signal was detected at 215 nm.

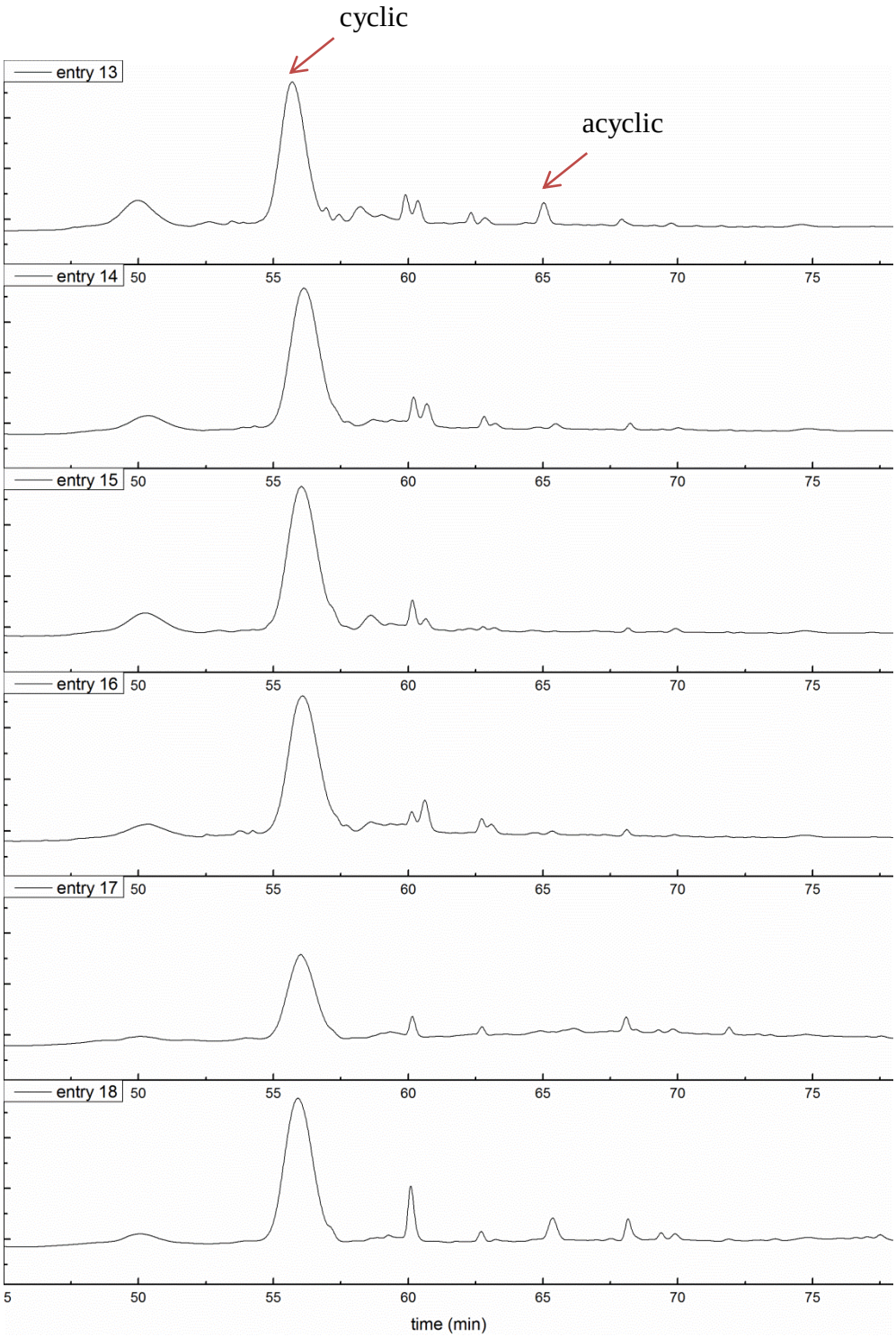

Figure 6.8-3. HPLC chromatograms (zoom 45-75 min) of reaction conditions **entry 13-18**. (MW, 30 min, 60°C). Analytical HPLC experiments were carried out with method 4; signal was detected at 215 nm.

6.8.2 Characterisation of U13, C13, U26, C26 (HPLC, MALDI-ToF, CD)

U13:(U)-Biotin-SGSG-KA*AYFZ*$_3$-NH_2

peptide	analytical t_R (min)	Purity after HPLC (%)
(U)-Biotin-SGSG-KA*AYFZ*$_3$-NH_2	65.9	94.4

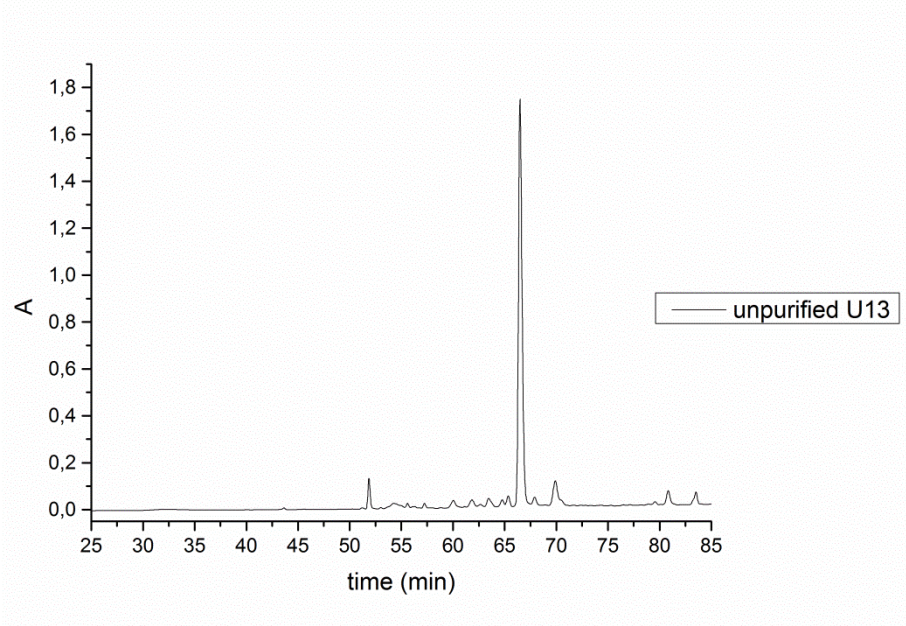

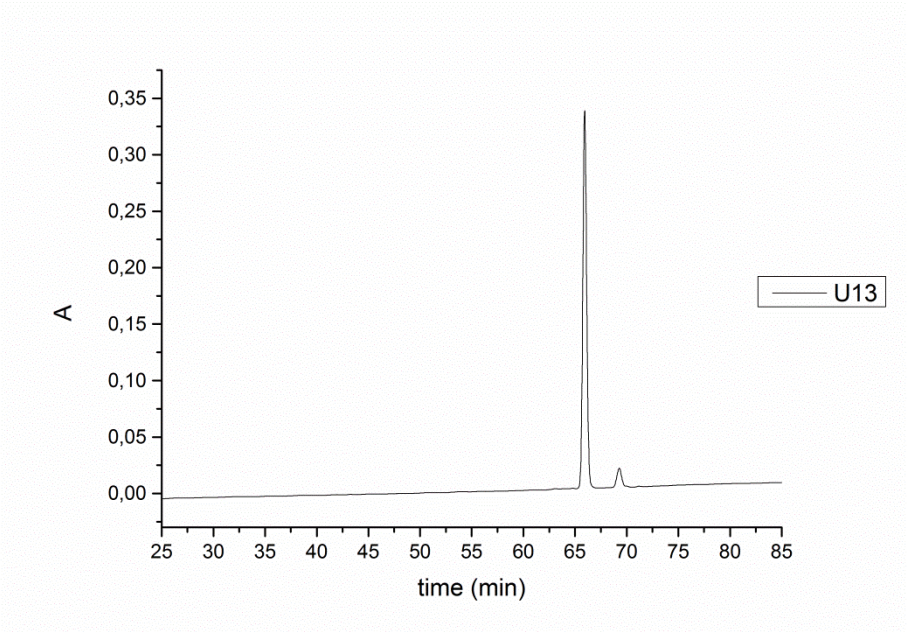

C13: (C)-Biotin-SGSG-KA*AYFZ$^{*}{}_{3}$-NH_2

	peptide	analytical t_R (min)	Purity after HPLC (%)
(on-bead synthesis)	(C)-Biotin-SGSG-KA*AYFZ$^{*}{}_{3}$-NH_2	53.4	85.4
(off-bead synthesis)	(C)-Biotin-SGSG-KA*AYFZ$^{*}{}_{3}$-NH_2	53.5	99.9

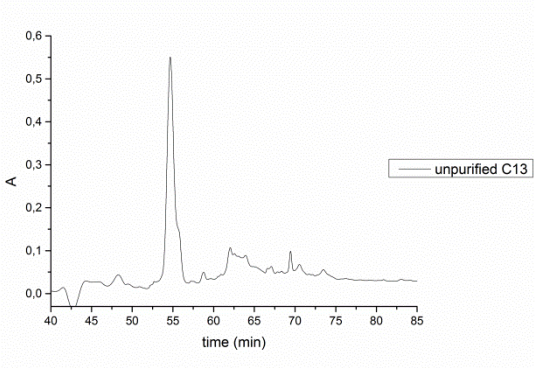

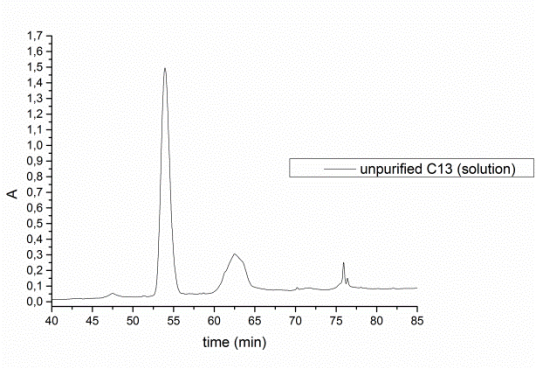

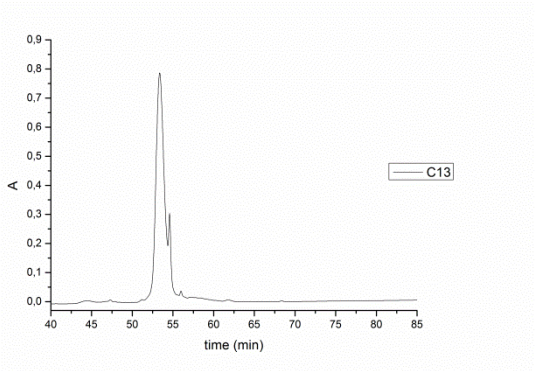

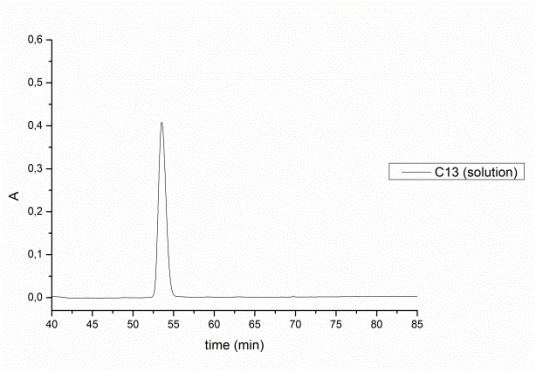

U26: (U)-Ac-KA*AYFZ*$_3$-NH_2

peptide	analytical t_R (min)	Purity after HPLC (%)
(U)-Ac-KA*AYFZ*$_3$-NH_2	68.3	77.2

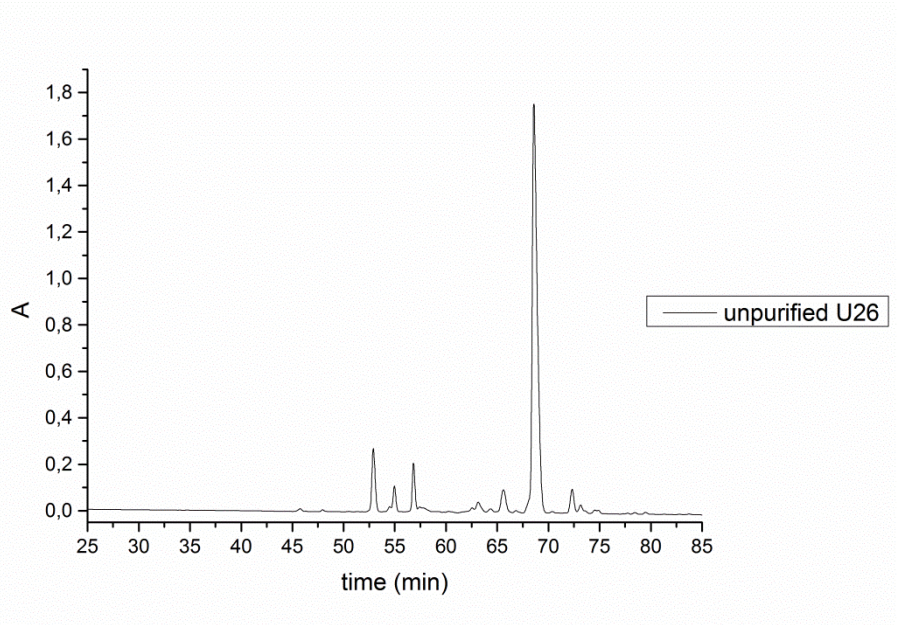

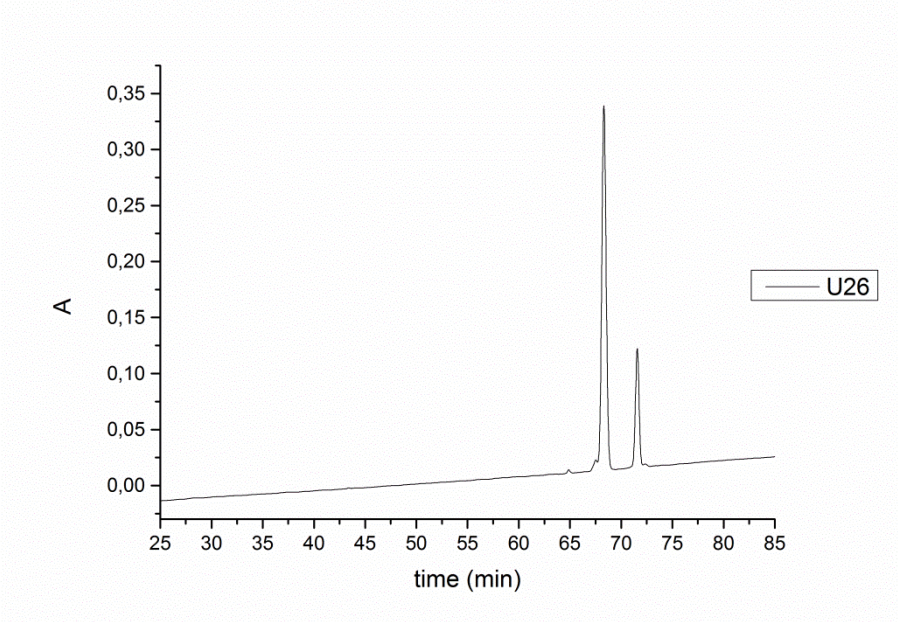

C26: (C)-Ac-KA*AYFZ*$_3$-NH_2

peptide	analytical t_R (min)	Purity after HPLC (%)
(C)-Ac-KA*AYFZ*$_3$-NH_2	53.2	95.0

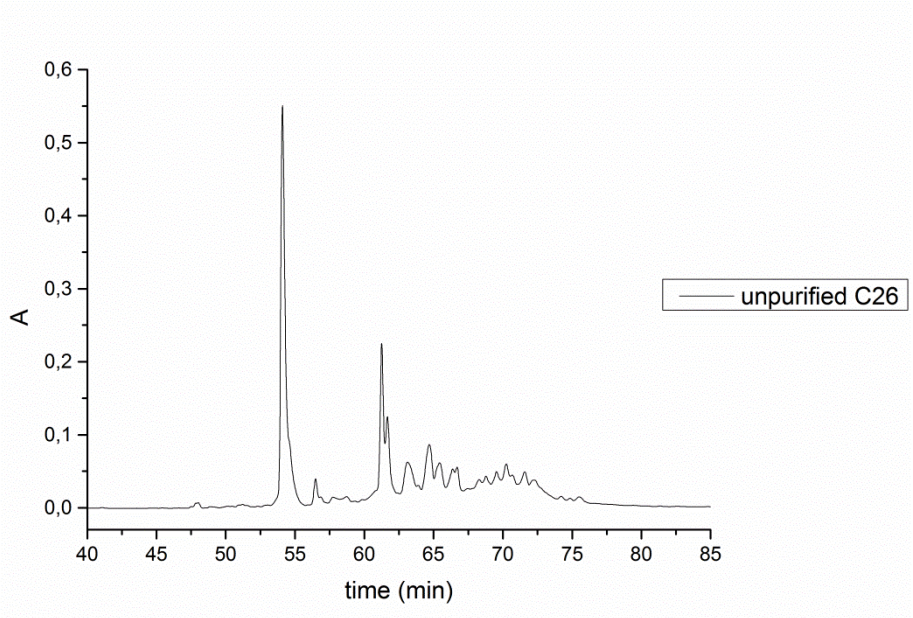

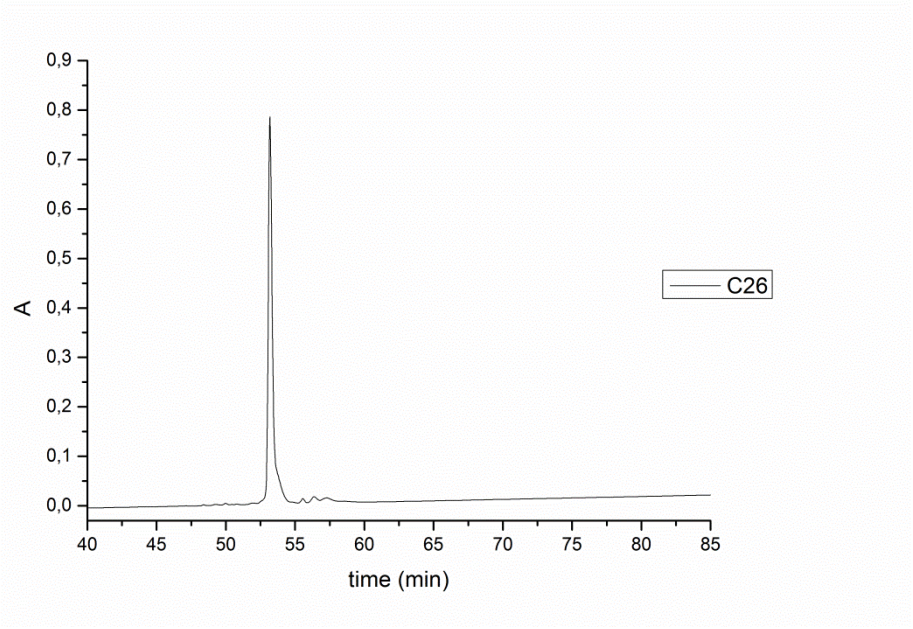

U13 (U)-Biotin-SGSG-KA*AYFZ*$_3$-NH_2

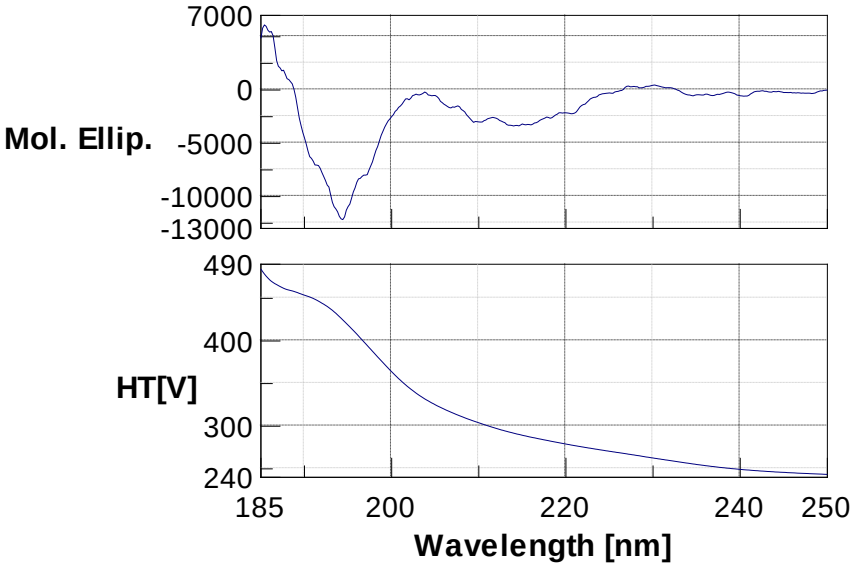

C13 (C)-Biotin-SGSG-KA*AYFZ*$_3$-NH_2

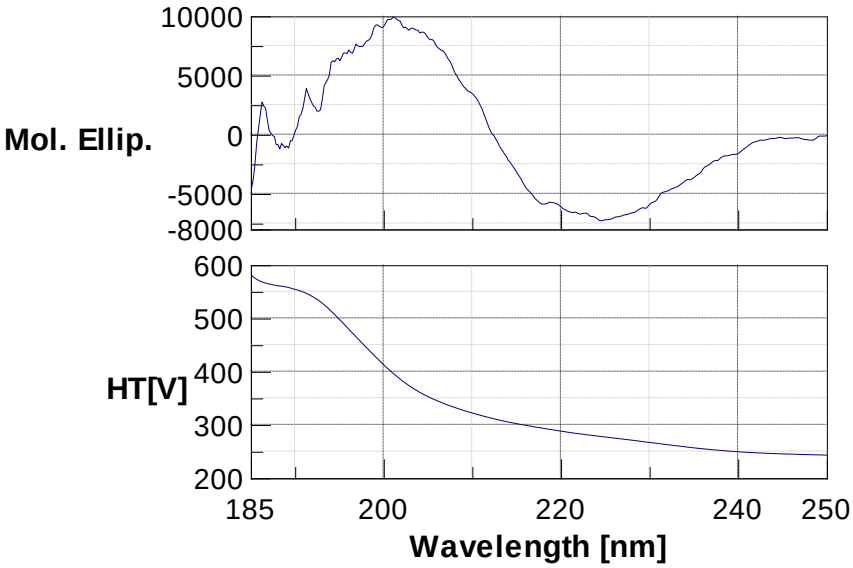

U26 (U)-Ac-KA*AYFZ*3-NH2

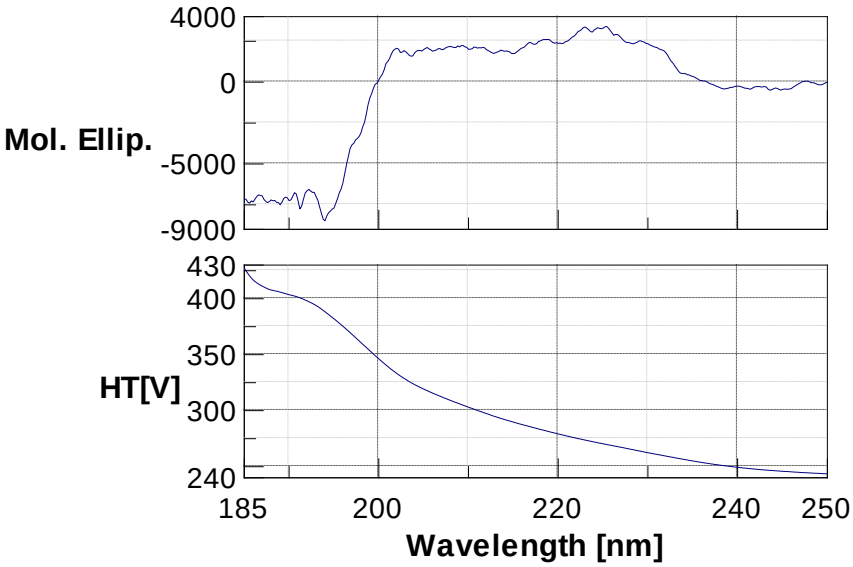

C26 (C)-Ac-KA*AYFZ*3-NH2

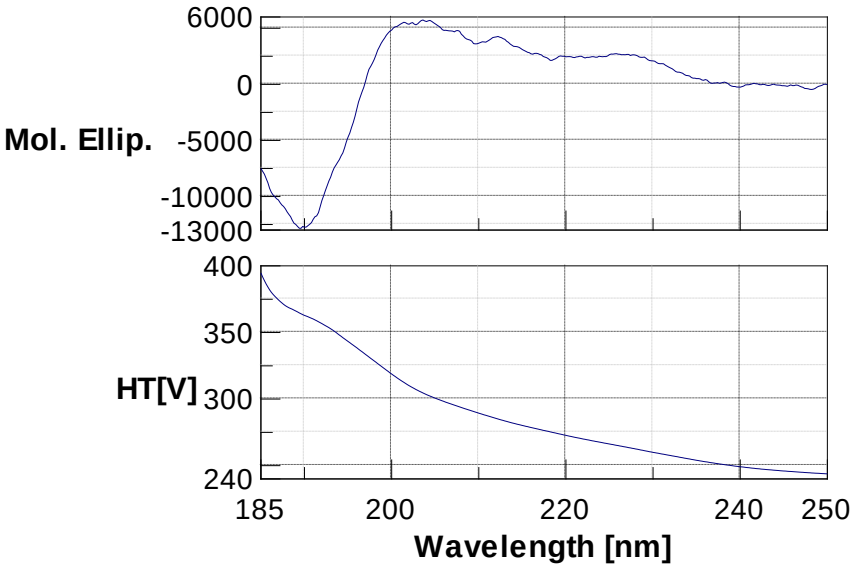

U13 (U)-Biotin-SGSG-KA*AYFZ*$_3$-NH_2

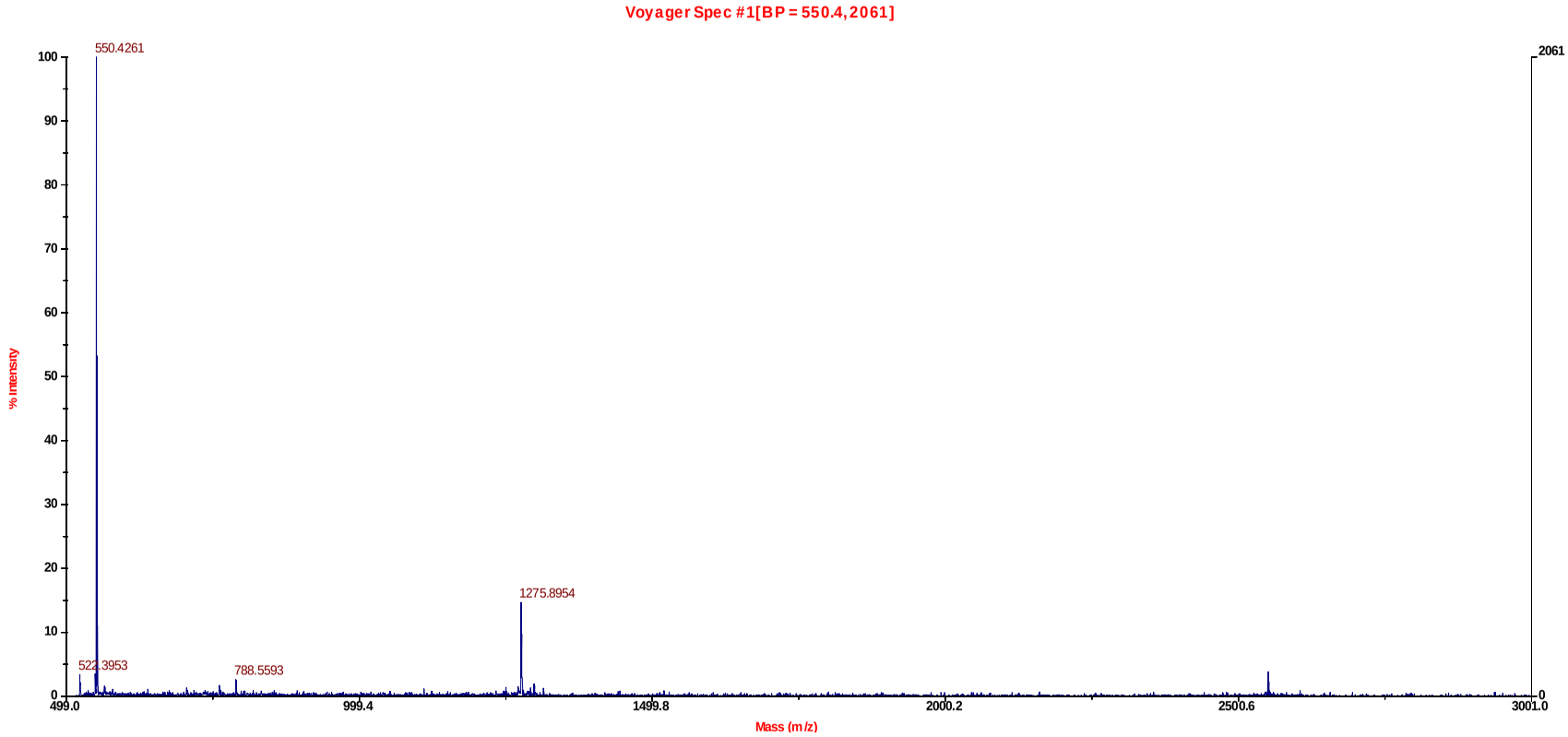

C13 (C)-Biotin-SGSG-KA*AYFZ*$_3$-NH_2

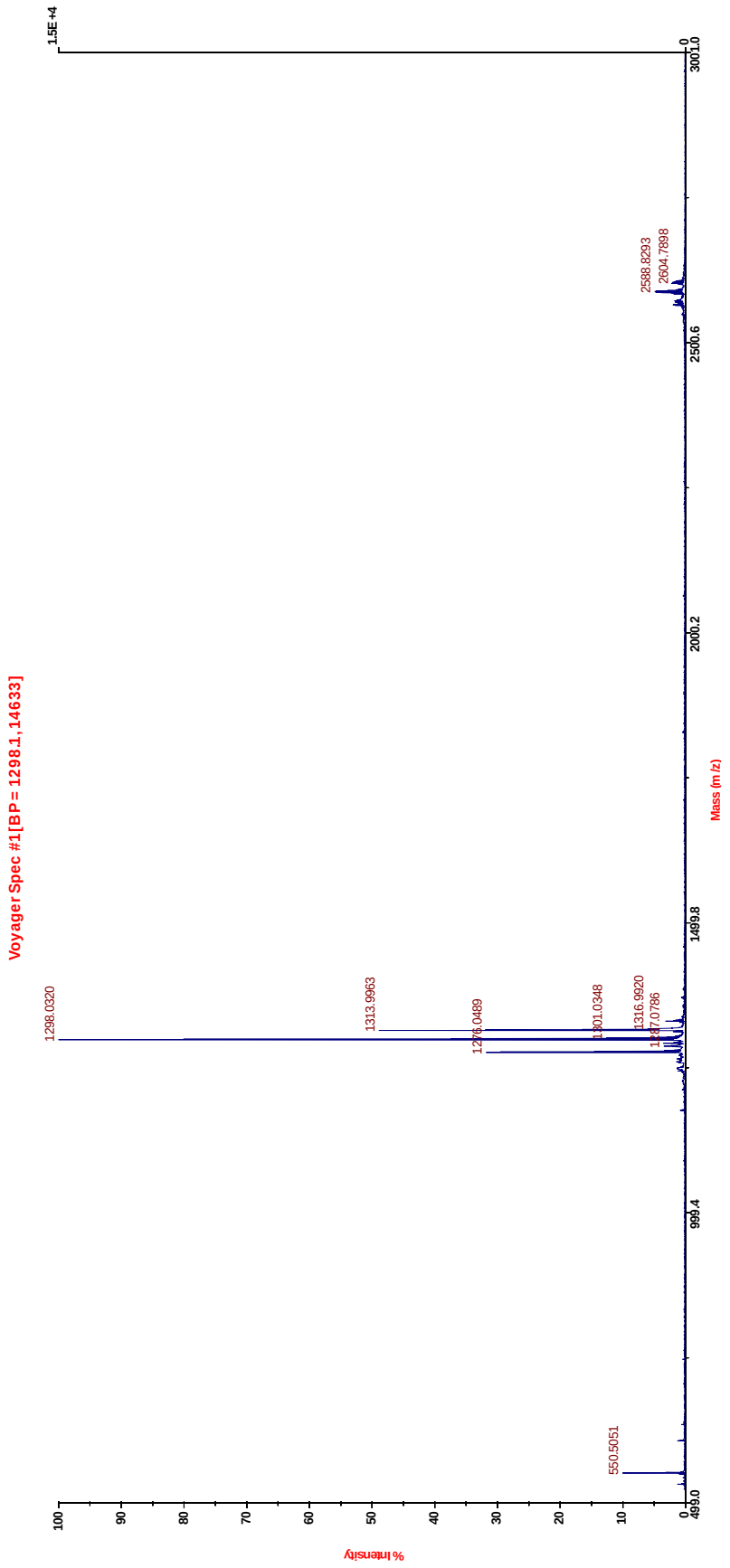

U26 (U)-Ac-KA*AYFZ*$_3$-NH_2

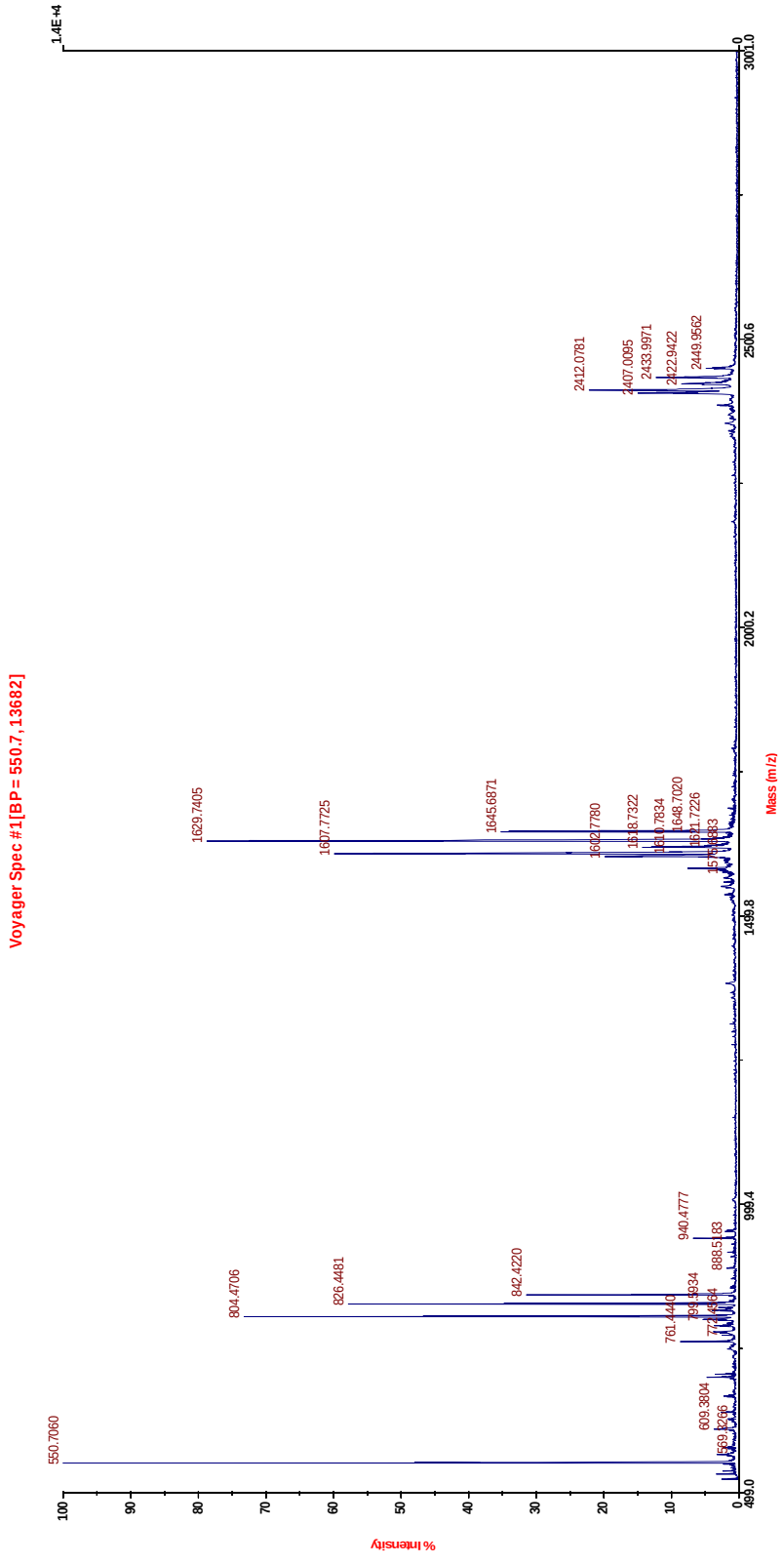

C26 (C)-Ac-KA*AYFZ$^{*}{}_{3}$-NH$_2$

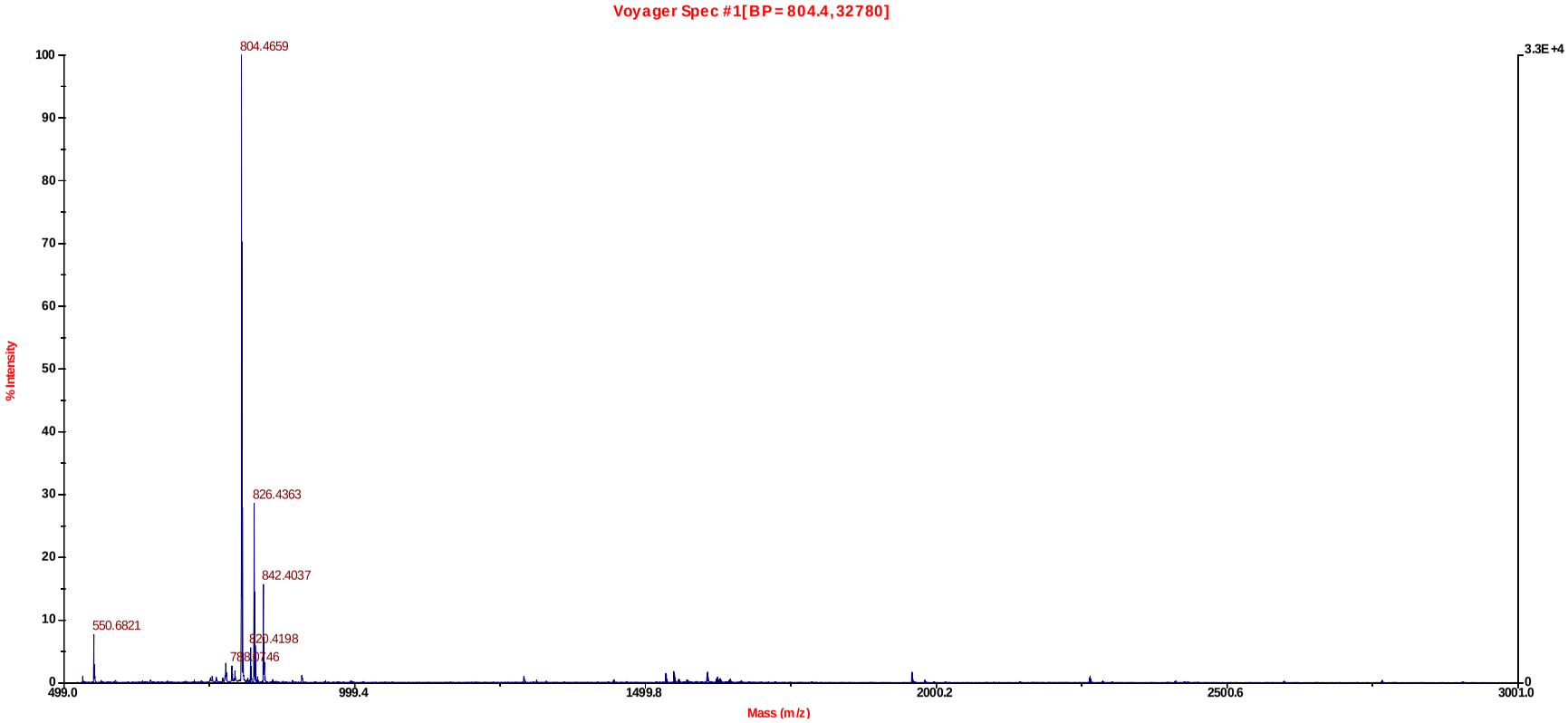

4.2.4 ^{1}H NMR of U13 and C13

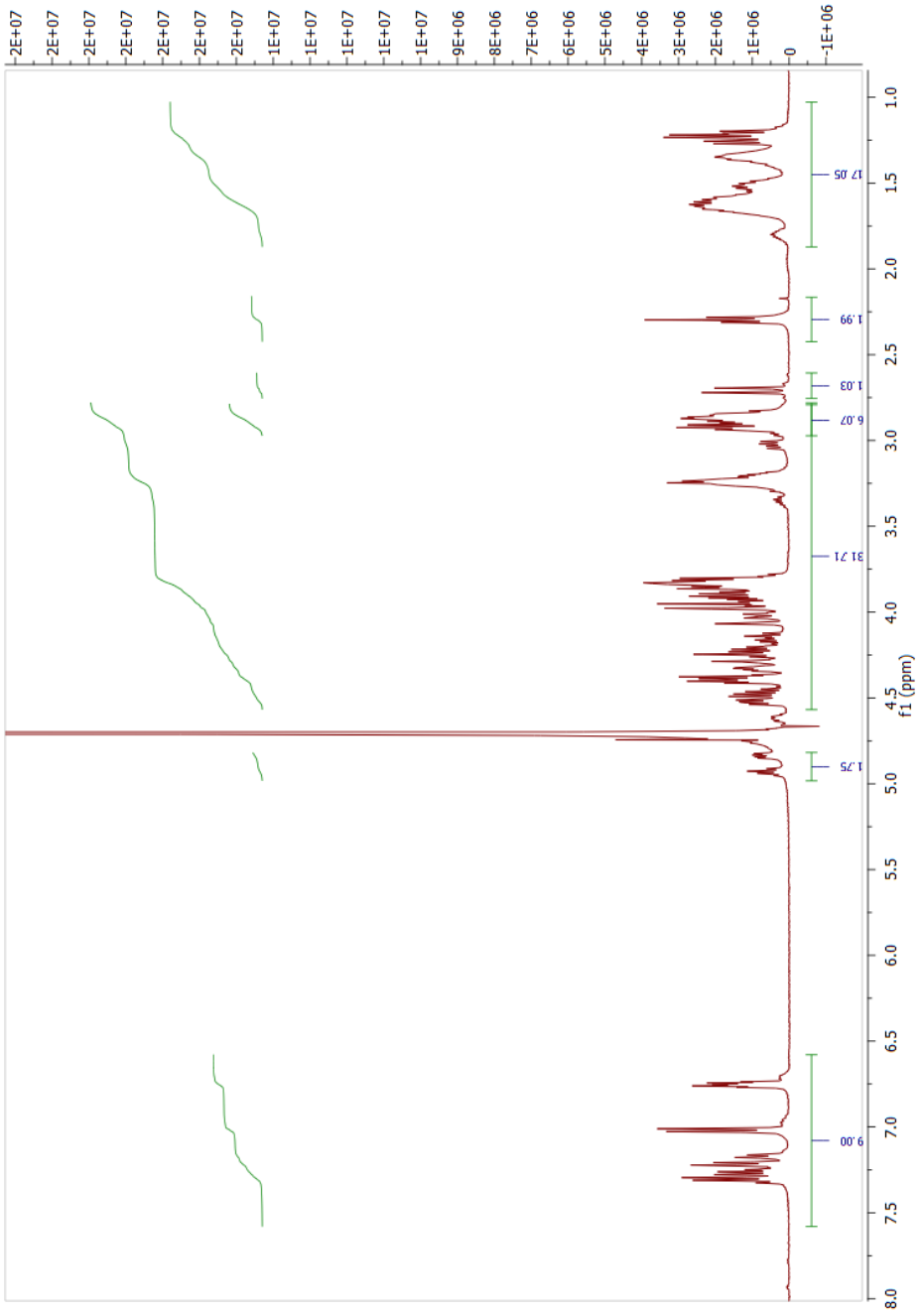

U13

C13

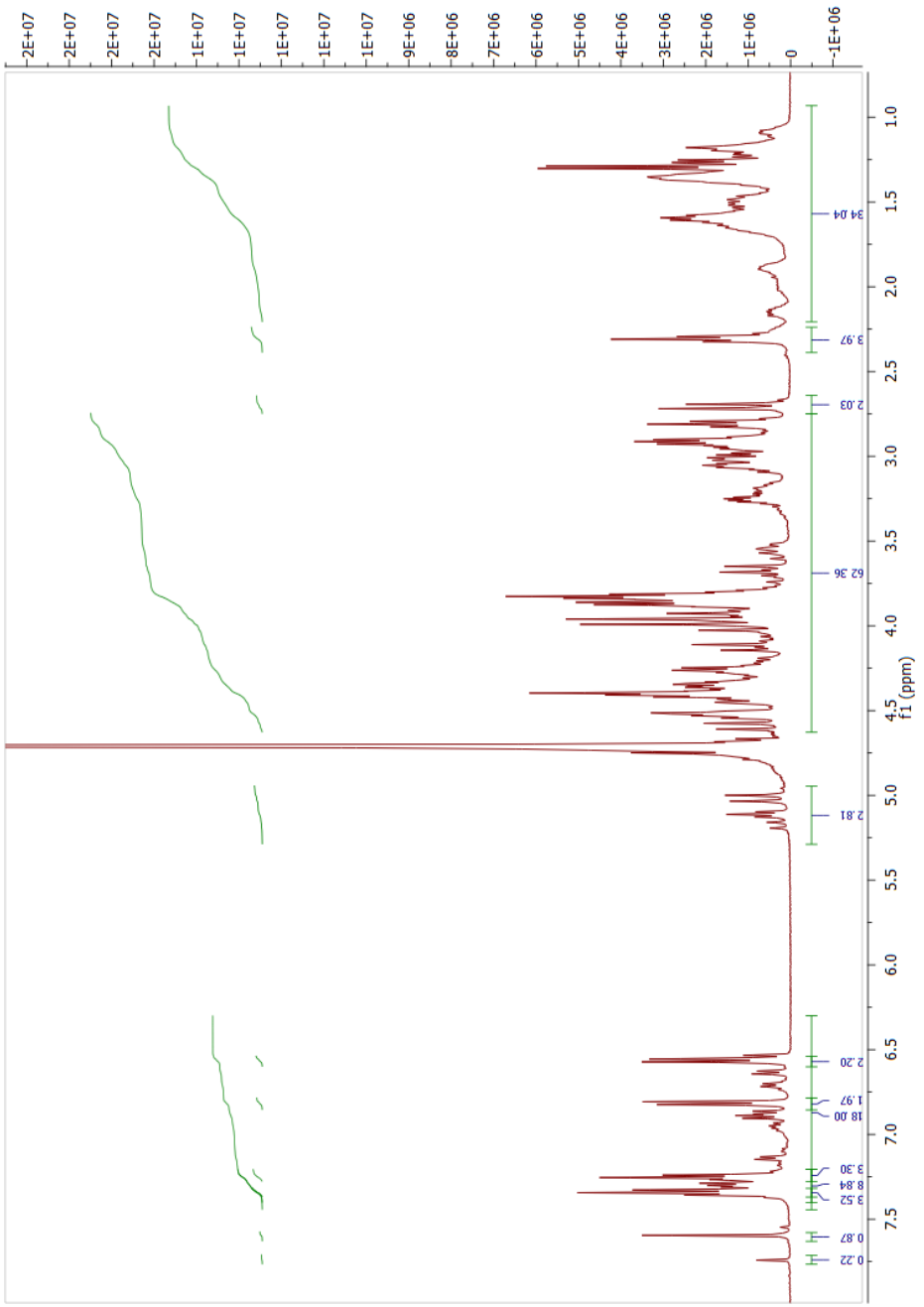

6.8.3 Electronic appendices

Detailed appendices are available on CD. Figures in these electronic appendices may be referenced in the present thesis. The table of contents is the following: